Electronic and Steric Modification of Divalent Group 14 Compounds Using Peripheral Boryl Substituents

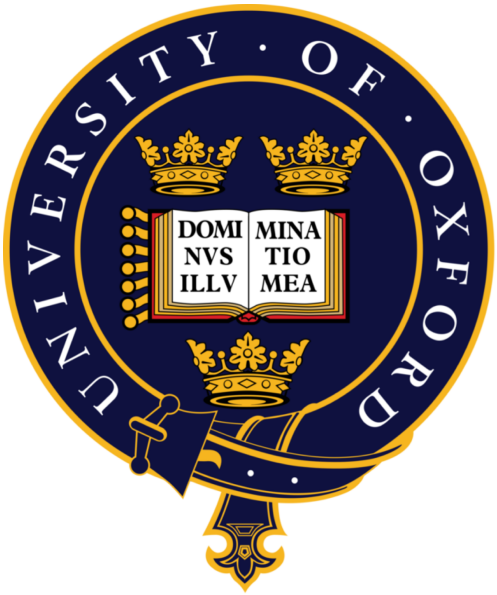

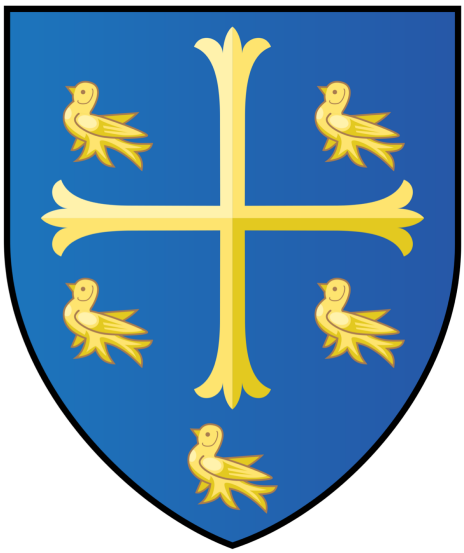

Lilja Kristinsdóttir

University College, Oxford

A thesis submitted for the degree of

Doctor of Philosophy

June 2018

Acknowledgements

Most importantly, I thank Prof. Simon Aldridge for accepting me into the group, for his guidance, support and brilliant ideas. I could not have wished for a better supervisor, a supervisor who is as supporting, non-judgemental and interested in the projects of the research group. His relentless enthusiasm and motivation kept me going when chemistry wasn't my best friend. I hope the Icelandic delicacies over the years have been a token of my gratitude.

I would also like to thank all the members of the Aldridge group, past and present, for their help, support, discussions and friendship. Thanks for all the coffee breaks, biscuits, pints, inside jokes and dance nights – you really made life in the lab and in Oxford a lot more fun. A special thank you to Jesús and Evgeny for taking me on, giving me advice and teaching me all the tricks when I arrived and to Andrey and his magic-like crystallization skills. Thank you Haoyu Niu and Dr. Petra Vasko for carrying out DFT calculations that contributed to my thesis. Nicola Oldroyd and Rachel Grabiner, Part II students, and Andreas Heilmann, summer student, made invaluable contributions to the chemistry on the tetrelenes reported in Chapter 5. Thank you for your collaboration, it was a fun and educating journey.

I'm most grateful to all the crystallographers for their countless hours of collecting and solving the X-ray data. Those late nights and weekends were undoubtedly unpleasant in many cases. Your help is immensely appreciated. Thank you to the group's crystallographers: Dr. Jesús Campos Manzano, Dr. Eugene Kolychev, Dr. Jamie Hicks and Dr. M. Ángeles Fuentes, as well as to of the Oxford Crystallography service staff: Dr. Amber L. Thompson and Dr. Kirsten E. Christensen.

Dr. Nick Rees has been very helpful throughout the course of this work with his help, advice, training and discussion on NMR spectroscopy. I will miss your cheerful music during instrument time in the basement.

Prof. Guy Bertrand kindly hosted my three months stay at the University of California San Diego. Thank you for the opportunity and your help. The rest of the group members in the Bertrand group I would like to thank for welcoming me into the group, helping me to settle in and offering advice and friendship. A special thank you to Cory for lively chats and lots of help in the lab, Rudy and his wife Liliane for their help and friendship and Eder for always being up for a beer and a game of pool, the discussions and travels. Also Max, Ryo and the rest of the non-chemists for the fun lunches and coffee breaks, trips and roof-parties.

I would like to thank the Clarendon Fund for funding my studies over the past three and a half years. I am also grateful for the funding offered by University College through the Old Members' Trust Graduate Conference and Academic Travel Fund,

which supported my travel to UCSD.

I would like to thank all my friends outside the lab, Anne, Claudia, Florence, Nate, Wiem and many more, who have made my stay in Oxford extremely fun and enjoyable, I will truly miss you. Sarah, thank you for your friendship and support, for our countless chats, walks, bike rides, wine and cheese nights and more and more – and not to mention the invaluable help with proofreading. Lakisa and all of the African dance group and the drummers, thanks for all the fun and performances. Thank you Dem for teaching me how to play the djembe and to all of Oxford Drum Troupe for fun practices, gigs and countless pints. Thank you to my friends who came to visit me in Oxford, it meant a lot and brought so many good memories.

I want to thank my parents for their support and understanding, for bringing me all the goodies from home and for spoiling me while writing my thesis back home. Thank you Hlynur for always being there, for listening to me rambling about chemistry and NMRs without having a clue, supporting me when things were downhill and for celebrating small victories with me. Thank you for moving to the UK so that we could spend time together and making our time in Oxford so special.

Lastly, I would like to dedicate this thesis to my grandmother. I am so grateful for the time we got together during the last months back in Iceland when I was writing up. She told me off every time I visited for a lunch-break as I shouldn't be wasting my time on her – I had more important things to do. It is as if she waited until the last minute – when she knew I was safely on the flight to hand in the thesis – and let go of life. Ég sakna þín amma.

Abstract

This thesis examines the use of sterically demanding boryl groups as peripheral substituents on *N*-heterocyclic carbenes and Group 14 tetrelenes.

Chapter III focuses on the syntheses of borylated imidazoles and imidazolium salts. With the aim of accessing an *N*,*N*'-bisborylated NHC or its metal complexes, the reactivity of bisborylated imidazolium salts with Brønsted bases and metal complexes was studied. The results highlight the lability of the N–B bond and electrophilicity of the boryl group as displacement of the boryl group was repeatedly observed.

Chapter IV deals with the syntheses and reactivity of unsymmetrical borylated imidazolium salts and the corresponding carbenes. An unsymmetrical bisborylated carbene has been observed and characterized both *in situ* and with a range of trapping experiments. This system is however characterized by a 1,2-shift of the *N*-bound boryl group to the C2 position. Slow rearrangement allowed for assessment of the kinetic properties of the reaction experimentally; computational studies provide consistent activation barriers and suggest an intramolecular migration pathway. Structural and spectroscopic studies of transition metal complexes and a selenium adduct of the carbene allowed for investigation of the steric and electronic properties of the carbene.

Chapter V examines the attempts to synthesize *N*,*N*'-bisborylated saturated *N*-heterocyclic carbenes and tetrelenes. Bisborylated *N*-heterocyclic germylenes and stannylenes were successfully synthesized and structurally characterized. Their reactivity towards small molecules was examined, with the pursuit of a germanone being of particular interest.

Numbering Scheme and Abbreviations

Known compounds will generally be numbered **x.y**, where x refers to the chapter where they are first mentioned and y is dependent on the order the compounds appear in the chapter. Compounds that were formed in the reactions reported in this thesis will be numbered in the order they appear (**1**-**35**) or using labelling derived there from.

The following abbreviations will be used throughout this report:

$\%V_{bur}$ – Percentage Buried Volume
acc. – Accurate
Ad – Adamantyl
ADF – Amseterdam Density Functional
Ar – Aryl
$Ar^{F}{}_{4}$ – 3,5-Bis(trifluoromethyl)phenyl
BICAAC – Bicyclic (Alkyl)(Amino)Carbene
br – Broad
ca. – Circa
CAAC – Cyclic (Alkyl)(Amino)Carbene
calc. – Calculated
cat. – Catalytic Amount
CI – Chemical Ionization
cod – Cyclooctadiene
COSY – Homonuclear Correlation Spectroscopy
CW – Continuous-Wave
Cy – Cyclohexyl
d – Doublet / Days / Distance
DAC – Diamidocarbene
DBU – 1,8-Diazabicyclo[5.4.0]undec-7-ene
DFT – Density Functional Theory
Dipp – 2,6-Diisopropylphenyl
DMPO – 5,5-Dimethyl-1-pyrroline *N*-oxide
EI – Electron Impact
EPR – Electron Paramagnetic Resonance
eq. – Equivalent
ESI – Electrospray Ionization
Et – Ethyl
FT – Fourier Transform
h – Hours
HMBC – Heteronuclear Multiple-Bond Correlation
HMDS – Hexamethyldisilazane (Bis(trimethylsilyl)amide)
HOMO – Highest Occupied Molecular Orbital

HSQC – Heteronuclear Single Quantum Correlation

i – *Ipso*

^{i}Pr – *Iso*-propyl

IR – Infrared

J – Coupling Constant

L – Ligand

LUMO – Lowest Occupied Molecular Orbital

m/m – *Meta*/Multiplet

MAAC – (Monoamido)(Amino)Carbene

Me – Methyl

Mes – 2,4,6-Trimethylphenyl

min – Minutes

mol – Moles

MS – Mass Spectroscopy

^{n}Bu – Normal-butyl

NHC – *N*-Heterocyclic Carbene

NHO – *N*-Heterocyclic Olefin

NMR – Nuclear Magnetic Resonance

o – *Ortho*

OTf – Trifluoromethanesulfonate

p – *Para*

Ph – Phenyl

ppm – Parts Per Million

q – Quartet

quin – Quintet

R – Substituent

r.t. – Room Temperature

ROESY - Rotating Frame Nuclear Overhauser Effect Spectroscopy

s – Singlet

SambVca – Salerno Molecular Buried Volume Calculation

sept – Septet

SPS – Solvent Purification System

t – Triplet

$t_{½}$ – Half-life

^{t}Bu – *Tert*-butyl

TEMPO – (2,2,6,6-Tetramethylpiperidin-1-yl)oxyl

TEP – Tolman Electronic Parameter

THF – Tetrahydrofuran

THT – Tetrahydrothiophene

TMEDA – *N*,*N*,*N*',*N*'-Tetramethylethylenediamine

vs – *versus*

xs. – Excess

Xyl – 2,6-Dimethylphenyl

ν – Frequency

δ – NMR Chemical Shift

Pr* – Ar = Ph
Pr*$^{(2\text{-Np})}$ – Ar = 2-Napthalene

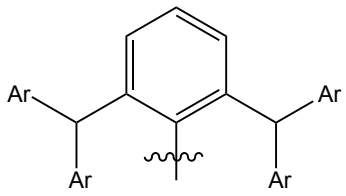

IMe – R = Me
IMes – R = Mes
IPr – R = Dipp
IPr* – R = Pr*
IPr*$^{(2\text{-Np})}$ – Ar = Pr*$^{(2\text{-Np})}$
ITr – R = CPh_3

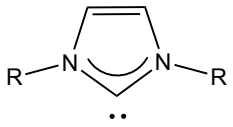

SIMes – Ar = Mes, n = 1
SIPr – Ar = Dipp, n = 1
6Mes – Ar = Mes, n = 2
6IPr – Ar = Dipp, n = 2
7Mes – Ar = Mes, n = 3
7IPr – Ar = Dipp, n = 3

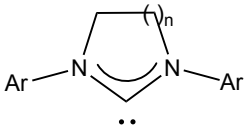

CAAC$^{\text{menthyl}}$ – RR' = menthyl
CAAC$^{\text{Cy}}$ – RR' = Cy
CAAC$^{\text{Me}}$ – R = R' = Me

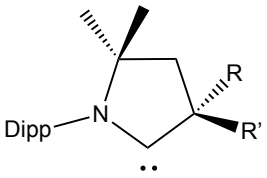

$C(N^iPr_2)_2$

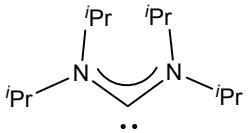

6MAAC$^{\text{Mes}}$

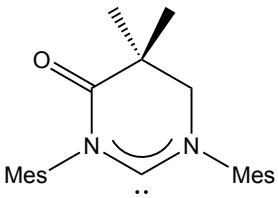

6DAC$^{\text{Mes}}$ – Ar = Mes
6DAC$^{\text{Dipp}}$ – Ar = Dipp

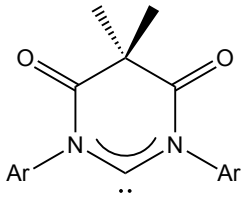

Table of Contents

Chapter I

Introduction

1.1 Divalent Group 14 Compounds

Divalent Group 14 compounds include carbenes and the heavier analogues, tetrelenes (silylenes, germylenes, stannylenes and plumbylenes), which feature a neutral Group 14 atom with two valence bonds and two non-bonded electrons (Figure 1.1). Such systems are typically unstable due to non-fulfilment of the octet rule. Two of the frontier orbitals (*n*s/*n*p-orbitals) of the carbene/tetrelene centre are occupied by bonding to the adjacent atoms (X), leaving two for the unpaired electrons to occupy. The electronic configuration adopted in the ground state depends on the central atom (E), the substituents (X) and the molecular geometry.

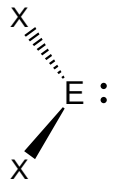

Carbenes E = C, Silylenes E = Si,
Germylenes E = Ge, Stannylenes E = Sn,
Plumbylenes E = Pb

Figure 1.1 Divalent Group 14 compounds.

A linear carbene can be viewed as sp-hybridized with two degenerate non-bonding orbitals (p_x and p_y) that are equivalent in energy.[1] According to Hund's rule, the two electrons would therefore be distributed between p_x and p_y, resulting in a triplet configuration (Figure 1.2). On bending, however, one of the p-orbitals gains s-character (the σ-orbital) at the expense of the C–X bonding orbitals, while the other

(now labelled p_π) is unchanged (Figure 1.2). This lowers the energy of the σ-orbital and opens up an energy gap between σ and p_π. At a certain energy gap (*ca*. 2 eV),[2] the pairing energy is outweighed and it is more favourable for both electrons to occupy the σ-orbital, resulting in a singlet configuration (Figure 1.2).

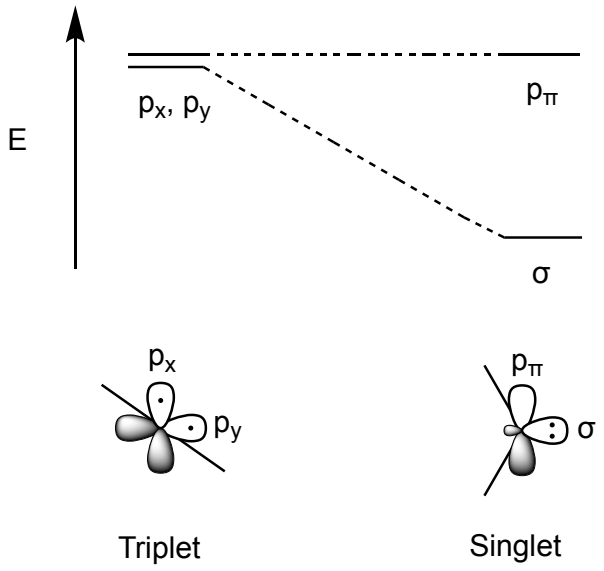

Figure 1.2 Frontier orbitals of a linear (left) and a bent (right) carbene.

As Group 14 is descended, the increasing number of radial nodes and poorer size match between the *n*s- and *n*p-orbitals means that s-p mixing becomes less effective. The calculated bond angles for systems of the type H_2E: (E = C, Si, Ge, Sn, Pb) decrease down the group (getting closer to 90°),[3] reflecting greater p-character in the bonding orbitals. This in turn confers more s-character on the σ-orbital, thereby stabilizing it and increasing the σ-p_π energy gap. This is reflected in an increasing energy difference between the singlet and triplet states on descending the group (Table 1.1)[3] and tetrelenes generally adopt a singlet ground state in contrast to carbenes, whose electronic ground state depends strongly on their substituents and the EX_2 bond angle.[4] In addition, the tendency to dimerize decreases down the group due to weaker E–E bonds.[3] The increased energy difference between the triplet and the singlet states

(ΔE_{ST} = E(triplet) – E(singlet)), and the decreased tendency to dimerize renders the tetrelenes more stable compared with carbenes, with increasing stability down the group.

	ΔE_{ST}
H_2C:	-58.6
H_2Si:	69.9
H_2Ge:	91.2
H_2Sn:	103.8
H_2Pb:	145.6

Table 1.1 Singlet-triplet energy gap (ΔE_{ST}, kJ mol^{-1}) for divalent Group 14 compounds.[3]

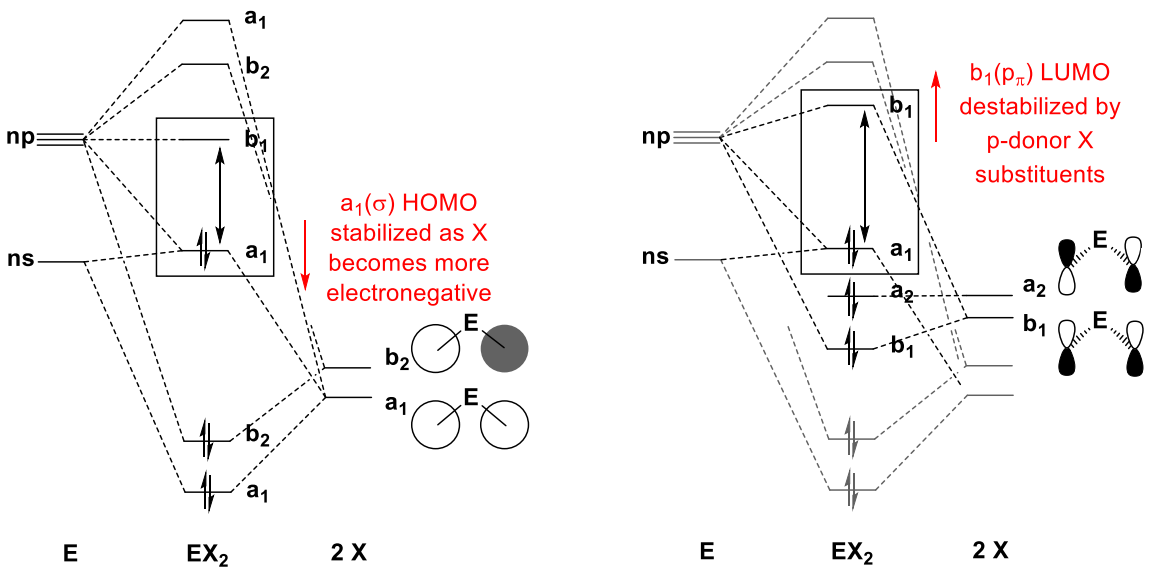

Figure 1.3: Perturbation orbital diagrams depicting inductive effects (left) and mesomeric effects (right) on the carbene/tetrelene centre (E = C, Si, Ge, Sn, Pb) induced by the substituents (X).[2]

For both carbenes and tetrelenes, the energy of the σ- and the p_π-orbitals can be tuned by changing the nature of the substituents or the geometry of the carbene/tetrelene centre. σ-Withdrawing substituents stabilize the σ-orbital of the divalent species and π-donating substituents destabilize the p_π-orbital, and *vice versa* (Figure 1.3). Reducing the EX_2 angle enhances the s-character in the σ-orbital and lowers its energy, and *vice versa*. Singlet carbenes and tetrelenes have an occupied σ-

orbital and an empty p_π-orbital and are thus σ-donating and π-accepting. Raising the energy of the σ-orbital causes increased σ-donation and lowering the p_π-orbital increases the π-accepting abilities of the carbene/tetrelene.

Generally, carbenes and tetrelenes are considered to be thermodynamically unstable (particularly for the lighter group 14 elements) and initial examples were therefore only observed and used *in situ*. Manipulation of the frontier orbitals of carbenes and tetrelenes affects their stability and reactivity; a large HOMO-LUMO (σ-p_π) energy gap renders the carbene/tetrelene less labile whereas a small HOMO-LUMO gap increases its reactivity. Careful adjustment of the HOMO-LUMO energy gap of the tetrelene centre can therefore be employed to design molecules that are thermally stable but still interact with/activate small molecules.

1.2 Carbenes

1.2.1 The Emergence of Carbenes and Their Metal Complexes

The first carbene metal complex was synthesized by Fischer and Maasböl in 1964.[5] The metal complex was obtained by the formal addition of two methyl groups to $W(CO)_6$, yielding $W(CO)_5[C(OMe)Me]$ (Scheme 1.1). This (Fischer) carbene has a singlet configuration and relies on a π-donating substituent to stabilize it. It is electrophilic due to its formally vacant p_π-orbital, neutrally charged and σ-donating/π-accepting.

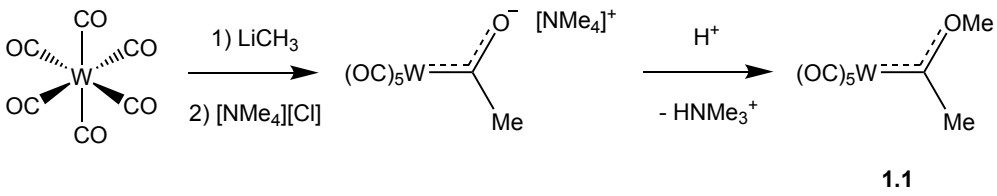

Scheme 1.1 Synthesis of the first metal carbene complex: a Fischer-type carbene.[5]

A new type of metal carbene was synthesized a decade later by Schrock.[6] Treatment of $Ta[CH_2CMe_3]_3Cl_2$ with two equivalents of neopentyllithium resulted in the formation of an alkylidene complex (Scheme 1.2). These Schrock carbenes, as they are also known, lack π-donating substituents and are, as a result, formally triplet carbenes. The metal-carbene bond is polarized towards the carbene, resulting in a formal charge of -2 on the ligand. The aforementioned polarity of the bond and the filled p_π-orbital renders these carbenes nucleophilic.

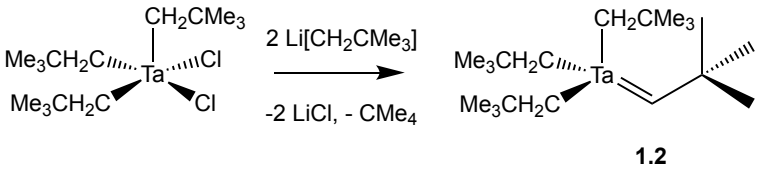

1.2

Scheme 1.2 Synthesis of the first Schrock carbene (alkylidene) complex.[6]

In an attempt to isolate a 'free' nucleophilic carbene, Wanzlick recognized that strongly electron-donating substituents would be needed to change the electrophilic nature of the carbene to nucleophilic and to offer the carbene enhanced stability.[7] The carbene he designed features a phenyl-substituted imidazoline heterocycle with π-donating nitrogen atoms adjacent to the carbene (**1.4**; Scheme 1.3). The free carbene was not isolated or indeed spectroscopically observed; instead the dimer **1.5** was formed and used as an *in situ* source of the carbene. The nucleophilic nature of the carbene was demonstrated by its reaction with methanol to give **1.6**, a reaction which implies the existence of an equilibrium between the dimer and the free carbene (now known as the Wanzlick equilibrium; Scheme 1.3). The existence of such equilibrium was initially debated[8,9] but has more recently been confirmed.[10] Sterically demanding substituents favour the formation of two molecules of the carbene, while less sterically demanding substituents shift the equilibrium towards the dimer.[10]

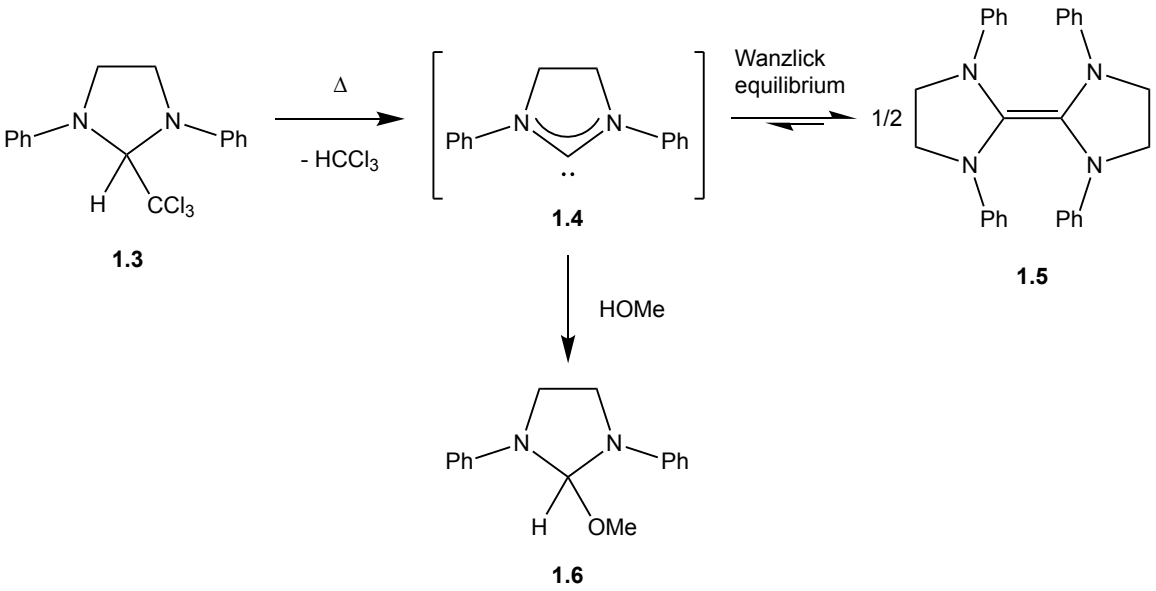

Scheme 1.3 A transient nucleophilic carbene (1.4) is suggested to be in equilibrium with the thermodynamically favoured dimer (1.5) at 170 °C but can be trapped with MeOH.[7]

In 1968, Wanzlick e*t al.*[11] and Öfele[12] independently reported the first examples of the direct formation of a metal carbene complex from a carbene precursor. Both methods rely on treating an imidazolium salt (**1.7** or **1.9**) with a basic metal source ($Hg(OAc)_2$ and $[HCr(CO)_5]^-$, respectively), which deprotonates the C–H bond and metallates the free carbene *in situ* (Scheme 1.4).

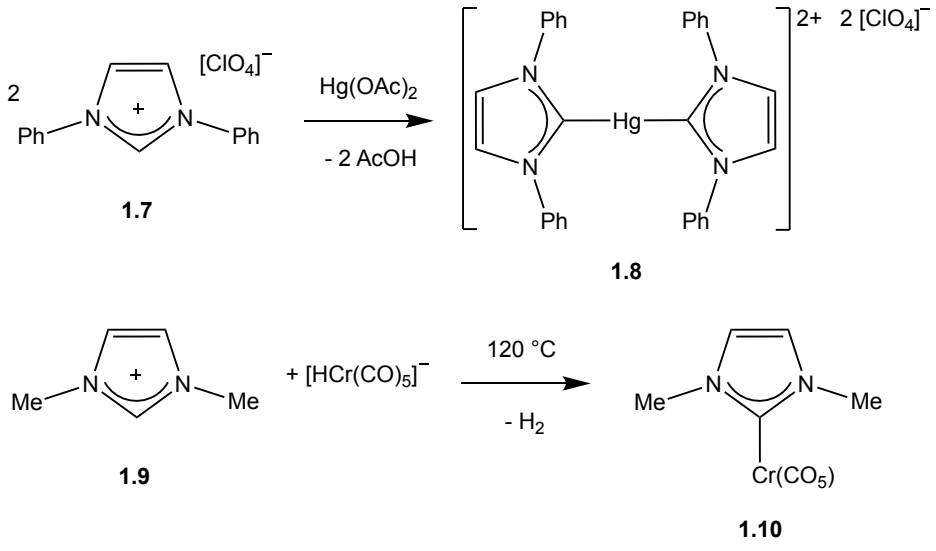

Scheme 1.4 Wanzlick's and Öfele's direct syntheses of metal carbene complexes from imidazolium salts 1.7 and 1.9.[11,12]

In 1970, Wanzlick *et al.* reported the first *in situ* observation of a free carbene (**1.11**; Scheme 1.5).[13] The steric profile in this case was sufficient to hinder dimerization, but the carbene was neither isolated nor structurally characterized; *in situ* reactions demonstrated nucleophilic properties of the carbene species.

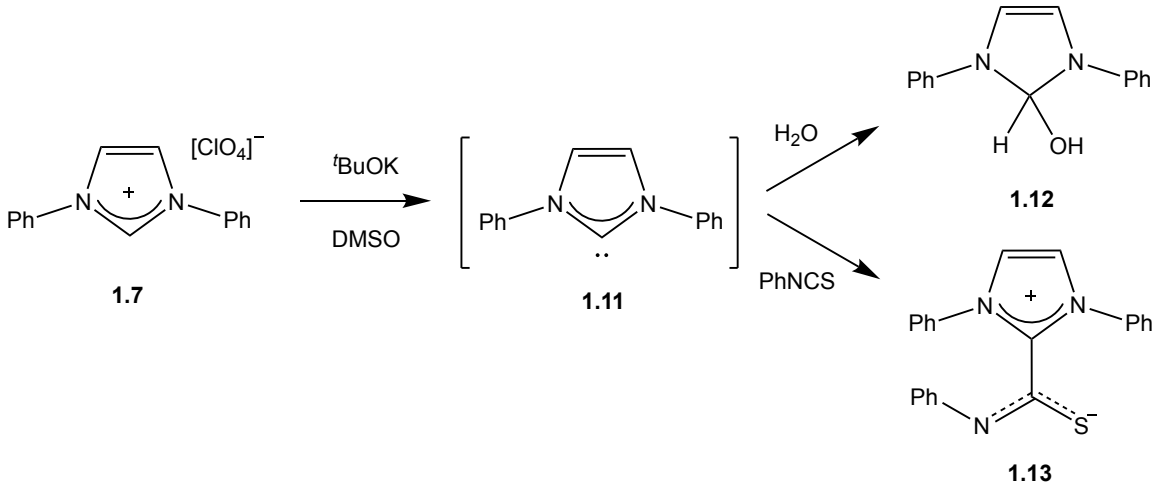

Scheme 1.5 First synthesis of an *N*-heterocyclic carbene (1.11) and subsequent electrophilic reactions with H_2O and PhNCS.[13]

In 1988, Igau *et al.* reported a stable λ^3-phosphinocarbene (**1.15**), which is in resonance with a λ^5-phosphaacetylene (**1.16**; Scheme 1.6).[14] Reactivity of the λ^3-phosphinocarbene/λ^5-phosphaacetylene suggested preference for the phospha-acetylene form, but carbenic reactivity was also observed. This carbene was not isolated nor structurally characterized, but isolation and structural characterization of a related analogue was later reported by the same group in 2000.[15]

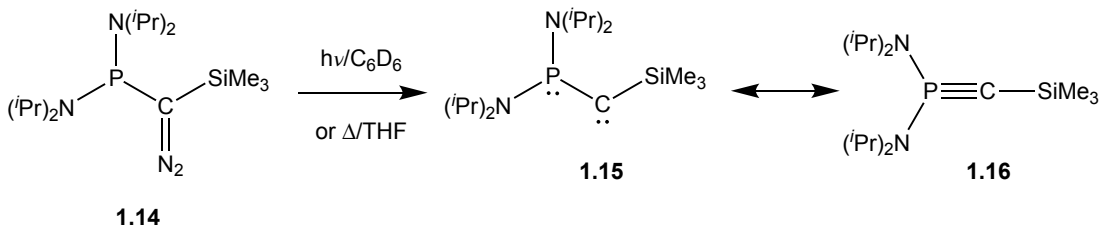

Scheme 1.6 Igau's synthesis of a λ^3-phosphinocarbene in resonance with λ^5-phosphaacetylene.[14]

In 1991, Arduengo *et al.* were the first to report an isolated free carbene as a thermodynamically stable crystalline compound (**1.18**; Scheme 1.7).[16] The carbene is thermodynamically stabilized by incorporation into an imidazolium ring and incorporates (a) inductive σ-withdrawing effects from the adjacent nitrogens that stabilize the σ-orbital, (b) mesomeric π-donation from the adjacent nitrogens that destabilizes the p_π-orbital, (c) a heterocyclic framework which forces bending of the carbene, thereby lowering the energy of the σ-orbital and (d) a formally aromatic 6π electron structure. Furthermore, the carbene is kinetically stabilized by the use of bulky adamantyl groups as the *N*-substituents, thereby preventing dimerization. This type of carbenes is known as an *N*-heterocyclic carbene (NHC), and subsequent isolated samples contain saturated as well as unsaturated backbones.

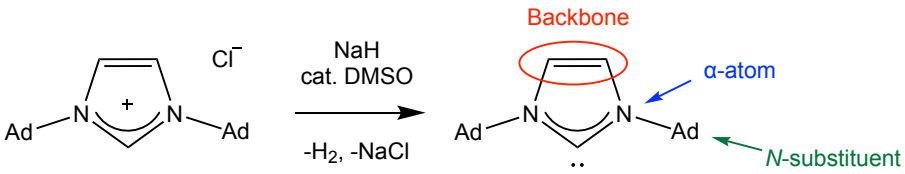

Scheme 1.7 Arduengo's synthesis of the first isolable free carbene.[16] The figure also outlines the key structural components of NHCs.

The work of Wanzlick, Bertrand and Arduengo ignited a new era in organometallic chemistry. A myriad of new carbenes – NHCs in particular – and their metal complexes have been synthesized. Carbenes have proved to be excellent ligands, especially in transition metal complexes employed as homogeneous catalysts. To understand their prominence, their electronic and steric properties will now be examined in more detail.

1.2.2 Carbene Predecessors: Tertiary Phosphines

Phosphines are commonly used spectator ligands in transition metal catalysis[17] and their properties are often compared with carbenes. Phosphines have been studied extensively, can be electronically and sterically tuned and their properties predicted empirically thanks to an extensive library of known systems. Like carbenes, simple phosphines are two-electron monodentate ligands. They are strong σ-donors and possess variable back-bonding capabilities (halophosphines and phosphites are strong acceptors whereas alkyl- and arylphosphines are relatively weak).[18] By changing the *P*-substituents, the electronic and steric properties of the ligand are changed simultaneously. Phosphines are in most cases conically shaped, with the substituents pointed away from the metal centre. As ligands, phosphines often suffer significant degradative reactions at elevated temperatures, such as oxidation, nucleophilic attack of the phosphine with electrophiles present in the reaction mixture or P–M bond cleavage (due to weak bond strength).[19] Evidently, degradation of the ligand reduces the productivity of the catalyst as well as its selectivity, as side reactions can take place at the denatured metal centre.[20]

The Tolman angle (or cone angle), θ, is used to quantify the steric bulk of tertiary phosphines.[21] It is the apex angle of a cone which is centred 2.28 Å away from the phosphorus centre and whose outlines just touches the edge of the van der Waals radii of the outermost atoms (Figure 1.4). For unsymmetrical phosphines, the half angles for each substituent are measured, giving the Tolman angle:

$$\theta = \frac{2}{3} \sum_{i=1}^{3} \theta_i / 2 \qquad (1.1)$$

(the half angles are depicted in Figure 1.4).

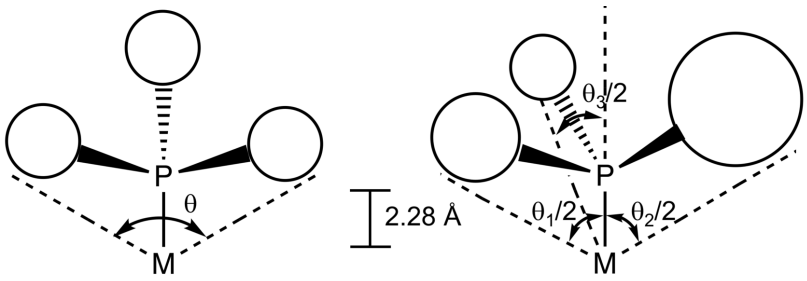

Figure 1.4 (Left) Tolman angle for a symmetrical tertiary phosphine. (Right) Method for measuring the Tolman angle for an unsymmetrical tertiary phosphine.

1.2.3 Electronic Properties of Singlet Carbenes

Singlet carbenes have a formally vacant p_π-orbital and a filled σ-orbital. The HOMO-LUMO energy gap can be tuned by changing the substituents on the carbene, the angle of the carbene as discussed in section 1.1 or the nature of the backbone of NHCs (see Scheme 1.7). They are σ-donating and thus nucleophilic and have the potential for π-back-donation. However, due to the p_π-orbital typically being high in energy, it does not interact well with the d-orbitals of metals, resulting in relatively weak π-back-bonding. Initially, as ligands within metal complexes, NHCs were considered to possess negligible π-backbonding.[22–24] More recent studies involving comparison of bond lengths,[25,26] UV-vis experiments,[27] NMR studies[28] and DFT calculations[25,29–32] suggest that π-back-donation accounts for over 10% of the metal-ligand bond strength; whether that is negligible or not is open to debate. In 2006, using annulated NHCs, Saravanakumar *et al*. showed that the π-back-donation can be increased by extending the π-system (Figure 1.5).[33]

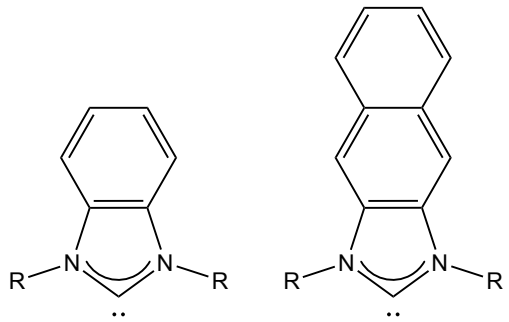

1.19 1.20

Figure 1.5 Annulation of NHCs by aromatic heterocycles extends the π-system.[33]

Carbenes are generally more σ-donating than even the most σ-donating phosphines,[17,34,35] which typically results in a stronger ligand-metal bond in metal complexes.[24,34,35] Unlike phosphines, the *N*-substituents on NHCs are peripherally substituted, and thus their electronic effects on the carbene are not as pronounced as phosphine substituents.[17] It is therefore possible to alter the steric effects considerably while maintaining the electronic properties of the carbene to a large extent. On the other hand, the electronic properties of carbenes can be altered by changing the nature of the backbone, the angle at carbon or the nature of the α-atoms. Various classes of NHCs and other carbenes will be discussed in section 1.2.5, along with their electronic properties.

Several methods are used to estimate the electronic properties of carbenes. *p*Ka measurements of the corresponding imidazolium precursors are one way of establishing the σ-donor properties, as more σ-donating carbenes have less acidic imidazolium precursors.[36] Another method, reported by Maji *et al.*, measures the nucleophilicity (N) and nucleophile-specific sensitivity parameter (s_N) of the carbene by measuring the rate of reaction with electrophiles whose electrophilicity (E) is known.[37] The higher the nucleophilicity, the more σ-donating the carbene is. One could, however, envision that steric bulk might affect the rate of these reactions.

Additionally, redox parameters of metal centres bearing carbenes can give insight into how electron-rich the metal centre is, and thus by implication what the electronic donor abilities of the carbene are.[36] One advantage of these methods is the relatively high precision compared to ^{13}C NMR and IR, spectroscopy for example.

The ^{13}C NMR chemical shift of the carbenic centre is frequently used to compare the electronic properties of carbenes. Carbenes have very high-field ^{13}C chemical shifts, ranging from 200 ppm upwards, due to the electron deficiency at the low-valent carbon centre.[38] An increase in the ^{13}C chemical shift is generally associated with increase in σ-donor properties of the carbene but this comparison can be quite ambiguous. The σ-orbital is in fact not the only characteristic component of the chemical shielding tensor in singlet carbenes and other shielding factors play as important, if not more important, roles.[39] Reduced electron density in the p_π-orbital similarly results in a higher chemical shift[40,41] and the angle at the carbene centre affects the chemical shift for example.[39,42] A small singlet-triplet gap also plays an important role and affects the σ_p shielding parameter due to an electron moving between the σ- and the p_π-orbital, permitting facile circulation of electrons; this paramagnetic current causes a downfield shift.[41] More σ-donating carbenes thus have higher chemical shifts compared with less σ-donating ones, but the chemical shift is not proportional to the σ-donor ability as other factors play important roles in the chemical shift. To sum up, the ^{13}C NMR chemical shifts of carbenes can give information on the electronic properties of carbenes but comparison needs to be made with care, especially between carbenes that are significantly different in structure.

The Tolman Electronic Parameter (TEP) is the most frequently used metric to

evaluate the donor properties of carbenes. It is obtained from the IR stretching frequency of the A_1 carbonyl stretching mode in $LNi(CO)_3$ (where L is the ligand).[21] Back-donation from the metal centre to the π*-orbital of CO results in weakening of the C=O bond. Hence a lower C=O stretching frequency indicates increased electron density at the metal centre and enhanced ligand donor properties of the ligand. The TEP was originally used for phosphines but can also be used for carbenes and so the electronic properties of ligands can be compared both within each ligand class and between them. There are a number of disadvantages to this method, however: it measures the overall electron density at the metal centre and therefore does not deconvolute the σ-donor and π-acceptor properties of the ligand, and the metal precursor (nickel tetracarbonyl) is very toxic. Due to the latter problem, $LIr(CO)_2Cl$ and $LRh(CO)_2Cl$ are more commonly used nowadays. A linear correlation is observed for the average CO stretching frequencies for the nickel, iridium and rhodium complexes, and so the TEP can be derived from the average CO stretching frequencies in $LIr(CO)_2Cl$ and $LRh(CO)_2Cl$.[36,43] The TEP does not offer separation of the σ-donor and π-acceptor abilities of carbenes, but reflects instead the total electronic properties of the ligand. Interpretation of the values therefore needs to be carried out in conjunction with other methods that give information on only one of the components.

Two experimental methods to evaluate the π-acceptor abilities of carbenes were reported by Back *et al.*[44] and Liske *et al.*[45] in 2013. The methods involve the syntheses of phosphinidene and selenium adducts of the carbenes. Both adducts can be described by two canonical structures, one of which features a dative E−C bond (E = P, Se), where two electron pairs are located at the phosphorus/selenium centre and the other a formal C=E double bond, in which one of the lone pairs of the phosphorous/selenium centre is donated into the p_π-orbital of the carbene centre

(Figure 1.6). Increasing π-acidity of the carbene centre leads to a stronger contribution of the structure on the right (Figure 1.6). This serves to decrease the shielding at the phosphorus/selenium centre, which in turn perturbs the $^{31}P/^{77}Se$ NMR resonance downfield. There is a linear correlation between the ^{31}P and ^{77}Se shifts, suggesting that either method can be used to evaluate π-acidity. Calculations have shown that σ-polarizations of the C–P bonds toward phosphorus exhibit a weak correlation with the ^{31}P chemical shifts but good correlations are observed with the π-polarizations.[46] Furthermore, the ^{77}Se and ^{31}P chemical shifts are strongly correlated with π-orbital interactions between the carbene centre and Se/P.[47] The advantage of using the selenium adduct is the ease of preparation and, the lack of an additional substituent means that the ^{77}Se shift is not affected by conformational effects in unsymmetrical carbenes. The advantage of using the phosphinidene adducts, on the other hand, is that it provides additional information as the phenyl group attached to the phosphorus allows for calculation of the barrier of rotation around the C–P bond and can give information on the double-bond character. It is worth noting that the ^{77}Se chemical shift is strongly affected by the solvent, concentration and temperature,[48] and thus it is important to compare the shifts in the same solvent system, which is generally acetone-d_6.

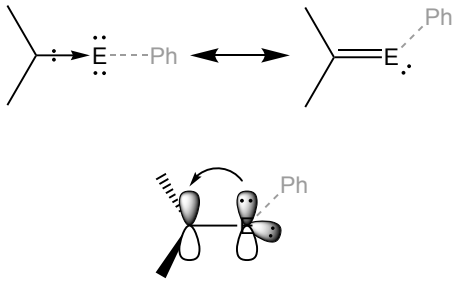

Figure 1.6 (Upper) Canonical structures of phosphinidene (E = P) and selenium (E = Se) adducts of carbenes. (Lower) Back-donation into the p_π-orbital of the carbene. The phenyl group is only present in the phosphinidene adduct.

In addition to experimental methods, several computational methods have been developed to probe the electronic structure of carbenes, some of which offer metrics that can be verified experimentally.[36] Calculations can be carried out either on the free ligand or by observing its properties as a ligand in a metal complex. The energies of the frontier orbitals of carbenes, either as ligands or as 'free' carbenes, are often calculated using Density Functional Theory (DFT) and give insight into the σ-donor and π-acceptor properties of the carbene.[35,49–54] The metal carbene bond can also be investigated by examining the instantaneous interaction, which represents the energy required to cleave the M–C bond into unrelaxed fragments.[53] This quantity can be sub-divided into three components, $\Delta E_{int} = \Delta E_{elstat} + \Delta E_{Pauli} + \Delta E_{orb}$. ΔE_{elstat} is responsible for electrostatic interaction between the unperturbed charge distributions of the two fragments, ΔE_{Pauli} describes the destabilizing interactions between occupied orbitals (steric repulsion) and the third, ΔE_{orb}, accounts for the charge transfer in the two fragments, including donor-acceptor interactions, and orbital mixing. ΔE_{orb} can be further sub-divided into $\Delta E_{orb}(\sigma)$ and $\Delta E_{orb}(\pi)$, the σ- and π-orbital interaction energies, which describe the σ-donor and π-acceptor properties of the carbene in the metal complex. Furthermore, the *trans*-influence of the carbene and the carbene–metal bond length can provide understanding of the σ-donor properties.[28] Zhu *et al.* offer a good explanation of the *trans*-influence of ligands of this type.[55] In a metal halide complex, LMX (where L is the ligand of interest, M the metal centre and X the halide), elongation of the metal–halide bond indicates an increased *trans*-influence of the L ligand, which is typically reflective of higher σ-donor capabilities. Moreover, strong σ-donor properties at L are also associated with lengthening of the M–L bond length itself, as increased σ-donor ability is associated with greater p-character in the σ-orbital.

1.2.4 Steric Properties of NHCs

The steric profiles of NHCs are typically very different from phosphines. Unlike most phosphines, the substituents are pointed *towards* the metal centre and the ligand can be considered to be umbrella-shaped (Figure 1.7). The steric bulk of the carbenes can therefore get closer to the metal centre, though, unlike phosphines, NHCs are highly anisotropic and thus non-chelating NHCs can rotate to minimize steric clash with other ligands or substrates bound to the metal centre. NHCs are therefore, generally speaking, more sterically demanding than phosphines but their anisotropic nature can mitigate this effect to some extent.

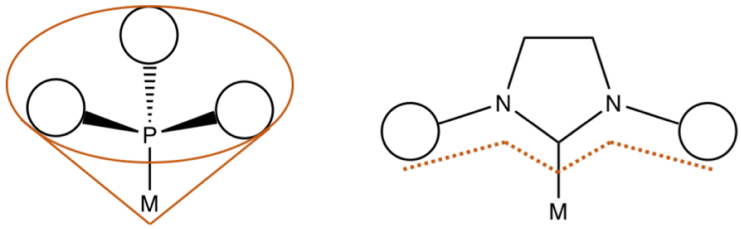

Figure 1.7 Cone shaped phosphines *vs* umbrella shaped NHCs.

As NHCs are not cone shaped, the Tolman angle is not suitable to evaluate their steric profile. Hillier *et al.* have developed a parameter, the 'percentage buried volume' ($\%V_{bur}$),[56] to quantify the steric demands of carbenes and this can be used to compare the steric demands of carbenes with phosphines (as a linear correlation is observed between the Tolman angle and the $\%V_{bur}$ for phosphines).[43] The $\%V_{bur}$ is calculated as the percentage volume occupied by the ligand within a sphere (usually with the radius of r = 3.5 Å) around the metal centre (Figure 1.8). The SambVca (Salerno molecular buried volume calculation) software, which was developed by Falivene *et al.*,[57] can be used to calculate the spatial occupation of the ligand from the crystallographic or computational structure of a metal complex. When comparing the

$\%V_{bur}$ of different carbenes, it is important that the parameters are derived from the analogous metal complexes, as the $\%V_{bur}$ of the same carbene can vary depending on the metal complex (for example by a few percentage points even between linear LCuCl, LAgCl and LAuCl systems).[58] Traditionally, the solid-state structure of a AuCl complex is chosen to calculate the $\%V_{bur}$. To date, the bulkiest carbenes reported are IPr*$^{(2\text{-Np})}$, synthesized by Dierick *et al.*, with a $\%V_{bur}$ of 57.4%[59] and ITr, synthesized by Roy *et al.*, with a $\%V_{bur}$ of 57.3%.[60] It is worth noting that the former is calculated from the structure of the LAgCl complex, whereas the latter is derived from the LAuCl complex and it is therefore not possible to precisely conclude which one is the more sterically demanding.

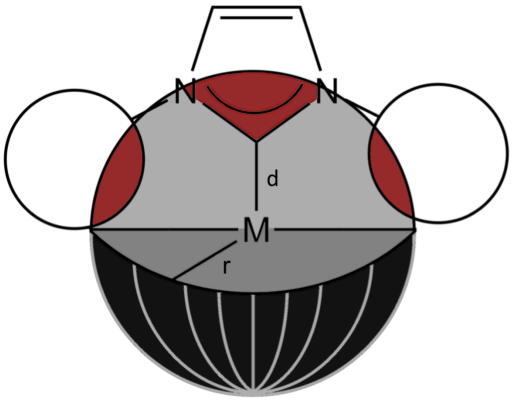

Figure 1.8 Representation of percentage buried volume, $\%V_{bur}$. The figure depicts a sphere around the metal centre, M, with radius r. The carbene–metal bond length is represented as d and the red area indicates the volume occupied by the ligand in the sphere ($\%V_{bur}$).

1.2.5 Different Classes of Carbene

This section will deal with different classes of carbene and detail, for example, how factors such as size, saturation and substitution pattern of the backbone, and the identity of the α-atoms affect the nature of the carbene, together with differences between cyclic and acyclic carbenes. Figure 1.9 depicts various classes of carbene and

Table 1.2 outlines the myriad of different carbenes explored in recent years, the scope greatly exceeds the capacity of the discussion herein, and so only key carbene classes are discussed.

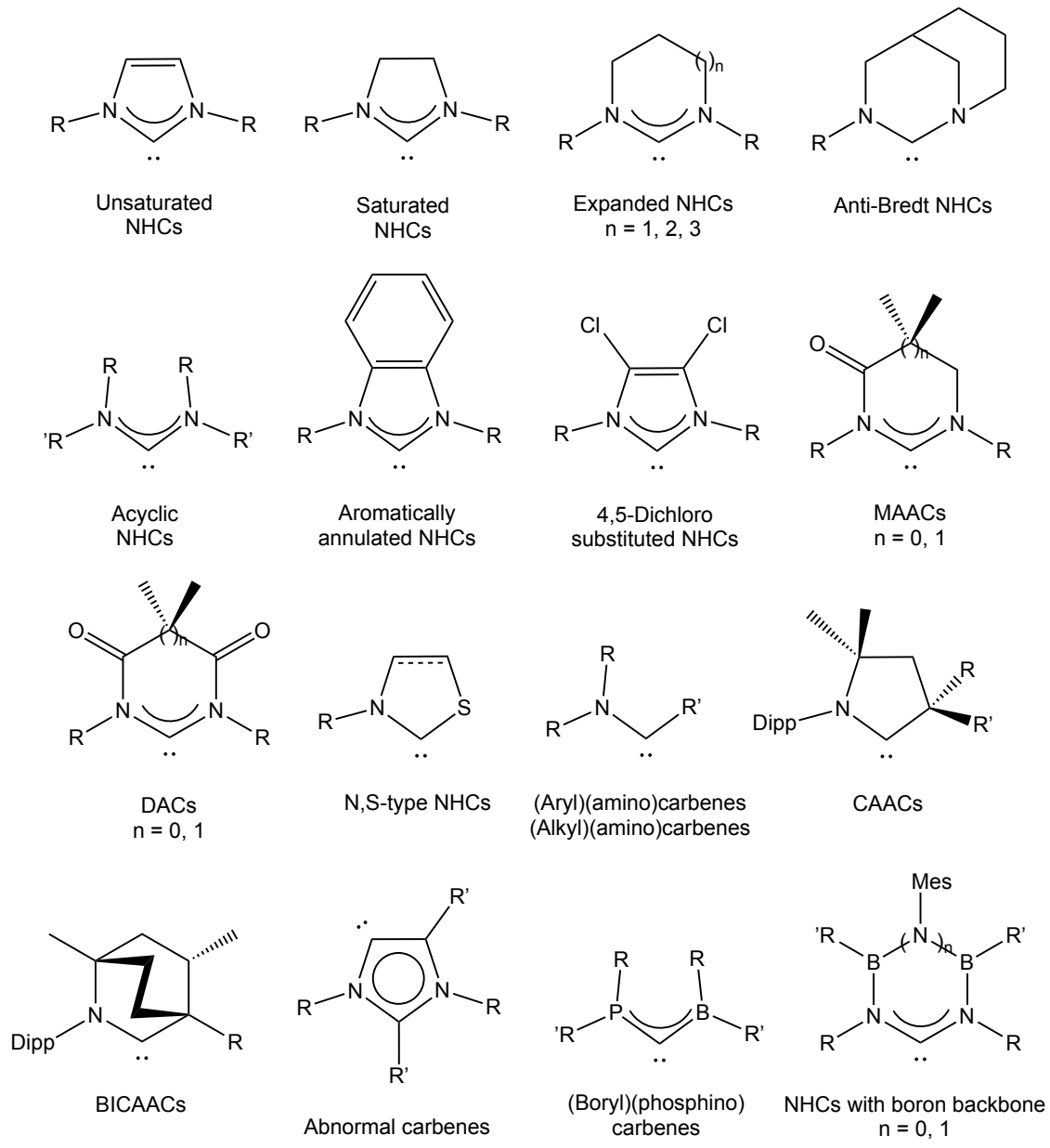

Figure 1.9 The examples of different carbene classes discussed in this section.

Carbene (L)	Free Carbene $\delta^{13}C$	Free Carbene TEP	LPPh $\delta^{31}P$	LSe $\delta^{77}Se$	$\%V_{bur}$
Unsaturated	[a]220.6[61]	[a]2051[43]	[a]-23.0[44]	[b]87[62]	[b]44.5[58]
Saturated	[a]243.8[61]	[a]2048[63]	[a]-10.4[44]	[b]181[62]	[b]47.0[58]
6-Membered	[a]244.9[64]	[a]2042[63]	[b]14.8[44]	[a]271[62]	[b]50.8[65]
Anti-Bredt	[b]282.0[66]	[b]2047[66]	[b]34.9[44]		[b]38.5[57,67]
Acyclic	[c]255.5[68]	[c]2050[69]	[c]69.5[44]	[c]593[62]	[f,h]44.3[70]
Benzannulated	[c]221.6[71]	[c]2045[72]	[c]-34.6[44]	[c]67[62]	
4,5-Dichloro substituted	[a]219.9[73]	[a]2053[72]		[b]174[74]	
MAAC	[a]260.6[75]	[a]2050[75]	[a]39.7[44]	[a]472[62]	
DAC	[a]278.4[76]	[a]2055[77]	[a]83.0[78]	[a]847[74]	[a]41.8[79]
N,S-Type	[b]254.3[80]	[b]2054[72]	[b]57.0[44]	[b]396[74]	
(Alkyl)(amino)	[c,i]326.3[81]	[d,i]2044[44]	[d,i]126.3[44]		
CAAC	[j]309.4[82]	[j]2051[83]	[j]68.9[44]	[e]492[84]	[k]51.0[36]
BICAAC	[e]334.4[85]	[e]2045[85]	[e]90.4[85]	[e]645[85]	[c]48.4[57,85]
Abnormal	[b,h]201.9[86]	[g,h]2039[87]			
Boron backbone	[d,h]221.6[88]	[d,h]2050[88]			

Table 1.2 Parameters often used to compare electronic and steric properties for the different carbene classes. ^{13}C chemical shifts (ppm) of the carbenic centres, Tolman Electronic Parameter (TEP, cm^{-1}) and ^{31}P and ^{77}Se chemical shifts (ppm) of the phosphinidene and selenium adducts of the carbenes. The structures of the carbenes are outlined in Figure 1.9, where R = [a]Mes, [b]Dipp, [c] *i*Pr, [d]Cy, [e]Me, [f] *t*Bu, [g](Me and *i*Pr), R' = [h]Ph, [i] *t*Bu or RR' = [j]Cy, [k]Menthyl. The values for MAAC and DAC correspond to the six-membered amidocarbenes, n = 1.

The most widely utilized carbenes are saturated and unsaturated five-membered *N*-heterocyclic carbenes, in which both α-atoms are nitrogens and the backbone positions are either substituted with hydrogens or alkyl groups. These carbenes offer a suitable baseline in the following discussion of other carbene classes. Compared with unsaturated NHCs, their saturated analogues are generally thought to be more σ-donating and π-accepting.[28,45,89] The increased bond length at the backbone increases the N−C−N angle and raises the energy of the σ-orbital (section 1.1), whereas the p_π-orbital lies lower in energy due to the lack of aromaticity of the imidazolylidene ring.

Ring-expanded NHCs, such as 6- and 7-membered saturated NHCs feature a larger N−C−N angle compared to their 5-membered analogues, resulting in higher σ-donor strength.[65] Additionally, by expanding the ring, the π-acidity increases somewhat. Although the reason has not been unambiguously established, this has been postulated to be due to a degree of pyramidalization of the α-nitrogens on account of increased flexibility in the heterocycle ring.[89] That pyramidalization of the α-nitrogens is known to increase the π-acidity of NHCs and can be seen in bicyclic NHCs or the so-called anti-Bredt NHCs. In such cases, one nitrogen is forced to pyramidalize and is thus restricted in the extent of its N-to-C π-donation, which results in increased carbene π-acidity.[44,66] In addition, expansion of the heterocycle forces the *N*-substituents closer to the metal centre in metal carbene complexes, and results in the ring-expanded NHCs being more sterically demanding compared to 5-membered analogues. Interestingly, this increase in steric bulk causes the isopropyl substituted 6-membered NHC to be resistant to dimerization,[90] unlike its 5-membered counterpart,[91] despite a lower HOMO-LUMO gap.

Incorporation into a heterocycle is not always necessary for the stabilization of a carbene. The first acyclic system, bis(diisopropylamino)carbene, was isolated by Alder *et al*. in 1996.[68] Since the carbene is not constrained by incorporation into a ring, the N−C−N angle is significantly wider (121.0(5)°), exceeding both 6- and 7-membered NHCs (114.7(1)° and 116.6(4)° for 6Mes and 7Mes, respectively).[64] As a consequence, acyclic carbenes are typically more σ-donating.[70] Moreover, due to their acyclic nature, the α-nitrogens are not forced to lie co-planar with the carbene centre and can pyramidalize, thereby lowering the energy of the p_π-orbital of the carbene.[41,44,45,52,70,92] Cyclic carbenes are in general more robust than acyclic ones, and acyclic carbenes have been shown to reduce metal carbonyl complexes.[93] The

application of acyclic carbenes in metal catalysis is therefore more limited.

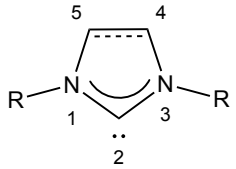

Figure 1.10 The numbering system for atoms of an *N*-heterocyclic NHC that will be used when discussing five-membered NHCs in the rest of the thesis.

Changing the backbone substituents of NHCs can also affect the electronic properties of the carbene to a large extent. As mentioned earlier, annulation of the backbone with an aromatic system results in slightly increased π-acidity compared with unsaturated NHCs due to delocalization of the π-electrons into the annulated aromatic system.[33] Consistently, naphthimidazol-2-ylidenes (**1.20**; Figure 1.5) exhibit more delocalization compared with benzimidazol-2-ylidenes (**1.19**; Figure 1.5). In terms of the σ-donor ability, Hahn *et al*. suggest that benzannulated NHCs lie between that of five-membered saturated and unsaturated carbenes, correlated with a C4−C5 bond length and, consequently, an N−C−N angle that lie between the two.[94] Recent results from the Aldridge group, however, suggest that the HOMO of benzannulated NHCs lie lower in energy than even the unsaturated counterparts, which is attributed to the electron-withdrawing effect of the benzene backbone.[95] Substitution of inductive electron withdrawing groups (*e.g*. chloride) on the backbone results in significant decrease in the energy of the σ-orbital of the carbene centre, which is highlighted by the stability of such carbenes to chloroform (and air for a limited amount of time).[73] Significant change in the π-acceptor properties is observed when carbonyl groups are introduced into the backbone. Delocalization of the π-electron density of *N*,*N*'-diamidocarbenes (DACs) into the carbonyl groups results in a great increase in their π-acidity, yet these carbenes are still sufficiently nucleophilic to

coordinate to transition metals.[44,45,75,76] Their monoamido-amino counterparts (MAACs) generally feature properties which lie between diamido- and diaminocarbenes in terms of π-acidity and σ-basicity.[44,45,75]

Changing the nature of the α-atom can also have a pronounced effect on the steric and electronic properties of the carbene. In 1997, Arduengo *et al.* isolated the first thiazol-2-ylidene, an N,S-type NHC, in which one of the α-nitrogens has formally been replaced with sulphur.[80] Due to sulphur being larger than both nitrogen and carbon, limited overlap of the π-orbitals of the carbene and the sulphur is expected,[80,89] and is reflected in the low lying p_π-orbital of thiozol-2-ylidenes.[89] In addition, as the sulphur atom does not bear a pendant substituent like nitrogen does, these carbenes are highly unsymmetrical and not very sterically demanding. It is not necessary to have two π-electron donating substituents adjacent to the carbene centre, as was demonstrated with the isolation of (aryl)(amino)carbenes by Solé *et al.* in 2001,[96] which were followed soon after by (alkyl)(amino)carbenes,[81] and their cyclic analogues, CAACs.[82] The substitution of a nitrogen atom with carbon, which is neither σ-withdrawing nor π-donating renders these carbenes very reactive (as will be discussed in section 1.2.6) with an extremely narrow HOMO-LUMO energy gap, reflecting the high energy of the σ-orbital and low energy of the p_π-orbital.[81,82] As the α-carbon atom is quaternary, the steric profile of the carbene changes significantly compared to other carbenes – the presence of two pendant substituents can render CAACs highly sterically demanding.[82] In 2017, Tomás-Mendivil *et al*. reported another analogue of CAACs, bicyclic (alkyl)(amino)carbenes (BICAACs) which are very stable and even more σ-donating and π-accepting than CAACs, potentially on account of an increased N–C–N angle.[85] Due to their bicyclic nature, the carbon bears only one pendant substituent

and thus the steric profile of BICAACs resembles more the steric profile of NHCs.

In 2001, Gründemann *et al.* reported an abnormal binding mode of carbenes in an iridium complex (Scheme 1.8).[97] This was the first report of an isolated imidazolylidene binding to a metal complex *via* the C5 (or C4) position rather than C2. The C–H bond at the C2 position is significantly more acidic compared to the C4 proton (p*K*a = 24 and 33, respectively) and according to calculations, relief of steric congestion is believed to be the principal reason for this unusual binding mode.[98] This initial observation opened up the field of abnormal (or mesoionic/remote) carbenes. In a similar fashion to CAACs, abnormal carbenes have one nitrogen and one carbon adjacent to the carbene centre, albeit with an additional peripheral nitrogen. As a result, abnormal carbenes are more σ-donating and π-accepting than their 'normal' counterparts.[86,99] It wasn't until 2009 that Aldeco-Perez *et al.* managed to isolate and structurally characterize the first abnormal carbene by substituting the C2 position with a phenyl group.[86] Their steric profile typically resembles normal NHCs, although an unsymmetrical profile results if the C4 position is unsubstituted.

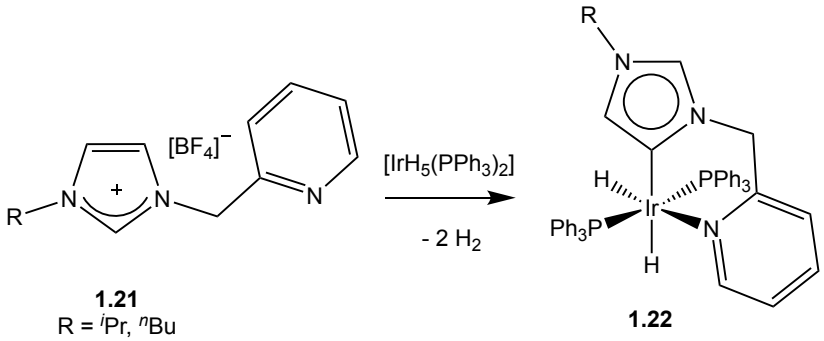

Scheme 1.8 First reported abnormal binding mode in NHCs.[97]

In 2005, Krahulic *et al*. published an NHC featuring a diboron backbone,[100] and later the same year Präsang *et al*. published a carbene analogue of a borazine (a six-membered carbene with a B–N–B backbone).[88] Due to the lower electronegativity of

boron compared with carbon,[101] these carbenes show enhanced σ-donor capabilities in comparison with other cyclic diamino carbenes, as well as marginally increased π-acidity.[88,100,102] In 2010, Lavigne *et al*. reported a carbene with a boryl group in the α-position, a (boryl)(phosphino)carbene, which is stable at room temperature for 24 h, but slowly undergoes a 1,2-rearrangement of the *P*-substituted mesityl group to the carbene centre.[103] The electronic properties of the carbene have not been studied extensively but DFT calculations suggest a low HOMO-LUMO gap. This is due in part to the weaker π-donor phosphino (as phosphorus achieves the optimum planar configuration for π-donation less easily than nitrogen),[104] and also due to the p-orbital interaction of the carbene and the adjacent boron centre, which has a formally vacant p-orbital and lies in plane with the carbene (at least in the solid state).

1.2.6 Applications of Carbenes

Carbenes, and NHCs in particular, are very important as ligands in transition metal complexes used in homogenous catalysis, and are often used as alternatives to tertiary phosphines. The NHC complexes tend to be less susceptible to air and moisture than phosphines, which can undergo degradation at elevated temperatures as discussed in section 1.2.2.[105] Carbenes are therefore often more effective and tolerate catalytic conditions better (leading to lower catalyst loadings). In cross-coupling reactions, for example, their strong σ-donor properties can aid the oxidative addition of the substrate, and their steric bulk can facilitate the reductive elimination of the target product.[106] The first example of the successful replacement of a tertiary phosphine with a carbene in catalysis was reported by Herrmann *et al.* in 1995 in a Heck coupling reaction. The use of an NHC (IMe) as a supporting ligand instead of triphenylphosphine resulted in high activity at a lower catalyst loading (Scheme 1.9).[107]

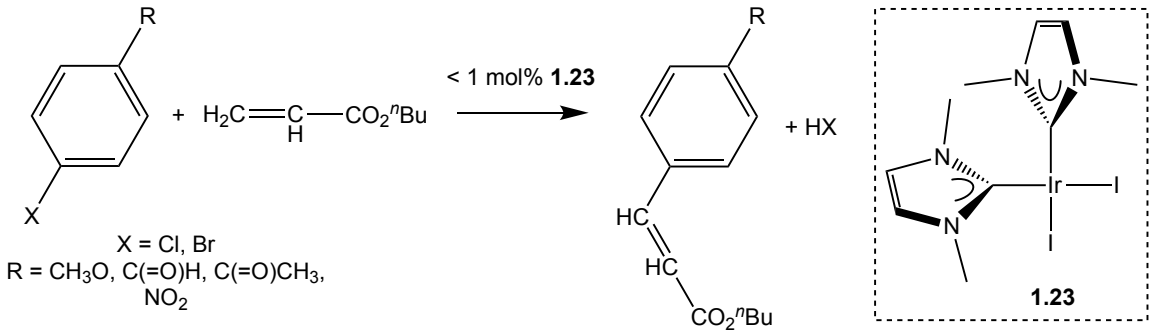

Scheme 1.9 A Heck coupling reaction improved by using an NHC as a ligand instead of a phosphine.[107]

Subsequently, the range of NHC-containing catalysts and catalytic reactions has increased hugely, with notable examples including their use in Suzuki,[108] Sonogashira,[109] Negishi,[110] and Buchwald-Hartwig[111] reactions as well as the well-known Grubbs 2nd generation catalyst (**1.24**; Figure 1.11).[112] The 'classic' NHCs are not the only carbenes of use in catalysis. For example, Anderson, Marx *et al.* have reported interesting changes in reactivity by replacing the NHC in the Hoveyda-Grubbs 2nd generation catalyst with a CAAC (*e.g.* **1.25**; Figure 1.11).[113,114]

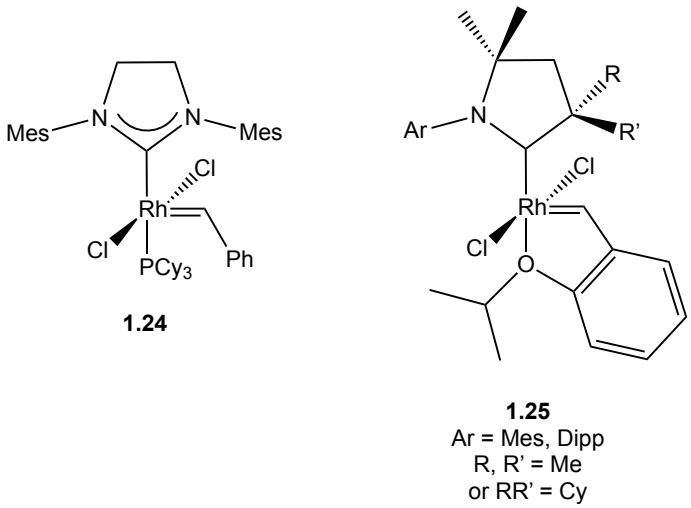

Figure 1.11 (Left) Grubbs 2nd generation catalyst and (right) CAAC substituted Hoveyda-Grubbs 2nd generation catalyst.[112,113]

Carbenes are also prominent in organocatalysis owing to the inversion of classical

reactivity ('Umpolung') which they can bring about. This opens up new reaction pathways, with reactivity towards carbonyl groups and Michael acceptors, for example, being of particular importance.[115] This type of reactivity (*in situ*) dates as far back as 1832, when Wöhler and Liebig observed the cyanide-catalyzed coupling of benzaldehyde to benzoin.[116] In 1958, Breslow proposed a mechanism for the thiazolium salt-catalyzed benzoin condensation (Scheme 1.10) which proceeded *via* a thiazolium zwitterion (**1.26**).[117] Since the isolation of free carbenes, their application in organocatalysis has developed rapidly. The first commercially available NHC – a triazol-5-ylidene, synthesized by Enders *et al.*[118] – has proven to be a powerful catalyst in benzoin-type condensations of formaldehydes.[119] Carbenes have subsequently been employed as organocatalysts in numerous reactions,[115] including benzoin condensations, Stetter reactions (which provide a new catalytic pathway for syntheses of 1,4-bifunctional molecules),[120] cross condensations of enals and aldehydes, imines, 1,2-diones or enones, Diels-Alder reactions, transesterifications (which has opened up a broad application in polymerization), 1,2-additions of aldehydes, ketones, aldimines and ketimines, and natural product synthesis. They are also prominent in polymer chemistry, and were, for example, employed in the first organocatalytic approach to the living ROP (ring-opening polymerization) of lactides. Sterically encumbered NHCs can be employed in stereoselective polymerization.[115] NHCs take part both in ring-opening polymerizations (*e.g*. lactones, lactides, epoxides and anhydrides) and step-growth polymerizations.[121] Moreover, nucleophilic catalysis by carbenes is not only limited to carbonyl groups and Michael acceptors; they can also catalyze ring-opening reactions of epoxides, aziridines and cyclopropanes, and have even shown Heck-type reactivity without the presence of a metal.[115,122] In addition, DAACs are capable of mediating [4+1] cycloadditions and reversible [2+1] cycloadditions.[123]

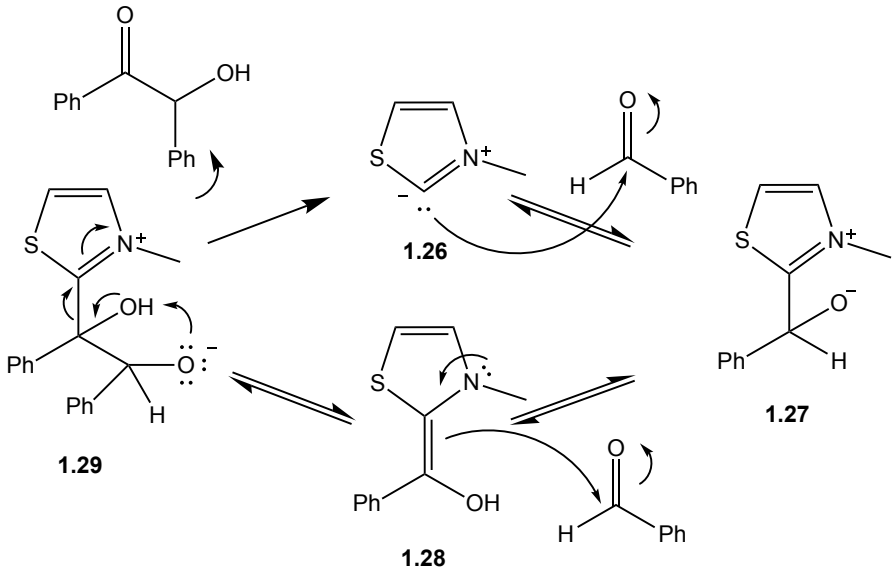

Scheme 1.10 Mechanism of benzoin condensation by thiazolium zwitterion 1.26 as proposed by Breslow.[117]

Within the realm of Main Group chemistry, carbenes are of significant importance and have been used to stabilize classes of compounds that were previously inaccessible. With their strong σ-donating abilities, they can donate electrons into the vacant p-orbitals of low-valent p-block elements. Phosphorus,[124] silicon[125] and carbon[126] have been isolated in the elemental oxidation state, by employing carbene stabilization, *e.g*. in systems of type (NHC)EE(NHC) (E = C, Si, P). The first isolated compound featuring a B≡B triple bond (reported by Braunschweig *et al*. in 2012) also relied on stabilization by an NHC.[127] In 2017, Rosas-Sánchez *et al*. stabilized the first borylidene–phosphorene (R(NHC)B=PR'$_3$), which was supported by an NHC.[128] Carbenes have also allowed for the isolation of Main Group radicals,[129,130] wherein the π-acidity of the carbene centre plays an important role in the delocalization of spin density. For example, a carbon-centred radical of this type has successfully been isolated, and characterized by X-ray crystallography; it is stable at room temperature owing to stabilization by a strongly π-acidic CAAC ligand.[131] Stabilization by IDipp has also allowed for the synthesis of the first examples of Group 14 metal (M) cations

containing M=E multiple bonds (E = C, N).[132]

CAACs and DACs have additionally demonstrated utility in the activation of small molecules, such as H_2,[52] NH_3[52,133] and CO[76,92] (Scheme 1.11). Notable is the reversible activation of CO by DACs. Moreover, in combination with bulky, electrophilic boranes, NHCs can display Frustrated Lewis Pair (FLP) reactivity. The two components – a bulky Lewis acid and a Lewis base (such as 6Dipp and $B(C_6F_5)_3$; Scheme 1.12) – do not form an adduct due to steric protection but can activate H_2 and other small molecules.[134]

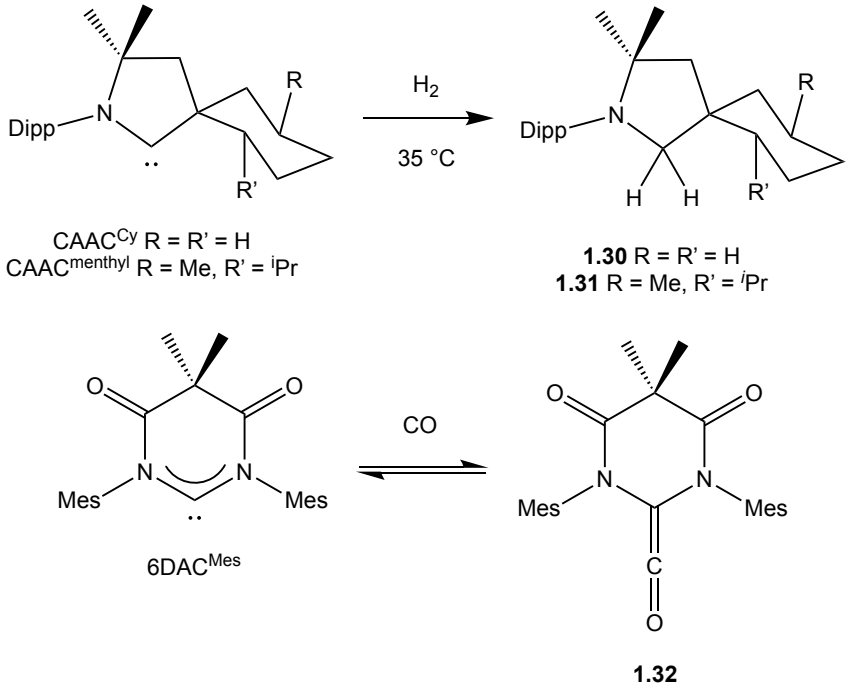

Scheme 1.11 (Upper) Activation of H_2 by CAACs.[52] (Lower) Reversible addition of CO by 6DAC^{Mes}.[77]

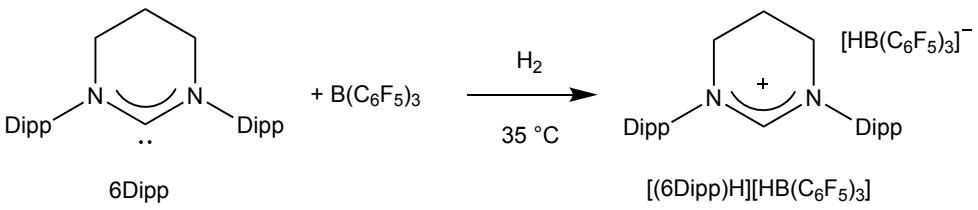

Scheme 1.12 FLP reactivity of 6Dipp in conjunction with $B(C_6F_5)_3$.[134]

Carbenes can also be coordinated to metal surfaces such as nanoparticles, forming

heterogeneous catalysts which can, for example, reduce alkenes in the presence of H_2.[135] Furthermore, carbene-containing organometallic materials such as metal-organic frameworks (MOFs) and liquid crystals also have been studied[136] and NHCs have also been used in metallopharmaceuticals.[137]

Interestingly, Bonnette *et al*. recently reported silicone derivatives which provide an efficient protecting medium to allow for NHCs to be handle under air, without inhibiting their reactivity.[138] This is likely to ease the employment of the ligand class and perhaps broaden their scope of application.

1.2.7 1,2-Rearrangement in Carbenes

Intramolecular 1,2-rearrangement in singlet carbenes is well established and involves interaction of the N−R σ-bond (where R is the migrating group) with the vacant p_π-orbital of the singlet carbene (Figure 1.13, left).[139–141] This interaction relies on the N−R σ-bond and the p_π-orbital being parallel. In order for the migration to take place in aromatic carbenes (unsaturated NHCs for example), the ring would therefore need to deform, and therefore dearomatize (Scheme 1.14). This is evidently highly unfavourable and calculations have confirmed high activation barriers for such migrations.[142–144] Heinemann *et al.* conclude that although imidazole-2-ylidenes are less stable than the isomeric rearranged imidazoles, the carbenes are kinetically stable to 1,2-rearrangement.[142] Nonetheless, Maier *et al.* observed the 1,2-shift of hydrogen in 2,3-dihydrothiazol-2-ylidene (**1.33**) in a matrix at 60 K (Scheme 1.15) and, due to the high activation barrier of the intramolecular pathway, suggested that an intermolecular 1,2-rearrangement takes place.[143] Intermolecular 1,2-rearrangement in NHCs was experimentally confirmed in 1998, when Solé *et al.* reported 1,2-silyl migration in aromatic carbenes.[141] They were unable to observe the

free carbenes, but crossover experiments supported an intermolecular 1,2-rearrangement (Scheme 1.16), which is suggested to proceed through a nucleophilic attack on the silyl group (Scheme 1.17).

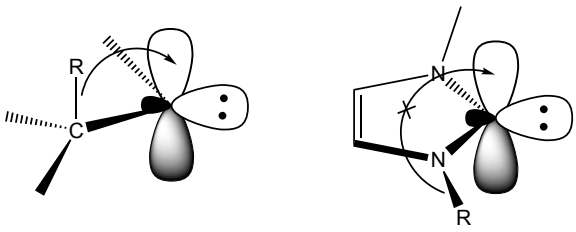

Figure 1.13 Interaction of the C–R σ-bond of the migrating group, R, with the p_π-orbital of the carbene centre in (left) an acyclic carbene and (right) an aromatic carbene.

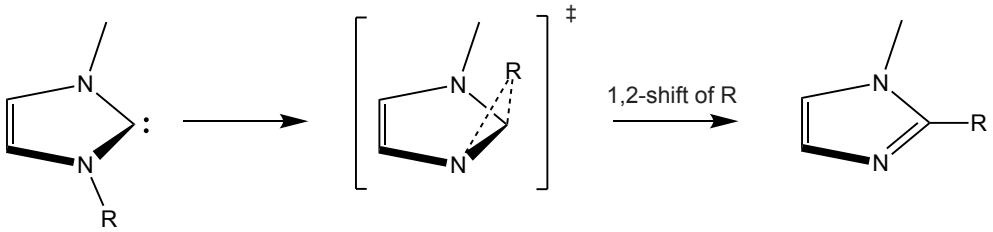

Scheme 1.14 Kinetically unfavourable intramolecular 1,2-rearrangement in imidazolylidenes *via* a dearomatized intermediate.

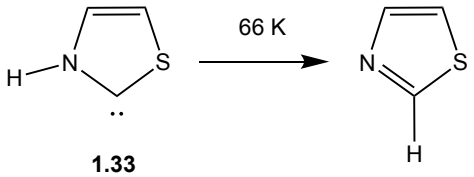

1.33 **1.34**

Scheme 1.15 1,2-Shift of hydrogen in 2,3-dihydrothiazol-2-ylidene 1.33 at 66 K.

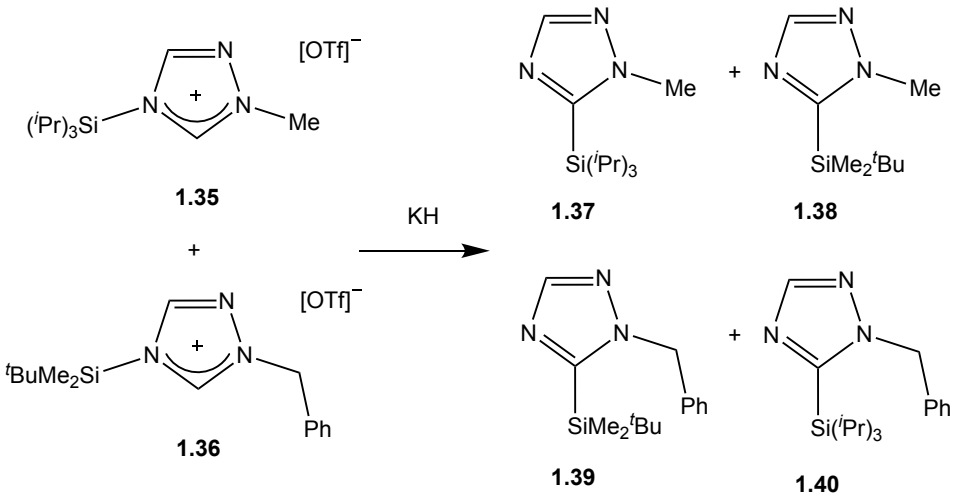

Scheme 1.16 Crossover experiment that confirms intramolecular 1,2-rearrangment of a silyl-substituted NHC.[141]

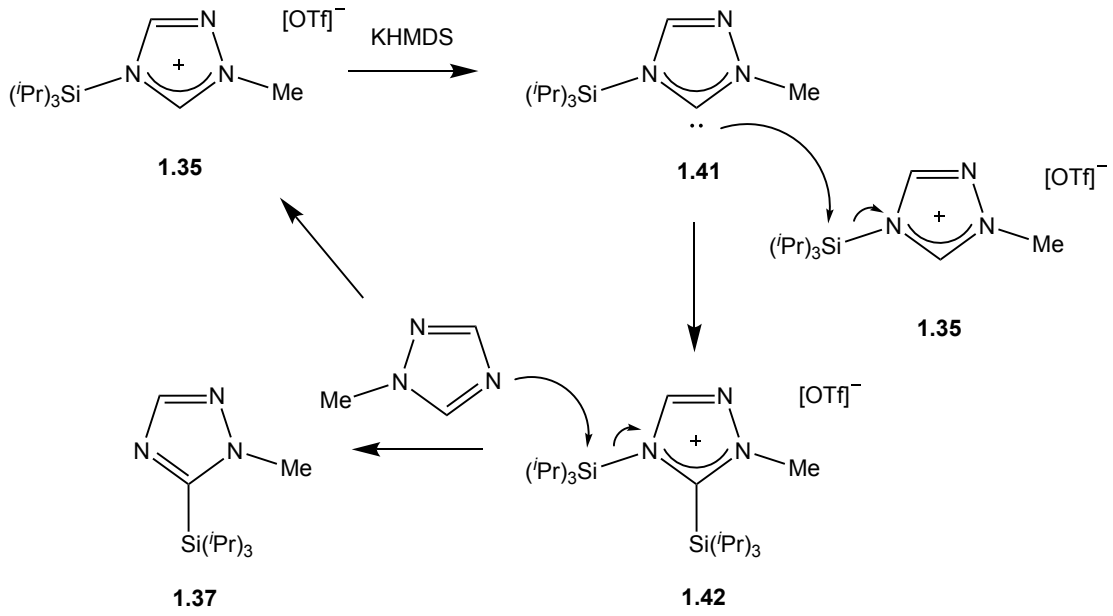

Scheme 1.17 Mechanism for the intermolecular 1,2-rearrangement in carbene 1.41 as suggested by Solé *et al.*[141]

Another plausible 1,2-rearrangement pathway was explored by DFT calculations by Cattoën *et al.* in 2007.[145] They suggested a radical pathway with homolytic fragmentation of an exocyclic N–N bond in acyclic amino-hydrazino-carbenes (Scheme 1.18). The possibility for intermolecular radical processes was further studied by Liu *et al.*,[146] where the 1,2-shift of $BMes_2$ was examined (Scheme 1.19).

They were unable to observe the free carbene, but crossover experiments support an intermolecular rearrangement. No signal could be detected in the electron paramagnetic resonance (EPR) measurement of an *in situ* deprotonation of the respective imidazolium salt (**1.47**). Nonetheless, EPR measurement of the *in situ* deprotonation reaction in the presence of 5,5-dimethyl-1-pyrroline *N*-oxide (DMPO, a commonly used spin trap) resulted in strong EPR signals, which match the signals of a simulated spectrum of a boryl/DMPO derivative (**1.52**) and $\{Me_3Si\}_2N^{\bullet}$ (Scheme 1.19).

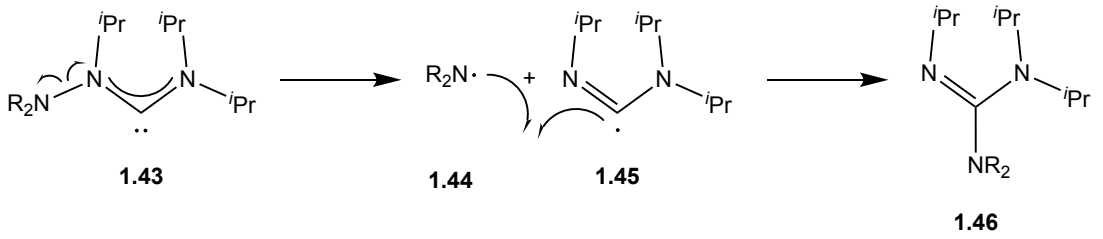

Scheme 1.18 Homolytic fragmentation of 1.43 to give 1,2-rearranged species 1.46 as proposed by Cattoën *et al.*[145]

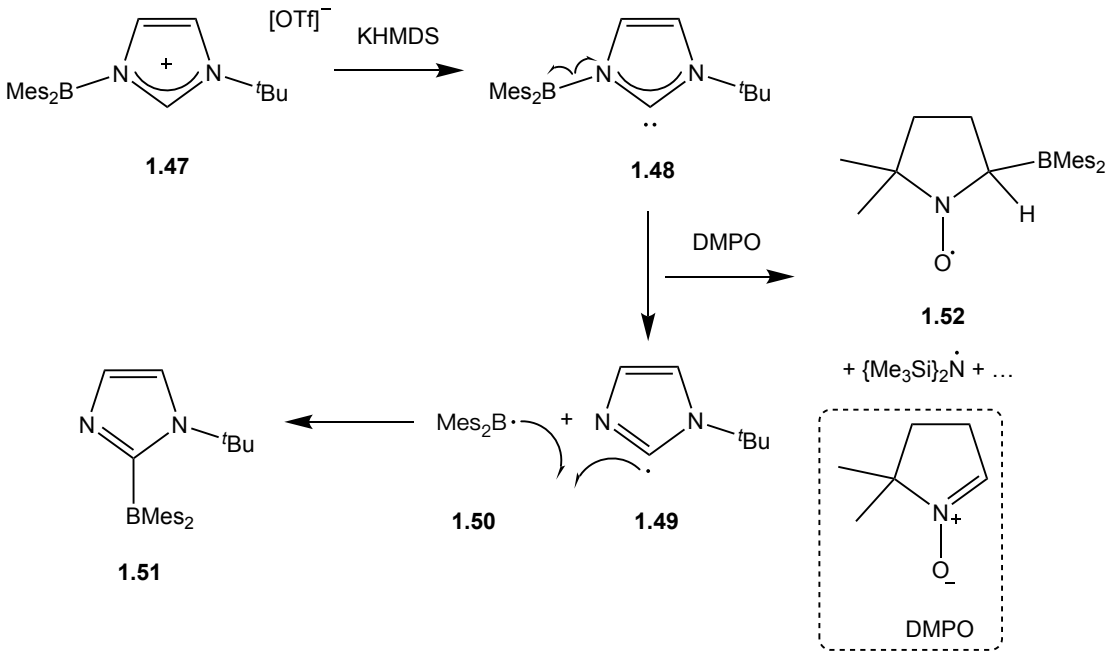

Scheme 1.19 Proposed mechanism for 1,2-rearrangement of 1.48 along with the proposed product from the *in situ* reaction of 1.48 with DMPO.[146]

1,2-Rearrangement in diaminocarbenes has been observed experimentally for a variety of *N*-substituents, including amide,[145] silyl,[143] boryl,[146] borane,[147,148] benzyl,[149] iminoyl,[150] phosphine[151] and phosphanyl,[152–155] as well as *P*-substituted mesityl in a boryl(phosphino)carbene[156] and *B*-substituted alkyl and allenyl groups in diboryl carbenes.[157] This indicates that N–R, P–R and B–R bonds (where R is the respective substituent) can be labile and that quenching of the carbene *via* C–R bond formation is often energetically favourable.

1.3 Heavier Carbene Analogues: Group 14 Tetrelenes

1.3.1 The Emergence of Group 14 Tetrelenes

As mentioned in section 1.1, the stability of the singlet state of divalent Group 14 compounds increases as the group is descended. It is therefore not surprising that the first Group 14 tetrelenes to be observed were a stannylene and a plumbylene, $Sn\{CH(SiMe_3)_2\}_2$ (**1.55**) and $Pb\{CH(SiMe_3)_2\}_2$ (**1.56**), synthesized by Davidson *et al.* in 1973 (Scheme 1.20).[158] Germylene $Ge\{CH(SiMe_3)_2\}_2$ (**1.54**) followed a few years later.[155] Although monomeric in solution, $Ge\{CH(SiMe_3)_2\}_2$ and $Sn\{CH(SiMe_3)_2\}_2$ were found to dimerize in the solid state.[159,160] A stannylene which is monomeric in the solid state (**1.57**) was isolated by using a more thermodynamically stabilizing amido ligand, $\{N(SiMe_3)_2\}$, which is σ- donating and π-accepting (Figure 1.13).[161] The first monomeric germylene, the heteroleptic system GeRR' (R = $CH(SiMe_3)_2$, R' = $C(SiMe_3)_3$; **1.58**; Figure 1.13), was isolated as a monomer in the solid state in 1991 by increasing the size of one of the alkyl ligands.[162]

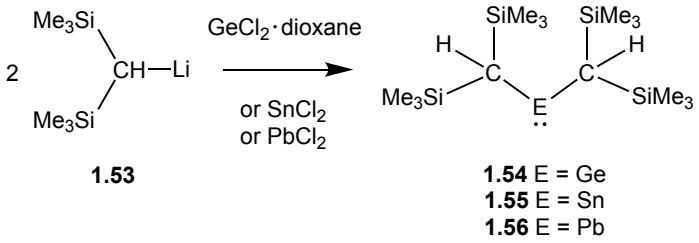

Scheme 1.20 The first observed monomeric Group 14 tetrelenes.[158,159]

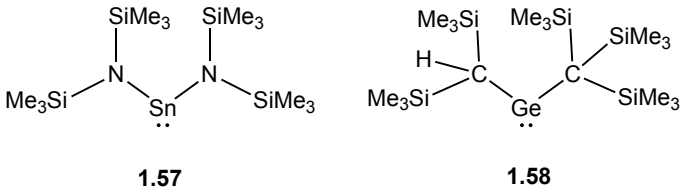

Figure 1.13 The first isolated monomeric stannylene and germylene.[161,162]

Historically, the syntheses of silylenes have proven the most challenging of all the tetrelenes, given their reduced stability compared to heavier analogues. An additional factor that resulted in the heavier analogues being easier to synthesize is the more ready availability of precursors of type MX_2/MX_2L (*e.g.* $GeCl_2$·dioxane, $SnCl_2$, $SnBr_2$, SnI_2, $PbCl_2$, $PbBr_2$, PbI_2).[161] Such halides have typically not been so readily accessible for silylenes. In 1981, West *et al.* observed, for the first time, a transient divalent silylene, $SiMes_2$, which dimerized at 77 K.[163] It was, however, not until 1994 that the same group managed to isolate the first silylene by incorporating the silicon centre into an *N*-heterocyclic ring (**1.60**; Scheme 1.21) in a manner that is reminiscent of NHCs.[164] In 2009, a new synthetic route to silylenes was opened up when Ghadwal *et al.* reported the carbene-stabilized dihalide IPr·$SiCl_2$, hence enabling syntheses of silylenes *via* salt metathesis, in a similar fashion to their heavier analogues.[165] Unlike the other Group 14 tetrelenes, whose acyclic monomers were known from the beginning, the first acyclic silylene was not reported until 2012 by Protchenko *et al.*,[166] followed by another example reported the same year by Rekken *et al.*[167]

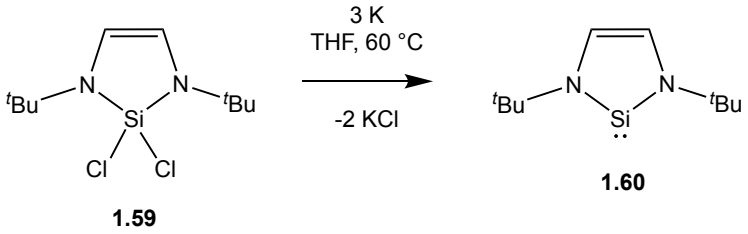

Scheme 1.21 The first isolated silylene, synthesized by West *et al.*[164]

1.3.2 Small Molecule Activation by Group 14 Tetrelenes

The lone pair at tetrelenes is nucleophilic, whereas the empty p_π-orbital is electrophilic and can act as an acceptor site.[168] It is this ambiphilic nature which enables the activation of small molecules, such as H_2 and NH_3, even under mild conditions.[166,169–172] The frontier orbitals of the tetrelene can be viewed in some ways to play an analogous role in the activation of small molecules to the d-orbitals in transition metals (Figure 1.14). The size of the HOMO-LUMO gap is therefore of critical importance to the reactivity of Group 14 tetrelenes towards small molecules. Synthesis is a careful balancing act: ensuring that the HOMO-LUMO gap is large enough for the molecule to be thermally stable but small enough to interact with/activate small molecules.

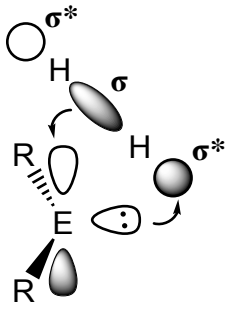

Figure 1.14 The ambiphilic nature of tetrelenes can allow for activation of small molecules, such as H_2.

As mentioned in section 1.3.1, the stability of divalent compounds increases upon descending Group 14. As a result, the ability of the tetrelenes to undergo oxidative

addition decreases.[1] A comparison of the reactivity of silylene **1.61** and germylene **1.63** towards NH_3 exemplifies this trend. The silylene undergoes formal oxidative addition of the N−H bond forming the four-coordinate 1,1-addition product with a +IV oxidation state at the silicon centre (**1.62**), whereas addition of NH_3 across the germylene and the ligand framework (to form **1.64**) results in no net change in the oxidation state of the tetrelene (Scheme 1.22).[171,172]

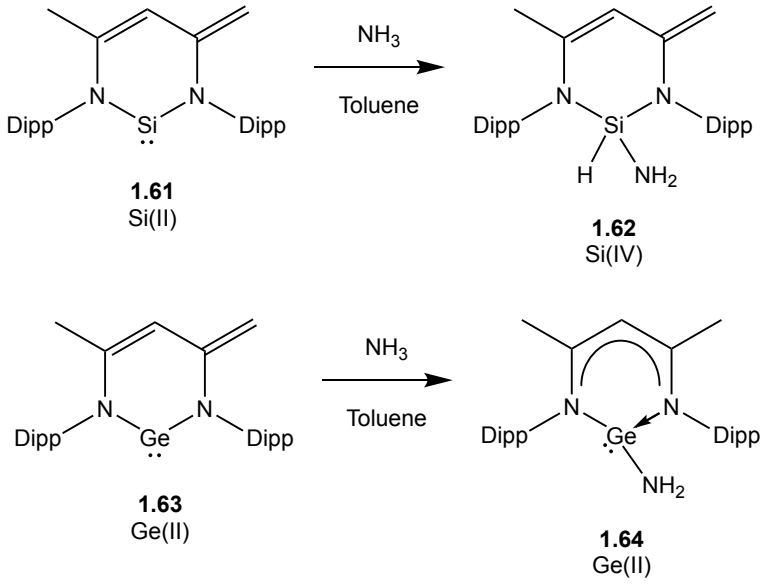

Scheme 1.22 (Upper) Oxidative addition of NH_3 by silylene 1.61 to give 1.62.[171] **(Lower) Activation of NH_3 by germylene 1.63 without formal change in oxidation state.**[172]

Of particular relevance to this thesis is the reactivity of silylenes and germylenes with oxygen transfer agents, with the aim of forming heavier analogues of ketones. Ketones usually exist in the monomeric form, but the heavier analogues have a high tendency to oligomerize or polymerize.[173] Upon descending Group 14, the E=O π-bond becomes intrinsically weaker and more polar, due to less effective p_π-overlap and the greater difference in electronegativity.[174] Attempts to synthesize a germanone date back to 1971 where Satgé *et al.* reported the first transient germanone.[4,175] Since then, there has been great interest and significant research dedicated to synthesizing

monomeric ketone analogues of the heavier Group 14 elements. Attempts have been made to access germanones, by the use of extremely bulky ligands such as 1,1,4,4-tetrakis(trimethylsilyl)butane-1,4-diyl for kinetic stabilization, for example, but almost all have been unsuccessful, with dimeric species often being produced instead.[176,177] From 2009 onwards, Yao *et al*. have reported a small number of Ge=O containing species featuring an additional coordinating Lewis base (such as an NHC or pyridine), which stabilizes the electron deficient germanium centre (Figure 1.15).[178,179]

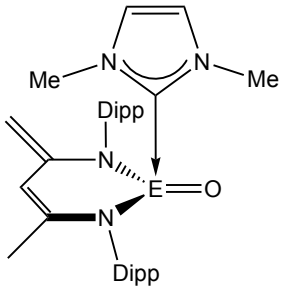

1.65 E = Ge
1.66 E = Si

Figure 1.15 Examples of a Lewis base supported germanone and silanone.[178,180]

To date, only one stable unsupported germanone has been isolated – *i.e*. one not additionally stabilized by an electron-donating Lewis base or a transition metal fragment.[174] This compound was synthesized by reacting a germylene supported by extremely bulky Eind substituents (Eind = 1,1,3,3,5,5,7,7-octaethyl-s-hydrindacen-4-yl) with trimethylamine *N*-oxide (Scheme 1.23). Theoretical studies have suggested that the Ge–O bond is highly polarized and that this compound could be considered as a charge-separated species. This renders the oxygen atom very nucleophilic and consistent patterns of reactivity are observed, such as the activation of CO_2.[174]

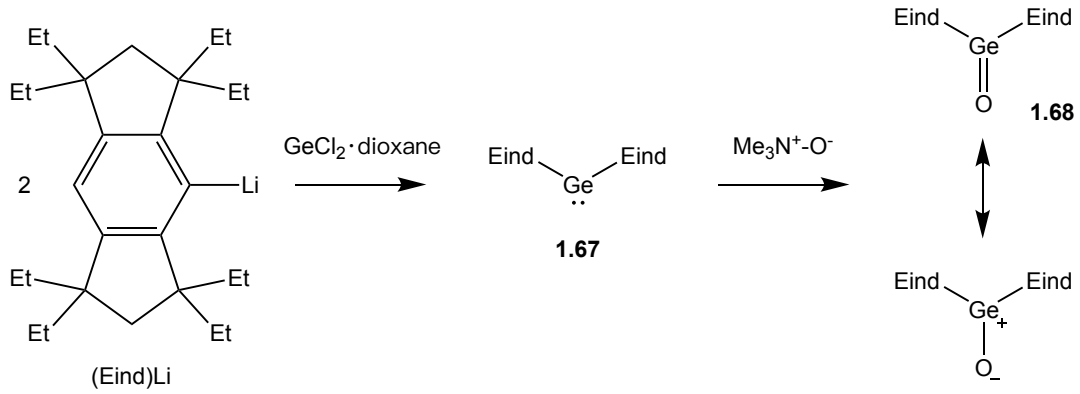

Scheme 1.23 Tamao's synthesis of the first unsupported monomeric germanone (1.68).[174]

As with germanones, silanones have also proved challenging to synthesize and reports of their chemistry been very limited. Kipping and Lloyd proposed the first silanone, $Ph_2Si{=}O$, as early as 1901 but attempts to synthesize it produced the corresponding polysiloxane instead.[182] Yao *et al.* have synthesized four-coordinate silanones similar to their Lewis base-stabilized germanones (*e.g.* **1.66**; Figure 1.15).[180] In 2015, Iwamoto *et al.* observed an unsupported silanone (**1.70**; Scheme 1.24), which was stable at -80 °C.[181] The silicon atom was incorporated into a cyclic system and the silanone stabilized with bulky silyl groups, one of which migrates to the oxygen at temperatures above -80 °C (Scheme 1.24). During the course of the work presented in this thesis, the first unsupported silanone (**1.74**; Scheme 1.25) was isolated and structurally characterized by Kato *et al*.[183] The silanone is, however, not stable at room temperature and dimerizes with a half-life of 30 min. Shortly after, the same group reported a second example of a silanone (**1.75**; Scheme 1.25), which has significantly increased stability towards dimerization (and subsequent rearrangement).[184]

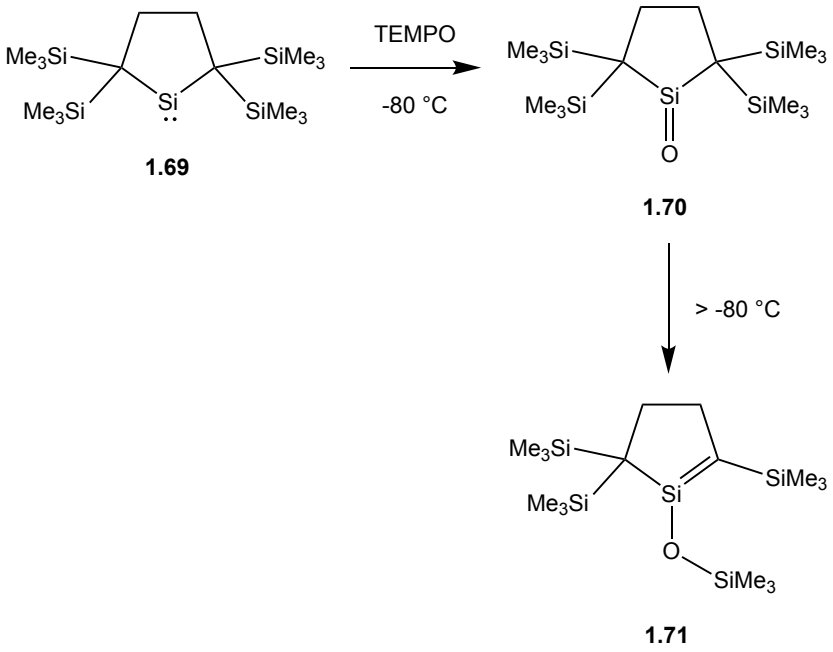

Scheme 1.24 The first observed unsupported silanone (1.70), which undergoes 1,3-rearrangement of one of the silyl groups above -80 °C.[181]

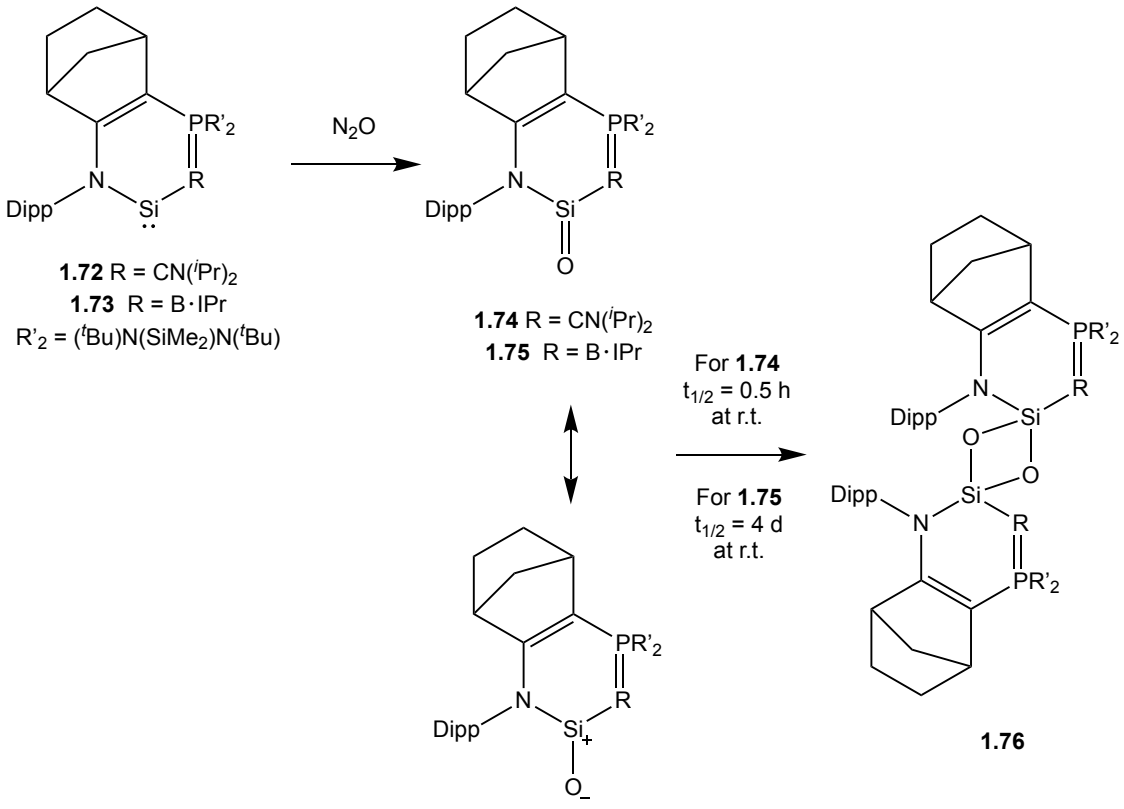

Scheme 1.25 Syntheses of monomeric silanones 1.74 (stable below -50 °C) and 1.75 (stable at room temperature).[183,184]

1.4 Boryl Ligands

1.4.1 Boryl Substituents

Organoboron compounds play a significant role in synthetic chemistry due to the C–B bond being easily converted to C–Cl, C–Br, C–O, C–N and C–C bonds. Charge-neutral boron has only six valence electrons and therefore does not fulfil the octet rule; three-coordinate boranes are archetypal Lewis acids. Traditionally, organoboron compounds are accessed synthetically through Grignard reactions or hydroboration, but developments in boron-metal chemistry in recent decades have opened the path to metal-catalyzed borylation. Transition-metal boryl complexes emerged in the 1960s with the work of Nöth and Schmid,[185] and are important intermediates in catalytic hydroboration, diboration and selective C–H bond activation processes.[186] The boron centre in these complexes is sp^2-hybridized and strongly σ-donating on account of its electropositivity. Due to the electron deficiency of three-coordinate boron, boryl complexes need to be stabilized *via* mesomeric π-donation from either its substituents or the metal centre; the former is nearly always the dominant source of π-stabilization.[186,187] Marder *et al.* studied the electronic properties of boryl ligands, demonstrating that they are amongst the most strongly σ-donating ligands known.[55]

For most of the p-block elements in the second row, anionic derivatives can be easily prepared as lithium salts such as LiF, LiOH, $LiNH_2$ and $LiCH_3$, but the synthesis of an anionic boron analogue had long proved to be very challenging.[188] Boranes are electron deficient and therefore most commonly react as strong Lewis acids to complete their octet. Attempts to synthesize a lithioborane *via* a simple deprotonation of an R_2BH species usually result instead in nucleophilic attack at the boron centre.[189] Moreover, the polarization of the B–H bond ($B^{\delta+}$–$H^{\delta-}$) gives the hydrogen atom

significant hydridic character, thereby making deprotonation even harder.[190] A reductive strategy starting from $R_2B–X$ (X = halogen) is also typically problematic due to the formation of very reactive transient boryl radicals.[191] In cases where the reduction process can be controlled, the formation of B–B bonds *via* dimerization is observed to be more facile than a second one-electron reduction process.[192,193]

Anionic, divalent boron atoms (BR_2^-) are isoelectronic with carbenes and are thus very unstable. For that reason, with the exception of metal boryl complexes, only electrophilic boranes were known until 2006, when Yamashita *et al*. reported the first isolated lithium boryl reagent (**1.78**; Scheme 1.26).[194] This formally anionic system is in principle stabilized in the same way as early examples of free carbenes, *i.e.* by incorporation into an *N*-heterocyclic ring bearing bulky Dipp *N*-substituents. A bulky *N*-substituent is needed to avoid formation of B–B bonded diborane and thus, only a few boryl anions have subsequently been isolated.[193] The B–Li bond is highly polarized due to the large difference in electronegativity between the boron (χ = 2.04) and lithium (χ = 0.96) atoms and therefore the boron centre is considered nucleophilic.[193] The nucleophilicity of the boryl anion has been confirmed through reactions with a wide range of electrophiles (a few examples are outlined in Scheme 1.27), although competing reductive behaviour can be problematic.[193,194]

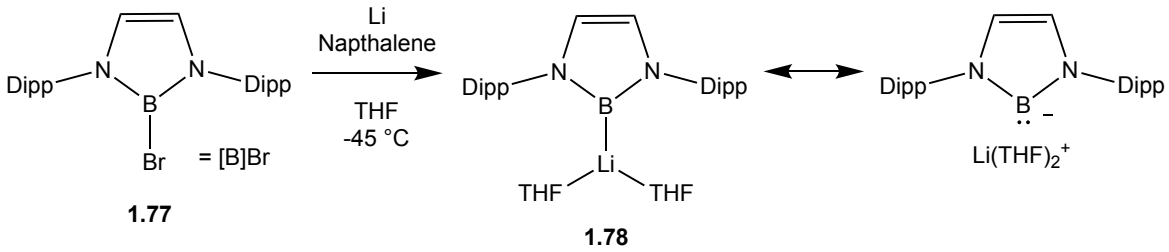

Scheme 1.26 Synthesis of the first boryl anion by Yamashita *et al*.[194]

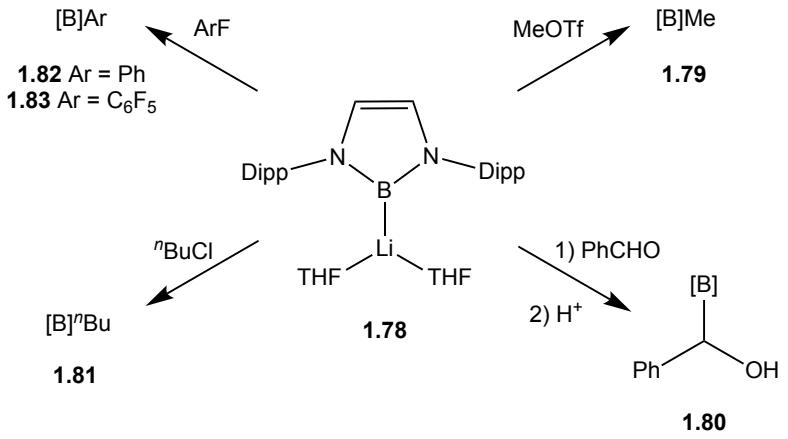

Scheme 1.27 Boryl anion 1.78 exhibits nucleophilic reactivity towards a range of electrophiles.[193,194]

Oxidative addition to a metal centre is often the rate determining step in a catalytic cycle and thus the use of more electron-donating ligands to promote faster oxidative addition could be envisaged as beneficial in delivering higher activity.[195,196] Boryl ligands are strongly σ-donating and potentially π-accepting, features which should result in a lower HOMO-LUMO energy gap at the metal centre, and greater intrinsic reactivity. The use of a bulky, strongly σ-donating boryl ligand could therefore be very valuable for synthesizing new species with interesting catalytic properties. The strong σ-donor properties and significant steric bulk of the {B(NDippCH)$_2$} ligand, and the propensity of boryllithium reagents to react with metal electrophiles have allowed for isolation of Group 14 systems of type E{B(NDippCH)$_2$}X (E = Si, Ge, Sn; X = boryl or amido group) that show interesting reactivity. Boryl-stannylene compounds, Sn{B(NDippCH)$_2$}$_2$ (**1.84**) and Sn{N(SiMe$_3$)Dipp}{B(NDippCH)$_2$} (**1.86**), synthesized by Aldridge *et al.*, highlight the role(s) played by the electronic properties of the boryl ligand. While the bis(boryl) stannylene **1.84** is able to activate a variety of E–H bonds (E = H, B, N, O, S), (amino)(boryl) stannylene **1.86** shows significantly lower reactivity towards small molecules (Scheme 1.28).[197] This is due to a higher HOMO-LUMO energy gap of the latter, as a result of the formal replacement of one

boryl group with an amino substituent. Density functional theory (DFT) calculations have shown that the singlet-triplet gap of the bis(boryl) and (amino)(boryl) systems vary significantly, being 53.6 kJ mol^{-1} and 98.3 kJ mol^{-1}, respectively.

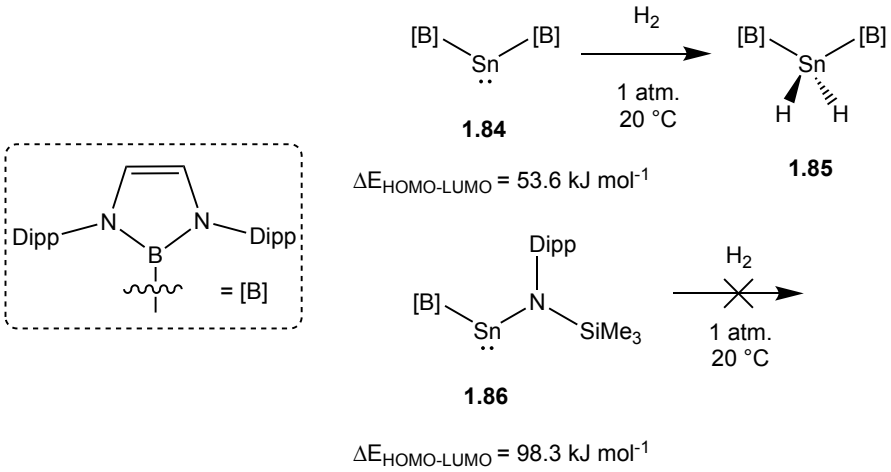

Scheme 1.28 Diboryl and (amido)(boryl) substituted stannylenes 1.84 and 1.86 exhibit different reactivity towards H_2 on account of different HOMO-LUMO energy gaps.[197]

The boryl ligand was also exploited to isolate one of the first stable acyclic silylenes, Si{B(NDippCH)$_2$}{N(SiMe$_3$)Dipp} (**1.88**), reported in 2012 by Aldridge *et al*. (Scheme 1.29). **1.88** has a wider angle at silicon than that found in cyclic analogues, such as **1.60** (Scheme 1.21), which, combined with the presence of the boryl substituent, leads to a narrower HOMO-LUMO energy gap and hence enhanced reactivity. **1.88** was the first silylene shown to be able to activate dihydrogen, which it can do even at 0 °C, with an activation barrier of approximately 98 kJ mol^{-1}.[198]

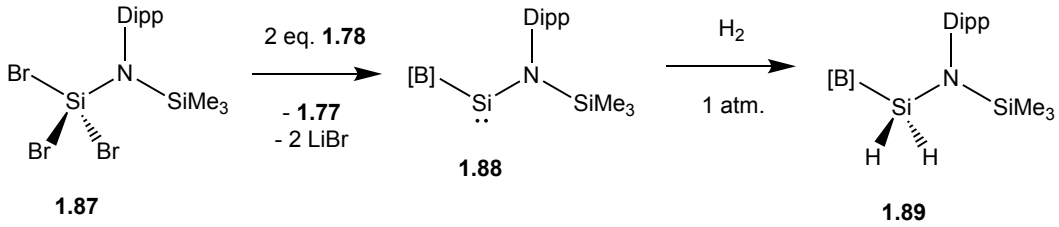

Scheme 1.29 Synthesis of the first acyclic silylene (1.88), which reacts with H_2 at ambient temperature.[166]

1.4.2 Peripheral Boryl Substituents

The boryllithium nucleophile (**1.78**) is challenging to synthesize and therefore the Aldridge group has, in recent years, also been interested in using boryl groups as peripheral substituents as part of C-, N- or O-donor ligands, since such systems can typically be accessed from the more readily available bromoborane precursor (**1.77**). **1.77**, for example, reacts readily with a variety of amines to form aminoboranes that are often stable to both air and moisture.[199,200] Scheme 1.30 outlines one example, in which bromoborane **1.77** reacts readily with ammonia to give the primary aminoborane **1.90**. This reaction has even proven to proceed in aqueous ammonia, with negligible formation of the hydrolysis product.[201] As a peripheral substituent on an amido ligand, the boryl group might still influence the electronic properties of the reactive centre, albeit to a somewhat lesser degree than *via* direct coordination.

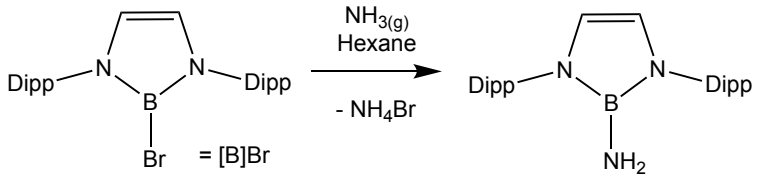

1.77 **1.90**

Scheme 1.30 Aminoborane 1.90 is readily synthesized from 1.77 and ammonia.[199]

Several monodentate borylamido ligands (**1.91**-**1.93**; Scheme 1.31) have been synthesized from **1.77**. These ligands have been shown to be able to stabilize a variety of low-valent Main Group compounds including silylenes, germylenes and stannylenes (Scheme 1.31).[199,200]

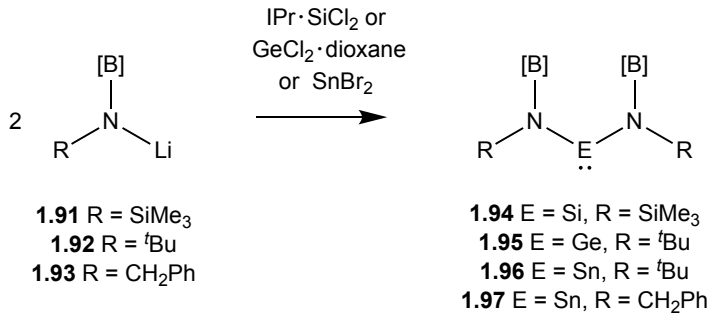

1.91 R = $SiMe_3$
1.92 R = ^tBu
1.93 R = CH_2Ph

1.94 E = Si, R = $SiMe_3$
1.95 E = Ge, R = ^tBu
1.96 E = Sn, R = ^tBu
1.97 E = Sn, R = CH_2Ph

Scheme 1.31 Syntheses of novel bis(borylamido) tetrelenes by salt metatheses.[199,200]

1.5 Research Outline

1.5.1 Borylated *N*-Heterocyclic Carbenes

As discussed in section 1.2.5, several boryl-containing carbenes have previously been synthesized, featuring both α- and β-borylation patterns.[88,100,103,202] Their electronic properties suggest that the boryl group increases the energy of the HOMO and reduces the energy of the LUMO as they are strongly σ-donating and have a formally vacant π-orbital. So far, no NHC bearing a pendant *N*-substituted boryl group has been isolated, nor has a metal complex of such an NHC been accessed. Chiu *et al*. have reported a 1,2-rearrangement in an NHC bearing $BMes_2$ as a pendant *N*-substituent (**1.48**; Scheme 1.19, section 1.2.7). Moreover, this process was reported to proceed too fast to allow even for detection of the free carbene.[146] Using Dipp-substituted diazaboryl groups ({$B(NDippCH)_2$}) as *N*-substituents could potentially allow for the isolation of *N*-borylated or *N*,*N'*-bisborylated NHCs. These boryl groups are *extremely* sterically bulky and are thus likely to provide a kinetic stability and thus a disincentive to a 1,2-shift of one of the boryl groups (Figure 1.16). Even if not completely prevented, a slow rearrangement process could allow for experimental insight into the kinetics of such migration.

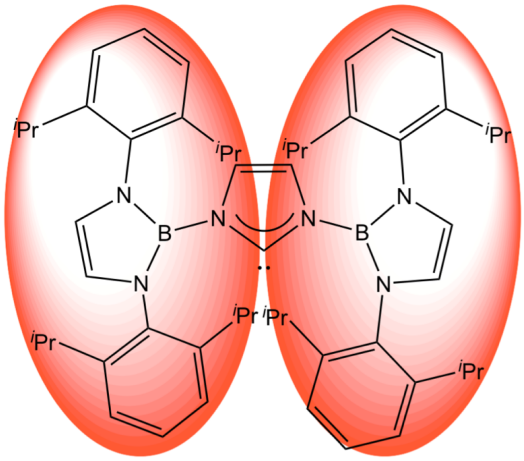

Figure 1.16 The steric bulk of Dipp substituted diazaboryl groups is likely to offer steric stabilization towards 1,2-rearrangement of the boryl groups in NHCs.

As peripheral substituents, the boryl groups are expected to raise the energy of the HOMO due to the strong σ-electron donating abilities of the boryl group. Three-coordinate boron centres feature a formally vacant p-orbital and as *N*-substituents, boryl groups might also serve to lower the energy of the LUMO of the carbene, provided p-orbital alignment of boron with the imidazole nitrogens can take place.

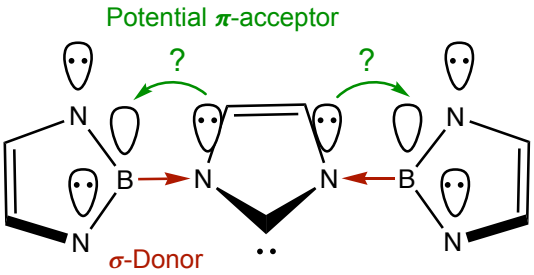

Figure 1.17 Electronic effects from peripherally substituted diazaboryl groups.

At the outset, the aim of the research reported in this thesis was the syntheses of NHCs bearing bulky peripheral diazaboryl substituents and assessment of their steric and electronic properties. The targeted NHCs are depicted in Figure 1.18, and include both bisborylated saturated, unsaturated, 4,5-disubstituted and benzannulated NHCs as well as abnormal NHCs.

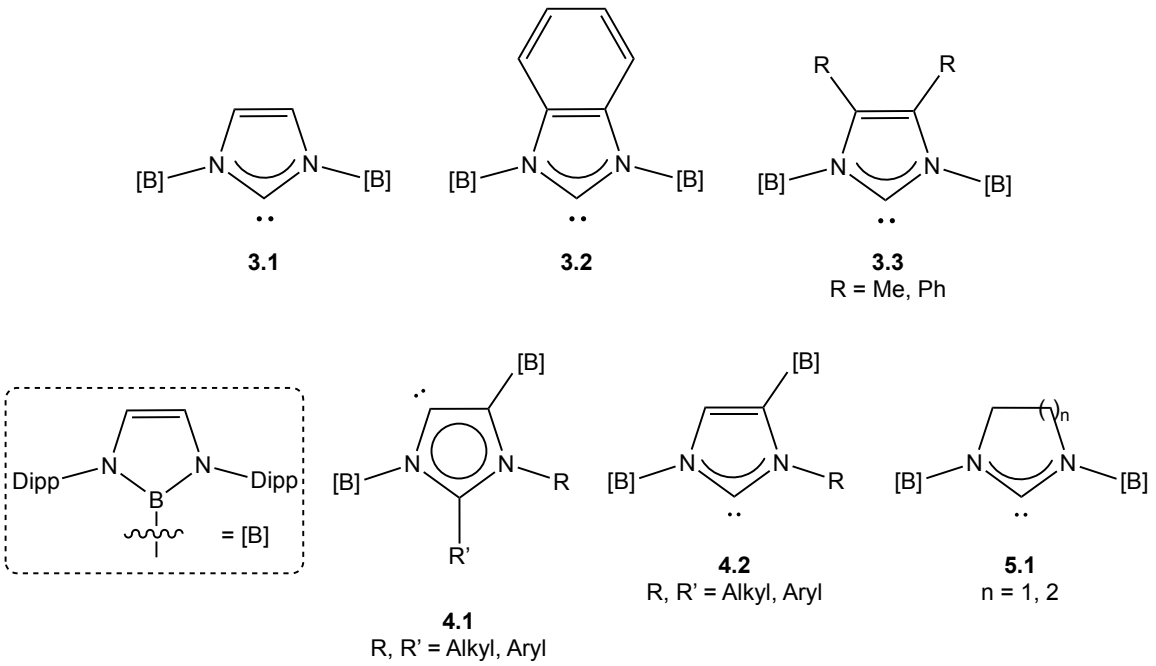

Figure 1.18 Targeted bisborylated NHCs.

1.5.2 *N,N'*-Bisborylated *N*-Heterocyclic Group 14 Tetrelenes

In addition to bisborylated *N*-heterocyclic carbenes, the focus of this thesis will include their heavier analogues, *N,N'*-bisborylated *N*-heterocyclic Group 14 tetrelenes. As for the carbenes, the peripherally substituted boryl groups are expected to reduce the HOMO-LUMO energy gap of tetrelenes. The electronic properties of these tetrelenes will be explored as well as their reactivity towards small molecules. Of particular interest is the reactivity of the germylenes towards oxygen transfer agents with isolation of an unsupported germanone in mind. The bulky boryl groups would be expected to provide great steric protection and hinder oligomerization of such a germanone. The targeted bisborylated 5- and 6-membered *N*-heterocyclic tetrelenes and germanone are depicted in Figure 1.19.

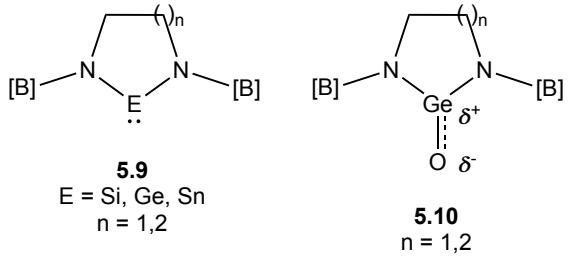

5.9
E = Si, Ge, Sn
n = 1,2

5.10
n = 1,2

Figure 1.19 Targeted Group 14 tetrelenes (left) along with the target germanone (right).

1.6 References

1 N. V. Sidgwick, *The Electronic Theory of Valency*, Oxford University Press, London, 1927.

2 R. Gleiter and R. Hoffmann, *J. Am. Chem. Soc.*, 1968, **90**, 5457–5460.

3 Y. Mizuhata, T. Sasamori and N. Tokitoh, *Chem. Rev.*, 2009, **109**, 3479–3511.

4 J. Satgé, *Adv. Organomet. Chem.*, 1982, **21**, 241–287.

5 E. O. Fischer and A. Maasböl, *Angew. Chem. Int. Ed.*, 1964, **3**, 580–581.

6 R. R. Schrock, *J. Am. Chem. Soc.*, 1974, **96**, 6796–6797.

7 H. W. Wanzlick, *Angew. Chem. Int. Ed.*, 1962, **1**, 75–80.

8 D. M. Lemal, R. A. Lovald and K. I. Kawano, *J. Am. Chem. Soc.*, 1964, **86**, 2518–2519.

9 H. E. Winberg, J. E. Carnahan, D. D. Coffman and M. Brown, *J. Am. Chem. Soc.*, 1965, **87**, 2055–2056.

10 V. P. W. Böhm and W. A. Herrmann, *Angew. Chem. Int. Ed.*, 2000, **39**, 4036–4038.

11 H. J. Schönherr and H. W. Wanzlick, *Angew. Chem. Int. Ed.*, 1968, **7**, 141–142.

12 K. Öfele, *J. Organomet. Chem.*, 1968, **12**, P42–P43.

13 H. J. Schonherr and H. W. Wanzlick, *Liebigs Ann. Chem.*, 1970, **179**, 176–179.

14 A. Igau, H. Grutzmacher, A. Baceiredo and G. Bertrand, *J. Am. Chem. Soc.*, 1988, **110**, 6463–6466.

15 T. Kato, H. Gornitzka, A. Baceiredo, A. Savin and G. Bertrand, *J. Am. Chem. Soc.*, 2000, **122**, 998–999.

16 A. J. Arduengo, R. L. Harlow and M. Kline, *J. Am. Chem. Soc.*, 1991, **113**, 361–363.

17 R. H. Crabtree, *J. Organomet. Chem.*, 2005, **690**, 5451–5457.

18 T. Leyssens, D. Peeters, A. G. Orpen and J. N. Harvey, *Organometallics*, 2007, **26**, 2637–2645.

19 P. W. N. M. van Leeuwen, C. Claver and ProQuest, *Rhodium Catalyzed Hydroformylation*, Boston: Kluwer Academic Publishers, Dordrecht, Netherlands, 2000.

20 J. P. Collman, L. S. Hegedus, J. R. Norton and F. R. J., *Principles and Applications of Organotransition Metal Chemistry.*, University Science Books, Mill Valley, CA, 2nd edn., 1987.

21 C. A. Tolman, *Chem. Rev.*, 1977, **77**, 313–348.

22 J. Cioslowski, *Int. J. Quantum Chem.*, 1993, **19**, 309–319.

23 A. J. Arduengo, D. A. Dixon, R. L. Harlow, H. V. R. Dias, W. T. Booster and T. F. Koetzle, *J. Am. Chem. Soc.*, 1994, **116**, 6812–6822.
24 C. Boehme and G. Frenking, *Organometallics*, 1998, **17**, 5801–5809.
25 X. Hu, Y. Tang, P. Gantzel and K. Meyer, *Organometallics*, 2003, **22**, 612–614.
26 A. A. D. Tulloch, A. A. Danopoulos, S. Kleinhenz, M. E. Light, M. B. Hursthouse and G. Eastham, *Organometallics*, 2001, **20**, 2027–2031.
27 M. J. Clarke and H. Taube, *J. Am. Chem. Soc.*, 1975, **97**, 1397–1403.
28 S. Fantasia, J. L. Petersen, H. Jacobsen, L. Cavallo and S. P. Nolan, *Organometallics*, 2007, **26**, 5880–5889.
29 D. Nemcsok, K. Wichmann and G. Frenking, *Organometallics*, 2004, **23**, 3640–3646.
30 M. Tafipolsky, W. Scherer, K. Öfele, G. Artus, B. Pedersen, W. A. Herrmann and G. S. McGrady, *J. Am. Chem. Soc.*, 2002, **124**, 5865–5880.
31 A. T. Termaten, M. Schakel, A. W. Ehlers, M. Lutz, A. L. Spek and K. Lammertsma, *Chem. Eur. J.*, 2003, **9**, 3577–3582.
32 X. Hu, I. Castro-Rodriguez, K. Olsen and K. Meyer, *Organometallics*, 2004, **23**, 755–764.
33 S. Saravanakumar, A. I. Oprea, M. K. Kindermann, P. G. Jones and J. Heinicke, *Chem. Eur. J.*, 2006, **12**, 3143–3154.
34 D. Bourissou, O. Guerret, F. P. Gabbaï and G. Bertrand, *Chem. Rev.*, 2000, **100**, 39–91.
35 R. Dorta, E. D. Stevens, N. M. Scott, C. Costabile, L. Cavallo, C. D. Hoff and S. P. Nolan, *J. Am. Chem. Soc.*, 2005, **127**, 2485–2495.
36 D. J. Nelson and S. P. Nolan, *Chem. Soc. Rev.*, 2013, **42**, 6723–6753.
37 B. Maji, M. Breugst and H. Mayr, *Angew. Chem. Int. Ed.*, 2011, **50**, 6915–6919.
38 D. Tapu, D. A Dixon and C. Roe, *Chem. Rev.*, 2009, **16**, 3385–3407.
39 D. Tapu, D. A. Dixon and C. Roe, *Chem. Rev.*, 2009, **109**, 3385–3407.
40 A. J. Arduengo, *Acc. Chem. Res.*, 1999, **32**, 913–921.
41 R. W. Alder and M. E. Blake, *J. Phys. Chem. A*, 1999, **103**, 11200–11211.
42 M. Nonnenmacher, D. Kunz, F. Rominger and T. Oeser, *Chem. Commun.*, 2006, **386**, 1378–1380.
43 R. A. Kelly, H. Clavier, S. Giudice, N. M. Scott, E. D. Stevens, J. Bordner, I. Samardjiev, C. D. Hoff, L. Cavallo and S. P. Nolan, *Organometallics*, 2008, **27**, 202–210.
44 O. Back, M. Henry-Ellinger, C. D. Martin, D. Martin and G. Bertrand, *Angew. Chem. Int. Ed.*, 2013, **52**, 2939–2943.
45 A. Liske, K. Verlinden, H. Buhl, K. Schaper and C. Ganter, *Organometallics*, 2013, **32**, 5269–5272.
46 S. V. C. Vummaleti, D. J. Nelson, A. Poater, A. Gómez-Suárez, D. B. Cordes, A. M. Z. Slawin, S. P. Nolan and L. Cavallo, *Chem. Sci.*, 2015, **6**, 1895–1904.
47 S. Dutta, B. Maity, D. Thirumalai and D. Koley, *Inorg. Chem.*, 2018, **57**, 3993–4008.
48 H. Duddeck, *Prog. Nucl. Magn. Reson. Spectrosc.*, 1995, **27**, 1–323.
49 A. A. Tukov, A. T. Normand and M. S. Nechaev, *Dalton Trans.*, 2009, **0**, 7015–7028.

50 B. Rao, H. Tang, X. Zeng, L. Liu, M. Melaimi and G. Bertrand, *Angew. Chem. Int. Ed.*, 2015, **54**, 14915–14919.
51 M. Z. Kassaee, F. A. Shakib, M. R. Momeni, M. Ghambarian and S. M. Musavi, *J. Org. Chem.*, 2010, **75**, 2539–2545.
52 G. D. Frey, V. Lavallo, B. Donnadieu, W. W. Schoeller and G. Bertrand, *Science*, 2007, **316**, 439–441.
53 H. Jacobsen, A. Correa, A. Poater, C. Costabile and L. Cavallo, *Coord. Chem. Rev.*, 2009, **253**, 687–703.
54 E. Karaca, M. Akkoç, E. Öz, S. Altin, V. Dorcet, T. Roisnel, N. Gürbüz, Çelik, A. Bayri, C. Bruneau, S. Yaşar and I. Özdemir, *J. Coord. Chem.*, 2017, **70**, 1270–1284.
55 J. Zhu, Z. Lin and T. B. Marder, *Inorg. Chem.*, 2005, **44**, 9384–9390.
56 A. C. Hillier, W. J. Sommer, B. S. Yong, J. L. Petersen, L. Cavallo and S. P. Nolan, *Organometallics*, 2003, **22**, 4322–4326.
57 L. Falivene, R. Credendino, A. Poater, A. Petta, L. Serra, R. Oliva, V. Scarano and L. Cavallo, *Organometallics*, 2016, **35**, 2286–2293.
58 H. Clavier and S. P. Nolan, *Chem. Commun.*, 2010, **46**, 841–861.
59 S. Dierick, D. F. Dewez and I. E. Markó, *Organometallics*, 2014, **33**, 677–683.
60 M. M. D. Roy, P. A. Lummis, M. J. Ferguson, R. McDonald and E. Rivard, *Chem. Eur. J.*, 2017, **23**, 11249–11252.
61 A. J. Arduengo, R. Krafczyk, R. Schmutzler, H. A. Craig, J. R. Goerlich, W. J. Marshall and M. Unverzagt, *Tetrahedron*, 1999, **55**, 14523–14534.
62 A. Liske, K. Verlinden, H. Buhl, K. Schaper and C. Ganter, *Organometallics*, 2013, **32**, 5269–5272.
63 M. Iglesias, D. J. Beetstra, B. Kariuki, K. J. Cavell, A. Dervisi and I. A. Fallis, *Eur. J. Inorg. Chem.*, 2009, **2009**, 1913–1919.
64 M. Iglesias, D. J. Beetstra, J. C. Knight, L. L. Ooi, A. Stasch, S. Coles, L. Male, M. B. Hursthouse, K. J. Cavell, A. Dervisi and I. A. Fallis, *Organometallics*, 2008, **27**, 3279–3289.
65 M. Mayr, K. Wurst, K. H. Ongania and M. R. Buchmeiser, *Chem. Eur. J.*, 2004, **10**, 1256–1266.
66 D. Martin, N. Lassauque, B. Donnadieu and G. Bertrand, *Angew. Chem.*, 2012, **124**, 6276–6279.
67 M. J. López-Gómez, D. Martin and G. Bertrand, *Chem. Commun.*, 2013, **49**, 4483–4485.
68 R. W. Alder, P. R. Allen, M. Murray and A. G. Orpen, *Angew. Chem. Int. Ed.*, 1996, **35**, 1121–1123.
69 K. Denk, P. Sirsch and W. A. Herrmann, *J. Organometalic Chem.*, 2002, **649**, 219–224.
70 H. Seo, B. P. Roberts, K. A. Abboud, K. M. Merz, S. Hong, V. Gaines and U. States, *Org. Lett.*, 2010, **12**, 1121–1123.
71 O. Starikova, G. Dolgushin, L. Larina, T. Komarova and V. Lopyrev, *Arkivoc*, 2003, **13**, 119–124.
72 D. J. Nelson and S. P. Nolan, *Chem. Soc. Rev.*, 2013, **42**, 6723–6753.
73 A. J. Arduengo, F. Davidson, H. V. R. Dias, J. R. Goerlich, D. Khasnis, W. J. Marshall and T. K. Prakasha, *J. Am. Chem. Soc.*, 1997, **7863**, 12742–12749.

74 K. Verlinden, H. Buhl, W. Frank and C. Ganter, *Eur. J. Inorg. Chem.*, 2015, **2015**, 2416–2425.
75 G. A. Blake, J. P. Moerdyk and C. W. Bielawski, *Organometallics*, 2012, **31**, 3373–3378.
76 T. W. Hudnall and C. W. Bielawski, *J. Am. Chem. Soc.*, 2009, **131**, 16039–16041.
77 V. César, N. Lugan and G. Lavigne, *Eur. J. Inorg. Chem.*, 2010, **2010**, 361–365.
78 R. R. Rodrigues, C. L. Dorsey, C. A. Arceneaux and T. W. Hudnall, *Chem. Commun.*, 2014, **50**, 162–164.
79 L. R. Collins, T. M. Rookes, M. F. Mahon, I. M. Riddlestone and M. K. Whittlesey, *Organometallics*, 2014, **33**, 5882–5887.
80 A. J. Arduengo, J. R. Goerlich and W. J. Marshall, *Liebigs Ann.*, 1997, **1997**, 365–374.
81 V. Lavallo, J. Mafhouz, Y. Canac, B. Donnadieu, W. W. Schoeller and G. Bertrand, *J. Am. Chem. Soc.*, 2004, **126**, 8670–8671.
82 V. Lavallo, Y. Canac, C. Präsang, B. Donnadieu and G. Bertrand, *Angew. Chem. Int. Ed.*, 2005, **44**, 5705–5709.
83 V. Lavallo, Y. Canac, A. DeHope, B. Donnadieu and G. Bertrand, *Angew. Chem. Int. Ed.*, 2005, **44**, 7236–7239.
84 M. Tretiakov, Y. G. Shermolovich, A. P. Singh, P. P. Samuel, H. W. Roesky, B. Niepötter, A. Visscher and D. Stalke, *Dalton Trans.*, 2013, **42**, 12940–12946.
85 E. Tomás-Mendivil, M. M. Hansmann, C. M. Weinstein, R. Jazzar, M. Melaimi and G. Bertrand, *J. Am. Chem. Soc.*, 2017, **139**, 7753–7756.
86 E. Aldeco-Perez, A. J. Rosenthal, B. Donnadieu, P. Parameswaran, G. Frenking and G. Bertrand, *Science*, 2009, **326**, 556–560.
87 A. R. Chianese, A. Kovacevic, B. M. Zeglis, J. W. Faller and R. H. Crabtree, *Organometallics*, 2004, **23**, 2461–2468.
88 C. Präsang, B. Donnadieu and G. Bertrand, *J. Am. Chem. Soc.*, 2005, **127**, 10182–10183.
89 O. Back, M. Henry-Ellinger, C. D. Martin, D. Martin and G. Bertrand, *Angew. Chem. Int. Ed.*, 2013, **52**, 2939–2943.
90 R. W. Alder, M. E. Blake, C. Bortolotti, S. Bufali, C. P. Butts, E. Linehan, J. M. Oliva, A. G. Orpen and M. J. Quayle, *Chem. Commun.*, 1999, **0**, 241–242.
91 M. K. Denk, A. Thadani, K. Hatano and A. J. Lough, *Angew. Chem. Int. Ed.*, 1997, **36**, 2607–2609.
92 V. Lavallo, Y. Canac, B. Donnadieu, W. W. Schoeller and G. Bertrand, *Angew. Chem. Int. Ed.*, 2006, **45**, 3488–3491.
93 D. Preysing, E. Herdtweck, W. A. Herrmann and O. Karl, *J. Organomet. Chem.*, 2003, **684**, 235–248.
94 F. E. Hahn and M. C. Jahnke, *Angew. Chem. Int. Ed.*, 2008, **47**, 3122–3172.
95 H. Niu, R. J. Mangan, A. V. Protchenko, N. Phillips, W. Unkrig, C. Friedmann, E. L. Kolychev, R. Tirfoin, J. Hicks and S. Aldridge, *Dalton Trans.*, 2018, Accepted Manuscript. DOI: 10.1039/C8DT01661E
96 S. Solé, H. Gornitzka, W. W. Schoeller, D. Bourissou and G. Bertrand, *Science*, 2001, **292**, 1901–1904.
97 S. Gründemann, A. Kovacevic, M. Albrecht, J. W. Faller and R. H. Crabtree, *Chem.*

Commun., 2001, **4**, 7–8.
98 J. B. Waters and J. M. Goicoechea, *Coord. Chem. Rev.*, 2014, **293–294**, 80–94.
99 S. Sarmah, K. Guha and A. K. Phukan, 2013, **13**, 3233–3239.
100 K. E. Krahulic, G. D. Enright, M. Parvez and R. Roesler, *J. Am. Chem. Soc.*, 2005, **127**, 4142–4143.
101 L. Pauling, *The Nature of the Chemical Bond and the Structure of Molecules and Crystals : an Introduction to Modern Structural Chemistry*, Cornell University Press, Ithaca, 3rd edn., 1960.
102 A. Kausamo, H. M. Tuononen, K. E. Krahulic and R. Roesler, *Inorg. Chem.*, 2008, **47**, 1145–1154.
103 F. Lavigne, E. Maerten, G. Alcaraz, N. Saffon-Merceron, C. Acosta-Silva and A. Baceiredo, *J. Am. Chem. Soc.*, 2010, **132**, 8864–8865.
104 Y. Leriche, H. Gornitzka, A. Baceiredo and G. Bertrand, 1998, 1539–1542.
105 W. A. Herrmann, *Angew. Chem. Int. Ed.*, 2002, **41**, 1290–1309.
106 M. N. Hopkinson, C. Richter, M. Schedler and F. Glorius, *Nature*, 2014, **510**, 485–496.
107 W. A. Herrmann, M. Elison, C. Kocher and G. R. J. Artus, *Angew. Chem. Int. Ed.*, 1995, **34**, 2371–2374.
108 W. A. Herrmann, C. P. Reisinger and M. Spiegler, *J. Organomet. Chem.*, 1998, **557**, 93–96.
109 S. Caddick, F. G. N. Cloke, G. K. B. Clentsmith, P. B. Hitchcock, D. McKerrecher, L. R. Titcomb and M. R. V. Williams, *J. Organomet. Chem*, 2001, **618**, 635–639.
110 N. Hadei, E. A. B. Kantchev, C. J. O'Brien and M. G. Organ, *Org. Lett.*, 2005, **7**, 3805–3807.
111 J. Huang, G. Grasa and S. P. Nolan, *Org. Lett.*, 1999, **1**, 1307–1309.
112 M. Scholl, S. Ding, C. W. Lee and R. H. Grubbs, *Org. Lett.*, 1999, **1**, 953–956.
113 D. R. Anderson, T. Ung, G. Mkrtumyan, G. Bertrand, R. H. Grubbs and Y. Schrodi, *Organometallics*, 2008, **27**, 563–566.
114 V. M. Marx, A. H. Sullivan, M. Melaimi, S. C. Virgil, B. K. Keitz, D. S. Weinberger, G. Bertrand and R. H. Grubbs, *Angew. Chem. Int. Ed.*, 2015, **54**, 1919–1923.
115 D. Enders, O. Niemeier and A. Henseler, *Chem. Rev.*, 2007, **107**, 5606–5655.
116 F. Wöhler and J. von Liebig, *Ann. der Pharm.*, 1832, **3**, 249–282.
117 R. Breslow, *J. Am. Chem. Soc.*, 1958, **80**, 3719–3726.
118 D. Enders, K. Breuer, G. Raabe, J. Runsink, J. H. Teles, J. Melder, K. Ebel and S. Brode, *Angew. Chem. Int. Ed.*, 1995, **34**, 1021–1023.
119 J. H. Teles, J. P. Melder, K. Ebel, R. Schneider, E. Gehrer, W. Harder, S. Brode, D. Enders, K. Breuer and G. Raabe, *Helv. Chim. Acta*, 1996, **79**, 61–83.
120 H. Stetter and K. Heinrich, *Org. React.*, 1991, **40**, 407–496.
121 S. Naumann and A. P. Dove, *Polym. Int.*, 2016, **65**, 16–27.
122 C. Fischer, S. W. Smith, D. A. Powell and G. C. Fu, *J. Am. Chem. Soc.*, 2006, **128**, 1472–1473.
123 J. P. Moerdyk and C. W. Bielawski, *Nat. Chem.*, 2012, **4**, 275–280.
124 Y. Wang, Y. Xie, P. Wei, R. B. King, H. F. Schaefer, P. V. R. Schleyer and G. H. Robinson, *J. Am. Chem. Soc.*, 2008, **130**, 14970–14971.
125 P. V. R. Schleyer and G. H. Robinson, *Science*, 2008, **321**, 1069–1071.

126 C. A. Dyker, V. Lavallo, B. Donnadieu and G. Bertrand, *Angew. Chem. Int. Ed.*, 2008, **47**, 3206–3209.
127 H. Braunschweig, R. D. Dewhurst, K. Hammond, J. Mies, K. Radacki and A. Vargas, *Science*, 2012, **336**, 1420–1422.
128 A. Rosas-Sánchez, I. Alvarado-Beltran, A. Baceiredo, D. Hashizume, N. Saffon-Merceron, V. Branchadell and T. Kato, *Angew. Chem.* 2017, 4892–4896.
129 C. D. Martin, M. Soleilhavoup and G. Bertrand, *Chem. Sci.*, 2013, **4**, 3020–3030.
130 S. H. Ueng, M. M. Brahmi, É. Derat, L. Fensterbank, E. Lacôte, M. Malacria and D. P. Curran, *J. Am. Chem. Soc.*, 2008, **130**, 10082–10083.
131 J. K. Mahoney, D. Martin, F. Thomas, C. E. Moore, A. L. Rheingold and G. Bertrand, *J. Am. Chem. Soc.*, 2015, **137**, 7519–7525.
132 A. Rit, R. Tirfoin and S. Aldridge, *Angew. Chem. Int. Ed.*, 2016, **55**, 378–382.
133 T. W. Hudnall, J. P. Moerdyk and C. W. Bielawski, *Chem. Commun.*, 2010, **46**, 4288–4290.
134 S. Kronig, E. Theuergarten, D. Holschumacher, T. Bannenberg, C. G. Daniliuc, P. G. Jones and M. Tamm, *Inorg. Chem.*, 2011, **50**, 7344–7359.
135 P. Lara, O. Rivada-Wheelaghan, S. Conejero, R. Poteau, K. Philippot and B. Chaudret, *Angew. Chem. Int. Ed.*, 2011, **50**, 12080–12084.
136 L. Mercs and M. Albrecht, *Chem. Soc. Rev.*, 2010, **39**, 1903–1912.
137 K. M. Hindi, M. J. Panzner, C. A. Tessier, C. L. Cannon and W. J. Youngs, *Chem. Rev.*, 2009, **109**, 3859–3884.
138 F. Bonnette, T. Kato, M. Destarac, G. Mignani, F. P. Cossío and A. Baceiredo, *Angew. Chem. Int. Ed.*, 2007, **46**, 8632–8635.
139 J. W. Storer and K. N. Houk, *J. Am. Chem. Soc.*, 1993, **115**, 10426–10427.
140 M. T. H. Liu, *Acc. Chem. Res.*, 1994, **27**, 287–294.
141 S. Solé, H. Gornitzka, O. Guerret and G. Bertrand, *J. Am. Chem. Soc.*, 1998, **120**, 9100–9101.
142 C. Heinemann and W. Thiel, *Chem. Phys. Lett.*, 1994, **217**, 11–16.
143 J. A. Montgomery, K. Raghavdchari, M. A. Alaham, V. G. Zakrzewski, E. S. Replogle, R. Gomperts, R. L. Martin, D. J. Fox, J. S. Binkley, G. Maier, J. Endres and H. P. Reisenauer, *Angew. Chem. Int. Ed.*, 1997, **36**, 69451–69454.
144 G. A. McGibbon, C. Heinemann, D. J. Lavorato and H. Schwarz, *Angew. Chemie Int. Ed. English*, 1997, **36**, 1478–1481.
145 X. Cattoën, H. Gornitzka, F. S. Tham, K. Miqueu, D. Bourissou and G. Bertrand, *Eur. J. Org. Chem.*, 2007, **2007**, 912–917.
146 W. C. Liu, Y. H. Liu, T. S. Lin, S. M. Peng and C. W. Chiu, *Inorg. Chem.*, 2017, **56**, 10543–10548.
147 D. Vagedes, G. Kehr, D. König, K. Wedeking, R. Fröhlich, G. Erker, C. Mück-lichtenfeld and S. Grimme, *Eur. J. Inorg. Chem.*, 2002, **2002**, 2015–2021.
148 A. Wacker, H. Pritzkow and W. Siebert, *Eur. J. Inorg. Chem.*, 1998, **6**, 1–7.
149 D. Zhang and H. Kawaguchi, *Organometallics*, 2006, **25**, 5506–5509.
150 G. Steiner, A. Krajete, H. Kopacka, K. H. Ongania, K. Wurst, P. Preishuber-Pflügl and B. Bildstein, *Eur. J. Inorg. Chem.*, 2004, **14**, 2827–2836.
151 A. P. Marchenko, H. N. Koidan, A. N. Huryeva, E. V. Zarudnitskii, A. A. Yurchenko and A. N. Kostyuk, *J. Org. Chem.*, 2010, **75**, 7141–7145.

152 A. P. Marchenko, H. N. Koidan, A. N. Hurieva, I. I. Pervak, S. V. Shishkina, O. V. Shishkin and A. N. Kostyuk, *European J. Org. Chem.*, 2012, **21**, 4018–4033.
153 A. P. Marchenko, H. N. Koidan, I. I. Pervak, A. N. Huryeva, E. V. Zarudnitskii, A. A. Tolmachev and A. N. Kostyuk, *Tetrahedron Lett.*, 2012, **53**, 494–496.
154 A. P. Marchenko, H. N. Koidan, E. V. Zarudnitskii, A. N. Hurieva, A. A. Kirilchuk, A. A. Yurchenko, A. Biffis and A. N. Kostyuk, *Organometallics*, 2012, **31**, 8257–8264.
155 P. Nägele, U. Herrlich, F. Rominger and P. Hofmann, *Organometallics*, 2013, **32**, 181–191.
156 F. Lavigne, E. Maerten, G. Alcaraz, N. Saffon-Merceron and A. Baceiredo, *Chem. Eur. J.*, 2014, **20**, 297–303.
157 M. Menzel, H. J. Winkler, T. Ablelom, D. Steiner, S. Fau, G. Frenking, W. Massa and A. Berndt, *Angew. Chem. Int. Ed.*, 1995, **34**, 1340–1343.
158 P. J. Davidson and M. F. Lappert, *J. Chem. Soc., Chem. Commun.*, 1973, **0**, 317.
159 D. E. Goldberg, D. H. Harris, M. F. Lappert and K. M. Thomas, *J. Chem. Soc. Chem. Commun.*, 1976, **227**, 1–2.
160 P. B. Hitchcock, M. F. Lappert, S. J. Miles and A. J. Thorne, 1984, **347**, 480–482.
161 D. H. Harris and M. F. Lappert, *J. Chem. Soc. Chem. Commun.*, 1974, **0**, 895–896.
162 P. Jutzi, A. Becker, H. G. Stammler and B. Neumann, 1991, **3**, 1647–1648.
163 R. West, M. J. Fink and J. Michl, *Science*, 1981, **214**, 1343–1344.
164 M. Denk, R. Lennon, R. Hayashi, R. West, A. V. Belyakov, H. P. Verne, A. Haaland, M. Wagner and N. Metzler, *J. Am. Chem. Soc.*, 1994, **116**, 2691–2692.
165 R. S. Ghadwal, H. W. Roesky, S. Merkel, J. Henn and D. Stalke, *Angew. Chem. Int. Ed.*, 2009, **48**, 5683–5686.
166 A. V. Protchenko, K. H. Birjkumar, D. Dange, A. D. Schwarz, D. Vidovic, C. Jones, N. Kaltsoyannis, P. Mountford and S. Aldridge, *J. Am. Chem. Soc.*, 2012, **134**, 6500–6503.
167 B. D. Rekken, T. M. Brown, J. C. Fettinger, H. M. Tuononen and P. P. Power, *J. Am. Chem. Soc.*, 2012, **134**, 6504–6507.
168 E. Rivard, *Dalton Trans.*, 2014, **43**, 8577–8586.
169 C. A. Caputo and P. P. Power, *Organometallics*, 2013, **32**, 2278–2286.
170 Y. Peng, B. D. Ellis, X. Wang and P. P. Power, *J. Am. Chem. Soc.*, 2008, **130**, 12268–12269.
171 A. Jana, C. Schulzke and H. W. Roesky, *J. Am. Chem. Soc.*, 2009, **131**, 4600–4601.
172 A. Jana, I. Objartel, H. W. Roesky and D. Stalke, *Inorg. Chem.*, 2009, **48**, 798–800.
173 J. Küpp, M. Remko and P. von R. Schleyer, *J. Am. Chem. Soc.*, 1996, **1118**, 5745–5751.
174 L. Li, T. Fukawa, T. Matsuo, D. Hashizume, H. Fueno, K. Tanaka and K. Tamao, *Nat. Chem.*, 2012, **4**, 361–365.
175 J. Barrau, M. Massol, D. Mesnard and J. Satgé, *J. Organomet. Chem.*, 1971, **30**, C67–C69.
176 T. Iwamoto, H. Masuda, S. Ishida, C. Kabuto and M. Kira, *J. Organomet. Chem.*, 2004, **689**, 1337–1341.
177 S. M. I. Al-Rafia, P. A. Lummis, M. J. Ferguson, R. McDonald and E. Rivard, *Inorg. Chem.*, 2010, **49**, 9709–9717.

178 S. Yao, Y. Xiong and M. Driess, *Chem. Commun.*, 2009, **0**, 6466–6468.
179 S. Yao, Y. Xiong, W. Wang and M. Driess, *Chem. Eur. J.*, 2011, **17**, 4890–4895.
180 S. Yao, Y. Xiong and M. Driess, *J. Am. Chem. Soc.*, 2009, **131**, 7562–7563.
181 S. Ishida, T. Abe, F. Hirakawa, T. Kosai, K. Sato, M. Kira and T. Iwamoto, *Chem. Eur. J.*, 2015, **2015**, 15100–15103.
182 F. S. Kipping and L. L. Lloyd, *J. Chem. Soc., Trans.*, 1901, **79**, 449–459.
183 I. Alvarado-Beltran, A. Rosas-Sánchez, A. Baceiredo, N. Saffon-Merceron, V. Branchadell and T. Kato, *Angew. Chem. Int. Ed.*, 2017, **56**, 10481–10485.
184 A. Rosas-Sánchez, I. Alvarado-Beltran, A. Baceiredo, N. Saffon-Merceron, S. Massou, D. Hashizume, V. Branchadell and T. Kato, *Angew. Chem. Int. Ed.*, 2017, **56**, 15916–15920.
185 G. Schmid, *Angew. Chem. Int. Ed.*, 1970, **9**, 819–830.
186 D. L. Kays and S. Aldridge, in *Contemporary Metal Boron Chemistry I: Borylenes, Boryls, Borane σ-Complexes, and Borohydrides*, eds. T. B. Marder and Z. Lin, Springer, Berlin, 2008, pp. 29–120.
187 G. J. Irvine, M. J. G. Lesley, T. B. Marder, N. C. Norman, C. R. Rice, E. G. Robins, W. R. Roper, G. R. Whittell and L. J. Wright, *Chem. Rev.*, 1998, **98**, 2685–2722.
188 M. Yamashita and K. Nozaki, *Pure Appl. Chem.*, 2008, **80**, 1187–1194.
189 H. Braunschweig, *Angew. Chem. Int. Ed.*, 2007, 46, 1946–1948.
190 L. Dang, Z. Lin and T. B. Marder, *Chem. Commun.*, 2009, **0**, 3987–3995.
191 R. Koster and G. Benedikt, *Angew. Chem. Int. Ed.*, 1964, **3**, 515.
192 J. Brotherton, A. L. McCloskey, L. L. Petterson and H. Steinberg, *J. Am. Chem. Soc.*, 1959, **82**, 6242–6245.
193 Y. Segawa, Y. Suzuki, M. Yamashita and K. Nozaki, *J. Am. Chem. Soc.*, 2008, **130**, 16069–16079.
194 Y. Segawa, M. Yamashita and K. Nozaki, *Science*, 2006, **314**, 113–115.
195 T. M. Boller, J. M. Murphy, M. Hapke, T. Ishiyama, N. Miyaura and J. F. Hartwig, *J. Am. Chem. Soc.*, 2005, **127**, 14263–14278.
196 H. Tamura, H. Yamazaki, H. Sato and S. Sakaki, *J. Am. Chem. Soc.*, 2003, **125**, 16114–16126.
197 A. V. Protchenko, J. I. Bates, L. M. A. Saleh, M. P. Blake, A. D. Schwarz, E. L. Kolychev, A. L. Thompson, C. Jones, P. Mountford and S. Aldridge, *J. Am. Chem. Soc.*, 2016, **138**, 4555–4564.
198 M. Driess, *Nat. Chem.*, 2012, **4**, 525–526.
199 T. J. Hadlington, J. A. B. Abdalla, R. Tirfoin, S. Aldridge and C. Jones, *Chem. Commun.*, 2016, **52**, 1717–1720.
200 A. Knights, Part II Thesis, University of Oxford, 2015.
201 A. V. Protchenko and S. Aldridge, *Unpubl. Results*.
202 Y. Ishida, B. Donnadieu and G. Bertrand, *Proc. Natl. Acad. Sci.*, 2006, **103**, 10–13.

Chapter II

General Methods and Instrumentation

2.1 Manipulation of Air-Sensitive Compounds

Some of the compounds used in the work presented in this thesis are air- or moisture-sensitive; preparation, manipulation and reactivity of these compounds therefore required handling under an inert atmosphere, unless otherwise stated.

2.1.1 Inert Atmosphere Techniques

Air- and moisture-sensitive compounds are most commonly stored and handled in the solution or solid phases using Schlenk lines and/or glove boxes which, in the case of this work, were maintained under an inert argon or nitrogen atmosphere, respectively.[1,2]

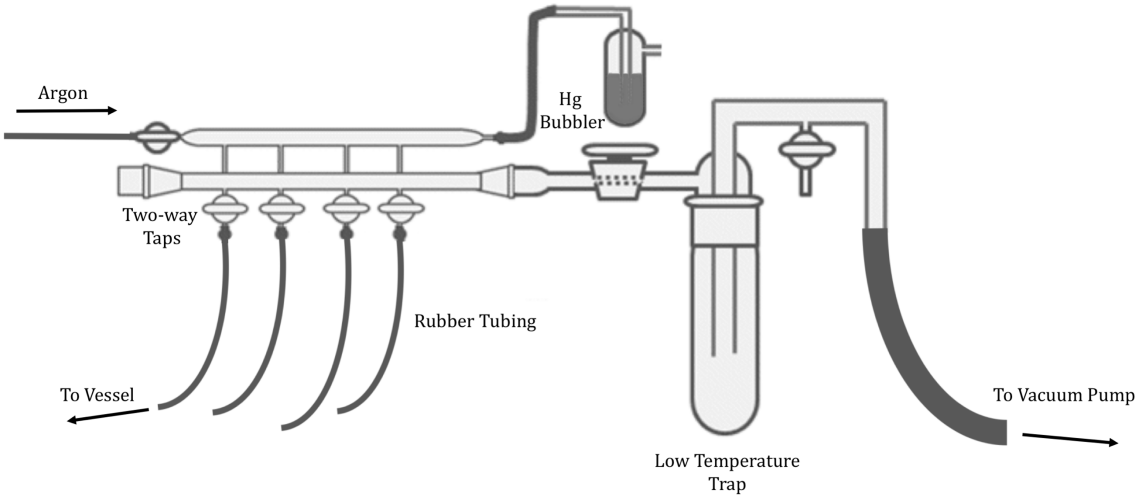

Figure 2.1 A Schlenk line. Figure adapted from Sarah Millar, copyright: Wiley-VCH Verlag GmbH & Co. KGaA, Weinheim.[3]

Solution-phase manipulations are generally conducted using Schlenk lines, which have shown to be a reliable way of minimizing exposure to oxygen and moisture.[4] They consist of a dual Pyrex glass manifold, one of which is connected to an argon inlet and the other to high vacuum. The pressure of the inert gas is maintained above atmospheric pressure by passing the argon stream through a mercury bubbler; the pressure in the vacuum manifold is monitored by a Pirani pressure gauge and generally maintained at 10^{-2} mbar. The reaction vessels can be connected to the Schlenk line *via* rubber tubing and opened to the vacuum or argon manifolds using either J. Young's taps or two-way taps with ground joints, lubricated with high vacuum grease, in order to produce an air-tight seal. Between the vacuum manifold and the vacuum pump is a trap, which is cooled using liquid nitrogen to ensure that solvents and other volatiles do not enter the pump. To ensure air- and moisture-free atmosphere in the reaction vessels, three 'pump-fill' cycles are applied, where the Schlenk tubes or J. Young's ampoules are evacuated to *ca.* 10^{-2} mbar, before being back-filled with argon. During the first vacuum cycle, the glass is thoroughly heated using a Bunsen burner to ensure removal of traces of moisture from the glass. The glass joints on the Schlenk tubes are also lubricated with high vacuum grease in order to produce an air-tight seal. Solutions are transferred using syringes (which are purged three times with argon prior to use) or cannulae by inducing a pressure gradient between the two vessels. The cannulae are fitted with glass-fibre filter paper for filtration of solutions.

Glove boxes were used for storage, manipulation of solids or preparation of NMR samples. The air- and moisture-free atmosphere is maintained by using nitrogen that has been passed through an activated copper catalyst and molecular sieves to remove oxygen and moisture, respectively. Compounds and apparatus are brought into the

box using an anti-chamber which is 'pump-filled' three times before being opened to the atmosphere of the glove box. Neoprene gloves are fitted to the glove box to allow access to the sealed box.

2.2 Spectroscopic and Analytical Techniques

The work presented in this thesis involved a range of spectroscopic and analytical characterization techniques. The details of each method are outlined below.

2.2.1 Nuclear Magnetic Resonance Spectroscopy

^{1}H, ^{7}Li, ^{11}B, ^{13}C, ^{19}F, ^{29}Si, ^{31}P, ^{77}Se and ^{119}Sn NMR spectra were measured using a Bruker Avance III HD nanobay 400 MHz spectrometer equipped with a 9.4 T magnet, a Bruker Avance 500 MHz spectrometer equipped with a 11.75 T magnet, or a Bruker Avance 500 MHz spectrometer equipped with a 11.75 T magnet and a ^{13}C detect cryoprobe. For ^{1}H and ^{13}C NMR spectroscopy, the residual peaks of the deuterated solvent were used as internal references. ^{7}Li, ^{11}B, ^{19}F, ^{29}Si, ^{31}P, ^{77}Se and ^{119}Sn NMR spectroscopy were externally referenced to: 1 M LiCl in D_2O, $BF_3{\cdot}OEt_3$ (both ^{11}B and ^{19}F) $SiMe_4$, 85% aqueous H_3PO_4 in C_6D_6, $SePh_2$ in $CDCl_3$ and Me_4Sn in C_6D_6, respectively. All ^{13}C NMR spectra were measured with proton decoupling. Measurements on the ^{13}C detect cryoprobe were carried out by Ms. Tina Jackson, University of Oxford. Homonuclear correlation spectroscopy (COSY), heteronuclear single-quantum correlation spectroscopy (HSQC), heteronuclear multiple-bond correlation spectroscopy (HMBC) and rotating frame nuclear Overhauser effect spectroscopy (ROESY) were used to aid assignment of resonances of ^{1}H and ^{13}C chemical shifts. Air- and moisture-sensitive NMR samples were prepared under an inert atmosphere in J. Young's valve NMR tubes and prepared using Schlenk line techniques or in a glove box.

2.2.2 Infrared Spectroscopy

Infrared spectra were measured on a Nicolet 500 FT-IR spectrometer. Samples were prepared on the Schlenk line with air- and moisture-free dichloromethane in a sealed solution phase IR cell.

2.2.3 Mass Spectroscopy

EI and CI measurements of charge-neutral molecules were carried out by Mr. Colin Sparrow and Dr. James Wickens, University of Oxford. Charged compounds were measured using a Bruker MicroTOF ESI mass spectrometer connected to a glove box *via* PEEK tubing.[5]

2.2.4 Elemental Microanalysis

Elemental microanalyses were carried out by Mr. Stephen Boyer, London Metropolitan University.

2.2.5 X-Ray Crystallography

Single crystals were mounted on MiTeGen MicroMounts using perfluoropolyether oil and cooled rapidly in a stream of cold N_2 using an Oxford Cryosystems Cryostream unit. X-ray data was collected on Bruker-Nonius KappaCCD and Oxford Diffraction (Agilent) SuperNova diffractometers using Mo-K_α or Cu-K_α radiation, respectively. For exceptionally small crystals ((**14**)$Rh(CO)_2Cl$ and (**28**)Sn), data were collected using I19-1 beamline at the Diamond Light Source at 100 K.[6] Data was reduced using the DENZO/SCALEPACK[7] or CrysAlisPro. Structure determinations were carried out using SIR92[8] or SuperFlip,[9] and refined with full-matrix least-squares within CRYSTALS[10,11] or SHELX.[12] Data collection and structure determinations were carried out by either Dr. Jesús Campos Manzano, Dr. Eugene Kolychev, Dr. Jamie Hicks or Dr.

M. Ángeles Fuentes, of the Aldridge group, or Dr. Amber L. Thompson or Dr. Kirsten E. Christensen, of the Oxford Crystallography service.

2.2.6 Theoretical Calculations

Density Functional Theory (DFT) calculations, including geometry optimizations, and determination of the energies of the frontier orbitals of the free carbenes and tetrelenes, along with fragmentation analyses for nickel carbene complexes were performed using the Amsterdam Density Functional (ADF) 2014 software package and were carried out by Haoyu Niu, of the Aldridge group. Vosko-Wilk-Nusair local density approximation with exchange from Becke,[13] were used with correlation correction from Perdew[14] and 3-dimensional dispersion effect (BP86-D3).[20] For the triple zeta basis set, Slater-type orbitals (STOs)[15] were used with an additional set of polarization functions (TZP).[16] The full-electron basis set approximation was applied with no molecular symmetry and geometric details and molecular orbital energies were obtained after unrestricted geometry optimization. Calculations were performed in the gas phase and general numerical quality was good.

The computational work on the activation barrier for the intramolecular 1,2-rearrangements of **14** and **20** utilized the DFT level within the Gaussian09 (Revision D.01) program package and was carried out by Dr. Petra Vasko, of the Aldridge group.[17] The PBE1PBE exchange-correlation functional with def-TZVP basis sets and a solvent model (pcm, toluene) was used for geometry optimizations.[18–22] Additionally, Grimme's empirical dispersion correction scheme was employed.[23,24] The nature of all stationary points found (minimum or saddle point) was confirmed by full frequency calculations.

2.2.7 Electron Paramagnetic Resonance Spectroscopy

X-band CW EPR experiments were performed at the Centre for Advanced ESR (CAESR) by Dr. William Myers on a Bruker BioSpin EMXmicro spectrometer equipped with an EMX Premium Gunn bridge and an ER 4122SHQE-W Bruker BioSpin cylindrical TE011 resonator. Spectra were measured at 294 K with a microwave frequency of 9.8352 GHz: the microwave power was 0.5 mW, the time constant was 20.48 ms for a sweep of 60 sec. over 200 Gauss, the modulation amplitude was 1 Gauss and the Q-value was 7800. The spectrum at each time point was the average of 5 field sweeps.

2.2.8 Percentage Buried Volume (%V_{bur})

%V_{bur} was calculated using the SambVca 2.0 program,[25] the radius of the sphere was set at 3.5 Å, the metal-carbene distance set at d = 2.00 Å, the Bondi radii scaled by 1.17 and the mesh spacing value set at 0.10 Å.

2.3 Preparation and Purification of Starting Materials

2.3.1 Commercially Available Starting Materials

Most commercially available compounds, solvents and gases were purified prior to use. The information on the supplier, purity and the method of further purification for these starting materials is provided as a table in the Appendix on the attached CD.

2.3.2 Syntheses of Starting Materials

Na[$BAr^F{}_4$] was synthesized by Haoyu Niu, Aldridge Group (University of Oxford), following methods reported in the primary literature.[26] Mesityllithium[27] and benzyl potassium[28] were synthesized by Dr. Arnab Rit, Aldridge Group, following methods reported in the primary literature. $[Rh(cod)Cl]_2$ was synthesized by Dr. Joseph Abdalla, Aldridge group, according to a procedure published by Crabtree *et al.*[29]

[(BICAAC^{Me})H][BF_4] was synthesized by Eder Tomás-Mendivil, Bertrand group (University of California, San Diego).[30] [(IPr)H][BF_4],[31] IPr[32] and IPr·$SiCl_2$[33] were synthesized by Rachel Grabiner, Aldridge group, following methods reported in the primary literature. Tris(pentafluorophenyl)borane was synthesized by Dr. Zhenbo Mo, Aldridge group, following methods reported in the primary literature.[34] Sn{$N(SiMe_3)_2$}$_2$ was synthesized by Alastair Knights, Aldridge group, following a modified method similar to procedures reported by Gynane *et al*.[35] and Heidemann *et al*.[36]

Preparation of PPh_3·BBr_3 (2.1)

The synthesis of **2.1** followed a modified method similar to that reported by Gee *et al*.[37] To a solution of triphenylphosphine (15 g, 59 mmol) in pentane (450 mL) was slowly added boron tribromide (5.6 mL, 59 mmol), which resulted in the immediate formation of a white precipitate. The reaction mixture was stirred overnight and after filtration, the resulting precipitate washed with pentane (3 x 25 mL) and dried *in vacuo* to afford **2.1** as a white powder. Yield: 28 g, 93%. A single product is observed in the ^{11}B and ^{31}P NMR spectra and the ^{11}B NMR spectrum is consistent with a four-coordinate boron centre.[38]

Preparation of *N,N*'-Bis(2,6-diisopropylphenyl)diazabutadine (2.2)

The synthesis of **2.2** followed a method similar to that reported by Jafarpour *et al*.[32] The reaction was not carried out under inert conditions. To a mixture of 2,6-diisopropylaniline (30 mL, 160 mmol) and glyoxal (9.0 mL of a 40% solution in H_2O, 80 mmol) in ethanol (170 mL) was added a few drops of formic acid, which resulted in the immediate formation of a yellow precipitate. The reaction mixture was stirred for 2 d and filtered. The resulting solid was washed with cold methanol (3 x 25 mL) and dried *in vacuo* to afford the product as a yellow powder. Yield: 22 g, 73% yield.

The ^{1}H NMR data is in accordance with literature values.[32]

Preparation of *N,N*'-Bis(2,6-diisopropylphenyl)-2-bromo-2,3-dihydro-1H-1,3,2-diazaborole (1)

The synthesis of **1** followed a modified procedure similar to that reported by Herrmannsdörfer *et al.*[39] **2.1** (20 g, 39 mmol) and **2.2** (15 g, 39 mmol) were refluxed for 48 h in diethyl ether (350 mL), producing a red solution with a white precipitate. Volatiles were removed *in vacuo* and the residue extracted into in hexane (300 mL and 3 x 50 mL). The filtrate was concentrated to *ca.* 20% of the original volume and stored at -20 °C, producing orange crystals. After filtration, the solid was washed with cold hexane (3 x 20 mL) to afford **1** as an orange crystalline solid. Yield: 13 g, 72%. The ^{1}H NMR data is in accordance with literature values.[39]

Preparation of *N,N*'-Bis(2,6-diisopropylphenyl)- 2,3-dihydro-1H-1,3,2-diazaborol-2-amine (2)

The synthesis of **2** followed a modified procedure similar to that reported by Hadlington *et al.*[40] Ammonia was purged through a stirred solution of **1** (16 g, 24 mmol) in dichloromethane (200 mL) for 30 min, resulting in an instant colour change from dark red to pale pink, with formation of white precipitate. The ammonia inlet was removed and the solution stirred overnight. After filtration, volatiles were removed *in vacuo* to afford **2** as a light brown solid. Yield: 14 g, 99%. The ^{1}H NMR data is in accordance with literature values.[40]

Preparation of Phenyllithium

The synthesis of phenyllithium followed a modified procedure similar to that reported by Fraenkel *et al.*[41] To a solution of bromobenzene (6.0 mL, 57 mmol) in

hexane (120 mL) was added dropwise ^{n}BuLi (38 mL of a 1.6 M solution in hexane, 60 mmol) at room temperature over 30 min. The reaction mixture was left to stand undisturbed for 24 h, which allowed for the gradual formation of colourless crystals. After filtration, the crystals were washed with hexane (3 x 20 mL) and dried *in vacuo* to afford phenyllithium as a white crystalline solid. Yield: 3.8 g, 79% yield. The ^{1}H NMR data is in accordance with literature values.[41]

Preparation of $H[AuCl_4]\cdot 4H_2O$

The synthesis of $H[AuCl_4]\cdot 4H_2O$ was adapted from a synthetic procedure reported by Brandys *et al.*[42] The reaction was not carried out under inert conditions. To a suspension of gold powder (2.4 g, 12 mmol) in HCl (31 mL) was added dropwise HNO_3 (7.9 mL). The solution was gently boiled and brown vapours evolved. More HCl was added until the brown colour of the vapours had disappeared. The HCl was boiled off, affording the crude product, which was used in the subsequent synthesis of (THT)AuCl without further purification.

Preparation of (THT)AuCl

(THT)AuCl was synthesized according to a procedure reported by Uson *et al.*[43] The reaction was not carried out under inert conditions. To a solution of $H[AuCl_4]\cdot 4H_2O$ in a mixture of water and diethyl ether (10 mL:50 mL) was added dropwise tetrahydrothiophene (2.2 mL, 0.025 mmol) and the solution stirred for 10 min. After filtration, the grey precipitate was washed with diethyl ether and dried *in vacuo* to afford the product as a grey powder. Yield: 2.6 g, 67%. In order to estimate the purity of the product, (THT)AuCl (20 mg, 0.076 mmol) and PPh_3 (24 mg, 0.076 mmol) were dissolved in THF in an NMR tube. Complete consumption of PPh_3 to form $(PPh_3)AuCl$ was observed by ^{31}P NMR spectroscopy,[44] indicating high purity of (THT)AuCl. The

product was stored under inert atmosphere in a schlenk tube at 5 °C.

Preparation of 4,5-Dimethylimidazole

4,5-Dimethylimidazole was synthesized according to a modified procedure similar to that reported by Li *et al*.[45] The work-up procedure reported in this paper was not found to be effective and an alternative work-up procedure reported by Serpell *et al*.[46] was used instead. The reaction was not carried out under inert conditions. 2,3-Butadione (0.70 mL, 8.0 mmol), paraformaldehyde (0.24 g, 8.0 mmol) and ammonium hydroxide (0.90 mL of a 35% solution, 16 mmol) were dissolved in water (140 mL) and stirred overnight. The reaction mixture was quenched with concentrated K_2CO_3 and the product extracted into diethyl ether (used as supplied, 4 x 50 mL). The combined extracts were dried over $MgSO_4$, filtered and the volatiles removed *in vacuo*. The brown oil was sublimed *in vacuo* at 80 °C to yield the product as a white powder. Yield: 0.16 g, 84%. The ^{1}H NMR data is in accordance with literature values.[45]

Preparation of $[Rh(CO)_2Cl]_2$

$[Rh(CO)_2Cl]_2$ was synthesized according to a procedure reported by Berre *et al.*[47] In a J. Young's ampoule, $RhCl_3 \cdot 3H_2O$ (1.0 g, 2.8 mmol) was dissolved in methanol (degassed, 25 mL) and CO purged through the solution for 30 min. The ampoule was sealed and the reaction mixture stirred at 65 °C for 20 h. Subsequent steps did not need to be carried out under inert atmosphere. The solvent was carefully removed *in vacuo* and sublimation of the product avoided. Red crystals were obtained, which were sublimed in static vacuum at 50 °C to yield the product as a red crystalline solid. Yield: 0.49 g, 66%. The product was used as is, without further purification and stored under argon in a Schlenk tube at 5 °C.

Preparation of 3,4,5,6-Tetrahydropyrimidine

3,4,5,6-Tetrahydropyrimidine was synthesized according to a slightly modified procedure based on that reported by Aoyagi *et al*.[48] In a J. Young's ampoule, a mixture of *N*,*N*-dimethylformamide dimethyl acetal (1.9 mL, 14 mmol) and 1,3-diaminopropane (1.2 mL, 14 mmol) was dissolved in toluene (8 mL), and the reaction mixture warmed to 100 °C. The reaction mixture was stirred and monitored by ^{1}H NMR spectroscopy, with complete conversion observed after 5 d. Volatiles were removed *in vacuo* at room temperature and the residue distilled under static vacuum at 80 °C to afford the product as a colourless viscous liquid. Yield: 0.60 mL, 55%. The product was stored in a J. Young's ampoule. The ^{1}H NMR data is in accordance with literature values.[48]

2.3.3 General Procedure for Addition of Dihydrogen to Tetrelenes

In a high pressure J. Young's NMR tube, a sample of (**28**)Ge, (**28**)Sn or (**29**)Sn (*ca*. 0.02 mmol) in C_6D_6 or toluene-d_8 (*ca*. 0.5 mL) was degassed by three freeze-pump-thaw cycles, and backfilled with H_2 at 77 K. The internal H_2 pressure on warming was *ca*. 4 atm.

2.4 References

1 R. E. Todd and P. L. Robinson, *Experimental Inorganic Chemistry. A Guide to Laboratory Practice*, Elsevier Publishing Co., Amsterdam, 1958.

2 R. J. Errington, *Advanced Practical Inorganic and Metalorganic Chemistry*, Blackie Academic and Professional, London, 1997.

3 S. Millar, Tips and Tricks for the Lab: Air-Sensitive Techniques, http://www.chemistryviews.org/details/education/3728881/Tips_and_Tricks_for_the_Lab_Air-Sensitive_Techniques_1.html, (accessed 16 March 2018).

4 D. F. Shriver and M. Drezdzon, *The Manipulation of Air-Sensitive Compounds,* Wiley-Interscience, 2nd edn., 1986.

5 A. T. Lubben, J. S. McIndoe and A. S. Weller, *Organometallics*, 2008, **27**, 3303–3306.

6 H. Nowell, S. A. Barnett, K. E. Christensen, S. J. Teat and D. R. Allan, *J. Synchrotron Radiat.*, 2012, **19**, 435–441.
7 Z. Otwinowski and W. Minor, *Methods Enzymol.*, 1997, **276**, 306–315.
8 G. Cascarano, C. Giacovazzo and A. Guagliardi, *J. Appl. Cryst.*, 1993, **26**, 343–350.
9 L. Palatinus and G. Chapuis, *J. Appl. Crystallogr.*, 2007, **40**, 786–790.
10 A. L. Thompson and D. J. Watkin, *J. Appl. Crystallogr.*, 2011, **44**, 1017–1022.
11 R. I. Cooper, A. L. Thompson and D. J. Watkin, *J. Appl. Crystallogr.*, 2010, **43**, 1100–1107.
12 G. M. Sheldrick, *Acta Cryst.*, 2008, **A64**, 112–122.
13 A. D. Becke, *Phys. Rev. A*, 1988, **38**, 3098–3100.
14 J. P. Perdew, *Phys. Rev. B*, 1986, **33**, 8822–8824.
15 J. C. Slater, *Phys. Rev.*, 1930, **36**, 57–64.
16 E. Lenthe and E. J. Baerends, *J. Comput. Chem.*, 2002, **24**, 1142–1156.
17 M. J. Frisch, G. W. Trucks, H. B. Schlegel, G. E. Scuseria, M. A. Robb, J. R. Cheeseman, G. Scalmani, V. Barone, B. Mennucci, G. A. Petersson, H. Nakatsuji, M. Caricato, X. Li, H. P. Hratchian, A. F. Izmaylov, J. Bloino, G. Zheng, J. L. Sonnenberg, M. Hada, M. Ehara, K. Toyota, R. Fukuda, J. Hasegawa, M. Ishida, T. Nakajima, Y. Honda, O. Kitao, H. Nakai, T. Vreven, J. A. J. Montgomery, J. E. Peralta, F. Ogliaro, M. Bearpark, J. J. Heyd, E. Brothers, K. N. Kudin, V. N. Staroverov, R. Kobayashi, J. Normand, K. Raghavachari, A. Rendell, J. C. Burant, S. S. Iyengar, J. Tomasi, M. Cossi, N. Rega, J. M. Millam, M. Klene, J. E. Knox, J. B. Cross, V. Bakken, C. Adamo, J. Jaramillo, R. Gomperts, R. E. Stratmann, O. Yazyev, A. J. Austin, R. Cammi, C. Pomelli, J. W. Ochterski, R. L. Martin, K. Morokuma, V. G. Zakrzewski, G. A. Voth, P. Salvador, J. J. Dannenberg, S. Dapprich, A. D. Daniels, J. B. F. Ö. Farkas, J. V. Ortiz and J. Cioslowski, *Gaussian 09, Revision D.01*, Gaussian, Inc., Wallingford CT, 2009.
18 J. P. Perdew, M. Ernzerhof, K. Burke, J. P. Perdew, M. Ernzerhof and K. Burke, *J. Chem. Phys.*, 1996, **105**, 9982–9985.
19 C. Adamo, V. Barone and C. Adamo, *J. Chem. Phys.*, 1995, **110**, 6158–6170.
20 J. P. Perdew, K. Burke and M. Ernzerhof, *Phys. Rev. Lett.*, 1996, **77**, 3865–3868.
21 J. P. Perdew, K. Burke and M. Ernzerhof, *Phys. Rev. Lett.*, 1997, **77**, 1396.
22 A. Schäfer, C. Huber, R. Ahlrichs, A. Schafer, C. Huber and R. Ahlrichs, *J. Chem. Phys. 100,* 2010, **100**, 5829–5835.
23 S. Grimme, J. Antony, S. Ehrlich, H. Krieg, S. Grimme, J. Antony, S. Ehrlich and H. Krieg, *J. Chem. Phys. 1*, 2010, **132**, 154104–154119.
24 S. Grimme, S. Ehrlich and L. Goerigk, *J. Comput. Chem.*, 2011, **32**, 1456–1465.
25 L. Falivene, R. Credendino, A. Poater, A. Petta, L. Serra, R. Oliva, V. Scarano and L. Cavallo, *Organometallics*, 2016, **35**, 2286–2293.
26 D. L. Reger, T. D. Wright, C. A. Little, J. J. S. Lamba and M. D. Smith, *Inorg. Chem.*, 2001, **40**, 3810–3814.
27 K. Kajiyama, M. Yoshimune, M. Nakamoto, S. Matsukawa, S. Kojima and K. Akiba, *Org. Lett.*, 2001, **3**, 12866–12867.
28 P. J. Bailey, R. A. Coxall, C. M. Dick, S. Fabre, L. C. Henderson, C. Herber, S. T. Liddle, D. Loroño-González, A. Parkin and S. Parsons, *Chem. Eur. J.*, 2003, **9**, 4820–4828.

29 Giordano G. H. and Crabtree R., *Inorg. Synth., Volume 28*, John Wiley & Sons, Inc., Hoboken, NJ, USA, 1990.
30 E. Tomás-Mendivil, M. M. Hansmann, C. M. Weinstein, R. Jazzar, M. Melaimi and G. Bertrand, *J. Am. Chem. Soc.*, 2017, **139**, 7753–7756.
31 L. Hintermann, *Beilstein J. Org. Chem.*, 2007, **3**, No. 22.
32 L. Jafarpour, E. D. Stevens and S. P. Nolan, *J. Organomet. Chem.*, 2000, **606**, 49–54.
33 R. S. Ghadwal, H. W. Roesky, S. Merkel, J. Henn and D. Stalke, *Angew. Chem. Int. Ed.*, 2009, **48**, 5683–5686.
34 W. E. Piers and T. Chivers, *Chem. Soc. Rev.*, 1997, **26**, 345–354.
35 B. M. J. S. Gynane, D. H. Harris, M. F. Lappert, P. P. Power and P. Rivière, Rivière-Baudet, *J. Chem. Soc. Dalt. Trans*, 1977, **20**, 2004–2009.
36 T. Heidemann and S. Mathur, *Eur. J. Inorg. Chem.*, 2014, **2014**, 506–510.
37 W. Gee, R. A. Shaw and B. C. Smith, *J. Chem. Soc.*, 1964, **0**, 4180–4183.
38 B. Wrackmeyer, *Nuclear Magnetic Resonance Spectroscopy of Boron Compounds Containing Two-, Three- and Four-Coordinate Boron*, 1988, vol. 20.
39 D. Herrmannsdorfer, M. Kaaz, O. Puntigam, J. Bender, M. Nieger and D. Gudat, *Eur. J. Inorg. Chem.*, 2015, **2015**, 4819–4828.
40 T. J. Hadlington, J. A. B. Abdalla, R. Tirfoin, S. Aldridge and C. Jones, *Chem. Commun.*, 2016, **52**, 1717–1720.
41 G. Fraenkel, S. Subramanian and A. Chow, *J. Am. Chem. Soc.*, 1995, **117**, 6300–6307.
42 M. C. Brandys, M. C. Jennings and R. J. Puddephatt, *J. Chem. Soc. Dalton Trans.*, 2000, **0**, 4601–4606.
43 R. Uson, A. Laguna, M. Laguna, D. A. Briggs, H. H. Murray and J. P. Fackler, *Inorg. Synth., Volume 26*, John Wiley & Sons, Inc., Hoboken, NJ, USA, 1989.
44 C. Nieto-Oberhuber, S. López and A. M. Echavarren, *J. Am. Chem. Soc.*, 2005, **127**, 6178–6179.
45 L. Li, V. S. Lelyveld, N. Prywes and J. W. Szostak, *J. Am. Chem. Soc.*, 2016, **138**, 3986–3989.
46 C. J. Serpell, N. L. Kilah, P. J. Costa, V. Félix and P. D. Beer, *Angew. Chem. Int. Ed.*, 2010, **49**, 5322–5326.
47 C. S. Berre, M. Etienne, J. Daran and P. Kalck, *Eur. J. Inorg. Chem.*, 2001, **2001**, 2689–2697.
48 N. Aoyagi, Y. Furusho, Y. Sei and T. Endo, *Tetrahedron*, 2013, **69**, 5476–5480.

Chapter III

Syntheses and Reactivity of *N*,*N*'-Bisborylated Imidazoles and Imidazolium Salts

---

3.1 Introduction

Singlet carbenes, and *N*-heterocyclic carbenes in particular, have attracted remarkable interest in the past three decades. Such species possess a formally vacant p_π-orbital (LUMO) and filled σ-orbital (HOMO). The HOMO-LUMO energy gap of the carbene can be tuned, for example by changing its substituents or by adjusting the angle at carbon (section 1.1). The most common class of carbenes are *N*-heterocyclic carbenes, which are stabilized by α-nitrogen substituents that are both σ-withdrawing and π-donating. These electronic properties, as well as the incorporation of the carbene into a cyclic structure (which narrows the angle at C), serve to increase the HOMO-LUMO energy gap of the carbene and thus stabilize it. In addition, sterically demanding *N*-substituents provide kinetic stabilization with respect to dimerization.

Using bulky Dipp-substituted diazaboryl groups ({$B(NDippCH)_2$} = [B]; Figure 3.1) as the *N*-substituents is likely to affect both the electronic and steric properties of the carbene. Strong σ-donation from the boryl substituents will likely augment the σ-donor capability of the carbene. In addition, provided that the π-systems of the boryl moiety and the nitrogen lie close to parallel, potential exocyclic N-to-B π-interactions could decrease the overall π-donation to carbon from the adjacent N-donors, resulting in a more π-acidic carbene centre. However, due to the great steric bulk of a Dipp-substituted boryl group, coplanarity of the boryl group and the imidazole ring

cannot be guaranteed – certainly not for both boryl substituents – and smaller groups may be required if significant tuning of the carbene π-properties is required. On the other hand, the presence of two bulky boryl groups as *N*-substituents is likely to confer great steric bulk and potentially result in a super bulky NHC.

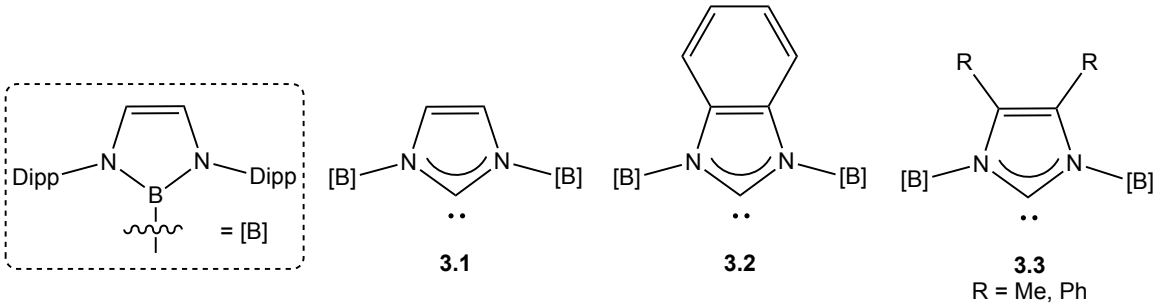

Figure 3.1 Targeted *N*,*N*'-bisborylated NHCs.

DFT calculations of the frontier orbitals of a hypothetical *N*,*N*'-bisborylated imidazolylidene (**3.1**; Figure 3.1) and other reported NHCs were carried out by Haoyu Niu, of the Aldridge group.[1] These indicate considerable changes in the σ-donating properties on incorporation of the boryl groups; with the σ-donor capability of **3.1** (as measured by the HOMO energy) being comparable with 6-membered saturated NHCs (Table 3.1).

	Free Carbene		
L	**HOMO**	**LUMO**	**ΔE**
3.1	-420.5	-28.9	398.3
IMes	-475.0	-33.1	441.9
SIMes	-462.9	-33.4	429.5
6Mes	-421.2	-41.9	379.3
7Mes	-402.8	-52.4	350.4

Table 3.1 DFT calculations on the frontier orbitals of 3.1 as well as other unsaturated and saturated NHCs. The table lists the energy of the HOMO (kJ mol^{-1}) and the LUMO (kJ mol^{-1}) of the free carbenes and their energy difference, ΔE (kJ mol^{-1}).[1]

From the calculated structure of the corresponding AuCl complex of **3.1** (Figure

3.2), the steric bulk of the hypothetical carbene can be calculated and compared with other carbenes. Using the SambVca 2.0 program,[2] a $\%V_{bur}$ of 70.4% is obtained for the bisborylated carbene, exceeding the bulkiest carbenes reported to date ($\%V_{bur}$ of 57.4% and 57.3%).[3,4]

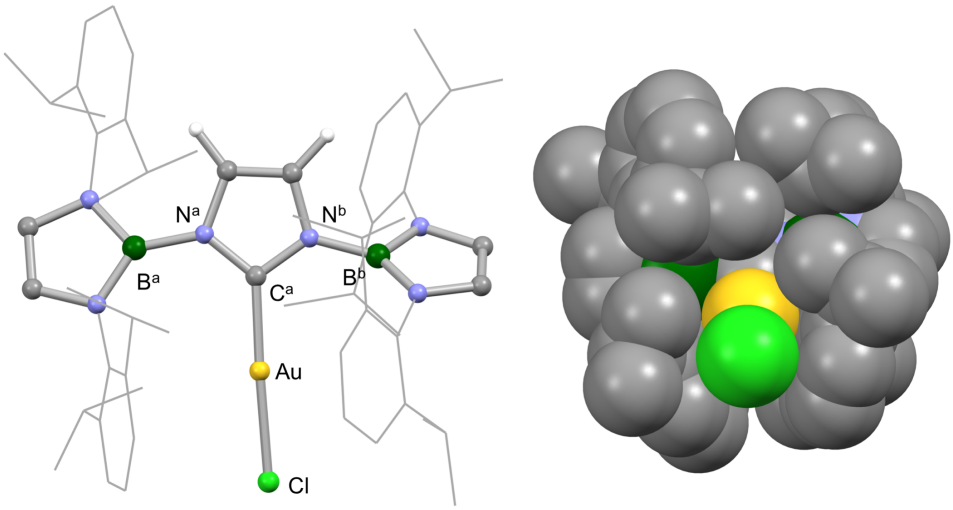

Figure 3.2 (Left) Molecular structure of (3.1)AuCl as determined by DFT calculations. Most hydrogen atoms omitted, and Dipp groups shown in wireframe format for clarity. (Right) Space-filling representation of (3.1)AuCl highlighting the extreme steric protection that the boryl groups offer.

It is worth emphasizing that a variety of *N*-substituents have previously been shown to be prone to migrate to the C2 carbon, thereby quenching the carbene function.[5–14] Very recently, Liu *et al.* reported such a 1,2-shift to be facile for a diarylboryl group (BAr_2, Ar = mesityl, 2,6-xylyl; Scheme 3.1) within an imidazole-derived skeleton.[14] The migration was reported to be so rapid that the putative carbenes could not be observed, presumably as the degree of steric bulk, both on the boryl group and the *N*-substituted butyl group, is not sufficient to hinder the rearrangement. Increasing the steric bulk of both *N*-substituents (*e.g.* by using bulky Dipp substituted diazaboryl groups), could allow for the isolation (or *in situ* metalation) of an NHC bearing pendant boryl groups as *N*-substituents, on the basis that the corresponding 1,2-

rearrangement would necessarily bring the two bulky groups much closer together.

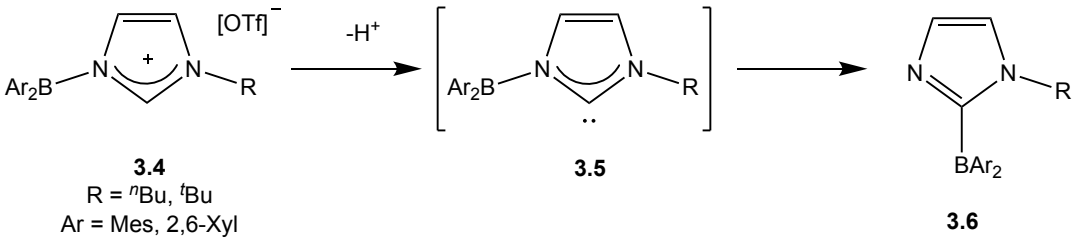

Scheme 3.1 1,2-Migration of an *N*- boryl group in the putative carbene 3.5.[14]

Among the most common NHC precursors are the corresponding imidazolium salts, which can be deprotonated to yield the free carbene. An extensively used method to synthesize the imidazolium precursors is cyclization of an *N*,*N*'-disubstituted diimine and a precarbenic unit, such as trialkyl orthoformate or paraformaldehyde. The diamines are often obtained from a reaction of glyoxal and the respective primary amine (Scheme 3.2).[15–17] Alternatively, the imidazolium precursors can be accessed by stepwise alkylation of an imidazolide anion (Scheme 3.2).[16,17]

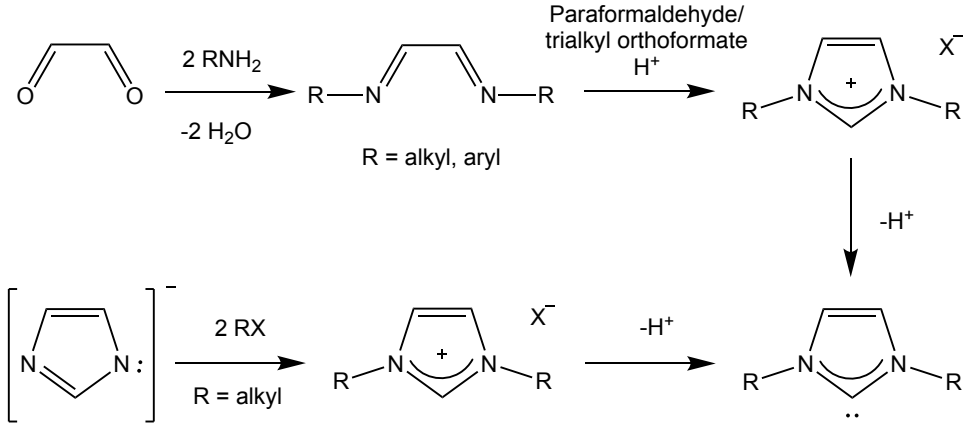

Scheme 3.2 Common syntheses of imidazolium salts: (upper) by introduction of a precarbenic unit to a diamine and (lower) alkylation of an imidazolide anion, and the subsequent deprotonation to give the respective NHCs.[15–17]

The aim of the research reported in this chapter is to establish viable syntheses of a range of *N*,*N*'-bisborylated imidazolium salts and thereby access the corresponding

NHCs and/or their metal complexes. The target carbenes are depicted in Figure 3.1. To aid discussion, especially of NMR assignments, key terms that are used throughout the thesis are outlined in Figure 3.3, which shows the structure of the boryl group on the left and the imidazole heterocycle on the right. Position *a* will generally be referred to as boryl group 'backbone' position, position *b* and *c* are the 'isopropyl methine/methyl groups', position *d* the 'imidazole backbone' and position *e* is 'C2 position'; or taken together, positions *d* and *e* will be collectively referred to as imidazole/imidazolium protons/carbons.

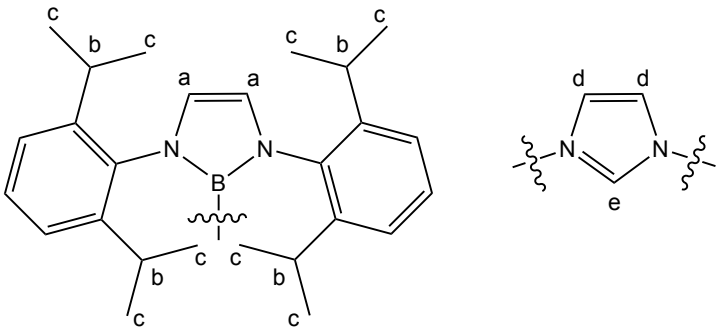

Figure 3.3 Labelling of various positions of the boryl group (left) and the imidazole heterocycle (right).

3.2 Results and Discussion

3.2.1 Syntheses of an *N*-Monoborylated Imidazole and *N,N'*-Bisborylated Imidazolium Salts

With the aim of accessing carbene **3.1** (Figure 3.1), the synthesis of an *N,N'*-bisborylated imidazolium salt was attempted. Initial attempts were made *via* the upper synthetic route depicted in Scheme 3.2, by reacting a diamine with a precarbenic unit. To access an *N,N'*-bisborylated diamine, aminoborane **2** was synthesized (Scheme 3.3) from a reaction of **1** and gaseous NH_3 in dichloromethane.[18] Subsequent reaction of **2** with glyoxal was attempted, targeting the borylated

diazabutadiene. Aminoborane **2** exhibits resistance to both water and acid but the reaction with glyoxal proved unsuccessful. Synthesis of the target imidazolium precursor *via* stepwise electrophilic attack at an imidazolide anion was therefore attempted instead (see Scheme 3.2, lower route).

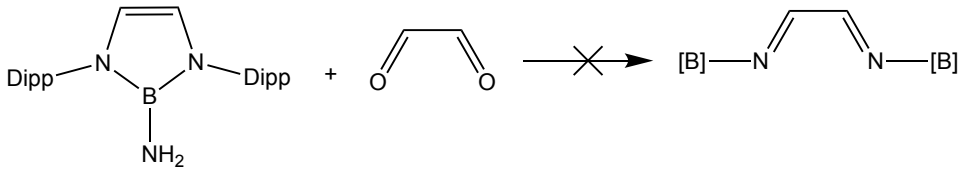

2

Scheme 3.3 Attempted reaction of aminoborane 2 with glyoxal.

The stoichiometric reaction of imidazole with **1** in acetonitrile can be monitored by ^{1}H NMR spectroscopy. Three inequivalent imidazole protons are present in the product, consistent with an unsymmetrical imidazole heterocycle and the uptake of a boryl group at one of the two nitrogen centres. Upon addition of a second equivalent of **1** in the presence of a base, symmetry is regained in the ^{1}H NMR spectrum; the two protons of the imidazole backbone are now equivalent, giving rise to a single resonance which integrates in a 2:1 ratio to the C2 proton. This suggests the formation of a bisborylated imidazolium species. This hypothesis is further supported by the 2:1 ratio of the ^{1}H NMR signals due to the backbone protons of the boryl heterocycles to the backbone protons of the imidazolium ring.

The monoborylated imidazole (**3**) can be selectively synthesized on a bulk scale *via* two (slightly) different routes, each involving the reaction of **1**, imidazole and a base: ^{n}BuLi in diethyl ether (78% yield) or sodium bis(trimethylsilyl)amide in benzene (41% yield) (Scheme 3.4). Recrystallization of **3** from hot acetonitrile tends to be the most convenient purification procedure for bulk quantities, but single crystals suitable for X-ray crystallography were grown by slow evaporation of

hexane. The crystal structure so obtained (Figure 3.4) confirms uptake of one boryl group by the imidazole heterocycle. The planes of the imidazole and the boryl moieties lie almost coplanar, rotated by only 5.9° with respect to each other. This orientation potentially allows for interaction between the p-orbitals of the imidazole nitrogen and the boron centre of the boryl heterocycle. The exocyclic B–N bond length of 1.515(3) Å does not, however, imply significant p-orbital overlap, being much longer than the average bond length of a typical coplanar B(3)–N(3) bond for $R_2B{=}NR'_2$ (R, R' = H, C, O, N), 1.409(34) Å.[19]

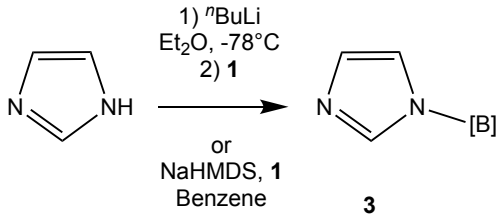

Scheme 3.4 Synthesis of monoborylated imidazole 3.

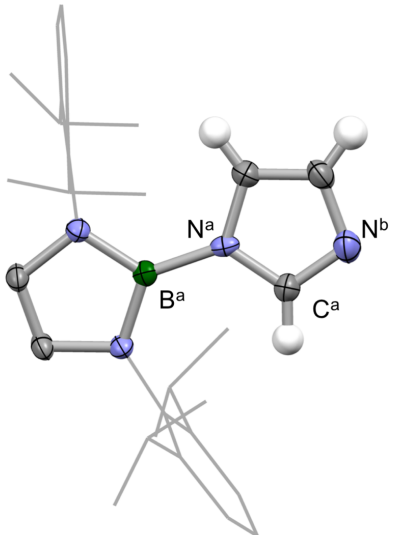

	(Å)/(°)
d(B[a]–N[a])	1.515(3)
d(C[a]–N[a])	1.346(3)
d(C[a]–N[b])	1.313(3)
∠(N[a]–C[a]–N[b])	111.1(2)
Θ([B[a]])	5.9

Figure 3.4 (Left) Molecular structure of 3 in the solid state, as determined by X-ray crystallography. Most hydrogen atoms omitted, and Dipp groups shown in wireframe format for clarity. Thermal ellipsoids set at the 40% probability level. (Right) Table of key structural parameters. Θ([B[a]]) indicates the angle between the plane of the boryl group and the imidazole heterocycle.

As mentioned above, *in situ* ^{1}H NMR spectroscopy suggests that upon addition of another equivalent of **1** to the monoborylated imidazole in MeCN-d_3, bisborylated imidazolium salt [(**4**)H]Br is obtained. Addition of a less polar solvent, such as benzene or THF, to [(**4**)H]Br results in complete (benzene) or partial (THF) reconversion to **3** and **1**, presumably *via* nucleophilic attack of Br^- on one of the boryl groups, which is driven in less polar media by generation of a charge neutral product. With this in mind, substitution of the Br^- counterion for a more weakly coordinating counterion (such as $[BPh_4]^-$, $[PF_6]^-$ or $[BAr^F{}_4]^-$) was thought to be needed in order to isolate the bisborylated imidazolium salt, $[(\mathbf{4})H]^+$ (Scheme 3.5). Accordingly, a one-pot procedure was developed for the formation of $[(\mathbf{4})H]^+$ in which 2.5 equivalents of **1** were initially reacted with imidazole in the presence of one equivalent of sodium bis(trimethylsilyl)amide. At this stage, one imidazole nitrogen is borylated. The solvent is then removed *in vacuo* and the residue redissolved in acetonitrile, under which conditions, a second boryl group is assimilated, and MX (MX = $Na[BPh_4]$, $K[PF_6]$, $Na[BAr^F{}_4]$) added in order to metathesize the anion. The bisborylated imidazolium salts, $[(\mathbf{4})H][BPh_4]$, $[(\mathbf{4})H][PF_6]$ and $[(\mathbf{4})H][BAr^F{}_4]$ were isolated in 64-87% yields (Scheme 3.5). Colourless single crystals of $[(\mathbf{4})H][BPh_4]$ suitable for X-ray crystallography were obtained by layering a dichloromethane solution with hexane.

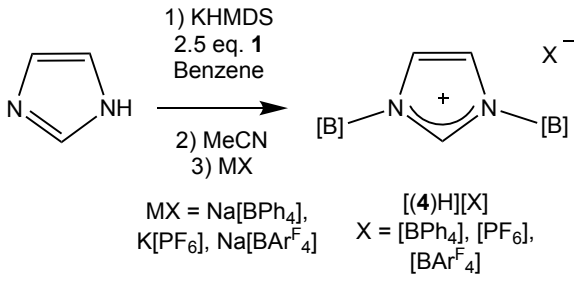

Scheme 3.5 Syntheses of bisborylated imidazolium salts [(4)H][BPh_4], [(4)H][PF_6] and [(4)H][$BAr^F{}_4$].

The crystal structure so obtained (Figure 3.5) confirms the nature of the bisborylated imidazolium cation in [(**4**)H][BPh_4]. Unsurprisingly, due to steric hindrance, only one of the boryl groups can now get close to coplanarity with the imidazolium heterocycle. An angle of 9.1° is found between the respective planes, whereas the other boryl group is rotated by 37.4°. The two exocyclic B–N bond lengths, however, are statistically identical (1.499(4) and 1.495(4) Å), despite the two different alignments, further suggesting that the π-interactions between the imidazole nitrogen and boron p-orbitals are not structurally significant.

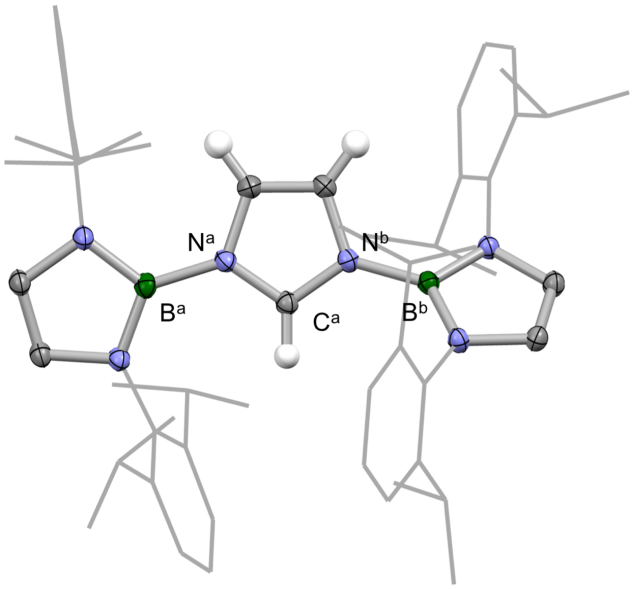

	(Å)/(°)
d(B^a–N^a)	1.499(4)
d(B^b–N^b)	1.495(4)
d(C^a–N^a)	1.342(3)
d(C^a–N^b)	1.343(3)
∠(N^a–C^a–N^b)	110.2(2)
Θ([B^a])	9.08
Θ([B^b])	37.4

Figure 3.5 (Left) Molecular structure of [(4)H][BPh_4] in the solid state, as determined by X-ray crystallography. Solvate molecule, counter-ion and most hydrogen atoms omitted, and Dipp groups shown in wireframe format for clarity. Thermal ellipsoids set at the 40% probability level. (Right) Table of key structural parameters. Θ([B]) indicates the angle between the plane of the boryl groups and the imidazolium heterocycle.

3.2.2 Reactivity of *N*,*N*'-Bisborylated Imidazolium Salts with Brønsted Bases

The most common Brønsted bases used for the deprotonation of carbene precursors are potassium *tert*-butoxide, lithium aluminum hydride, ^{n}BuLi, alkali metal

bis(trimethylsilyl)amides and 1,8-diazabicyclo[5.4.0]undec-7-ene (DBU).[16] Due to the oxophilicity of the boryl group, potassium *tert*-butoxide was not considered to be a convenient base for the deprotonation of [(**4**)H]$^+$. The reactivity of other Brønsted bases with [(**4**)H]$^+$ was therefore explored.

Deprotonation of [(**4**)H][BPh_4] was attempted using ^{n}BuLi in toluene at -78 °C. The ^{1}H NMR spectrum of an aliquot taken from the reaction mixture is consistent with a lowering of local symmetry in the 2,6-diisopropylphenyl (Dipp) groups, with two inequivalent isopropyl methine septets and four inequivalent isopropyl methyl doublets being observed, compared to one septet and two doublets for [(**4**)H]$^+$. The backbone protons and carbons of both the imidazole heterocycle and the boryl groups give rise to one singlet each in both the ^{1}H and ^{13}C NMR spectra, suggesting that the lowering of symmetry is unlikely to be caused by the presence of two inequivalent boryl groups. Additionally, several signals are observed in the range of 1.1-1.5 ppm and 23-38 ppm in the ^{1}H and ^{13}C NMR spectra, consistent with an alkyl group being present in the product. Colourless single crystals of the new product suitable for X-ray crystallography could be grown from diethyl ether. The structure of **4**(H)(^{n}Bu) so obtained (Figure 3.6) reveals attack of the *n*-butyl group at the C2 position of the imidazolium moiety and a lowering of symmetry above/below the central heterocycle plane consistent with the NMR data (Scheme 3.6).

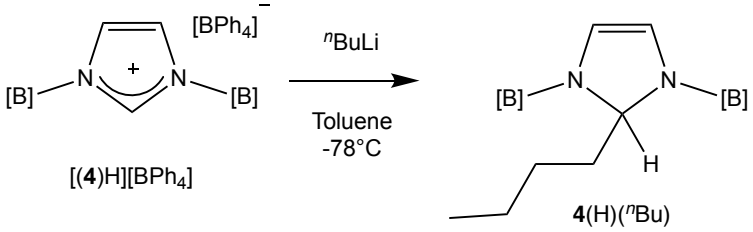

Scheme 3.6 Nucleophilic attack of ^{n}BuLi at C2 position of [(4)H]$^+$ to yield 4(H)(^{n}Bu).

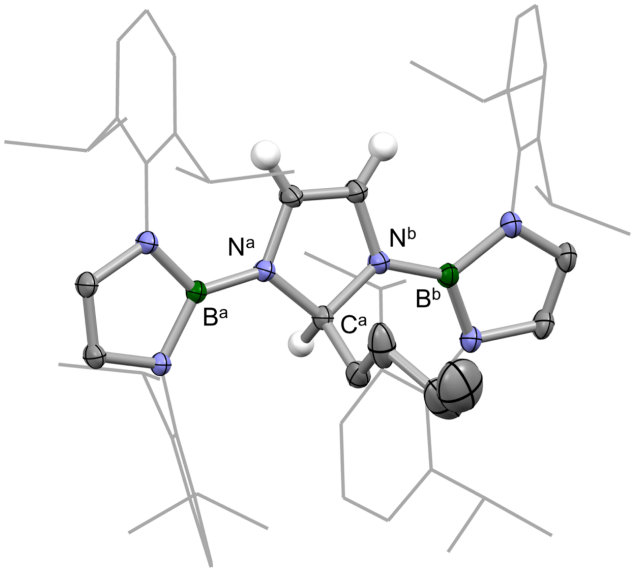

	(Å)/(°)
d(Bᵃ–Nᵃ)	1.433(3)
d(Bᵇ–Nᵇ)	1.430(3)
d(Cᵃ–Nᵃ)	1.484(3)
d(Cᵃ–Nᵇ)	1.488(2)
∠(Nᵃ–Cᵃ–Nᵇ)	103.1(1)
Θ([Bᵃ])	20.4
Θ([Bᵇ])	6.0

Figure 3.6 (Left) Molecular structure of 4(H)(^{n}Bu) in the solid state, as determined by X-ray crystallography. Solvate molecule and most hydrogen atoms omitted, and Dipp groups shown in wireframe format for clarity. Thermal ellipsoids set at the 40% probability level. (Right) Table of key structural parameters.

The steric and electronic consequences of uptake of the additional alkyl group at C2 are reflected in the increased co-planarity of the boryl and imidazole skeletons (inter-plane angles of 20.34 and 6.0°) in the solid state and in the exocyclic B–N bond lengths, 1.433(3) and 1.430(3) Å, which are somewhat shorter compared with [(**4**)H][BPh_4] (1.499(4) and 1.495(4) Å).

In order to reduce the possibility for nucleophilic attack at the electrophilic C2 centre, the more sterically demanding base, ^{t}BuLi, was employed (in toluene at -78 °C). In this case the ^{1}H NMR spectrum of the product shows a singlet integrating to two protons at 4.43 ppm which, according to HSQC, correlates to a carbon at 66.5 ppm These ^{1}H and ^{13}C chemical shifts are similar to the C2 proton and carbon of **4**(H)(^{n}Bu), implying that there are two protons attached to C2, a hypothesis that is supported by the phase-sensitive COSY and HSQC spectra which shows that the ^{13}C signal belongs to a secondary carbon. Thus, instead of removing the C2 proton, the *tert*-butyl group

appears to undergo beta-hydride elimination, resulting in a nucleophilic attack of the hydride at the C2 position (Scheme 3.7). β-Hydride elimination is a well-known decomposition pathway for metal alkyls.[20] The condition for such elimination is the availability of an empty valance orbital on the metal centre to interact with the C_β–H bond and thus β-hydride elimination plays a more important role in Group 1, 2 and 13 metals. Wehmschulte *et al*. have, for example, used ^{t}BuLi as a hydride source in the preparation of alanes and gallanes.[21]

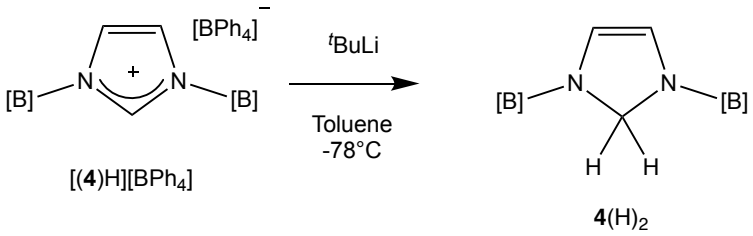

Scheme 3.7 Suggested attack of a β-hydride of ^{t}BuLi at C2 on [(4)H][BPh$_4$] to yield 4(H)$_2$.

To circumvent the attack of the base at the C2 centre (as an alkyl group or a hydride), the use of bulkier bases that lack β-hydrogens was studied. The combination of [(**4**)H][BPh$_4$] and either phenyllithium or mesityllithium was dissolved in a mixture of C_6D_6 and diethyl ether (10:1) in a J. Young's NMR tube and the reaction mixture sonicated. The *in situ* ^{1}H NMR spectrum of the reaction between phenyllithium and [(**4**)H][BPh$_4$] reveals the formation of a species with signals identical to those of the phenylborane **5** (Scheme 3.8), reported by Yamashita *et al*.[22] This in turn implies nucleophilic attack by the phenyl group on one of the boryl functions. In the case of mesityllithium, the reaction mixture – as probed by ^{1}H NMR spectroscopy – is apparently complex, but colourless single crystals suitable for X-ray crystallography could be grown by extracting the residual reaction mixture into hexane. The crystal structure reveals a complex composed of two monoborylated imidazoles coordinated to the lithium metal centre of Li[BPh$_4$] (**6**, Scheme 3.8 and Figure 3.7). This supports

the conclusion that the boryl group is being attacked by the nucleophilic aryl group (yielding a monoborylated imidazole heterocycle) rather than deprotonation taking place at C2 (Scheme 3.8).

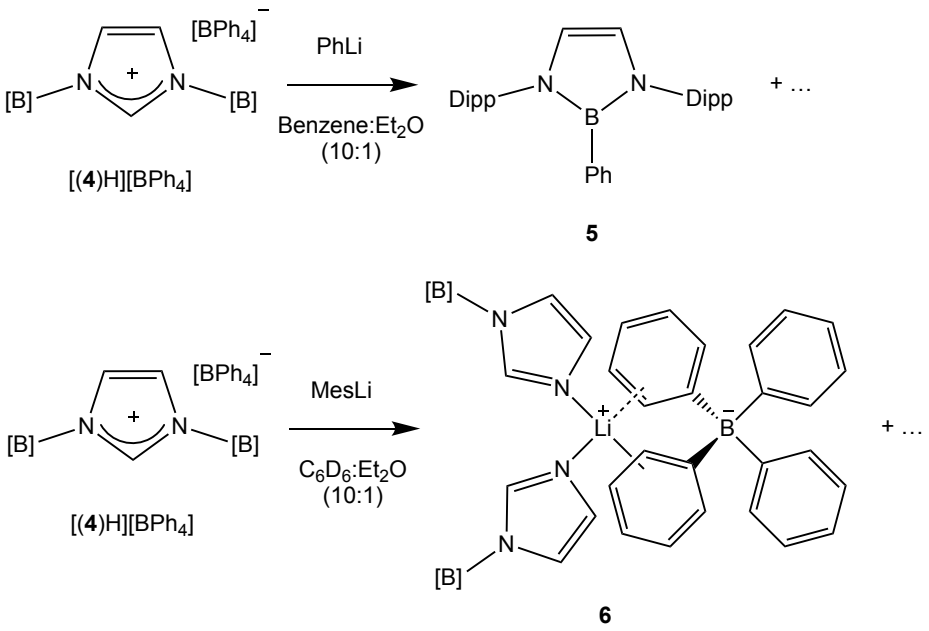

Scheme 3.8 Reaction of [(4)H][BPh$_4$] with aryllithiums results in nucleophilic attack of the base at the boron centre of one of the boryl groups.

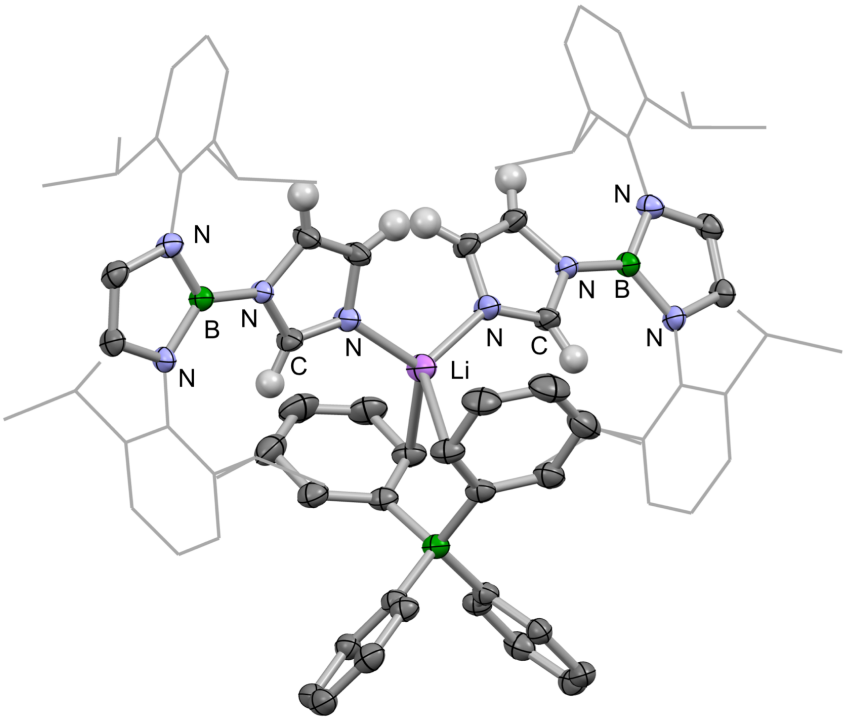

Figure 3.7 Molecular structure of 6 in the solid state, as determined by X-ray crystallography. Solvate molecule and most hydrogen atoms omitted, and Dipp groups shown in wireframe format for clarity. Thermal ellipsoids set at the 40% probability level.

Bis(trimethylsilyl)amides are strong relatively non-nucleophilic bases that do not react with **1**,[23] and are therefore good candidates for deprotonation of [(**4**)H]$^+$. The ^{1}H NMR spectra obtained from the reaction mixtures comprised of [(**4**)H]$^+$ and potassium bis(trimethylsilyl)amide, however, imply a lowering of symmetry in the product. These spectra show two inequivalent isopropyl methine septets and four inequivalent isopropyl methyl doublets. Unlike **4**(H)(^{n}Bu), however, the product gives rise to *two* singlets assigned to the backbone protons of the boryl groups, implying that the two boron-containing heterocycle fragments are inequivalent. Colourless single crystals suitable for X-ray crystallography were obtained from diethyl ether. The solid state structure of **7** so obtained (Figure 3.8) reveals migration of one of the boryl groups to the backbone of the imidazole heterocycle (Scheme 3.9).

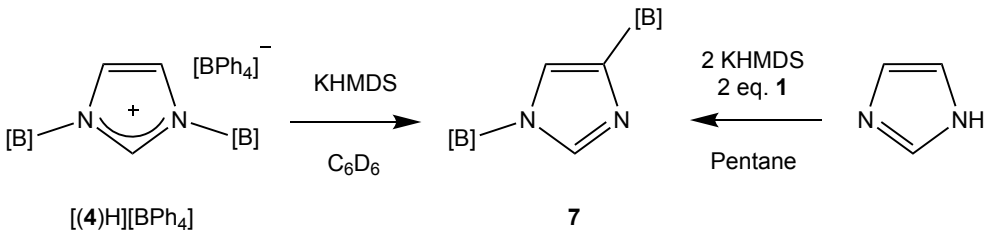

Scheme 3.9 Deprotonation of [(4)H][BPh$_4$] using potassium bis(trimethylsilyl)amides results in migration of one of the boryl groups to the backbone. Migrated species 7 can also be synthesized in one-pot directly from imidazole.

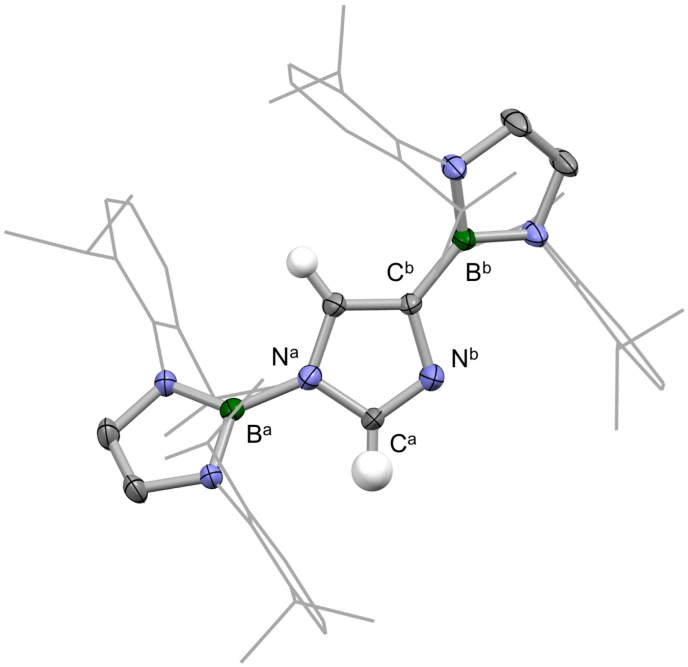

	(Å)/(°)
d(B^a–N^a)	1.501(3)
d(B^b–C^b)	1.512(3)
d(C^a–N^a)	1.374(3)
d(C^a–N^b)	1.294(4)
∠(N^a–C^a–N^b)	111.1(3)
Θ([B^a])	41.5
Θ([B^b])	26.5

Figure 3.8 (Left) Molecular structure of 7 in the solid state, as determined by X-ray crystallography. Most hydrogen atoms omitted, and Dipp groups shown in wireframe format for clarity. Thermal ellipsoids set at the 40% probability level. (Right) Table of key structural parameters.

The crystal structure implies successful deprotonation at the imidazole heterocycle to give an abnormal NHC, which is subsequently quenched by a 1,2-shift of the boryl group to the carbene centre. 1,2-Rearrangement in this fashion has been reported for various hetero substituents (boryl, iminoyl, benzyl, silyl and phosphanyl).[5–14] From a metrical perspective, the exocyclic B^a–N^a and B^b–C^b bond

lengths are statistically the same (1.501(3) Å and 1.512(3) Å respectively) and both boryl groups are significantly twisted out of the plane of the imidazole moiety: 41.5° and 26.5° for the *N*- and *C*-bound boryl groups, respectively.

The solid-state structure suggests that net deprotonation takes place at the C4 position, to give an abnormal NHC (imidazole-4-ylidene), rather than the more acidic C2 position to give imidazole-2-ylidene (Figure 3.9). DFT calculations were therefore carried out by Haoyu Niu, of the Aldridge group, to probe the relative energies of the various potential isomeric products (Figure 3.9). The structures of the carbenes and their corresponding rearranged species, along with their relative internal energies, are given in Figure 3.9. These studies indicate that, although imidazole-2-ylidene is the thermodynamically more favourable carbene isomer, rearranged species involving *N*- rather than *C*-centred lone pairs are globally lower in energy. The 1,4-bisborylated imidazole is calculated to be more stable than the 1,2-isomer, presumably due to steric hindrance, which provides a thermodynamic driving force for overall deprotonation at C4 rather than C2.

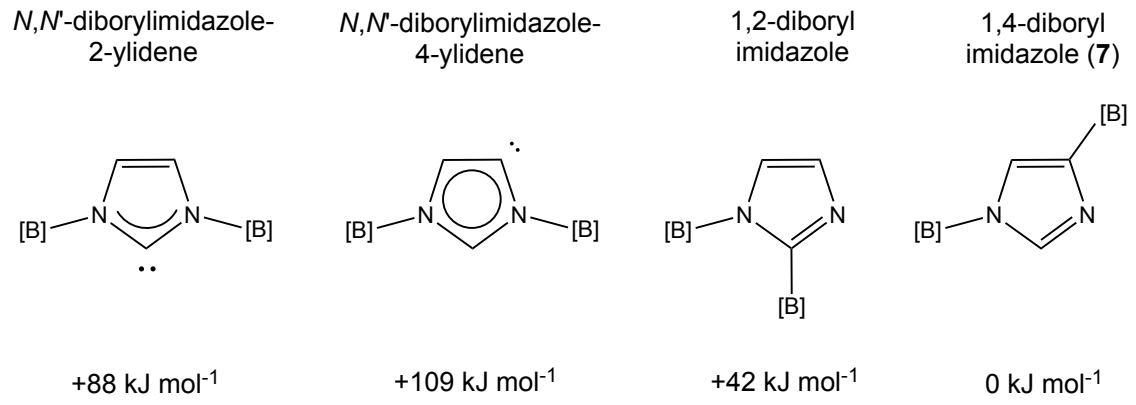

Figure 3.9: Comparison of the internal energies (kJ mol^{-1}) of carbenes and the respective 1,2-rearranged species derived from deprotonation of [(4)H]$^{+}$.

For synthetic ease, it was found that **7** can also be synthesized in one-pot by the reaction of one equivalent of imidazole and two equivalents of both **1** and potassium

bis(trimethylsilyl)amide and isolated in 55% yield (Scheme 3.9).

All attempts to isolate, or observe, the free carbene using lithium, sodium or potassium bis(trimethylsilyl)amides as the base were unsuccessful. Under a range of conditions, involving variation of temperature and solvent (C_6D_6, toluene-d_8, THF-d_8, C_6D_{12} and C_6D_5Br), the reaction invariably leads to the formation of **7** (Table 3.2). Since the free carbene could not be isolated, *in situ* metalation was pursued instead.

Counterion	Base	Solvent	Temperature (°C)	Product (%)[b]
$[BPh_4]^-$	NaHMDS	THF-d_8	-78 °C - 25 °C	**7** (100)
$[BPh_4]^-$	NaHMDS	C_6D_6	r.t.	**7** (100)
$[BPh_4]^-$	LiHMDS	C_6D_6	r.t.	**7** (100)
$[PF_6]^-$	NaHMDS	C_6D_{12}	r.t.	**7** (100)
$[PF_6]^-$	NaHMDS	$C_6D_5CD_3$	-78 °C - 25 °C	**7** (100)
$[BPh_4]^-$	KHMDS	C_6D_5Br	r.t.	**7** (100)
$[BPh_4]^-$	KHMDS	C_6D_5Br:C_6F_5Br [a]	r.t.	**7** (50), **3** (50)

Table 3.2 Reactions of [(4)H][BPh_4] and [(4)H][PF_6] with alkali metal bis(trimethylsilyl)amides under various reaction conditions. [a]In 10:1 ratio. [b]Approximately according to ^{1}H NMR spectroscopy.

3.2.3 *In Situ* Metalation Studies

Initial attempts to trap the carbene revolved around the use of Group 11 metal electrophiles, given the known propensity of gold(I) systems in particular to form strong bonds to carbene donors. ^{1}H NMR spectroscopy was used to monitor the reactions of [(**4**)H][BPh_4], sodium bis(trimethylsilyl)amide and either CuCl or (THT)AuCl in THF or fluorobenzene. Identical spectra are obtained from both metal complexes, each featuring two different species, one of which is the known chloroborane **8** (Scheme 3.10).[22] Three inequivalent imidazolium protons are observed for the second species, each of which integrates as one proton (compared to two protons for the backbone C*H* singlet of the boryl group), implying that only one diazaboryl group is bonded to the imidazole fragment. Furthermore, two broad

singlets are apparent in the ^{11}B NMR spectrum at 20 and 0 ppm, consistent with the presence of the diazaboryl group and a four-coordinate boron centre, respectively.

Colourless single crystals suitable for X-ray crystallography were obtained from hexane at -20 °C. The solid-state structure so obtained reveals exchange of one of the boryl groups for BPh_3, resulting in an unsymmetrical imidazolium zwitterion with a diazaboryl group attached to one nitrogen and a triphenylborane group to the other (Figure 3.10). From a metrical perspective, (**3**)BPh_3 features a diazaboryl group which is rotated by 20.1° compared to the imidazole plane, and a $B^a–N^a$ bond length which is shorter (at 1.470(4) Å) than those found in both monoborylated imidazole **3** and bisborylated imidazolium [(**4**)H][BPh_4] (1.515(3) and 1.499(4)/1.495(4) Å, respectively). The $C^a–N^a$ bond length is considerably longer than the $C^a–N^b$ bond length, which is consistent with the predominant resonance structure of (**3**)BPh_3 shown in Scheme 3.10.

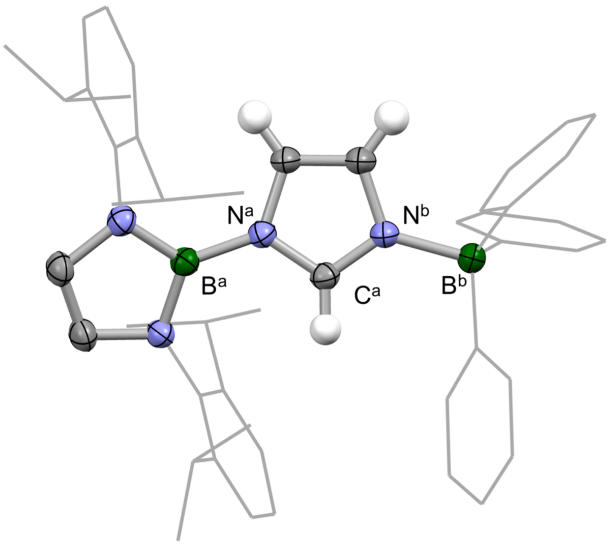

	(Å)/(°)
d($B^a–N^a$)	1.470(4)
d($B^b–N^b$)	1.617(3)
d($C^a–N^a$)	1.350(3)
d($C^a–N^b$)	1.306(4)
∠($N^a–C^a–N^b$)	111.1(2)
Θ([B^a])	20.1

Figure 3.10 (Left) Molecular structure of (3)BPh_3 in the solid state, as determined by X-ray crystallography. Most hydrogen atoms omitted, and Dipp groups shown in wireframe format for clarity. Thermal ellipsoids set at the 40% probability level. (Right) Table of key structural parameters.

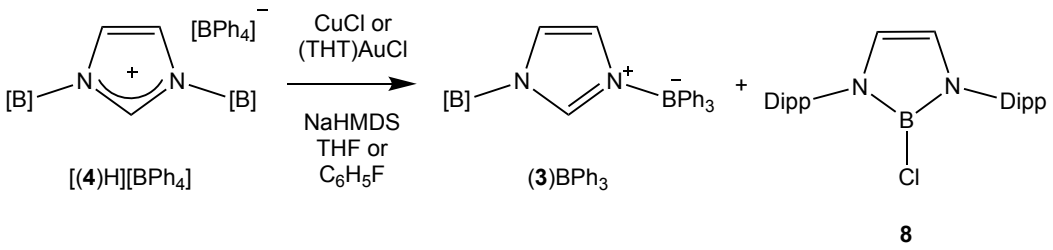

Scheme 3.10 Deprotonation of [(4)H][BPh_4] in the presence of CuCl or (THT)AuCl results in substitution of one of the boryl groups with BPh_3.

B–C bond cleavage of a tetraarylborate anion is not unprecedented. The breakage of a B–C bond in $[BPh_4]^-$, $[BAr^F{}_4]^-$ and $[B(C_6F_5)_4]^-$ mediated by transition metals and by bismuth has been reported.[24–30] The mechanism for the displacement of the diazaboryl group is unknown, but the reaction appears to be mediated by the metal centre. This hypothesis is supported by the fact that in the absence of CuCl or AuCl, the reaction of [(**4**)H][BPh_4] and a alkali metal bis(trimethylsilyl)amide leads to complete conversion to migrated species **7** and no sign of (**3**)BPh_3 is observed by NMR spectroscopy. Furthermore, the chloride component of **8** is likely to originate from the copper- or gold-bound Cl^- chloride ligand.

In a more logical fashion, (**3**)BPh_3 can be synthesized directly from **3** and BPh_3 in acetonitrile, whereupon (**3**)BPh_3 precipitates cleanly from the reaction mixture and can be isolated in 37% yield.

The *in situ* metalation of [(**4**)H][PF_6] was therefore examined, with the aim to circumvent the substitution of the boryl group by BPh_3. The ^{1}H NMR spectrum of an aliquot taken from the reaction mixture obtained from [(**4**)H][PF_6], sodium bis(trimethylsilyl)amide and (THT)AuCl in benzene is complicated, apparently featuring a number of different species. Similar findings are obtained using CuCl or AgOTf in C_6D_6. In the case of (THT)AuCl and CuCl, **8** is observed in the ^{1}H NMR spectra. Furthermore, one major species is apparent in all of the spectra. This species exhibits

lower symmetry in the imidazole moiety, with three inequivalent imidazolium protons being observed, each of which integrates to one proton (compared to the 2H backbone C*H* singlet of the boryl group), implying that only one diazaboryl group is bonded to the imidazole fragment. This is reminiscent of the pattern observed in the ^{1}H NMR spectrum of (**3**)BPh_3. Furthermore, the ^{19}F NMR spectrum in each case shows that the simple doublet due to the hexafluorophosphate counterion of the starting material, [(**4**)H][PF_6], has been replaced by a doublet of doublets and a doublet of quintets, indicating lowering of symmetry of the phosphorane unit.

Colourless single crystals suitable for X-ray crystallography could be obtained from the (THT)AuCl reaction mixture by recrystallization from hexane. The solid-state structure so obtained (Figure 3.11) reveals the exchange of one of the boryl groups for a pentafluorophosphorane unit, resulting in an unsymmetrical imidazolium zwitterion with a diazaboryl group attached to one nitrogen and a PF_5 group to the other. The ^{1}H NMR spectrum of the crystals confirms that (**3**)PF_5 is the common product formed in the *in situ* deprotonation of [(**4**)H][PF_6] in the presence all three of the aforementioned metal complexes. The cleavage of the counter-anion in this case is presumably driven by similar factors to those leading to the formation of (**3**)BPh_3.

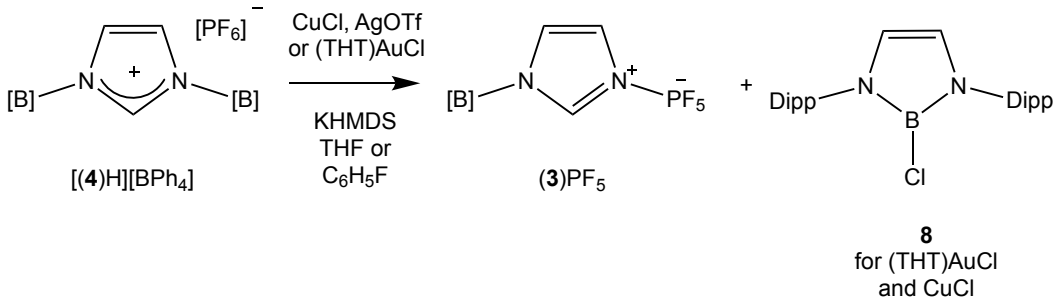

Scheme 3.11 Deprotonation of [(4)H][PF_6] in the presence of CuCl, (THT)AuCl or AgOTf resulting in substitution of one of the boryl groups with PF_5.

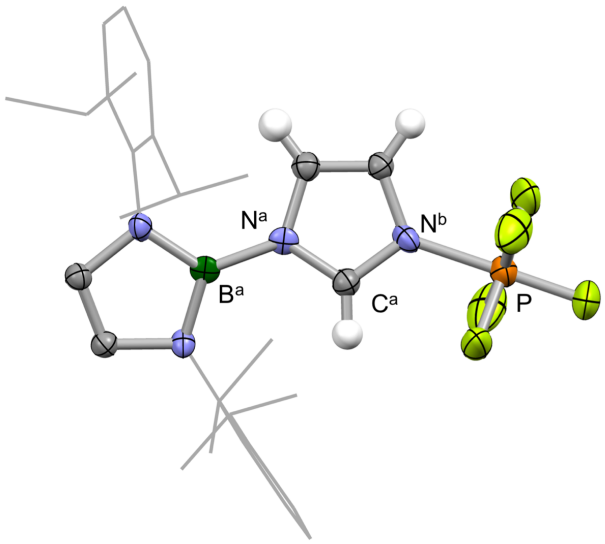

	(Å)/(°)
d(B^a–N^a)	1.50(2)
d(N^b–P)	1.84(1)
d(C^a–N^a)	1.34(2)
d(C^a–N^b)	1.33(2)
∠(N^a–C^a–N^b)	110(1)
Θ([B^a])	13.2

Figure 3.11 (Left) Molecular structure of (3)PF_5 in the solid state, as determined by X-ray crystallography. Most hydrogen atoms omitted, and Dipp groups shown in wireframe format for clarity. Thermal ellipsoids set at the 40% probability level. (Right) Table of key structural parameters.

Incorporation of CF_3 groups in the *meta*-position on the phenyl rings on $[BPh_4]^-$ reduces the negative charge on the *ipso*-carbons, which renders $[BAr^F{}_4]^-$ more stable than $[BPh_4]^-$ under highly electrophilic conditions.[31] With this in mind, the corresponding *in situ* trapping reactions were attempted with [(**4**)H][$BAr^F{}_4$]. However, the reaction of [(**4**)H][$BAr^F{}_4$] with a range of metal complexes either resulted in the formation of **8** (with either ZnCl{$N(SiMe_3)_2$} or (THT)AuCl/Na{$N(SiMe_3)_2$}) or in no reaction at all (either (Ph_3P)Au{$N(SiMe_2)_2$}, Zn{$N(SiMe_2)_2$}$_2$, Zn{N^{i}Bu$_2$}$_2$, $ZnMe_2$ and Sn{$N(SiMe_2)_2$}$_2$; Scheme 3.12).

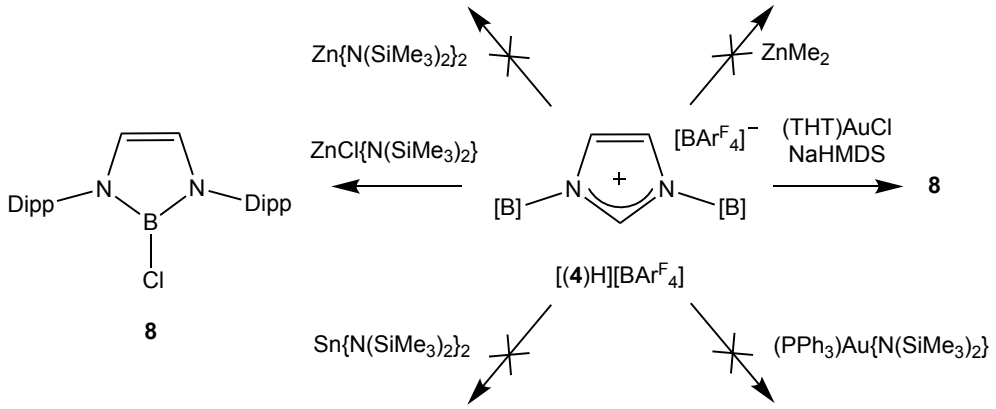

Scheme 3.12 *In situ* reactivity of [(4)H][BAr$^F_4$] with various metal complexes.

In addition to the traditional methods for the metalation of carbenes *in situ*, an alternative method, in which copper (I) NHC complexes are formed using an electrochemical procedure, has been developed by Lake *et al*.[32] The method relies on the electrochemical reduction of the imidazolium salt at a copper electrode (with release of H_2), with the carbene formed *in situ* being trapped by coordination to a Cu(I) centre (example given on the left hand side in Scheme 3.13). This method has allowed for the isolation of copper complexes of carbenes whose ligand precursors have, for example, several acidic protons, as it provides selective deprotonation at C2. Several attempts have for example been made to deprotonate **3.7** (Scheme 3.13) or react it with metal precursors in order to access the corresponding free carbene or its metal complexes but all were unsuccessful (Scheme 3.13). With reduction in the presence of copper, however, Lake *et al*. managed to isolate the copper complex of the NHC (**3.8**; Scheme 3.13). This method could thus be a potential solution to the problematic removal of the proton at C5 in the case of [(**4**)H][BPh$_4$] and could allow for direct metalation at the C2 position. Electrochemical reduction of [(**4**)H][BPh$_4$] and [(**4**)H][BAr$^F_4$] was explored in collaboration with the Willans group at the University of Leeds. Unfortunately, this did not result in the isolation of the desired complex as carbene rearrangement also seems to occur in this case.

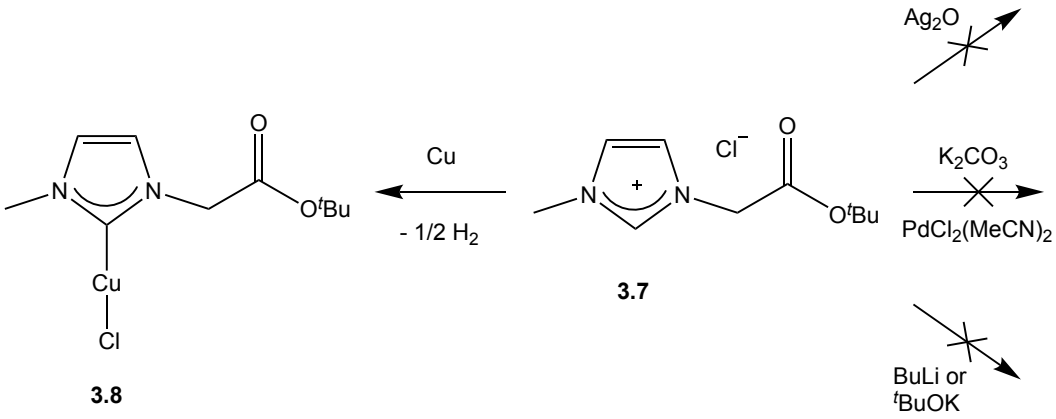

Scheme 3.13 Electrochemical reduction of imidazolium salt 3.7 by copper.[32]

3.2.4 Blocking the Backbone: Borylation of 4,5-Disubstituted Imidazoles and Their Reactivity

Attempts to access the free *N,N*'-bisborylated carbene or its metal complexes have been frustrated for systems based around the parent imidazole. By preventing the migration of the boryl group to C4 upon deprotonation, it was hypothesized that a carbene, or its metal complexes, might be isolated. This might be achieved by blocking the backbone sites of the imidazole heterocycle, *i.e*. by using 4,5-disubstituted imidazoles as building blocks (Figure 3.12). In such systems, the only acidic site on the imidazole moiety would be expected to be at the C2 position. Moreover, due to steric hindrance, the 1,2-shift of one of the boryl groups to the carbenic centre at the C2 position might not be favourable (due to the presence of the second *N*-bound boryl group), or at least potentially slow enough to allow for isolation of the free carbene at low temperature or *via in situ* metalation.

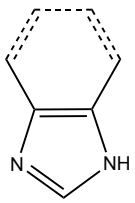

Figure 3.12 4,5-Disubstituted Imidazoles.

Monoborylated benzimidazole (**9**; Scheme 3.14) was synthesized in a similar way to monoborylated imidazole **3**, from benzimidazole, potassium bis(trimethylsilyl)amide and **1**, which afforded **9** in 41% yield. Colourless single crystals suitable for X-ray crystallography were obtained from hexane. The solid-state structure of **9** so obtained is shown in Figure 3.13. The B^a–N^a bond length is 1.467(2) Å, which is considerably shorter than the analogous bond length of **3** (1.515(3) Å) and [(**4**)H][BPh_4] (1.499(4) and 1.495(4) Å). The boryl group is significantly twisted; 39.8° between the plane of the boryl group compared to the imidazole moiety. From the structure of [(**4**)H][BPh_4], it is clear that the alignment of the boryl group does not affect the B–N bond length as the bond lengths are statistically the same despite one lying almost in plane and the other not. This suggests that p-orbital interaction of the boron and nitrogen does not affect the bond length, indicating that the property of the σ-bond might be responsible for the shortening of the bond length. The electron-withdrawing nature of the annulated benzene ring serves to lower the electron density at the imidazole nitrogen and might result in greater s-character of the B^a–N^a bond and hence shorter bond length. Similar trends for reported unsaturated NHCs have, however, not been observed. The exocyclic C–N bonds (the bond between the nitrogen of the imidazole heterocycle and the *ipso*-carbon) in a Dipp substituted unsaturated NHC, benzannulated NHC and 4,5-dichloro substituted NHC (whose chloride groups are also electron-withdrawing) are, for example, not statistically different[33,34] and the same is true for the Mes substituted counterparts.[34–36]

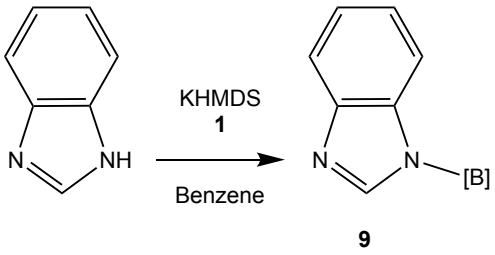

9

Scheme 3.14 Synthesis of monoborylated benzimidazole 9.

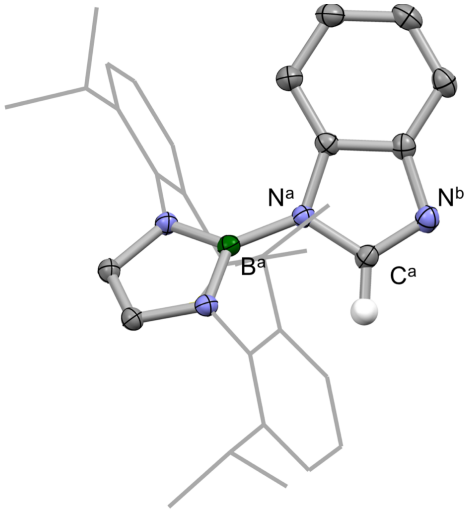

	(Å)/(°)
d(B^a–N^a)	1.467(2)
d(C^a–N^a)	1.382(2)
d(C^a–N^b)	1.306(2)
∠(N^a–C^a–N^b)	115.3(1)
Θ([B^a])	39.8

Figure 3.13 (Left) Molecular structure of 9 in the solid state, as determined by X-ray crystallography. Most hydrogen atoms omitted, and Dipp groups shown in wireframe format for clarity. Thermal ellipsoids set at the 40% probability level. (Right) Table of key structural parameters.

With the aim of attaching the second boryl group onto monoborylated benzimidazole, **9** and **1** were dissolved in MeCN-d_3 in a J. Young's NMR tube and the reaction mixture monitored by ^{1}H NMR spectroscopy. No change was observed at room temperature nor at 80 °C, even after heating the reaction mixture for four days. This lack of reactivity is believed to be due to lower nucleophilicity of benzimidazole compared with imidazole. This in turn is caused by the annulated aromatic ring on the backbone, which is electron-withdrawing and serves to reduce the nucleophilicity

of the nitrogen of **9** compared to **3**. Recent results from Eugene Kolychev, of the Aldridge group, show that in the presence of pyridine, **1** is in equilibrium with pyridine coordinated borane ([**10**]Br; Scheme 3.15), and that this cationic species is more labile to nucleophilic substitution at boron.[37] The boryl cation can be isolated as the corresponding $[PF_6]^-$ salt ([**10**][PF_6]; Scheme 3.15), which has been structurally characterized.[37] In an attempt to substitute the second boryl group onto the benzimidazole fragment, the reaction was therefore carried out in pyridine-d_5 in order to increase the electrophilicity of the boryl fragment. A mixture of **9** and **1** were dissolved in pyridine-d_5 in a J. Young's NMR tube and the reaction mixture monitored by ^{1}H NMR spectroscopy. No change was observed at room temperature nor at 115 °C, even after heating the reaction mixture for four days.

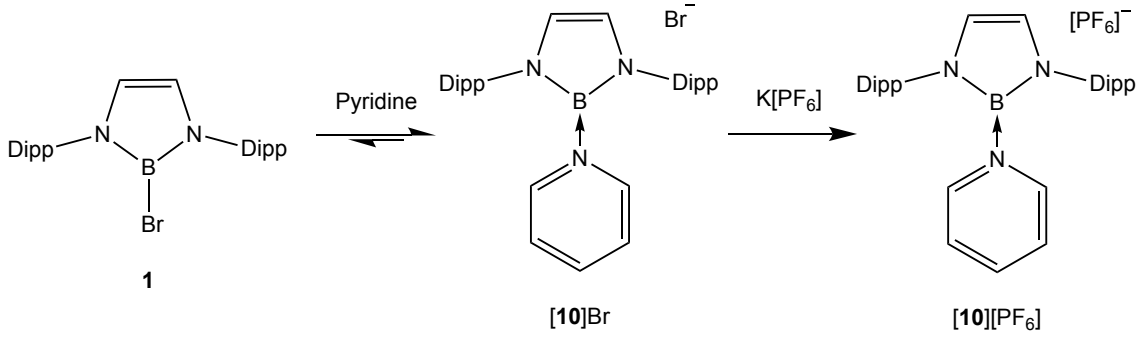

Scheme 3.15 In pyridine, 1 is in equilibrium with pyridine ligated borenium species [10]Br. The equilibrium can be driven towards $[10]^+$ by the addition of K[PF_6].[37]

Given the difficulty in diborylating benzimidazole, alternative 'protected' imidazoles were targeted. 1,3-Disubstituted 4,5-dimethylimidazolium salts have successfully been deprotonated in the past to yield the corresponding free carbene (see, for example, Scheme 3.16).[38,39] Conveniently, the bisborylated 4,5-dimethylimidazolium salt, [(**11**)H][BPh_4], could readily be synthesized in a similar manner to [(**4**)H][BPh_4] and isolated in 31% yield (Scheme 3.17). Colourless single crystals suitable for X-ray crystallography were obtained from C_6D_6 and Figure 3.14

shows the solid-state structure of [(**11**)H][BPh_4] so obtained. Both boryl groups are significantly twisted with respect to the imidazole plane; 63.7° and 53.3° compared with 9.1° and 37.4° in [(**4**)H][BPh_4]. The exocyclic B–N bond lengths are, however, statistically the same in the two structures (1.501(2) and 1.502(2) Å *vs* 1.499(4) and 1.495(4) Å, respectively).

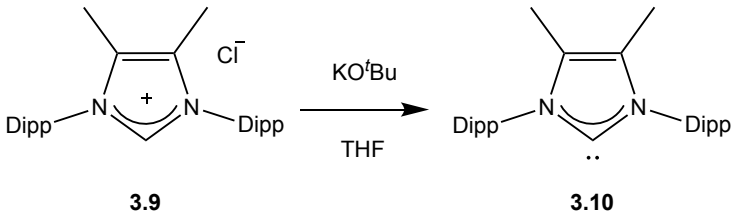

Scheme 3.16 4,5-Dimethyl substituted imidazolium salt 3.9 can be deprotonated to give free carbene 3.10.[38]

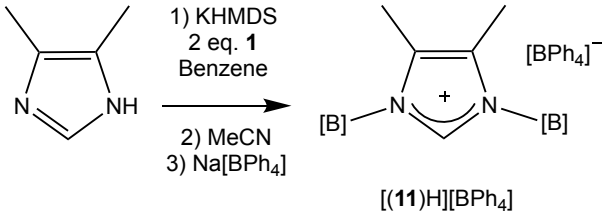

Scheme 3.17 Synthesis of *N*,*N*'-bisborylated 4,5-dimethylimidazolium salt [(11)H][BPh_4].

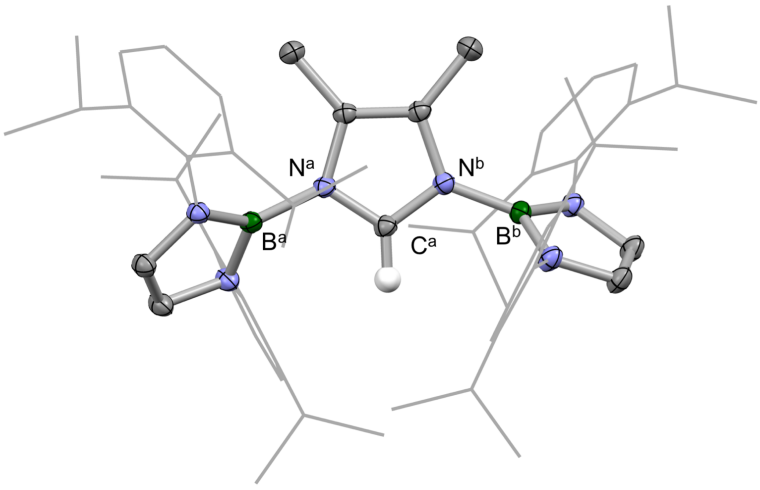

	(Å)/(°)
d(B^a–N^a)	1.501(2)
d(B^b–N^b)	1.502(2)
d(C^a–N^a)	1.334(2)
d(C^a–N^b)	1.331(2)
∠(N^a–C^a–N^b)	110.6(1)
Θ([B^a])	63.7
Θ([B^b])	53.3

Figure 3.14 (Left) Molecular structure of [(11)H][BPh_4] in the solid state, as determined by X-ray crystallography. Solvate molecule, counter-ion and most hydrogen atoms omitted, and Dipp groups shown in wireframe format for clarity. Thermal ellipsoids set at the 40% probability level. (Right) Table of key structural parameters.

In the hope of accessing the free bisborylated carbene *via* deprotonation at the C2 position, [(**11**)H][BPh_4] was reacted with potassium bis(trimethylsilyl)amide in benzene. The product was isolated and washed with acetonitrile, affording the isolated product in 30% yield. Two inequivalent boryl groups are apparent in the ^1H NMR spectrum of the product, as signalled by two backbone singlets, two isopropyl methine septets and four isopropyl methyl doublets. Furthermore, the singlet for the C2 proton is still present. This suggest that the desired carbene has not been formed. The product has high solubility in hexane, indicating a charge neutral species. Mass spectrometry (including accurate mass, m/z = 866.6526 ($[M]^+$) supports the idea of deprotonation of the imidazolium salt and that both boryl groups are still attached to the compound. Interestingly, a singlet integrating to six protons analogous to that observed for the C4/C5 methyl groups of the imidazolium precursor is not observed, nor are two separate signals integrating to 3 protons each. Instead, two singlets integrating to two and three protons each are present. This, in addition to the presence of the C2 proton suggest that 1,2-shift of the boryl group to the C2 position has not taken place, but rather that a 1,3-shift to one of the methyl groups on the backbone, to give **12** (Scheme 3.18), could be a possibility. The ^1H NMR spectrum of the product, along with proposed assignment of the signals is depicted in Figure 3.15. The reaction presumably proceeds *via* a remote (or abnormal) *N*-heterocyclic olefin formed *in situ* upon deprotonation of one of the methyl groups on the imidazole backbone. Attempts to obtain single crystals suitable for X-ray crystallography from either acetonitrile or hexane were unfortunately unsuccessful.

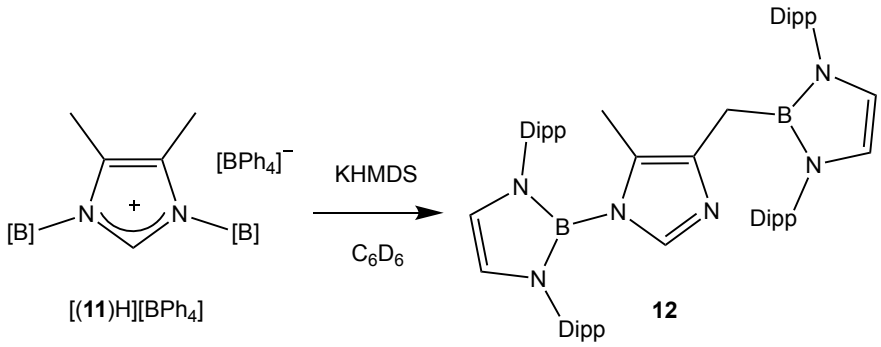

Scheme 3.18 Deprotonation of [(11)H][BPh$_4$] is believed to result in migration of one of the boryl groups to the methyl group on the backbone.

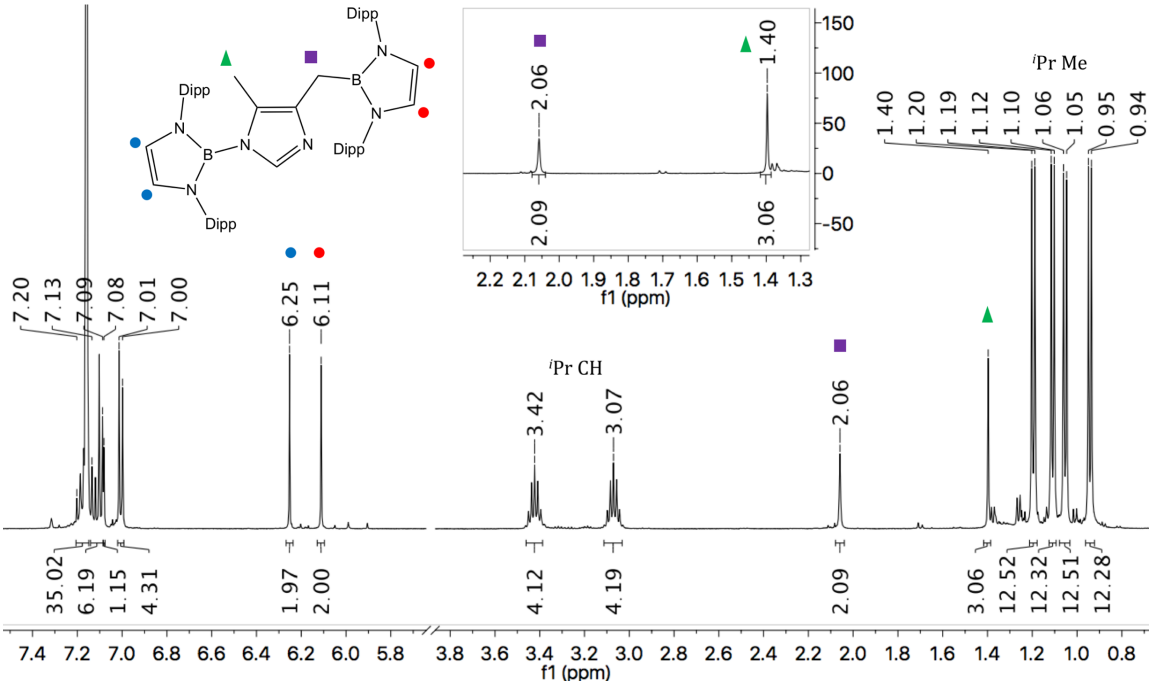

Figure 3.15 The ^{1}H NMR spectrum of 12 in C_6D_6 along with proposed assignment of peaks.

With this in mind, the synthesis of a 1,3-diboryl-4,5-diphenyl imidazolium salt, (which would possess less acidic protons at the 4,5-substituents) was attempted in a similar manner to [(**4**)H][BPh$_4$] and [(**11**)H][BPh$_4$]. 4,5-Diphenylimdiazole was stirred with two equivalents of **1** and one equivalent of potassium bis(trimethylsilyl)amide in pyridine. The ^{1}H NMR spectra of aliquots taken from the reaction mixture in MeCN-d$_3$ reveal the presence of one predominant species, identified as **1**, along with a second (minor) species. The ratio of the two species does

not change considerably with time nor on heating the reaction mixture (three days at 110 °C). Bearing in mind that the bisborylated imidazolium species would typically have high solubility in acetonitrile, complete conversion to the bisborylated species would be expected to be signalled by only one main species in the ^{1}H NMR spectrum in MeCN-d_3 with only minimal (or no) residual **1**. The ^{1}H NMR spectra thus indicate either minimal reaction of 4,5-diphenylimdiazole with **1**, or conversion to a monoborylated imidazole, which conceivably has low solubility in acetonitrile, with one equivalent of **1** remaining in solution. Volatiles were removed *in vacuo* and the residue extracted into dichloromethane and filtered. The bulk of the residue of the filtrate was insoluble in acetonitrile and thus the residue was washed repeatedly with acetonitrile. The ^{1}H NMR spectrum obtained for the product in C_6D_6 shows the presence of a single product. The ratio of the integrals of the imidazole C2 proton (singlet at 7.59 ppm), the signal for the backbone of the boryl ligand (singlet at 6.17 ppm), the isopropyl methine protons (septet at 3.12 ppm) and the isopropyl methyl groups (two doublets at 1.07 ppm and 0.94 ppm) is 1:2:4:12:12, suggesting that the 4,5-dimethylimidazole moiety and boryl units are present in a 1:1 ratio, and thus that the main product from the reaction is the monoborylated species **13** (Scheme 3.19). Colourless single crystals of the product suitable for X-ray crystallography were obtained from toluene and the solid-state structure so obtained (Figure 3.16) confirms the structure of **13**. The boryl group is significantly twisted out of the imidazole plane; 50.0° compared with **3** (5.9°), yet the exocyclic B–N bond is considerable shorter (at 1.482(2) Å) than the analogous bond in **3** (1.515(3) Å), and close to that of monoborylated benzimidazole **9** (1.467(2) Å). As with the benzannulated system **9**, this might be attributed to the electron withdrawing properties of the phenyl groups in the 4 and 5 positions.

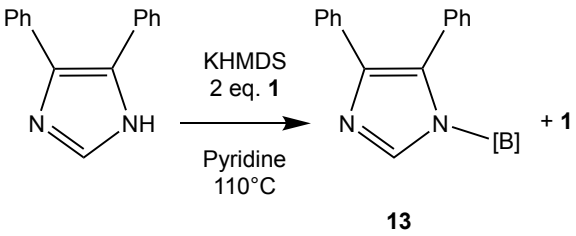

Scheme 3.19 Synthesis of monoborylated 4,5-diphenylimidazole 13.

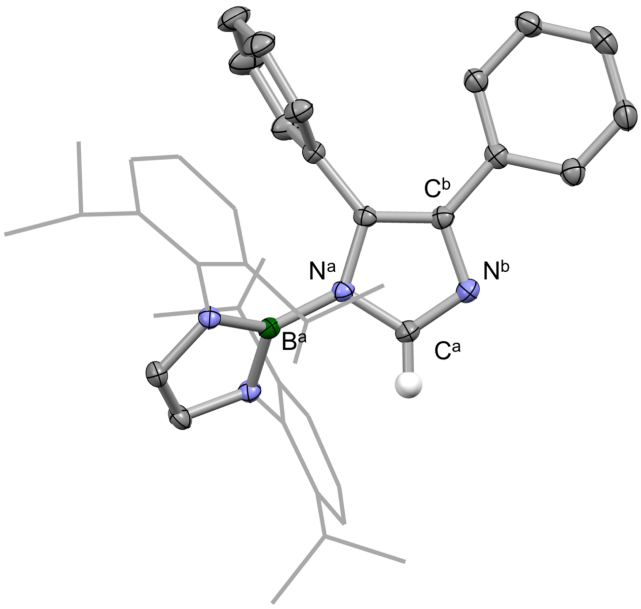

	(Å)/(°)
d(B^a–N^a)	1.482(2)
d(C^a–N^a)	1.371(2)
d(C^a–N^b)	1.303(2)
∠(N^a–C^a–N^b)	113.7(1)
Θ([B^a])	50.0
Θ(Ph)	5.9

Figure 3.16 (Left) Molecular structure of 13 in the solid state, as determined by X-ray crystallography. Most hydrogen atoms omitted, and Dipp groups shown in wireframe format for clarity. Thermal ellipsoids set at the 40% probability level. (Right) Table of key structural parameters. Θ([Ph]) indicates the angle between the plane of the C^b-bound phenyl group and the imidazole heterocycle.

In an attempt to add a second boryl group onto the imidazole heterocycle, a mixture of **13** and **1** was dissolved in pyridine-d_5 or MeCN-d_3 in a J. Young's NMR tube. The reactions were monitored *in situ* by ^{1}H NMR spectroscopy. No change was observed, even upon heating at 115 °C in pyridine-d_5 and 60 °C in MeCN-d_3 over five days in each case. As in the case of benzimidazole, the lack of reactivity is believed to be due to lower nucleophilicity on account of the electron withdrawing effects of the backbone phenyl groups.

3.3 Conclusions

An *N,N'*-bisborylated carbene, where the boryl group is a Dipp substituted 1,3,2-diazaboryl function ({B(NDippCH)$_2$}), is a ligand of great interest from both electronic and steric perspectives. DFT calculations of the free carbene indicate similar σ-donor properties to saturated 6-membered NHCs and the %V_{bur} of the carbene (derived from the calculated structure of its gold complex) places it far beyond the most sterically demanding carbenes reported to date.[3,4]

As potential synthetic intermediates, bisborylated imidazolium salts, containing the [(**4**)H]$^+$ cation have been successfully synthesized. All attempts to isolate or observe the free carbene *via* deprotonation have, however, either (a) resulted in a nucleophilic attack at the C2 centre of the imidazole heterocycle or at the boron of the diazaboryl group, or (b) following successful deprotonation, resulted in 1,2-rearrangement of the boryl group to give an unsymmetrical charge neutral species. Attempts to metalate the carbene *in situ* have either led to displacement of one of the boryl groups by the displaced halide or in no reaction.

Syntheses of bisborylated benzimidazole and 4,5-diphenylimidazole were unsuccessful due to the reduced nucleophilicity of the imidazole nitrogens; bisborylation of 4,5-dimethylimidazole could, in contrast, be successfully carried out. However, deprotonation of the imidazolium salt in this case apparently results in a 1,3-rearrangement of one of the boryl groups to give an unsymmetrical charge neutral species featuring a backbone activated methyl group.

All efforts to isolate the bisborylated free carbene or its respective metal complexes have thus, regrettably, been unsuccessful. **7** could, nonetheless, offer an interesting building block for other bisborylated normal and abnormal NHCs and

attempted syntheses of such NHCs will be the topic of Chapter 4.

3.4 Experimental Procedures

Preparation of 3

Method (a): To a solution of imidazole (0.29 g, 4.3 mmol) and **1** (2.0 g, 4.3 mmol) in diethyl ether (20 mL) at -78 °C was added dropwise ^{n}BuLi (2.6 mL of a 2.5 M solution in hexane, 6.4 mmol). The stirred solution was allowed to slowly reach room temperature overnight. After filtration, the filtrate was concentrated and recrystallized at -20 °C. Colourless crystals were isolated and dried *in vacuo* to yield the product as a white crystalline solid (shown to be the diethyl ether solvate). Yield: 2.3 g, 89%. Slow evaporation of a hexane solution yielded colourless single crystals suitable for X-ray crystallography.

Method (b): A mixture of imidazole (0.058 g, 0.86 mmol), potassium bis(trimethylsilyl)amide (0.17 g, 0.86 mmol) and **1** (0.40 g, 0.86 mmol) was dissolved in benzene (10 mL) and stirred for 15 min. After filtration, volatiles were removed *in vacuo* and the resulting residue redissolved in acetonitrile at 80 °C. The solution was slowly allowed to reach room temperature in the oil bath, before being further cooled to -20 °C to yield colourless crystals. After filtration, the crystals were washed with cold acetonitrile (3 x 3 mL) and dried *in vacuo* to yield the product as a white solid. Yield: 0.16 g, 41%.

Spectroscopic Data for 3

^{1}H NMR (MeCN-d_3, 400 MHz, 298 K): δ_H 7.44-7.48 (2H, m, *p*-*H* of Dipp), 7.34-7.36 (4H, m, *m*-*H* of Dipp), 6.73 (br m, NCHC*H*N[B] of imidazole), 6.64 (1H, br m, NC*H*CHN[B] of imidazole), 6.40 (2H, s, N(C*H*)$_2$N of boryl ligand), 6.18 (1H, br m, 1H, NC*H*N), 3.44 (4H,

q, $^{3}J_{HH}$ = 7.0 Hz, CH_2 of coordinated Et_2O), 3.00 (4H, sept, $^{3}J_{HH}$ = 6.9 Hz, CHMe$_2$), 1.23 (12H, d, $^{3}J_{HH}$ = 6.9 Hz, CH*Me*$_2$), 1.14 (6H, t, $^{3}J_{HH}$ = 7.0 Hz, *Me* of coordinated Et_2O), 0.98 (12H, d, $^{3}J_{HH}$ = 6.9 Hz, CH*Me*$_2$) ppm. ^{1}H NMR (C_6D_6, 400 MHz, 298 K): δ_H 7.28 (1H, s, NC*H*CHN or NC*H*N of imidazole), 7.19-7.23 (2H, br m, *p-H* of Dipp), 7.10-7.12 (4H, m, *m-H* of Dipp), 6.96 (1H, br m, NC*H*CHN or NC*H*N of imidazole), 6.40 (1H, br m, NC*H*CHN or NC*H*N of imidazole), 6.02 (2H, s, N(C*H*)$_2$N of boryl ligand), 3.27 (4H, q, $^{3}J_{HH}$ = 7.0 Hz, CH_2 of coordinated Et_2O), 3.14 (4H, sept, $^{3}J_{HH}$ = 6.9 Hz, CHMe$_2$), 1.16 (12H, d, $^{3}J_{HH}$ = 6.9 Hz, C*H*Me$_2$), 1.11 (6H, t, $^{3}J_{HH}$ = 7.0 Hz, *Me* of coordinated Et_2O), 1.03 (12H, d, $^{3}J_{HH}$ = 6.9 Hz, CH*Me*$_2$) ppm. ^{13}C{^{1}H} NMR (MeCN-d_3, 101 MHz, 298 K): δ_C 147.0 (*o-C* of Dipp), 140.0 (N*C*HCHNB of imidazole), 137.8 (*i-C* of Dipp), 129.9 (NCH*C*HNB of imidazole), 129.5 (*p-C* of Dipp), 125.1 (*m-C* of Dipp), 120.2 (N*C*HN), 119.9 (N(*C*H)$_2$N of boryl ligand), 66.2 (*C*H$_2$ of coordinated Et_2O), 29.3 (*C*HMe$_2$), 24.6 (CH*Me*$_2$), 23.4 (CH*Me*$_2$), 15.6 (*Me* of coordinated Et_2O) ppm. ^{11}B NMR (C_6D_6, 128 MHz, 298 K): δ_B 21 (br s, boryl ligand) ppm. MS (CI): *m/z* (assignment, %) 455.3 ([M]H$^+$, 6%). Acc. Mass EI: calc. for $C_{29}H_{40}{}^{10}BN_4$: 454.3382; found: 454.3383. Elemental microanalysis: found (calc. for $C_{29}H_{39}BN_4$): C 76.26 (76.64)%, H 8.76 (8.65)%, N 12.06 (12.33)%.

Crystallographic Data for 3

a = 18.977(4) Å, *b* = 10.871(2) Å, *c* = 12.988(3) Å, α = β = γ = 90°, V = 2679.4(9) Å^3, Orthorhombic, *Pna*2$_1$, *Z* = 4, R_1 for 5209 [data intensity $I > 2\sigma(I)$] unique data = 0.047, wR_2 (all 5836 unique data) = 0.120.

Preparation of [(4)H][BPh$_4$]

A mixture of imidazole (0.084 g, 1.2 mmol), sodium bis(trimethylsilyl)amide (0.23 g, 1.2 mmol) and **1** (1.5 g, 3.2 mmol) was dissolved in benzene (15 mL) and stirred for 1 h. Volatiles were subsequently removed *in vacuo* and acetonitrile (15 mL) added. The

resulting mixture was stirred for 1 h, Na[BPh_4] (0.42 g, 1.2 mmol) added and the solution stirred for further 15 min. Volatiles were again removed *in vacuo*, and the residue extracted into dichloromethane and filtered. Volatiles were removed from the filtrate *in vacuo* and the resulting residue washed with benzene (3 x 10 mL) to yield the product as a light brown powder. Yield: 1.2 g, 86%. Single crystals suitable for X-ray crystallography were obtained by layering of a dichloromethane solution with hexane.

Spectroscopic Data for [(4)H][BPh_4]

^{1}H NMR (MeCN-d_3, 400 MHz, 298 K): δ_H 7.45-7.49 (4H, m, *p*-*H* of Dipp), 7.30-7.36 (8H, m, *o*-*H* of [BPh_4]$^-$), 7.28-7.30 (8H, m, *m*-*H* of Dipp), 7.01-7.04 (9H, overlapping m, *m*-*H* of [BPh_4]$^-$ and NC*H*N), 6.86-6.89 (4H, m, *p*-*H* of [BPh_4]$^-$), 6.62 (2H, br s, N(C*H*)$_2$N of imidazole), 6.43 (4H, s, N(C*H*)$_2$N of boryl ligand), 2.74 (8H, sept, $^3J_{HH}$ = 6.9 Hz, C*H*Me$_2$), 1.15 (12H, d, $^3J_{HH}$ = 6.9 Hz, CH*Me*$_2$), 0.85 (12H, d, $^3J_{HH}$ = 7.0 Hz, CH*Me*$_2$) ppm. ^{13}C{^{1}H} NMR (MeCN-d_3, 101 MHz, 298 K): δ_C 164.8 (q, $^1J_{CB}$ = 49.3 Hz, *i*-*C* of [BPh_4]$^-$), 145.7 (*o*-*C* of Dipp), 136.8 (br m, *o*-*C* of [BPh_4]$^-$), 136.1 (N*C*HN), 135.6 (*i*-*C* of Dipp), 130.5 (*p*-*C* of Dipp), 126.6 (br q, $^3J_{CB}$ = 2.7 Hz, *m*-*C* of [BPh_4]$^-$), 126.1 (*m*-*C* of Dipp), 125.9 (N(*C*H)$_2$N of imidazole), 122.7 (*p*-*C* of [BPh_4]$^-$), 121.5 (N(*C*H)$_2$N of boryl ligand), 29.5 (*C*HMe$_2$), 24.5 (CH*Me*$_2$), 23.8 (CH*Me*$_2$) ppm. ^{11}B NMR (MeCN-d_3, 128 MHz, 298 K): δ_B 19 (br s, boryl ligand), -7 (s, [BPh_4]$^-$). MS (ESI): *m/z* (assignment, %) 841.6 ([M]$^+$, 97%). Acc. Mass ESI: calc. for $C_{55}H_{75}B_2N_6$: 841.6251; found: 841.6246. Elemental microanalysis: found (calc. for $C_{79}H_{95}B_3N_6$): C 81.60 (81.72)%, H 8.36 (8.25)%, N 7.21 (7.24)%.

Crystallographic Data for [(4)H][BPh_4]

a = 12.553(3) Å, *b* = 17.613(4) Å, *c* = 18.596(4) Å, α = 83.63(3)°, β = 73.84(3)°, γ = 72.41(3)°, V = 3762.7(15) Å^3, Triclinic, *P*1, *Z* = 2, R_1 for 10796 [data intensity $I > 2\sigma(I)$] unique data = 0.075, wR_2 (all 13459 unique data) = 0.227.

Preparation of [(4)H][PF_6]

[(**4**)H][PF_6] was synthesized in the same fashion as [(**4**)H][BPh_4] from imidazole (0.073 g, 1.1 mmol), sodium bis(trimethylsilyl)amide (0.20 g, 1.1 mmol), **1** (1.0 g, 2.1 mmol) and K[PF_6] (0.20 g, 1.1 mmol) but the resulting product was washed with hexane (3 x 15 mL), rather than benzene, to yield the product as a light brown solid. Yield: 0.70 g, 64%.

Spectroscopic Data for [(4)H][PF_6]

^{1}H NMR (toluene-d_8, 400 MHz, 298 K): δ_H 7.21-7.24 (4H, m, *p*-*H* of Dipp), 7.02-7.04 (8H, m, *m*-*H* of Dipp), 5.92 (4H, s, N(C*H*)$_2$N of boryl ligand), 2.75 (8H, sept, $^3J_{HH}$ = 6.8 Hz, C*H*Me$_2$), 1.06 (12H, d, $^3J_{HH}$ = 6.8 Hz, CH*Me*$_2$), 0.90 (12H, d, $^3J_{HH}$ = 6.9 Hz, CH*Me*$_2$) ppm. N(C*H*)$_2$N of imidazole and NC*H*N could not be located unambiguously due to potential overlap with $C_6D_4HCD_3$. ^{19}F NMR (toluene-d_8, 376 MHz, 298 K): δ_F -70.99 (d, $^1J_{FP}$ = 771.3 Hz, [PF_6]$^-$) ppm.

Preparation of [(4)H][BAr^F_4]

[(**4**)H][BAr^F_4] was synthesized in the same fashion as [(**4**)H][PF_6] from imidazole (0.058 g, 0.86 mmol), sodium bis(trimethylsilyl)amide (0.16 g, 0.86 mmol), **1** (1.0 g, 2.1 mmol) and Na[BAr^F_4] (0.76 g, 0.86 mmol), yielding the product as a brown solid. Yield: 1.3 g, 87%.

Spectroscopic Data for [(4)H][BAr^F_4]

^{1}H NMR (MeCN-d_3, 400 MHz, 298 K): δ_H 7.73 (8H, m, *o*-*H* of [BAr^F_4]$^-$), 7.69 (4H, m, *p*-*H* of [BAr^F_4]$^-$), 7.44-7.48 (2H, m, *p*-*H* of Dipp), 7.34-7.36 (4H, d, $^3J_{HH}$ = 7.8 Hz, *m*-*H* of Dipp), 7.03 (1H, br m, NC*H*N), 6.60 (2H, br m, N(C*H*)$_2$N of imidazole), 6.44 (4H, s, N(C*H*)$_2$N of boryl ligand), 2.72 (8H, sept, $^3J_{HH}$ = 6.9 Hz, C*H*Me$_2$), 1.12 (12H, d, $^3J_{HH}$ = 6.8

Hz, CH*Me*$_2$), 0.83 (12H, d, $^3J_{HH}$ = 7.0 Hz, CH*Me*$_2$) ppm. ^{13}C{^{1}H} NMR (MeCN-d$_3$, 101 MHz, 298 K): δ_C 162.6 (q, $^1J_{CB}$ = 49.9 Hz, *i-C* of [BAr$^F_4$]$^-$), 145.8 (*o-C* of boryl ligand), 136.1 (N*C*HN), 135.7 (overlapping s, *i-C* of Dipp and *o-C* of [BAr$^F_4$]$^-$), 130.5 (*p-C* of Dipp), 130.0 (qq, $^2J_{CF}$ = 31.6 Hz, $^2J_{CB}$ = 2.9 Hz, *m-C* of [BAr$^F_4$]$^-$), 126.1 (*m-C* of Dipp), 125.9 (N(*C*H)$_2$N of imidazole), 125.5 (q, $^2J_{CF}$ = 271.7 Hz, *C*F$_3$), 121.5 (N(*C*H)$_2$N of boryl ligand), 118.7 (sept, $^3J_{CF}$ = 3.9 Hz, *p-C* of BAr$^F_4$), 29.5 (*C*HMe$_2$), 24.5 (CH*Me*$_2$), 23.7 (CH*Me*$_2$) ppm. ^{11}B NMR (MeCN-d$_3$, 128 MHz, 298 K): δ_B 19 (br s, boryl ligand), -7 ppm (s, [BAr$^F_4$]$^-$). ^{19}F NMR (MeCN-d$_3$, 377 MHz, 298 K): δ_F -63.26 (br s, C*F*$_3$) ppm.

Preparation of 4(H)(^{n}Bu)

To a suspension of [(**4**)H][BPh$_4$] (0.20 g, 0.17 mmol) in toluene (5 mL) at -78 °C was added dropwise ^{n}BuLi (0.07 mL of a 2.5 M solution in hexane, 0.2 mmol). The solution was allowed to warm slowly to room temperature over 4 h. The ^{1}H NMR spectrum of an aliquot taken from the reaction mixture measured at this point indicates full conversion to the product, contaminated with *ca*. 5% of **7**. After filtration, volatiles were removed *in vacuo* to yield the crude product as an off-white powder. Yield: 0.05 g, 40%. Colourless single crystals suitable for X-ray crystallography were obtained from diethyl ether at -20 °C.

Spectroscopic Data for 4(H)(^{n}Bu)

^{1}H NMR (C$_6$D$_6$, 400 MHz, 298 K): δ_H 7.07-7.13 (4H, overlapping m, *p-H* of Dipp), 6.97-7.03 (8H, overlapping m, *m-H* of Dipp), 5.86 (4H, s, N(C*H*)$_2$N of boryl ligand), 5.12 (2H, s, N(C*H*)$_2$N of imidazole), 4.65 (1H, s, NC(*H*)(^{n}Bu)N), 3.33 (4H, sept, $^3J_{HH}$ = 6.8 Hz, C*H*Me$_2$), 3.25 (4H, sept, $^3J_{HH}$ = 6.9 Hz, C*H*Me$_2$), 1.49-1.67 (4H, overlapping m, ^{n}*Bu*), 1.21-1.27 (26H, overlapping m, CH*Me*$_2$ and ^{n}*Bu*), 1.13-1.17 (31H, overlapping m,

CH*Me*$_2$ and ^{n}*Bu*) ppm. ^{13}C{^{1}H} NMR (C_6D_6, 101 MHz, 298 K): δ_C 146.7 (*o-C* of Dipp), 146.0 (*o-C* of Dipp), 139.7 (*i-C* of Dipp), 127.7 (*p-C* of Dipp), 124.0 (*m-C* of Dipp), 119.1 (N(*C*H)$_2$N of boryl ligand), 114.1 (N(*C*H)$_2$N of imidazole), 75.9 (N*C*(H)(^{n}Bu)N), 38.1 (NC(H)(*C*H$_2$(CH$_2$)$_3$CH$_3$)N), 28.7 (*C*HMe$_2$), 28.4 (*C*HMe$_2$), 26.2 (CH*Me*$_2$), 25.7 (CH*Me*$_2$), 24.6 (^{n}*Bu*), 24.5 (^{n}*Bu*), 23.8 (overlapping s, CH*Me*$_2$ and ^{n}*Bu*), 23.6 (^{n}*Bu*), 23.4 (CH*Me*$_2$), 14.9 (*C*H$_3$ of ^{n}Bu) ppm. ^{11}B NMR (C_6D_6, 128 MHz, 298 K): δ_B 20 (br s, boryl ligand) ppm.

Crystallographic Data for 4(H)(^{n}Bu)

a = 23.9614(5) Å, b = 12.7450(3), Å, *c* = 41.0029(10) Å, α = γ = 90°, β = 105.169(2)°, V = 12085.5(5) Å^3, Monoclinic, *P*2$_1$/*c*, *Z* = 8, R_1 for 18174 [data intensity $I > 2\sigma(I)$] unique data = 0.062, wR_2 (all 25084 unique data) = 0.189.

Reaction of [(4)H][BPh$_4$] and ^{t}BuLi

To a suspension of [(**4**)H][BPh$_4$] (0.052 g, 0.045 mmol) in toluene (5 mL) at -78 °C was added dropwise ^{t}BuLi (0.03 mL of a 1.6 M solution in hexane, 0.05 mmol). The solution was allowed to warm slowly to room temperature and stirred for a further 72 h. Volatiles were removed *in vacuo* and an NMR spectra of the crude product obtained.

Spectroscopic Data for the Reaction of [(4)H][BPh$_4$] and ^{t}BuLi

^{1}H NMR (C_6D_6, 400 MHz, 298 K): δ_H 7.07-7.11 (4H, m, *p-H* of Dipp), 6.98-7.00 (8H, m, *m-H* of Dipp), 5.81 (4H, s, N(C*H*)$_2$N of boryl ligand), 5.02 (2H, s, N(C*H*)$_2$N of imidazole), 4.43 (2H, s, NC(*H*)$_2$N), 3.26 (8H, sept, $^3J_{HH}$ = 6.9 Hz, C*H*Me$_2$), 1.18 (48 H, overlapping d, CH*Me*$_2$) ppm. ^{13}C{^{1}H} NMR (C_6D_6, 126 MHz, 298 K): δ_C 146.1 (*o-C* of Dipp), 139.5 (*i-C* of Dipp), 127.9-128.4 (overlapping signals, *p-C* of Dipp and C_6D_6), 123.9 (*m-C* of Dipp), 118.3 (N(*C*H)$_2$N of boryl ligand), 114.2 (N(*C*H)$_2$N of imidazole), 66.5 (N*C*(H)$_2$N), 28.7

(*C*HMe$_2$), 24.6 (CH*Me*$_2$), 23.6 (CH*Me*$_2$) ppm. ^{11}B NMR (toluene, 128 MHz, 298 K): δ_B 20 (br s, boryl ligand) ppm.

Reaction of [(4)H][BPh$_4$] and Phenyllithium

[(**4**)H][BPh$_4$] (0.11 g, 0.095 mmol) and phenyllithium (0.008 g, 0.1 mmol) were dissolved in a mixture of benzene and diethyl ether (1 mL:0.1 mL) and the resulting mixture stirred at room temperature overnight. The ^{1}H NMR spectrum of an aliquot taken from the reaction measured at this point shows conversion to the known compound **5**,[22] in addition to several other minor species.

Reaction of [(4)H][BPh$_4$] and Mesityllithium

[(**4**)H][BPh$_4$] (0.10 g, 0.086 mmol) and mesityllithium (0.011 g, 0.086 mmol were dissolved in a mixture of C_6D_6 and diethyl ether (0.5 mL:0.05 mL) in a J. Young's NMR tube. The solution was sonicated at room temperature for 3 h, at which point the ^{1}H NMR spectrum of an aliquot of the reaction mixture contains multiple unidentifiable species. The solvent was removed *in vacuo* and the residue redissolved in hexane and filtered. A small number of colourless single crystals of **6** suitable for X-ray crystallography were obtained from the filtrate.

Crystallographic Data of 6

a = 28.5139(17) Å, b = 20.5280(8) Å, c = 32.219(2) Å, α = γ = 90°, β = 118.725(9)°, V = 16538(2) Å^3, Monoclinic, $C2/c$, Z = 4, R_1 for 8511 [data intensity $I > 2\sigma(I)$] unique data = 0.107, wR_2 (all 14427 unique data) = 0.297.

Preparation of 7

Method (a) (*in situ*): [(**4**)H][BPh$_4$] (10 mg, 0.0086 mmol) and sodium

bis(trimethylsilyl)amide (2 mg, 0.009 mmol) were dissolved in THF-d_8 (0.5 mL) in a J. Young's NMR tube. The solution turned dark brown immediately. The ^{1}H NMR spectrum measured after 10 min shows complete conversion to a single new product. Variation in the solvent, temperature and base (potassium bis(trimethylsilyl)amide) and lithium bis(trimethylsilyl)amide) employed does not appear to affect the nature of the product formed.

Method (b) (preparative scale): Imidazole (0.15 g, 2.1 mmol), potassium bis(trimethylsilyl)amide (0.85 g, 4.3 mmol) and **1** (2.0 g, 4.3 mmol) were dissolved in pentane (40 mL) and stirred at room temperature. A white precipitate formed immediately and the solution was stirred overnight. After filtration, the residual solid was extracted with pentane (2 x 5 mL) and the filtered extracts combined, concentrated and stored at -20 °C overnight producing colourless crystals. After filtration at -20 °C, the crystals were dried *in vacuo* to yield the product as a white crystalline solid. Yield: first crop – 0.54 g, 30%; second crop – 0.45 g, 25%. Colourless single crystals suitable for X-ray crystallography were obtained from diethyl ether at -20 °C.

Spectroscopic Data for 7

^{1}H NMR (THF-d_8, *in situ*, 400 MHz, 298 K): δ_H 7.24-7.31 (12H, overlapping m, *p*-*H* of Dipp and *o*-*H* of Na[BPh_4]), 7.12-7.18 (6H, overlapping m, *m*-*H* and *p*-*H* of Dipp), 7.01-7.03 (4H, m, *m*-*H* of Dipp), 6.55 (1H, d, $^4J_{HH}$ = 1.0 Hz, NC*H*N), 6.14 (2H, s, N(C*H*)$_2$N of boryl ligand), 6.06 (2H, s, N(C*H*)$_2$N of boryl ligand), 5.81 (1H, d, $^4J_{HH}$ = 1.0 Hz, NC*H*C[B]N of imidazole), 2.95 (4H, sept, $^3J_{HH}$ = 6.9 Hz, C*H*Me$_2$), 2.88 (4H, sept, $^3J_{HH}$ = 6.9 Hz, C*H*Me$_2$), 1.11 (12H, d, $^3J_{HH}$ = 6.9 Hz, CH*Me$_2$*), 1.07 (12H, d, $^3J_{HH}$ = 6.9 Hz, CH*Me$_2$*), 1.06 (12H, d, $^3J_{HH}$ = 6.9 Hz, CH*Me$_2$*), 0.76-0.80 (24H, overlapping d, CH*Me$_2$*) ppm. ^{1}H NMR (C_6D_6, 400 MHz, 298 K): δ_H 7.16-7.19 (4H, overlapping m, *p*-*H* of *C*-boryl ligand

and C_6D_5H), 7.09-7.13 (6H, overlapping m, *m*-*H* of *C*-boryl ligand and *p*-*H* of *N*-boryl ligand), 6.96-6.98 (4H, m, *m*-*H* of *N*-boryl ligand), 6.86 (1H, d, $^4J_{HH}$ = 0.8 Hz, NC*H*N), 6.15 (2H, s, N(C*H*)$_2$N of *C*-boryl ligand), 6.03 (1H, d, $^4J_{HH}$ = 0.8 Hz, NC*H*C[B]N of imidazole), 5.90 (2H, s, N(C*H*)$_2$N of *N*-boryl ligand), 3.25 (4H, sept, $^3J_{HH}$ = 6.9 Hz, C*H*Me$_2$ of *C*-boryl ligand), 2.97 (4H, sept, $^3J_{HH}$ = 6.9 Hz, C*H*Me$_2$ of *N*-boryl ligand), 1.24 (12H, d, $^3J_{HH}$ = 6.9 Hz, *C*H*Me$_2$* of *C*-boryl ligand), 1.10 (12H, d, $^3J_{HH}$ = 6.9 Hz, CH*Me$_2$* of *N*-boryl ligand), 1.06 (12H, d, $^3J_{HH}$ = 6.9 Hz, *C*H*Me$_2$* of *C*-boryl ligand), 0.82 (12H, d, $^3J_{HH}$ = 6.9 Hz, CH*Me$_2$* of *N*-boryl ligand) ppm. Integration of *p*-*H* of *C*-boryl ligand is slightly higher than expected due to partial overlap with C_6D_5H. $^{13}C\{^1H\}$ NMR (C_6D_6, 101 MHz, 298 K): δ_C 145.8 (*o*-*C* of *C*-boryl ligand), 145.4 (*o*-C of *N*-boryl ligand), 140.5 (*i*-*C* of *C*-boryl ligand), 140.1 (N*C*HN), 137.6 (*i*-*C* of *N*-boryl ligand), 128.5 (*p*-*C* of *N*-boryl ligand), 127.4 (*p*-*C* of *C*-boryl ligand), 124.8 (N*C*HC[B]N of imidazole), 124.5 (*m*-*C* of *N*-boryl ligand), 123.6 (*m*-*C* of *C*-boryl ligand), 119.8 (N(*C*H)$_2$N of *C*-boryl ligand), 118.9 (N(*C*H)$_2$N of *N*-boryl ligand), 28.7 (*C*HMe$_2$ of *C*-boryl ligand), 28.7 (*C*HMe$_2$ of *N*-boryl ligand), 24.6 (CH*Me$_2$* of *C*-boryl ligand), 24.5 (CH*Me$_2$* of *N*-boryl ligand), 24.1 (CH*Me$_2$* of *C*-boryl ligand), 23.4 (CH*Me$_2$* of *N*-boryl ligand) ppm. *C*[B] cannot be observed. ^{11}B NMR (C_6D_6, 128 MHz, 298 K): δ_B 21-24 (overlapping br s, *C*- and *N*-ligand) ppm. MS (CI): *m/z* (assignment, %) 841.6 ([M]H$^+$, 2%). Acc. Mass EI: calc. for $C_{55}H_{76}{}^{10}B^{11}BN_4$: 840.6261; found: 840.6276. Elemental microanalysis: found (calc. for $C_{55}H_{75}B_2N_6$): C 76.55 (78.47)%, H 8.64 (8.98)%, N 9.97 (9.98)%.

Crystallographic Data for 7

a = 10.4216(2) Å, *b* = 42.5113(7) Å, *c* = 23.5431(4) Å, α = γ = 90°, β = 92.6228(16)°, V = 10419.5(3) Å^3, Monoclinic, *Cc*, *Z* = 8, R_1 for 17715 [data intensity $I > 2\sigma(I)$] unique data = 0.050, wR_2 (all 18450 unique data) = 0.130.

Preparation of (3)BPh_3

Method (a): To a solution of [(**4**)H][BPh_4] (0.10 g, 0.086 mmol) and CuCl (0.13 g, 1.3 mmol) in THF (15 mL) was added sodium bis(trimethylsilyl)amide (0.016 g, 0.086 mmol) and the resulting solution stirred overnight, over which time it turned grey in colour. Volatiles were removed *in vacuo* and the residue extracted into hot hexane and filtered. A small number of colourless single crystals suitable for X-ray crystallography were obtained from the filtrate at -20 °C.

Method (b): To a solution of [(**4**)H][BPh_4] (0.10 g, 0.086 mmol) and (THT)AuCl (0.10 g, 0.31 mmol) in fluorobenzene (15 mL) was added sodium bis(trimethylsilyl)amide (0.016 g, 0.086 mmol) and the resulting solution stirred for 2 h. The ^{1}H NMR spectrum of an aliquot from the reaction mixture indicates full conversion to (**3**)BPh_3 and the known compound **8**.[22] Performing the reaction in THF rather than fluorobenzene gives a similar mixture of products.

Method (c): **3** (250 mg, 0.55 mmol) and BPh_3 (130 mg, 0.55 mmol) were dissolved in acetonitrile (15 mL) leading to the immediate formation of a precipitate. The reaction mixture was stirred for 1 h, at which point it was filtered and the solid washed with acetonitrile (2 x 5 mL) and dried *in vacuo*, yielding the product as an off-white solid. Further crops of the product could be obtained from a concentrated solution of the filtrate stored at -20 °C. Yield: first crop – 70 mg, 18%; second crop – 75 mg, 19%.

Spectroscopic Data for (3)BPh_3

^{1}H NMR (C_6D_6, 400 MHz, 298 K): δ_H 7.38 (1H, s, NC*H*N), 7.32-7.34 (6H, m, *o*-*H* of Ph), 7.12-7.25 (12H, overlapping m, *p*-*H* and *m*-*H* of Ph, *p*-*H* of Dipp and C_6D_5H), 6.97-6.98 (4H, m, *m*-*H* of Dipp), 6.51 (1H, s, [B]NCHC*H*NBPh_3), 6.06 (1H, s, [B]NC*H*CHNBPh_3),

5.90 (2H, s, N(C*H*)$_2$N of boryl ligand) 2.88 (4H, sept, $^3J_{HH}$ = 6.9 Hz, C*H*Me$_2$), 1.07 (12H, d, $^3J_{HH}$ = 6.9 Hz, CH*Me*$_2$), 0.88 (12H, d, $^3J_{HH}$ = 6.9 Hz, CH*Me*$_2$) ppm. Integration of *p-H* and *m-H* of Ph and *p-H* of Dipp is slightly higher than expected due to partial overlap with C_6D_5H. $^{13}C\{^1H\}$ NMR (C_6D_6, 101 MHz, 298 K): δ_C 153.6 (br m, *i-C* of Ph), 145.5 (*o-C* of Dipp), 139.7 (N*C*HN), 135.9 (*i-C* of Dipp), 135.0 (*o-C* of Ph), 129.5 (*p-C* of Dipp), 128.7 ([B]NCH*C*HNBPh$_3$), 127.4 (*p-C* or *m-C* of Ph), 125.1 and 124.8 (*m-C* of Dipp and *p-C* or *m-C* of Ph), 119.4 and 119.3 (N(*C*H)$_2$N of boryl ligand and [B]N*C*HCHNBPh$_3$), 28.8 (*C*HMe$_2$), 24.5 (CH*Me*$_2$), 23.3 (CH*Me*$_2$) ppm. ^{11}B NMR (C_6D_6, 128 MHz, 298 K): δ_B 20 (br s, boryl ligand), 0 (br s, N*B*Ph$_3$) ppm.

Crystallographic Data for (3)BPh$_3$

a = 13.052(3) Å, *b* = 13.739(3) Å, *c* = 14.567(3) Å, α = 67.86(3)°, β = 78.61(3)°, γ = 75.61(3)°, V = 2327.9(8) Å^3, Triclinic, *P*1, *Z* = 2, R_1 for 6251 [data intensity $I > 2\sigma(I)$] unique data = 0.077, wR_2 (all 8307 unique data) = 0.236.

Preparation of (3)PF$_5$

To a solution of [(**4**)H][PF$_6$] (150 mg, 0.15 mmol) and (THT)AuCl (49 mg, 0.15 mmol) in benzene (15 mL) was added sodium bis(trimethylsilyl)amide (28 mg, 0.15 mmol) and the resulting solution stirred for 48 h. The ^1H NMR spectrum of an aliquot taken from the reaction mixture indicates full consumption of [(**4**)H][PF$_6$] and conversion to the product, along with other unknown species. Volatiles were removed *in vacuo*, the residue dissolved in hexane and filtered. A few colourless single crystals suitable for X-ray crystallography were obtained from the filtrate at -20 °C.

Similar products were observed by ^1H NMR spectroscopy from the reaction of [(**4**)H][PF$_6$] (70 mg, 0.071 mmol) and CuCl (7 mg, 0.07 mmol) or AgOTf (18 mg, 0.071

mmol) in C_6D_6 (0.5 mL) in a J. Young's NMR tube, sonicated at room temperature for 8 or 15 h, respectively.

Spectroscopic Data for (3)PF_5

^{1}H NMR (C_6D_6, 400 MHz, 298 K): δ_H 7.70 (1H, br s, NC*H*CN), 7.16-7.23 (22H, overlapping m, *p-H* of Dipp and C_6D_5H), 7.05-7.07 (4H, m, *m-H* of Dipp), 6.79 (1H, br s, NC*H*CHN of imidazole), 5.97 (1H, br s, NC*H*CHN of imidazole), 5.91 (2H, s, N(C*H*)$_2$N of boryl ligand), 2.85 (4H, septet, $^3J_{HH}$ = 6.9 Hz, C*H*Me$_2$), 1.05 (12H, d, $^3J_{HH}$ = 6.9 Hz, CH*Me*$_2$), 0.91 (12H, d, $^3J_{HH}$ = 6.9 Hz, CH*Me*$_2$) ppm. Integration of *p-H* of Dipp is higher than expected due to partial overlap with C_6D_5H. ^{11}B NMR (C_6D_6, 128 MHz, 298 K): δ_B 20-21 (br m, boryl ligand) ppm. ^{19}F NMR (C_6D_6, 376 MHz, 298 K): δ_F -59.61 (dd, $^2J_{FF}$ = 59.4 Hz, $^1J_{FP}$ = 766.2 Hz), -82.24 (dquin, $^2J_{FF}$ = 59.4 Hz, $^1J_{FP}$ = 776.7 Hz) ppm. ^{31}P NMR (C_6D_6, 162 MHz, 298 K): δ_P -148.0 (m) ppm.

Crystallographic Data for (3)PF_5

a = 9.0872(7) Å, *b* = 22.005(2) Å, *c* = 15.4010(19) Å, α = γ = 90°, β = 101.019(10)°, V = 3022.9(5) Å^3, Monoclinic, $P2_1/n$, *Z* = 4, R_1 for 2117 [data intensity $I > 2\sigma(I)$] unique data = 0.168, wR_2 (all 4294 unique data) = 0.384.

Preparation of 9

Benzimidazole (0.13 g, 1.1 mmol), **1** (0.50 g, 1.1 mmol) and potassium bis(trimethylsilyl)amide (0.21 g, 1.1 mmol) were dissolved in benzene (15 mL) and the resulting mixture stirred for 1 h. After filtration, volatiles were removed *in vacuo.* The crude product is *ca.* 90% pure by ^{1}H NMR spectroscopy and can used for subsequent steps without further purification. Yield: 0.40 g, 74%. The product was purified by dissolving the crude solid in a minimal amount of acetonitrile at 80 °C and

allowing the solution to cool slowly in the oil bath, producing colourless crystals. The supernatant was filtered off and the crystals washed with acetonitrile (4 x 5 mL) and dried *in vacuo* to afford the product as a white solid. Yield: 0.22 g, 41%. Colourless single crystals suitable for X-ray crystallography were obtained from hexane at -20 °C.

Spectroscopic Data for 9

^{1}H NMR (C_6D_6, 400 MHz, 298 K): δ_H 7.87 (1H, d, $^{3}J_{HH}$ = 7.8 Hz, NCC*H*(CH)$_3$CN), 7.83 (1H, br s, NC*H*N), 7.14-7.18 (3H, overlapping m, *p-H* of Dipp and C_6D_5*H*), 7.04-7.06 (4H, m, *m-H* of Dipp), 6.96-6.99 (1H, m, NCCHC*H*(CH)$_2$CN), 6.90-6.94 (2H, overlapping m, NC(CH)$_2$C*H*CHCN and NC(CH)$_3$C*H*CN), 6.23 (2H, s, N(C*H*)$_2$N of boryl ligand), 3.27 (4H, sept, $^{3}J_{HH}$ = 6.8 Hz, C*H*Me$_2$), 1.14 (12H, d, $^{3}J_{HH}$ = 6.8 Hz, CH*Me*$_2$), 0.93 (12H, d, $^{3}J_{HH}$ = 6.8 Hz, CH*Me*$_2$) ppm. Integration of *p-H* of Dipp is slightly higher than expected due to partial overlap with C_6D_5H. ^{13}C{^{1}H} NMR (C_6D_6, 101 MHz, 298 K): δ_C 145.7 (*o-C* of Dipp), 145.7 (N*C*CN), 145.0 (N*C*HN), 137.8 (*i-C* of Dipp), 135.7 (NC*C*N), 128.6 (*p-C* of Dipp), 124.6 (*m-C* of Dipp), 122.9 (NC*C*H(CH)$_3$CN or NCCH*C*H(CH)$_2$CN), 122.8 (NC(CH)$_2$*C*HCHCN), 120.7 (NC*C*H(CH)$_3$CN), 119.7 (N(*C*H)$_2$N of boryl ligand), 113.0 (NC(CH)$_3$*C*HCN or NCCH*C*H(CH)$_2$CN), 28.9 (*C*HMe$_2$), 25.4 (CH*Me*$_2$), 23.0 (CH*Me*$_2$) ppm. ^{11}B NMR (C_6D_6, 128 MHz, 343 K): δ_B 22 (br s, boryl ligand) ppm. MS (EI): *m/z* (assignment, %) 504.3 ([M]$^+$, 14%). Acc. Mass EI: calc. for $C_{33}H_{41}{}^{10}BN_4$: 503.3455; found: 503.3405. Elemental microanalysis, found (calc. for $C_{33}H_{41}BN_4$): C 78.54 (78.56)%, H 8.59 (8.19)%, N 11.33 (11.11)%.

Crystallographic Data for 9

a = 10.6579(1) Å, *b* = 14.5434(2) Å, *c* = 19.6235(3) Å, α = γ = 90°, β = 105.1023(7)°, V = 2936.63(7) Å^3, Monoclinic, $P2_1/n$, *Z* = 4, R_1 for 5190 [data intensity $I > 2\sigma(I)$] unique data = 0.047, wR_2 (all 6691 unique data) = 0.121.

Preparation of [(11)H][BPh_4]

A mixture of **1** (0.15 g, 0.32 mmol), potassium bis(trimethylsilyl)amide (0.064 g, 0.32 mmol) and 4,5-dimethylimidazole (0.031 g, 0.32 mmol) in benzene (10 mL) was stirred for 1 h. Volatiles were removed *in vacuo* and a further portion of **1** added (0.15 g, 0.32 mmol). After redissolving in acetonitrile (10 mL), the resulting mixture was stirred for 15 min, whereupon Na[BPh_4] (0.11 g, 0.32 mmol) was added and the solution stirred for a further 15 min. Volatiles were removed *in vacuo*, and the residue extracted into dichloromethane and filtered. Volatiles were again removed *in vacuo* and the resulting residue washed with hot hexane (3 x 3 mL) to yield the product as a light brown powder. Yield: 0.12 g, 31%. Single crystals suitable for X-ray crystallography were obtained from a concentrated C_6D_6 solution at room temperature.

Spectroscopic Data for [(11)H][BPh_4]

^{1}H NMR (MeCN-d_3, 400 MHz, 298 K): δ_H 7.37-7.38 (4H, m, *p-H* of Dipp), 7.27-7.30 (m, 8H, *o-H* of [BPh_4]$^-$), 7.16-7.18 (8H, m, *m-H* of Dipp), 6.98-7.01 (8H, m, *m-H* of [BPh_4]$^-$), 6.83-6.86 (4H, m, *p-H* of [BPh_4]$^-$), 6.49 (4H, s, N(C*H*)$_2$N of boryl ligand), 2.73 (8H, sept, $^3J_{HH}$ = 6.8 Hz, C*H*Me$_2$), 1.85 (6H, s, N(C*Me*)$_2$N), 1.11 (24H, d, $^3J_{HH}$ = 6.7 Hz, CH*Me*$_2$), 0.74 (24H, $^3J_{HH}$ = 6.9 Hz, CH*Me*$_2$) ppm. NC*H*N could not be located. ^{13}C{^{1}H} NMR (MeCN-d_3, 101 MHz, 298 K): δ_C 164.8 (q, $^1J_{CB}$ = 49.3 Hz, *i-C* of [BPh_4]$^-$), 145.7 (*o-C* of boryl ligand), 136.7 (br m, *o-C* of [BPh_4]$^-$), 135.3 (*i-C* of Dipp), 132.5 (N(*C*Me)$_2$N), 130.0 (*p-C* of Dipp), 129.3 (N*C*HN), 126.5 (br q, $^3J_{CB}$ = 2.7 Hz, *m-C* of [BPh_4]$^-$), 125.5 (*m-C* of Dipp), 122.7 (*p-C* of [BPh_4]$^-$), 122.2 (N(*C*H)$_2$N of boryl ligand), 29.4 (*C*HMe$_2$), 25.7 (CH*Me*$_2$), 23.3 (CH*Me*$_2$), 10.4 (N(C*Me*)$_2$N) ppm. ^{11}B NMR (MeCN-d_3, 160 MHz, 298 K): δ_B 20 (br s, boryl ligand), -7 (s, [BPh_4]$^-$) ppm. MS (ESI): *m/z* (assignment, %) 869.7 ([M]$^+$, 97%). Acc. Mass ESI: calc. for $C_{57}H_{79}B_2N_6$: 869.6636; found: 869.6564.

Crystallographic Data for [(11)H][BPh$_4$]

a = 15.2400(2) Å, b = 19.7389(3) Å, c = 27.9978(4) Å, α = γ = 90°, β = 93.2466(13)°, V = 8408.8(2) Å^3, Monoclinic, $P2_1/n$, Z = 4, R_1 for 13871 [data intensity $I > 2\sigma(I)$] unique data = 0.049, wR_2 (all 17462 unique data) = 0.128.

Reaction of [(11)H][BPh$_4$] with Potassium Bis(trimethylsilyl)amide

[(**11**)H][BPh$_4$] (26 mg, 0.022 mmol) and potassium bis(trimethylsilyl)amide (5 mg, 0.02 mmol) were dissolved in benzene (1 mL) and the reaction mixture stirred for 2 h. Volatiles were removed *in vacuo* and the residue washed with a minimal amount of acetonitrile and dried *in vacuo* to yield the product as a light brown solid. Yield: 6 mg, 30%.

Spectroscopic Data for the Reaction of [(11)H][BPh$_4$] with Potassium Bis(trimethylsilyl)amide

^{1}H NMR (C_6D_6, 500 MHz, 298 K): δ_H 7.17-7.20 (35H, overlapping m, *p-H* of Dipp of *C*- or *N*-boryl ligand and C_6D_5H), 7.08-7.13 (6H, overlapping m, *m-H* of Dipp of *N*-boryl ligand and *p-H* of Dipp of *C*- and *N*-boryl ligand), 7.08 (1H, s, NC*H*N), 7.00-7.01 (4H, m, *m-H* of Dipp of *C*-boryl ligand), 6.25 (2H, s, N(C*H*)$_2$N of *N*-boryl ligand), 6.11 (2H, s, N(C*H*)$_2$N of *C*-boryl ligand), 3.42 (4H, sept, $^3J_{HH}$ = 6.9 Hz, C*H*Me$_2$ of *C*- or *N*-boryl ligand), 3.07 (4H, sept, $^3J_{HH}$ = 6.9 Hz, C*H*Me$_2$ of *C*- or *N*-boryl ligand), 2.06 (2H, s, NCC*H*$_2$[B]), 1.40 (3H, s, NC*Me*), 1.20 (12H, d, $^3J_{HH}$ = 6.9 Hz, CH*Me*$_2$ of *C*- or *N*-boryl ligand), 1.11 (12H, d, $^3J_{HH}$ = 6.8 Hz, CH*Me*$_2$ of *C*- or *N*-boryl ligand), 1.05 (12H, d, $^3J_{HH}$ = 6.9 Hz, CH*Me*$_2$ of *C*- or *N*-boryl ligand), 0.94 (12H, d, $^3J_{HH}$ = 6.9 Hz, CH*Me*$_2$ of *C*- or *N*-boryl ligand). Integration of *p-H* of Dipp is higher than expected due to partial overlap with C_6D_5H. ^{13}C{^{1}H} NMR (C_6D_6, 126 MHz, 298 K): δ_C 146.9 (*o-C* of Dipp of *C*- or *N*-boryl ligand), 145.7 (*o-C* of Dipp of *C*- or *N*-boryl ligand), 139.5 (*i-C* of Dipp of *N*-boryl

ligand), 137.5 (overlapping s, N*C*Me or N*C*CH_2[B] and *i-C* of Dipp of *C*-boryl ligand), 137.1 (N*C*Me or N*C*CH_2[B]), 127.4-128.6 (overlapping signals, *p-C* of Dipp of *C*- and *N*-boryl ligands and C_6D_6), 124.2 (*m-C* of Dipp of *C*-boryl ligand), 123.5 (*m-C* of *N*-boryl ligand), 122.9 (N*C*HN), 119.5 (overlapping s, N(*C*H)$_2$N of *C*- and *N*-boryl ligand), 28.8 (*C*HMe_2 of *C*- or *N*-boryl ligand), 28.3 (*C*HMe_2 of *C*- or *N*-boryl ligand), 25.9 (CH*Me*$_2$ of *C*- or *N*-boryl ligand), 25.7 (CH*Me*$_2$ of *C*- or *N*-boryl ligand), 23.8 (CH*Me*$_2$ of *C*- or *N*-boryl ligand), 23.1 (CH*Me*$_2$ of *C*- or *N*-boryl ligand), 10.0 (NC*Me*) ppm. NC*C*H_2[B] cannot be observed. ^{11}B NMR (C_6D_6, 128 MHz, 298 K): δ_B 22-29 (br s, boryl ligands) ppm. MS (ESI): *m/z* (assignment, %) 825.6 ([M]$^+$, 8%). Acc. Mass ESI: calc. for $C_{57}H_{78}{}^{10}B_2N_6$: 866.6541; found: 866.6526.

Preparation of 13

A mixture of 4,5-diphenylimdiazole (0.14 g, 0.64 mmol), **1** (0.60 g, 1.3 mmol) and potassium bis(trimethylsilyl)amide (0.13 g, 0.64 mmol) was dissolved in pyridine (15 mL) and the reaction mixture stirred at 110 °C for 3 d. Volatiles were removed *in vacuo* and the residue extracted into dichloromethane. After filtration, and removal of volatiles again *in vacuo*, the residue was washed with acetonitrile (3 x 5 mL) and dried *in vacuo* to yield the product as an off-white solid. Yield: 0.19 g, 49%. Colourless single crystals suitable for X-ray crystallography were obtained from a concentrated toluene solution.

Spectroscopic Data for 13

^{1}H NMR (C_6D_6, 400 MHz, 298 K): δ_H 7.59 (1H, s, NC*H*N), 7.53 (2H, m, Ar-*H* of Ph), 7.10-7.14 (2H, m, *p-H* of Dipp), 6.94-7.00 (7H, overlapping m, Ar-*H* of Ph and *m-H* of Dipp), 6.87-6.91 (3H, m, Ar-*H* of Ph), 6.78-6.79 (2H, m, Ar-*H* of Ph), 6.17 (2H, s, N(C*H*)$_2$N of boryl ligand), 3.12 (4H, sept, $^3J_{HH}$ = 6.8 Hz, C*H*Me_2), 1.07 (12H, d, $^3J_{HH}$ = 6.8 Hz, CH*Me*$_2$),

0.94 (12H, d, $^{3}J_{HH}$ = 6.9 Hz, CH*Me*$_2$). $^{13}C\{^{1}H\}$ NMR (C_6D_6, 126 MHz, 298 K): δ_C 145.4 (*o-C* of Dipp), 141.4 (*i-C* of Ph), 140.5 (N*C*HN), 137.2 (*i-C* of Dipp), 135.6 (Ar-*C* of Ph), 132.8 (Ar-*C* of Ph), 130.9 (Ar-*C* of Ph), 129.6 (*i-C* of Ph), 128.7 (Ar-*C* of Ph), 127.9-128.4 (overlapping signals, Ar-*C* of Ph and *C*$_6$D$_6$) 127.5 (*p-C* of Dipp,), 126.4 (Ar-*C* of Ph), 124.4 (*m-C* of Dipp), 119.6 (N(*C*H)$_2$N of boryl ligand), 28.7 (*C*HMe$_2$), 26.0 (CH*Me*$_2$), 22.9 (CH*Me*$_2$) ppm. ^{11}B NMR (C_6D_6, 128 MHz, 298 K): δ_B 22 (br s, boryl ligand) ppm. MS (ESI): *m/z* (assignment, %) 606.4 ([M]$^+$, 10%). Acc. Mass ESI: calc. for $C_{41}H_{47}{}^{10}BN_4$: 605.3925; found: 605.3934.

Crystallographic Data for 13

a = 15.5481(2) Å, *b* = 13.1165(2) Å, *c* = 34.0186(4) Å, α = γ = 90°, β = 93.156(1)°, V = 6927.12(16) Å^3, Monoclinic, *C*2/*c*, *P*2$_1$2$_1$2$_1$, *Z* = 8, R_1 for 6627 [data intensity $I > 2\sigma(I)$] unique data = 0.048, wR_2 (all 7204 unique data) = 0.133.

3.5 References

1 H. Niu, R. J. Mangan, A. V. Protchenko, N. Phillips, W. Unkrig, C. Friedmann, E. L. Kolychev, R. Tirfoin, J. Hicks and S. Aldridge, *Dalton Trans.*, 2018, Accepted Manuscript. DOI: 10.1039/C8DT01661E

2 L. Falivene, R. Credendino, A. Poater, A. Petta, L. Serra, R. Oliva, V. Scarano and L. Cavallo, *Organometallics*, 2016, **35**, 2286–2293.

3 S. Dierick, D. F. Dewez and I. E. Markó, *Organometallics*, 2014, **33**, 677–683.

4 M. M. D. Roy, P. A. Lummis, M. J. Ferguson, R. McDonald and E. Rivard, *Chem. Eur. J.*, 2017, **23**, 11249–11252.

5 D. Vagedes, G. Kehr, D. König, K. Wedeking, R. Fröhlich, G. Erker, C. Mück-lichtenfeld and S. Grimme, *Eur. J. Inorg. Chem.*, 2002, **2002**, 2015–2021.

6 D. Zhang and H. Kawaguchi, *Organometallics*, 2006, **25**, 5506–5509.

7 A. Wacker, H. Pritzkow and W. Siebert, *Eur. J. Inorg. Chem.*, 1998, **6**, 1–7.

8 G. Steiner, A. Krajete, H. Kopacka, K. H. Ongania, K. Wurst, P. Preishuber-Pflügl and B. Bildstein, *Eur. J. Inorg. Chem.*, 2004, **14**, 2827–2836.

9 A. P. Marchenko, H. N. Koidan, A. N. Huryeva, E. V. Zarudnitskii, A. A. Yurchenko and A. N. Kostyuk, *J. Org. Chem.*, 2010, **75**, 7141–7145.

10 A. P. Marchenko, H. N. Koidan, A. N. Hurieva, I. I. Pervak, S. V. Shishkina, O. V. Shishkin and A. N. Kostyuk, *European J. Org. Chem.*, 2012, **21**, 4018–4033.

11 A. P. Marchenko, H. N. Koidan, I. I. Pervak, A. N. Huryeva, E. V. Zarudnitskii, A. A.

Tolmachev and A. N. Kostyuk, *Tetrahedron Lett.*, 2012, **53**, 494–496.
12 A. P. Marchenko, H. N. Koidan, E. V. Zarudnitskii, A. N. Hurieva, A. A. Kirilchuk, A. A. Yurchenko, A. Biffis and A. N. Kostyuk, *Organometallics*, 2012, **31**, 8257–8264.
13 S. Solé, H. Gornitzka, O. Guerret and G. Bertrand, *J. Am. Chem. Soc.*, 1998, **120**, 9100–9101.
14 W. C. Liu, Y. H. Liu, T. S. Lin, S. M. Peng and C. W. Chiu, *Inorg. Chem.*, 2017, **56**, 10543–10548.
15 L. Benhamou, E. Chardon, G. Lavigne, S. Bellemin-Laponnaz and V. César, *Chem. Rev.*, 2011, **111**, 2705–2733.
16 P. de Frémont, N. Marion and S. P. Nolan, *Coord. Chem. Rev.*, 2009, **253**, 862–892.
17 W. A. Herrmann, *Angew. Chem. Int. Ed.*, 2002, **41**, 1290–1309.
18 T. J. Hadlington, J. A. B. Abdalla, R. Tirfoin, S. Aldridge and C. Jones, *Chem. Commun.*, 2016, **52**, 1717–1720.
19 C. R. Groom, I. J. Bruno, M. P. Lightfoot and S. C. Ward, *Acta Crystallogr. Sect. B Struct. Sci. Cryst. Eng. Mater.*, 2016, **72**, 171–179.
20 C. Elschenbroich, *Organometallics*, Weinheim : Wiley-VCH, New York, 2006.
21 R. J. Wehmschulte, J. J. Ellison, K. Ruhlandt-Senge and P. P. Power, *Inorg. Chem.*, 1994, **2**, 6300–6306.
22 Y. Segawa, Y. Suzuki, M. Yamashita and K. Nozaki, *J. Am. Chem. Soc.*, 2008, **130**, 16069–16079.
23 A. V. Protchenko and S. Aldridge, *Unpubl. Results*.
24 S. G. Weber, D. Zahner, F. Rominger and B. F. Straub, *Chem. Commun.*, 2012, **48**, 11325–11327.
25 H. Salem, L. J. W. Shimon, G. Leitus, L. Weiner and D. Milstein, *Organometallics*, 2008, **27**, 2293–2299.
26 W. V Konze, B. L. Scott and G. J. Kubas, *Chem. Commun.*, 1999, **3**, 1807–1808.
27 V. Stavila, J. H. Thurston, D. Prieto-Centurión and K. H. Whitmire, *Organometallics*, 2007, **26**, 6864–6866.
28 H. Dengel and C. Lichtenberg, *Chem. Eur. J.*, 2016, **22**, 18465–18475.
29 T. V. Ashworth, M. J. Nolte, R. H. Reimann and E. Singleton, *J. Chem. Soc., Chem. Commun.,* 1977, **0**, 937–939.
30 N. Phillips, T. Dodson, R. Tirfoin, J. I. Bates and S. Aldridge, *Chem. Eur. J.*, 2014, **20**, 16721–16731.
31 S. H. Strauss, *Chem. Rev.*, 1993, **93**, 927–942.
32 B. R. M. Lake, E. K. Bullough, T. J. Williams, A. C. Whitwood, M. A. Little and C. E. Willans, *Chem. Commun.*, 2012, **48**, 4887–4889.
33 A. J. Arduengo, R. Krafczyk, R. Schmutzler, H. A. Craig, J. R. Goerlich, W. J. Marshall and M. Unverzagt, *Tetrahedron*, 1999, **55**, 14523–14534.
34 A. A. Berkessel, M. Paul, P. Sudkaow, N. E. Schlörer and J. M. Neudörfl, *Angew. Chemie Int. Ed.*, 2018, Accepted Manuscript. DOI: 10.1002/anie.201801676.
35 M. Movassaghi and M. A. Schmidt, *Org. Lett.*, 2005, **7**, 2453–2456.
36 A. J. Arduengo, F. Davidson, H. V. R. Dias, J. R. Goerlich, D. Khasnis, W. J. Marshall and T. K. Prakasha, *J. Am. Chem. Soc.*, 1997, **7863**, 12742–12749.

37 E. L. Kolychev and S. Aldridge, *Unpubl. Results*.
38 S. J. Ryan, S. D. Schimler, D. C. Bland and M. S. Sanford, *Org. Lett.*, 2015, **17**, 1866–1869.
39 N. E. Kamber, W. Jeong, S. Gonzalez, J. L. Hedrick and R. M. Waymouth, *Macromolecules*, 2009, **42**, 1634–1639.

Chapter IV

Syntheses and Reactivity of Unsymmetrical Borylated Imidazoliums and Carbenes

---

4.1 Introduction

By blocking the C2 position of an *N*-substituted 1,4-diborylimidazole framework ([(**4.1**)H]$^+$; Scheme 4.1), the only imidazolium proton would be the one at the C5 position. Successful deprotonation at that position would result in the formation of an abnormal NHC (**4.1**), which would have two adjacent sterically demanding boryl groups. Following successful deprotonation, migration of the *N*-boryl group to C5 would be expected to be either slow or completely hindered, due to the steric bulk of both boryl groups, and could allow for isolation of the free carbene and/or its metal complexes.

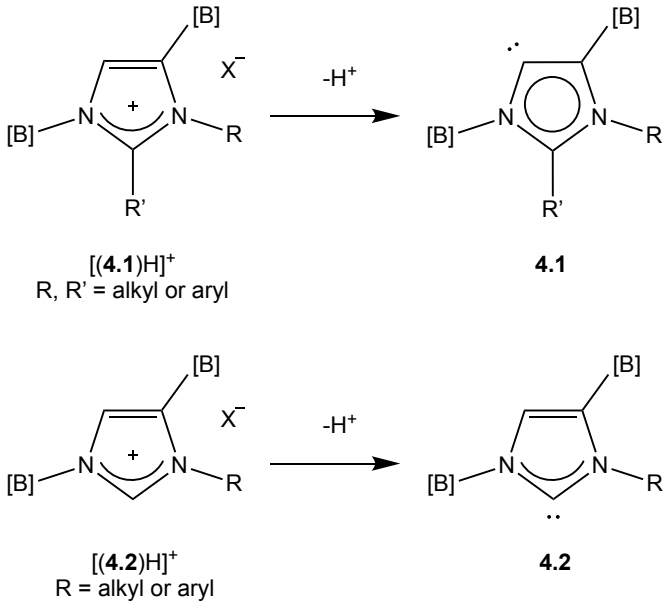

Scheme 4.1 Potential precursors for unsymmetrical bisborylated abnormal and normal NHCs, 4.1 and 4.2.

Using a similar synthon, where the C2 position is not blocked (*e.g.* [(**4.2**)H]$^+$, Scheme 4.1), one can envisage that an unsymmetrical carbene (**4.2**) could be accessed. Then the acidic protons of the imidazole are the ones in C5 and C2 positions. The results from Chapter 3 show that the C2 position does not need to be blocked for deprotonation of the backbone to take place, although the C2 position is expected to be more acidic. Removal of the C5 proton would result in an abnormal NHC, as discussed above, but removal of the more acidic C2 proton would result in a normal (but unsymmetrical) NHC. 1,2-Rearrangement of the boryl group is expected to be slowed down or hindered due to steric clash with the other *N*-substituent (R), which could allow for isolation of the free carbene and/or its metal complexes, depending on the steric protection of the other substituent.

Spectroscopic properties of free carbenes as well as their metal complexes and main group (*e.g.* Se, PR) adducts can give valuable information concerning their electronic and steric properties (see sections 1.2.3 and 1.2.4 for more details). The $\%V_{bur}$ can be obtained from the solid-state structure of metal carbene complexes (commonly AuCl systems) and can be used as a tool to compare the steric properties of the carbenes.[1–3] The Tolman electronic parameter (TEP) can be obtained from the IR spectra of metal carbonyl complexes, for example of the type $LRh(CO)_2Cl$, and compared with other carbenes.[4–6] The TEP is proportional to the C=O stretching frequency, which is inversely related to the degree of electron density present at the metal centre. Highly σ-donating carbenes thus result in a low TEP. It is, nonetheless, important to note that the TEP does not deconvolute the σ-donor and π-acceptor properties of the carbene, and that enhanced π-back-donation can result in a TEP which underestimates the true σ-donor capabilities. ^{13}C chemical shifts of free

carbenes are often used to compare their electronic properties, but this method is also ambiguous to some extent. A high degree of p-character in the σ-orbital and a low energy LUMO have both been reported to cause a downfield shift in the ^{13}C NMR signal, as well as a small singlet-triplet gap and large angle at the carbene centre.[7–10] Since these latter two characteristics are intimately related to the former two, the downfield shift is not definitive but can give implication of the electronic properties of the carbene centre to some degree. π-Acidity of carbene centres can be compared *via* the ^{31}P and ^{77}Se chemical shifts of phosphinidene and selenium adducts of the respective carbene.[11–14] A downfield shifted ^{31}P or ^{77}Se resonance indicates greater carbene π-acidity. With the availability of all these experimental probes, it is therefore highly desirable to combine the results obtained from several different methods to get a complete picture of the electronic properties of the carbene. In addition, DFT calculations can give information on the σ- and p_π-orbitals and their properties are easily separated.[5,15] The energy of each orbital can be calculated for the free carbene and the interaction of these orbitals with the orbitals of a chosen metal centre.

The aim of the research reported in this chapter is the syntheses of various unsymmetrical bisborylated imidazolium salts of type [(**4.1**)H]$^+$ and [(**4.2**)H]$^+$ (Scheme 4.1) with the aim of isolating bisborylated abnormal and normal NHCs (**4.1** and **4.2**) and/or their metal complexes.

4.2 Results and Discussion

4.2.1 Pursuing 1,4-Diborylimidazole-5-ylidenes, Bisborylated Abnormal NHCs

In order to obtain an imidazolium salt of type [(**4.1**)H]$^+$ (Scheme 4.1), both the nitrogen and C2 positions need to be alkyl- or arylated. Migrated species **7** (section 3.2.2) is potentially a good starting point for such a species: alkylation at the

unsubstituted imidazole nitrogen would generate a positively charged imidazolium salt which in turn might be alkylated at C2 by deprotonation followed by quenching with an appropriate electrophile. With this in mind, **7** was reacted with methyl trifluoromethanesulfonate to afford [(**14**)H][OTf] in 61% yield (Scheme 4.2). Colourless single crystals suitable for X-ray crystallography were grown by layering a benzene solution with pentane. The solid-state structure so obtained confirms successful methylation of the imidazole heterocycle (Figure 4.1). The *N*-substituted boryl group is slightly rotated compared with the imidazole heterocycle, by 18.0°, which is significantly less than for **7** (41.4°) for example and more in line with bisborylated imidazolium salt [(**4**)][BPh_4] (9.1° and 37.4°). Imidazolium salt [(**14**)H][OTf] can also be synthesized *via* a one-pot synthesis from imidazole and two equivalents of both **1** and potassium bis(trimethylsilyl)amide, with subsequent addition of one equivalent of methyl trifluoromethanesulfonate affording the product in 84% yield.

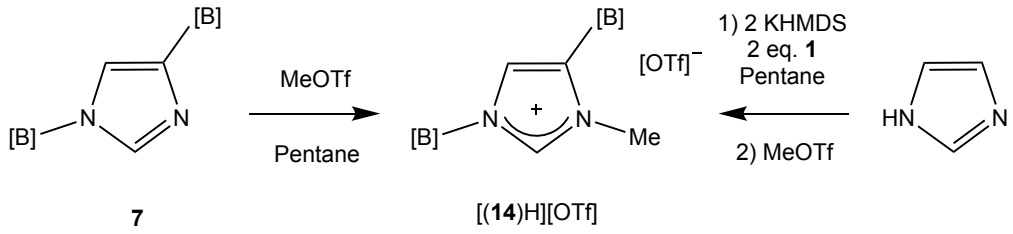

7 [(**14**)H][OTf]

Scheme 4.2 Syntheses of [(14)H][OTf] from 7 or directly from imidazole.

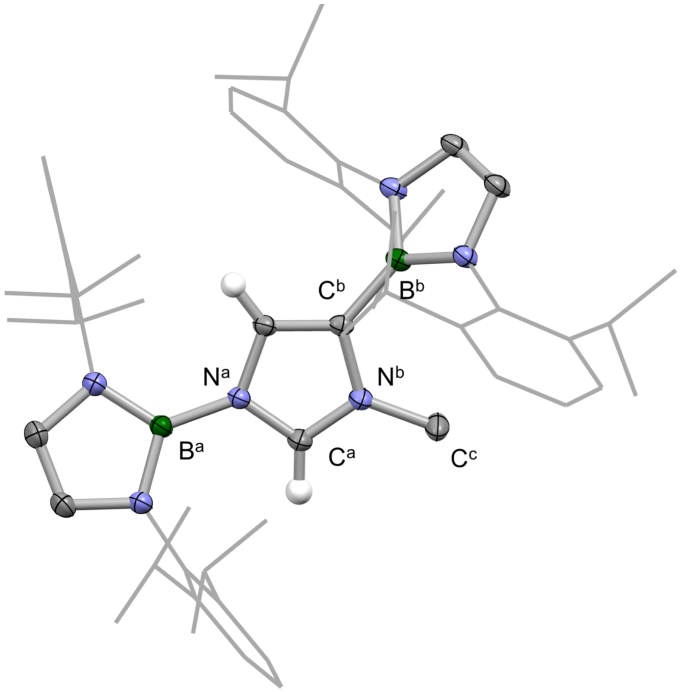

	(Å)/(°)
d(B^a–N^a)	1.491(2)
d(B^b–C^b)	1.567(2)
d(C^a–N^a)	1.344(2)
d(C^a-N^b)	1.320(2)
∠(N^a–C^a–N^b)	109.7(1)
Θ([B^a])	18.0
Θ([B^b])	49.6

Figure 4.1 (Left) Molecular structure of [(14)H][OTf] in the solid state, as determined by X-ray crystallography. Counter-ion and most hydrogen atoms omitted, and Dipp groups shown in wireframe format for clarity. Thermal ellipsoids set at the 40% probability level. (Right) Table of key structural parameters.

With the aim of blocking the C2 position to access an imidazolium salt of type [(**4.1**)H]$^+$, [(**15**)H][OTf] was accessed from [(**14**)H][OTf] in 65% yield by deprotonation/methylation at the C2 position (Scheme 4.3). Single crystals suitable for X-ray crystallography could be obtained by layering a benzene solution with pentane. The solid-state structure so obtained is depicted in Figure 4.2 and confirms successful methylation at C2.

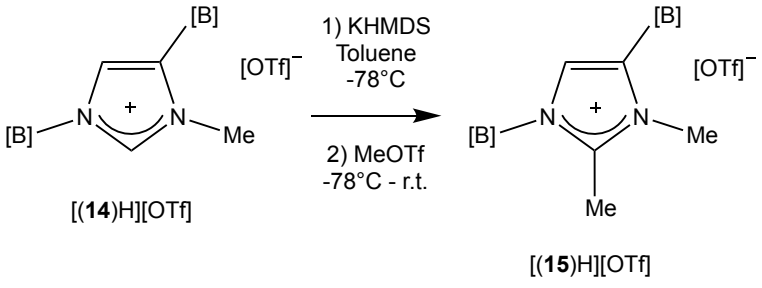

Scheme 4.3 Synthesis of [(15)H][OTf] by deprotonation/methylation of [(14)H][OTf].

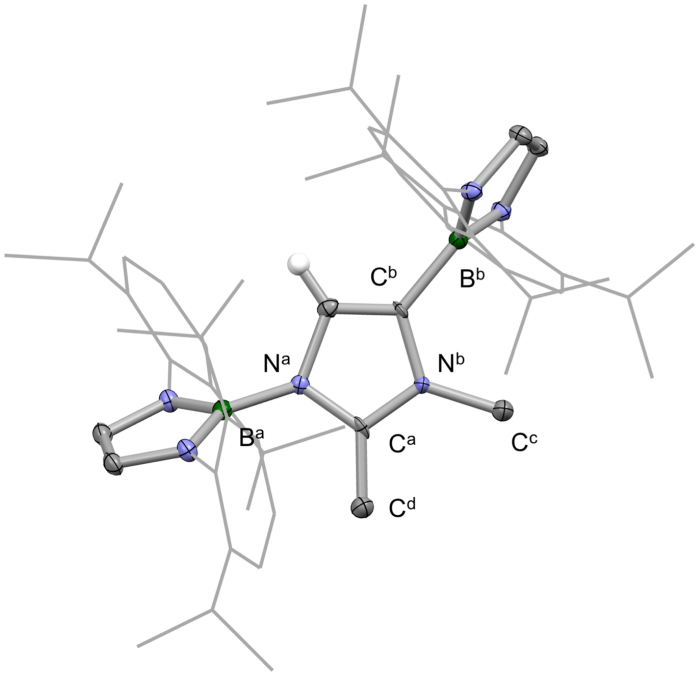

	(Å)/(°)
d(B^a–N^a)	1.45(1)
d(B^b–C^b)	1.62(1)
d(C^a–N^a)	1.33(1)
d(C^a–N^b)	1.33(2)
∠(N^a–C^a–N^b)	110(1)
Θ([B^a])	65.9
Θ([B^b])	73.3

Figure 4.2 (Left) Molecular structure of [(15)H][OTf] in the solid state, as determined by X-ray crystallography. Solvate molecule, counter-ion and most hydrogen atoms omitted, and Dipp groups shown in wireframe format for clarity. Thermal ellipsoids set at the 40% probability level. (Right) Table of key structural parameters.

Following successful synthesis of [(**15**)H][OTf], deprotonation at the C5 position was pursued with the aim of accessing an abnormal NHC. The ^{1}H NMR spectrum of the *in situ* reaction of [(**15**)H][OTf] with potassium bis(trimethylsilyl)amide in C_6D_6 shows complete consumption of the imidazolium salt and clean conversion to a single new species (Figure 4.3). The C5 proton is, however, still present as shown by a singlet at 5.50 ppm in the ^{1}H NMR spectrum and, apart from the isopropyl groups, only one methyl group can be observed, which gives rise to a singlet at 2.41 ppm integrating to three protons. Moreover, in addition to the peaks belonging to the boryl groups, two mutually coupled doublets are observed at 2.43 and 2.91 ppm, each integrating to one proton, with a coupling constant of 2.1 Hz. Furthermore, HSQC measurements indicate that both hydrogens couple to the same carbon atom and the phase-sensitive

COSY and HSQC spectra indicate that it is a secondary carbon. The product has high solubility in hexane, indicating a charge neutral species and thus implying that deprotonation has successfully taken place. The ^{1}H and ^{13}C NMR spectra, however imply that instead of the C5 proton, one proton of the *C2*-bound methyl group has been removed (**16**; Scheme 4.4). All attempts to obtain single crystals suitable for X-ray crystallography failed due to its very high solubility in hydrocarbon solvents and its moisture sensitivity.

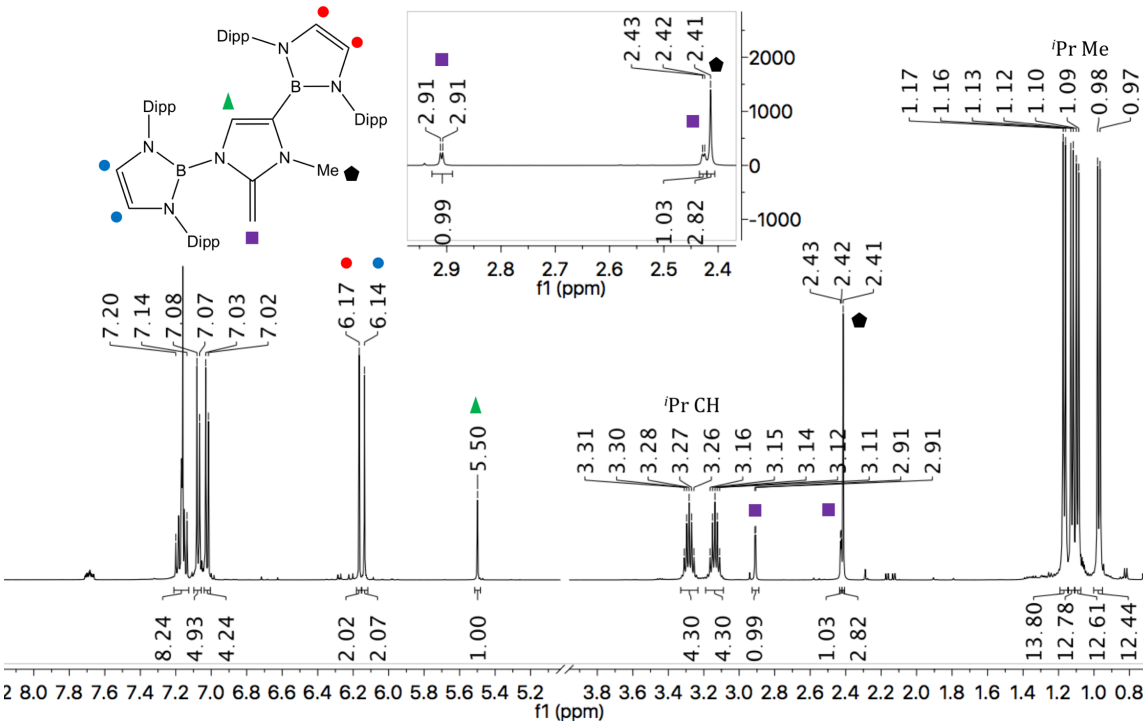

Figure 4.3 The *in situ* ^{1}H NMR spectrum of 16 in C_6D_6 at room temperature.

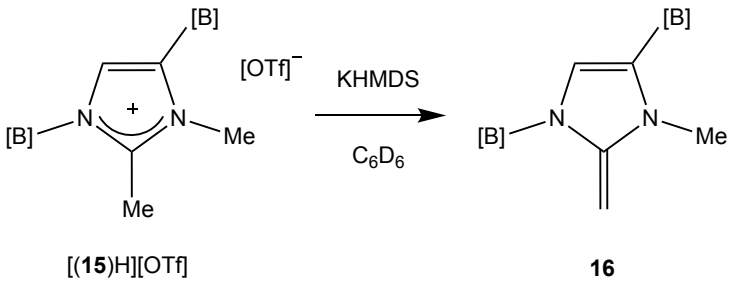

Scheme 4.4 *In situ* deprotonation of [(15)H][OTf].

Compounds of this type are well known in the literature and known as *N*-heterocyclic olefins (NHO).[16] Comparison of the ^{1}H and ^{13}C NMR spectra of **16** with those of the related Dipp-substituted species **4.3** (Scheme 4.5) supports the proposed structure of **16**.[17] The olefinic ^{1}H and ^{13}C chemical shifts for **4.3** are 2.42 ppm (singlet, two protons) and 44.3 ppm, respectively. The corresponding signals fall at 2.43, 2.91 and 46.6 ppm, respectively for **16**, the olefinic protons being chemically inequivalent due to the unsymmetrically substituted backbone. The geminal coupling constant, $^{2}J_{HH}$ = 2.1 Hz, is in good agreement with literature precedent (*ca*. 0-3 Hz).[18] NHOs are interesting ligands in their own right and the reactivity of **16** in metal complexes could be of great interest.

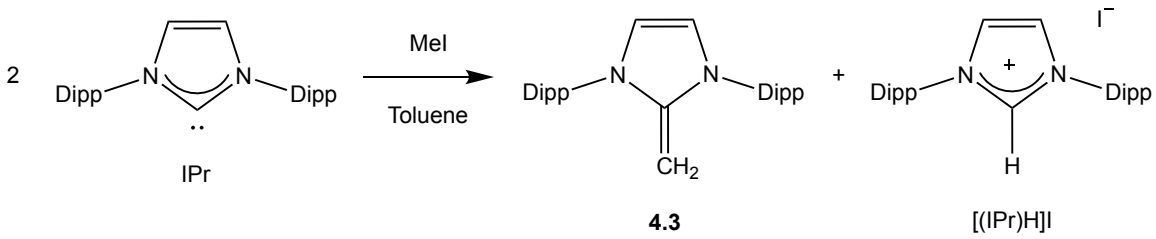

Scheme 4.5 Synthesis of a Dipp substituted *N*-heterocyclic olefin (NHO), 4.3.[17]

It is clear that in order to synthesize the target abnormal carbene, a non-acidic substituent is needed to block the C2 position. Alkyl- or arylation at C2 of [(**14**)H][OTf] relies on the use of a non-halogenated electrophile (such as triflate) due to the risk of nucleophilic attack of a halide on the *N*-substituted boryl group. Thus, readily available options other than methyl – which do not possess potentially acidic hydrogens – are limited. Access to imidazolium precursors of type [(**4.1**)H]$^{+}$ was therefore sought *via* a different synthetic approach. One possibility is the use of a C2-substituted imidazole as a building block for borylation, and conveniently 2-phenylimidazole is commercially available. Two proposed retrosynthetic routes to imidazolium precursor **4.6** are depicted in Scheme 4.6.

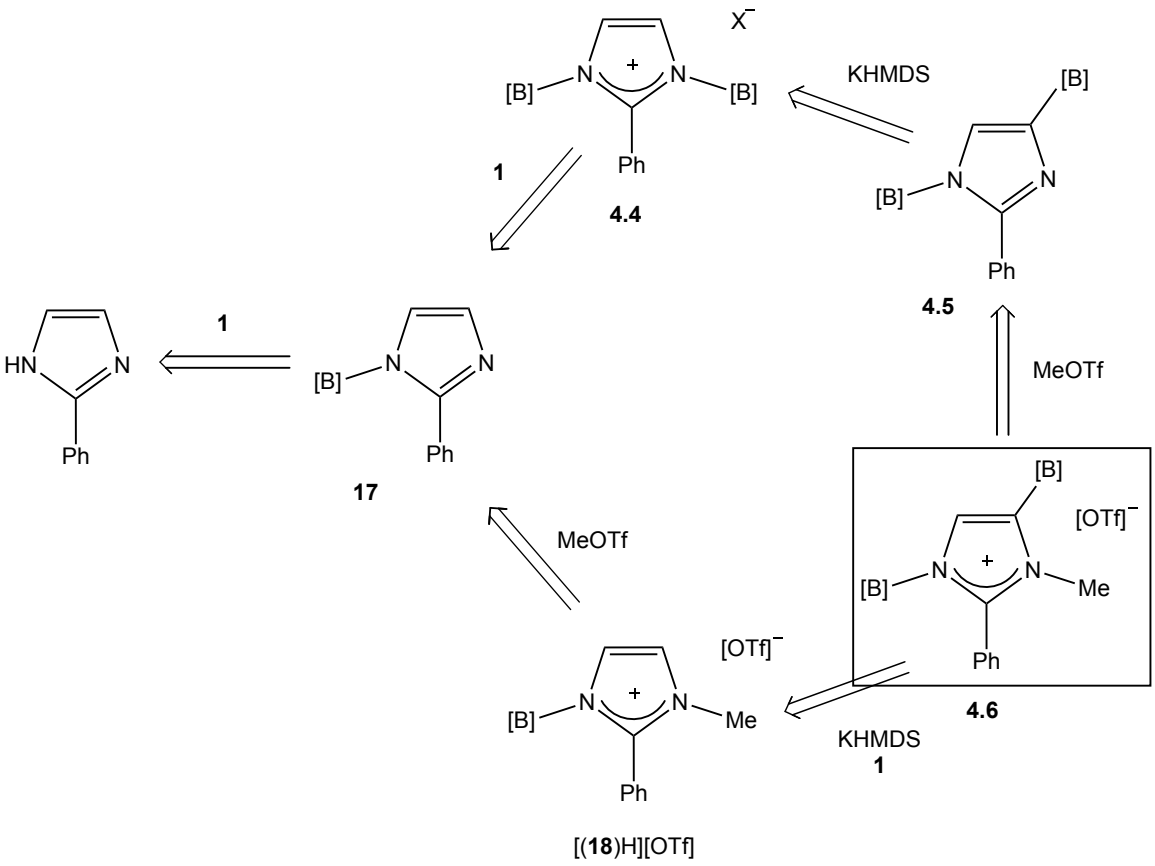

Scheme 4.6 Proposed retrosynthetic approach for 4.6, a potential precursor to an abnormal NHC.

The first step for both synthetic routes involves borylation of 2-phenylimidazole. In the forward sense, deprotonation of 2-phenylimidazole with ^{n}BuLi and subsequent addition of one equivalent of **1** gives rise to full consumption of 2-phenylimidazole and clean conversion to a single new species in the ^{1}H NMR spectrum of the reaction mixture. The new product, **17**, was isolated in 59% yield (Scheme 4.7). The product has not been structurally characterized by X-ray crystallography, but the ^{1}H NMR spectrum is consistent with successful borylation of 2-phenylimidazole. Following the upper route in Scheme 4.6, the second step relies on borylation of the unsubstituted nitrogen in **17** to give **4.4**. However, the *in situ* ^{1}H NMR spectrum of the reaction of imidazole **17** with **1** that has been heated in pyridine-d_5 at 110 °C for four days indicates no reactivity, presumably due to the relatively low nucleophilicity of the arylated imidazole, in agreement with results discussed in section 3.2.4.

Furthermore, **4.5** could not be accessed directly by reacting **17** in the presence of one equivalent of both **1** and potassium bis(trimethylsilyl)amide in C_6D_6 at 80 °C.

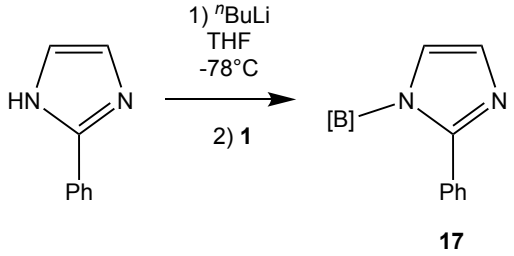

17

Scheme 4.7 Reaction of 2-phenylimidazole with ^{n}BuLi and 1.

Since these reactions were unsuccessful, the lower route in Scheme 4.6 was attempted and methylation of imidazole **17** was therefore of interest. The *in situ* ^{1}H NMR spectrum of the reaction of **17** with methyl trifluoromethanesulfonate in CD_2Cl_2 shows full consumption of the starting materials and conversion to a new product. The spectrum is consistent with successful methylation of **17** (Scheme 4.8), although the product has not been structurally characterized by X-ray crystallography.

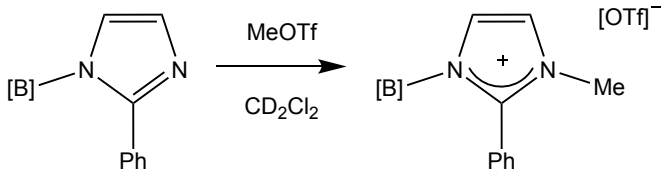

17 [(**18**)H][OTf]

Scheme 4.8 Reaction of 17 with methyl trifluoromethanesulfonate.

The last step towards accessing target imidazolium salt **4.6** relies on borylation of [(**18**)H][OTf] at C4. [(**18**)H][OTf] was reacted with potassium bis(trimethylsilyl)amide in the presence of **1** and, although the ^{1}H NMR spectrum of the reaction mixture shows full consumption of [(**18**)H][OTf] and conversion to a single new species, the data is not consistent with successful borylation. The signals for **1**, for example, remain unchanged but the nature of the imidazole-derived product is unknown. 1,2-

rearrangement might be taking place, although no concrete evidence is available.

4.2.2 Synthesis and Properties of 1,4-Diboryl-3-methylimidazol-2-ylidene

Imidazolium salt [(**14**)H][OTf] also represents a potential precursor for a 'normal' NHC (**4.2**; Scheme 4.1): successful deprotonation at the C2 position would allow access to an unsymmetrical NHC with one adjacent boryl group. Its reactivity towards strong bases was therefore examined. Upon addition of potassium bis(trimethylsilyl)amide to a solution of [(**14**)H][OTf] in toluene-d_8 or C_6D_6, immediate full consumption of the imidazolium salt and clean conversion to a single new species is observed by ^{1}H NMR spectroscopy. Moreover, a peak at 225.8 ppm is observed in the ^{13}C NMR spectrum, in the region characteristic of NHCs (Figure 4.4).[7] At room temperature, the signals for the new product slowly disappear in both the ^{1}H and ^{13}C NMR spectra and a new set of resonances appears. Full consumption of the product is observed after 12 h, at which stage no signal is retained above 150 ppm in the ^{13}C NMR spectrum.

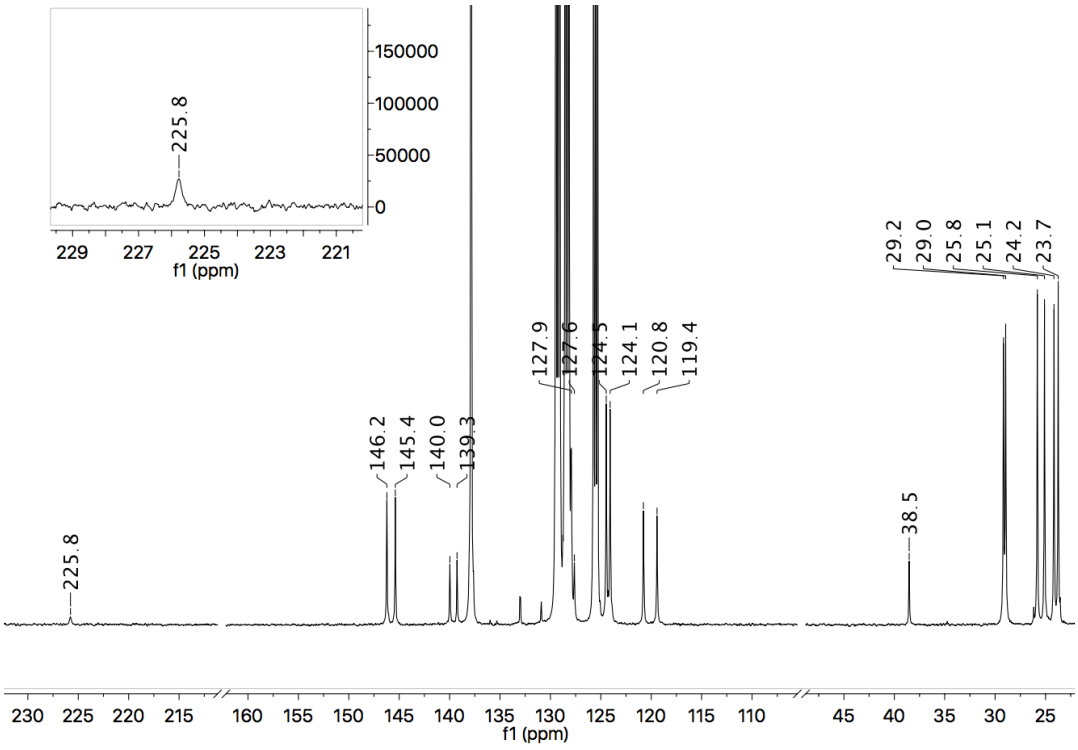

Figure 4.4 The *in situ* ^{13}C NMR spectrum of 14 in toluene-d_8.

These observations suggest the formation of carbene **14**, which apparently then undergoes 1,2-rearrangement (N-to-C) of the boryl group to the C2 position to give **19** (Scheme 4.9). The identity of **19** could be established by X-ray crystallography. Single crystals were obtained by recrystallization from diethyl ether. The solid-state structure so determined (Figure 4.5) shows an imidazole heterocycle with *C2*- and *C4*-substituted boryl groups and an *N*-bound methyl group, and therefore corroborates the structure of **19** proposed in Scheme 4.9. Along with the *in situ* NMR spectroscopic data, this structure offers encouragement that the free carbene had in fact successfully been synthesized. Unfortunately, all attempts to crystalize the free carbene were unsuccessful and its characterization relies instead on a range of trapping experiments (see section 4.2.4).

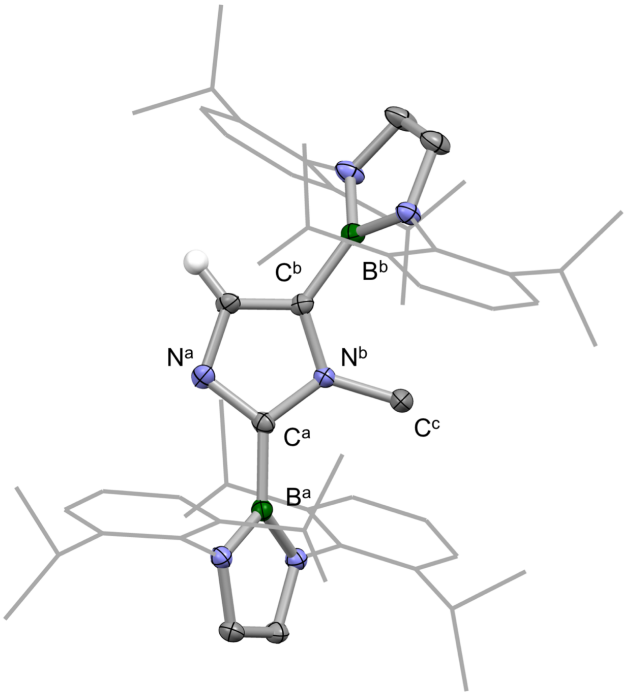

	(Å)/(°)
d(B^a–C^a)	1.560(5)
d(B^b–C^b)	1.563(4)
d(C^a–N^a)	1.360(6)
d(C^a–N^b)	1.371(3)
∠(N^a–C^a–N^b)	105.7(4)
Θ([B^a])	51.2
Θ([B^b])	59.3

Figure 4.5 (Left) Molecular structure of 19 in the solid state, as determined by X-ray crystallography. Most hydrogen atoms omitted, and Dipp groups shown in wireframe format for clarity. Thermal ellipsoids set at the 40% probability level. (Right) Table of key structural parameters.

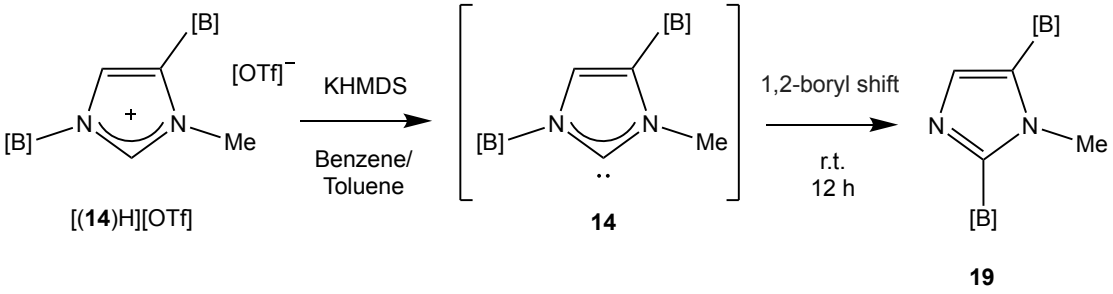

Scheme 4.9 *In situ* deprotonation of [(14)H][OTf] with subsequent 1,2-rearrangement of the *N*-substituted boryl group at room temperature.

While intramolecular 1,2-rearrangement in singlet carbenes are well studied,[19–21] such rearrangement in aromatic carbenes has, until now, been considered too thermodynamically unfavourable due to dearomatization.[22,23] Intermolecular pathways in NHCs have been confirmed with crossover experiments carried out by Solé *et al.*[19] and Liu *et al.*[24] The former group suggests that the rearrangement proceeds through a nucleophilic attack by the carbene centre on the *N*-substituent (Scheme 1.17; section 1.2.7), whereas the latter group predicts a radical pathway (Scheme 1.19; section 1.2.7). The two mechanisms are discussed in more details in section 1.2.7. The rate determining step in an intermolecular pathway that proceeds through nucleophilic attack is expected to be bimolecular, which would have high negative entropy change. In the homolytic radical pathway, the rate determining step is undeniably the homolytic cleavage to form the two radical fragments and has thus high positive entropy change.

In order to establish whether the reaction proceeds *via* an intra- or intermolecular pathway, kinetic experiments were carried out, with the conversion of the free carbene to the rearranged species being monitored as a function of time at different temperatures. A bimolecular rate determining step might be expected to yield second order kinetics, whereas a monomolecular rate determining step might be expected to

yield first order kinetics. Therefore, imidazolium salt [(**14**)H][OTf] and potassium bis(trimethylsilyl)amide were placed in a J. Young's NMR tube along with a sealed capillary tube containing an internal standard (4-bromobenzaldehyde in toluene-d_8). The starting materials were dissolved in toluene-d_8 at -78 °C and maintained at -78 °C until inserted into the NMR spectrometer. The sample was then warmed to a given temperature and the conversion of **14** to **19** monitored by ^{1}H NMR spectroscopy as a function of time. The probe temperature was varied between each individual experiment, measurements being conducted at 298, 303, 308, 318 and 323 K. The changes in intensity of three resonances in the ^{1}H NMR spectra were monitored with time (Figure 4.6): the boryl backbone protons of the carbene **14** (a1 or a2; 5.97 ppm), the backbone imidazole proton of the migrated species **19** (b; 6.58 ppm) and the *N*-methyl protons of **19** (c; 2.84 ppm). These peaks were chosen as they do not overlap with other peaks in the spectrum. The internal standard, 4-bromobenzaldehyde, was chosen as its signals do not overlap with the signals of interest, and the aldehydic proton (9.39 ppm) is well separated and can therefore be integrated accurately. Figure 4.7 shows the ^{1}H NMR spectra of the reaction mixture after 25 min, 2 h, 6 h and 20 h at 298 K.

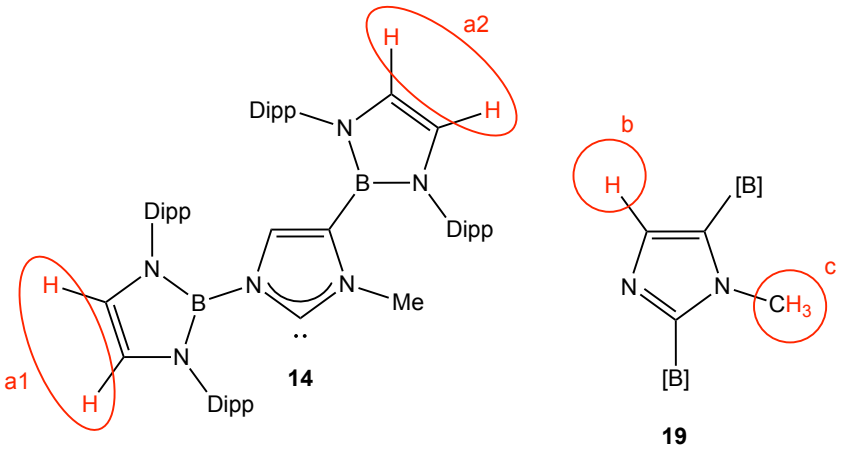

Figure 4.6 The protons of 14 and 19 monitored as a function of time.

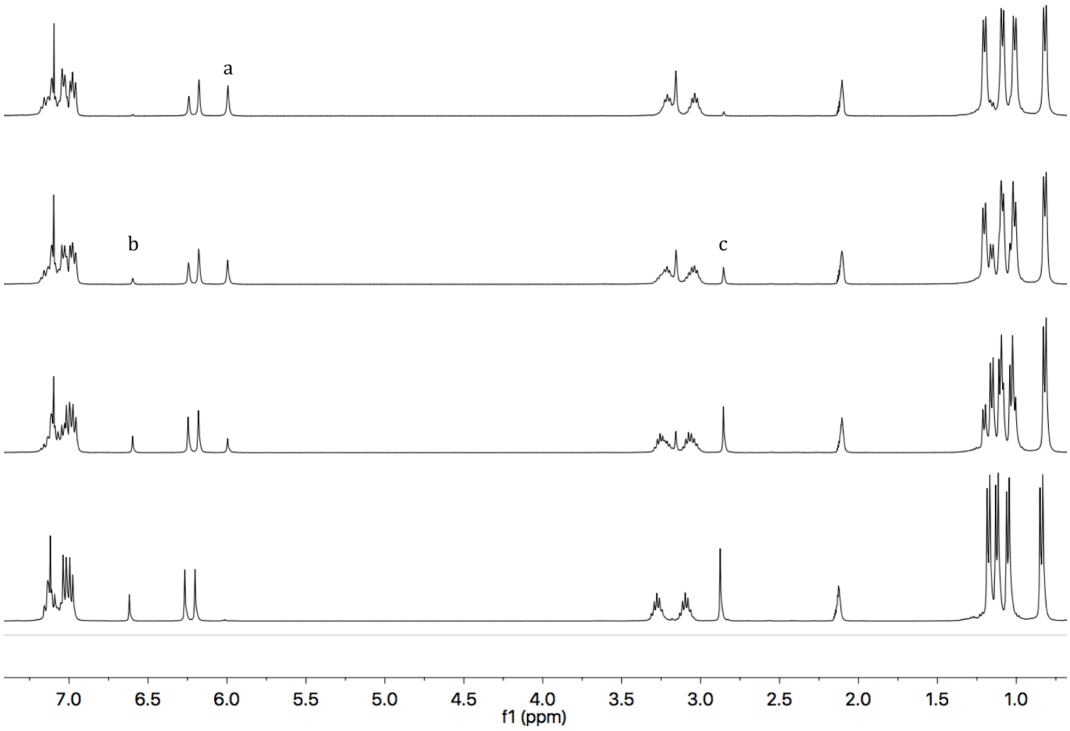

Figure 4.7 1,2-Rearrangement of carbene 14 monitored *in situ* by ^{1}H NMR spectrometry in toluene-d_8 at 298 K. The changes in intensity of resonances labelled a, b and c (Figure 4.6) were monitored with time. The spectra were recorded after 25 min (top), 2 h, 6 h and 20 h (bottom).

The ratio of the proportion of free carbene **14** and migrated species **19** was calculated from the integrals listed above at each given time and temperature (Figure 4.8). An exponential plot is obtained when the percentage of the free carbene is plotted with respect to time at all temperatures, and the plots are linear (R^2 = 0.995 - 0.999) for the natural logarithm of the percentage of free carbene **14** (ln(%**14**)) with respect to time at each temperature (Figure 4.8). This suggests that the rate determining step of the 1,2-rearrangement is first-order, and is therefore not likely to be intermolecular – as has previously been reported for other NHCs.[19,24,25] From the data obtained at 298 K, the rate constant, k = (4.80 ± 0.04) x 10^{-5} s^{-1}, and half-life, $t_{½}$ = 4.01 ± 0.04 h, could be determined for the reaction at room temperature.[26,27]

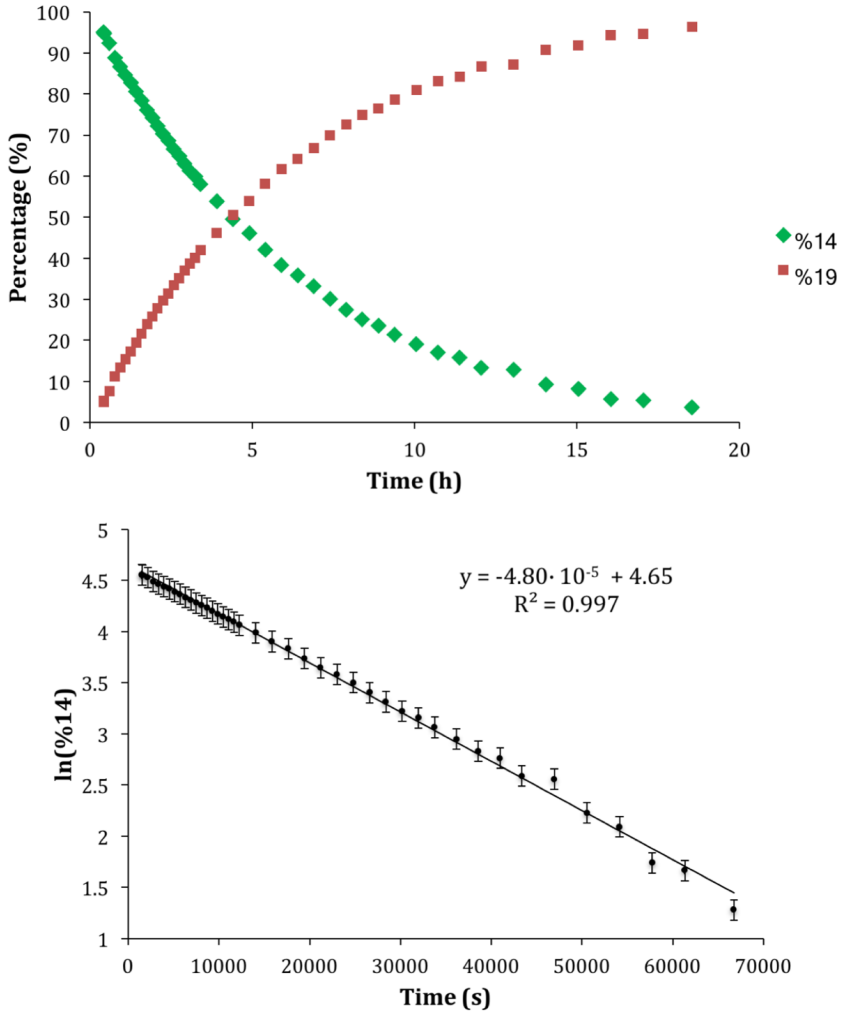

Figure 4.8 (Upper) Percentage free carbene 14 and rearranged species 19 with respect to time. (Lower) Natural logarithm of the percentage of free carbene 14 with respect to time.

The rate constants and half-lives of the carbene were calculated at different temperatures and an Eyring plot (ln(k/T) *vs* 1/T; Figure 4.9) used to estimate both the enthalpy and entropy of activation: $\Delta H^{\ddagger} = 97 \pm 2$ kJ mol^{-1} and $\Delta S^{\ddagger} = -3.1 \pm 0.2$ J mol^{-1} K^{-1}, respectively.[28] A mechanism involving a bimolecular rate-determining step typically would proceed with a large negative entropy, while dissociative radical process would usually give rise to a large positive entropy of activation. In this case, however, a small negative entropy of activation is observed. These data suggest therefore that the 1,2-shift of the boryl group is unlikely to proceed through an intermolecular nucleophilic or dissociative radical pathway.

T (K)	k (s^{-1})	$t_{½}$
298	(4.80 ± 0.08) x 10^{-5}	4.01 ± 0.07 h
303	(9.14 ± 0.07) x 10^{-5}	2.10 ± 0.02 h
308	(1.90 ± 0.04) x 10^{-4}	1.01 ± 0.02 h
318	(6.3 ± 0.2) x 10^{-4}	18.4 ± 0.4 min
323	(1.03 ± 0.02) x 10^{-3}	11.2 ± 0.3 min

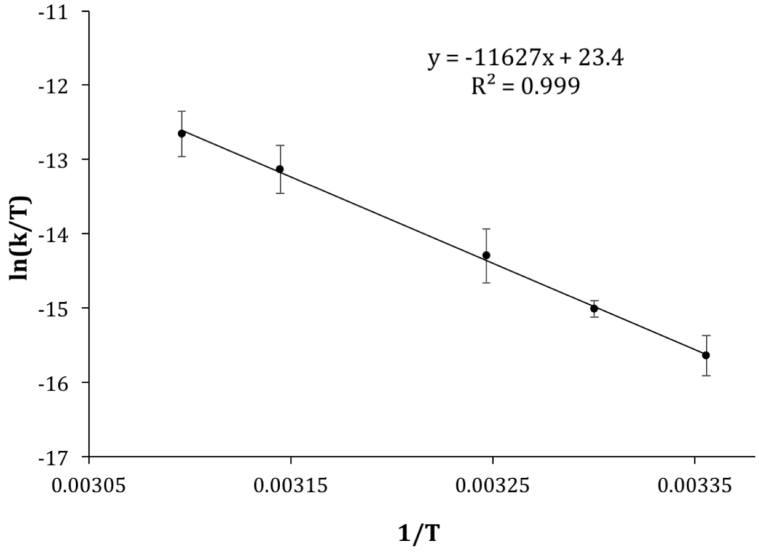

Figure 4.9 (Upper) Rate constant (k) of the 1,2-rearrangement and the half-life ($t_{½}$) of 14 at given temperatures (T). (Lower) Eyring plot: natural logarithm of k/T with respect to 1/T.

Experiments were carried out to see if any radicals could be detected during the 1,2-rearrangement of **14**. An EPR spectrum of the *in situ* reaction of [(**14**)H][OTf] with potassium bis(trimethylsilyl)amide in C_6D_6 was measured but no relevant radical species could be observed in the spectrum. The *in situ* reactivity with radical traps was also investigated. It is, however, worth noting that addition of such reagents to the reaction mixture might alter the mode of reactivity and the interpretation of the product distribution therefore need to be made with caution. Carrying out the reaction of [(**14**)H][OTf] with potassium bis(trimethylsilyl)amide in the presence of either one equivalent of (2,2,6,6-tetramethylpiperidin-1-yl)oxidanyl (TEMPO) or 20 equivalents of 2,3-dimethylbutadiene had no effect on the course of the reaction, with the 1,2-rearrangement proceeding to completion in a similar fashion. Specifically, to rule out

the possibility that a radical intermediate was formed in the reaction with TEMPO, but reacted with TEMPO to give a product which is not directly observable by ^{1}H NMR spectroscopy, the signals for the migrated species **19** were integrated and compared to that of bis(trimethylsilyl)amine (at 0.10 ppm). Comparison of the respective integrals reveals that equimolar amounts of the two products are present in solution, suggesting full conversion to **19** and that no intermediate has reacted with TEMPO.

As discussed in section 1.2.7, the barriers to intramolecular 1,2-shifts in aromatic carbenes have been calculated to be too high to be mechanistically compatible with the observed reactivity. In part, this reflects the need for dearomatization to allow for interaction of the exocyclic σ-bond of the migrating group and the empty p_{π}-orbital of the carbene. The kinetic data for the 1,2-shift of the boryl group in **14** (notably the first order kinetics and entropy of activation close to zero) do not appear to be consistent with the reaction being intermolecular, implying the possibility of a different mechanism in this case. To gain insight into the mechanism, DFT calculations for an intramolecular rearrangement were carried out by Dr. Petra Vasko (of the Aldridge group), using solvent model (continuum model, toluene) and replacing the Dipp groups with Xyl (2,6-dimethylphenyl) for geometry optimizations. The results are in broad agreement with the experimental kinetic data. Thus the enthalpy and entropy of activation derived from DFT calculations are: $\Delta H^{\ddagger}$ = 95 kJ mol^{-1} and $\Delta S^{\ddagger}$ = 9 J mol^{-1} K^{-1}, compared with the experimental values: $\Delta H^{\ddagger}$ = 97 ± 2 kJ mol^{-1} and $\Delta S^{\ddagger}$ = -3.1 ± 0.2 J mol^{-1} K^{-1}. The activation barrier ($\Delta G^{\ddagger}$ = 92 kJ mol^{-1} at 298 K) is not only consistent with the experimental value ($\Delta G^{\ddagger}$ = 98 ± 2 kJ mol^{-1} at 298 K), but significantly lower than the values calculated for other *N*-heterocyclic systems, *e.g*. 288 kJ mol^{-1} for the 1,2-shift of hydrogen in 2,3-dihydroimidazol-2-ylidene[29] and 177 kJ mol^{-1} for the 1,2-

shift of hydrogen in 2,3-dihydrothiazol-2-ylidene.[23] This data does therefore provide some support that an intramolecular pathway is feasible in this system.

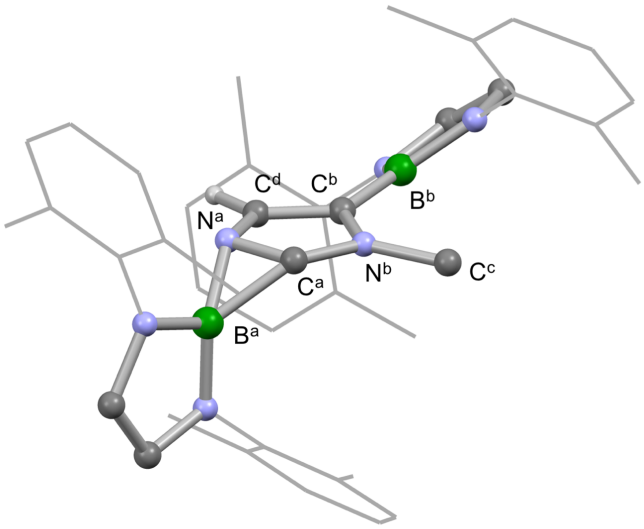

	(Å)/(°)
d(B^a–N^a)	1.598
d(B^a–C^a)	1.698
d(C^a–N^a)	1.351
d(C^a–N^b)	1.350
d(N^a–C^d)	1.375
d(N^b–C^b)	1.395
d(C^b–C^d)	1.370
∠(N^a–C^a–N^b)	109.0
Θ([B^a])	89.9
Θ([B^a-N^a-C^a])	37.3

Figure 4.10 (Left) Molecular structure of the transition state for the 1,2-shift of the boryl group in the Xyl analogue of 14 as determined by DFT calculations. Most hydrogen atoms omitted, and Xyl groups shown in wireframe format for clarity. (Right) Table of key structural parameters. Θ([B^a]) indicates the angle between the plane of the *N*-substituted boryl group and the imidazole heterocycle. Θ([B^a-N^a-C^a]) indicates the angle between the B^a/N^a/C^a plane and the imidazole heterocycle.

The structure of the transition state is depicted in Figure 4.10. The boron of the migrating boryl group is projected 37.3° out of the imidazole heterocycle plane (Θ([B^a-N^a-C^a]); Figure 4.10). Comparison of the bond lengths of the imidazole heterocycle in the transition state with the solid-state structure of imidazolium salt [(**14**)H][OTf] and the calculated structure of carbene **14** (Figures 4.1 and 4.23, respectively), however, do not imply dearomatization of the ring. The C^a–N^a bond length (1.351 Å) lies between the corresponding bond lengths in [(**14**)H][OTf] (1.344(2) Å) and **14** (1.390 Å). The C^a–N^b bond length (1.350 Å) is very similar to the C^a–N^a bond length, but slightly shorter than the corresponding bond length in **14** (1.358 Å), and longer than in [(**14**)H][OTf] (1.320(2) Å).

In the calculated mechanisms that have been reported in literature,[22,23] dearomatization is observed as the migrating group needs to lie above/below the plane of the aromatic system to allow for interaction of the (now parallel) σ-bond of the migrating group and the p_π-orbital of the carbene (Scheme 1.14). In this system, however, the calculated position of the boryl group, projected only 37.3° out of the imidazole heterocycle plane does not imply that the N–B σ-bond and the p_π-orbital at C^a are aligned parallel. Several reactions reported in this thesis imply that the *N*-bound boryl group in systems of this type are strongly electrophilic. It is therefore possible that instead of migration proceeding *via* formal donation of the electrons of the N–B σ-bond into the p_π-orbital at C2 (*i.e*. formal migration of an anionic boryl fragment), the boryl group might be migrating as an electrophilic (formally cationic) species, which 'shuttles' between the exocyclic N- and C2-centred lone pairs, and as such does not bring about dearomatization in the imidazole heterocycle (Figure 4.11). If the orientation of the migrating boryl group is examined in more detail, one can see that its plane lies perpendicular to the imidazole heterocycle. This orientation would allow for interaction of the vacant p_π-orbital at boron with the σ-orbitals (lone pairs) of both N^a and the carbene carbon; the migrating boryl electrophile is therefore stabilized in the transition state by both N/C lone pairs (Figure 4.11). In addition, this alignment of the boryl group below the imidazole heterocycle plane would allow for additional stabilization of the electron deficient boron centre *via* donation from the aromatic π-system of the imidazole heterocycle into the formally vacant boron σ-orbital (Figure 4.11).

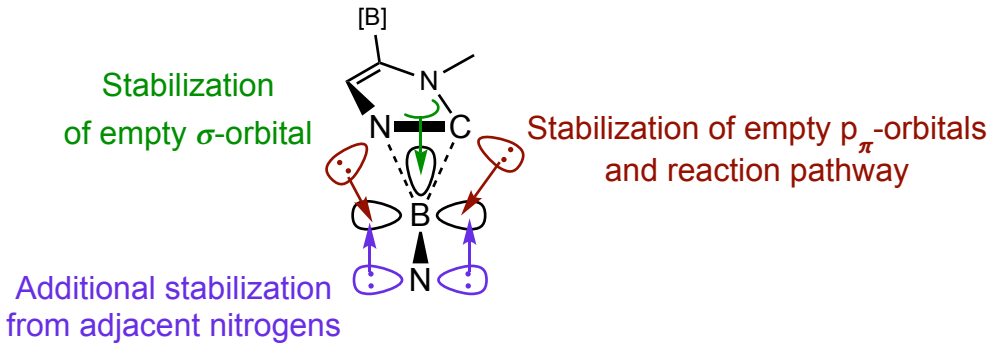

Figure 4.11 Proposed stabilization of the migrating 'cationic' boryl group in the transition state.

The reason underpinning this alternative pathway might arise from the fact that the migrating groups in the systems that have previously been explored computationally do not possess a vacant p_π-orbital, and thus rely solemnly on the aforementioned interaction of the N–R σ-bond with the p_π-orbital at C2 (and thus results in dearomatization). On the other hand, experimental data on a previously reported 1,2-shift of a $BMes_2$ group, which does possess a vacant p_π-orbital, suggests an intermolecular (radical) pathway.[24] A significant difference between $BMes_2$ and the diazaboryl moiety is the presence of the nitrogen atoms α to the boron centre in the latter which are π-donating and could serve to provide additional stabilization of the migrating diazaboryl 'cation' and thus lower the energy of the transition state. This would not be the case for $BMes_2$ and the transition state of the corresponding 1,2-shift would therefore be higher in energy.

4.2.3 Kinetic Experiments on Other *N*-Boryl-*N*'-Methyl NHCs

Given the mechanistic issues discussed above, comparison of the kinetic parameters associated with the boryl group migration in **14** with other *N*-borylated NHCs would clearly be of interest. Two examples which were thought to be synthetically feasible are carbenes **20** and **21** (Figure 4.12), both of which lack the boryl group at the backbone position but contain one boryl group and one methyl group as *N*-

substituents. The steric properties around the carbene centre are therefore similar to **14**, but the absence of the second boryl group might influence the electronic properties of the carbene and thus the rate of the 1,2-shift.

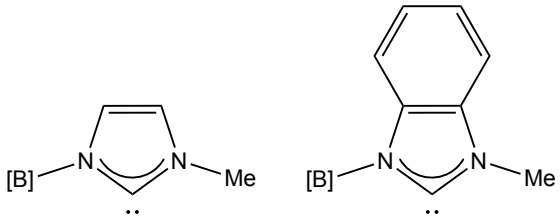

20 **21**

Figure 4.12 Other *N*-boryl-*N'*-methyl NHCs.

Monoborylated imidazole **3** (section 3.2.1) and benzimidazole **9** (section 3.2.4) represent potential precursors for the syntheses of the parent imidazolium salts, [(**20**)H]$^+$ and [(**21**)H]$^+$ (Scheme 4.10). Accordingly, **3** and **9** were readily methylated using methyl trifluoromethanesulfonate to give [(**20**)H][OTf] and [(**21**)H][OTf] in 87% and 85% isolated yields, respectively. Colourless single crystals suitable for X-ray crystallography could be obtained from hot acetonitrile and hot hexane, respectively. The solid-state structures (Figures 4.13 and 4.14) so obtained confirm successful *N*-methylation of the two imidazole precursors.

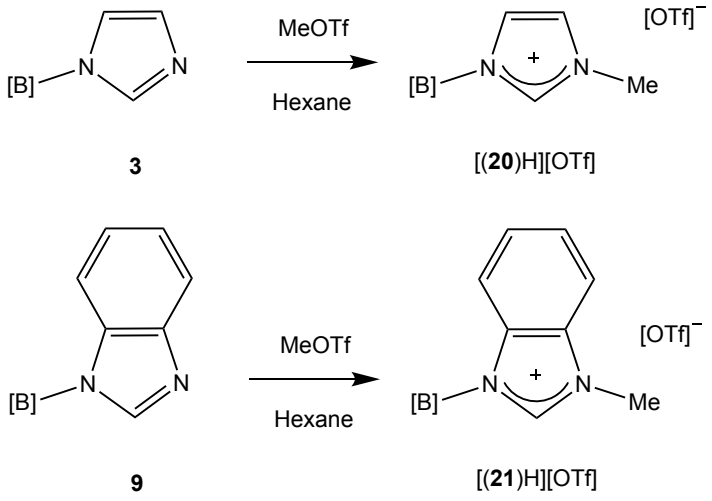

3 [(**20**)H][OTf]

9 [(**21**)H][OTf]

Scheme 4.10 Syntheses of [(20)H][OTf] and [(21)H][OTf] by methylation of 3 and 9, respectively.

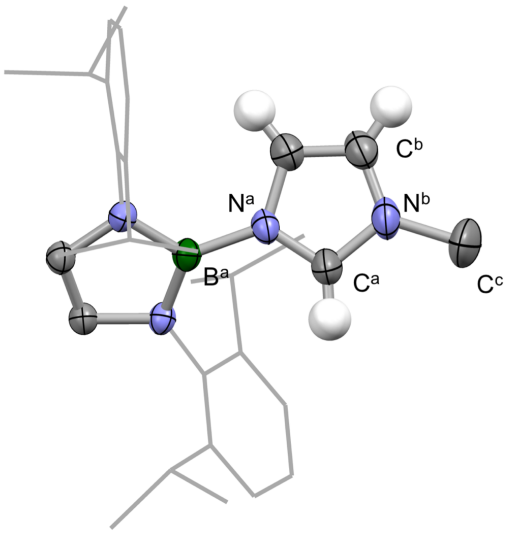

	(Å)/(°)
d(B^a–N^a)	1.515(3)
d(C^a–N^a)	1.346(3)
d(C^a–N^b)	1.313(3)
∠(N^a–C^a–N^b)	111.1(2)
Θ([B^a])	5.9

Figure 4.13 (Left) Molecular structure of [(20)H][OTf] in the solid state, as determined by X-ray crystallography. Most hydrogen atoms omitted, and Dipp groups shown in wireframe format for clarity. Thermal ellipsoids set at the 40% probability level. (Right) Table of key structural parameters.

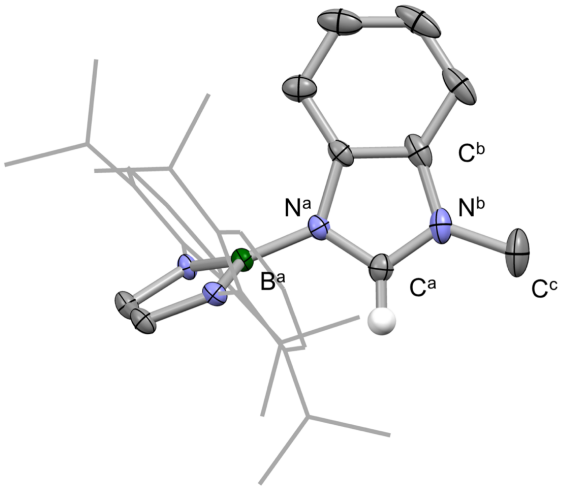

	(Å)/(°)
d(B^a–N^a)	1.467(2)
d(C^a–N^a)	1.382(2)
d(C^a–N^b)	1.306(2)
∠(N^a–C^a–N^b)	115.3(1)
Θ([B^a])	39.8

Figure 4.14 (Left) Molecular structure of [(21)H][OTf] in the solid state, as determined by X-ray crystallography. Most hydrogen atoms omitted, and Dipp groups shown in wireframe format for clarity. Thermal ellipsoids set at the 40% probability level. (Right) Table of key structural parameters.

Deprotonation of the respective imidazolium salts was subsequently attempted in order to probe the stabilities of the corresponding carbenes and their potential to undergo analogous 1,2-rearrangements. The ^{1}H and ^{13}C NMR spectra obtained *in situ*

of the reaction mixtures derived from [(**20**)H][OTf] or [(**21**)H][OTf] and potassium bis(trimethylsilyl)amide support the hypothesis of C2 deprotonation: no imidazolium NC*H*N signal can be observed in either ^{1}H NMR spectrum, and signals at 231.8 ppm and 223.6 ppm, respectively, appear in the ^{13}C NMR spectra. These data are consistent with the successful generation of the respective free carbenes (**20** and **21**; Scheme 4.11). As in the case of carbene **14**, the reaction mixtures were monitored by ^{1}H and ^{13}C NMR spectroscopy at room temperature with the resonances for the carbenes slowly disappearing to be replaced by a new set of peaks in both cases. Ultimately, no resonances are visible above 150 ppm in the ^{13}C NMR spectrum of either species after *ca*. one week (**20**) and two days (**21**).

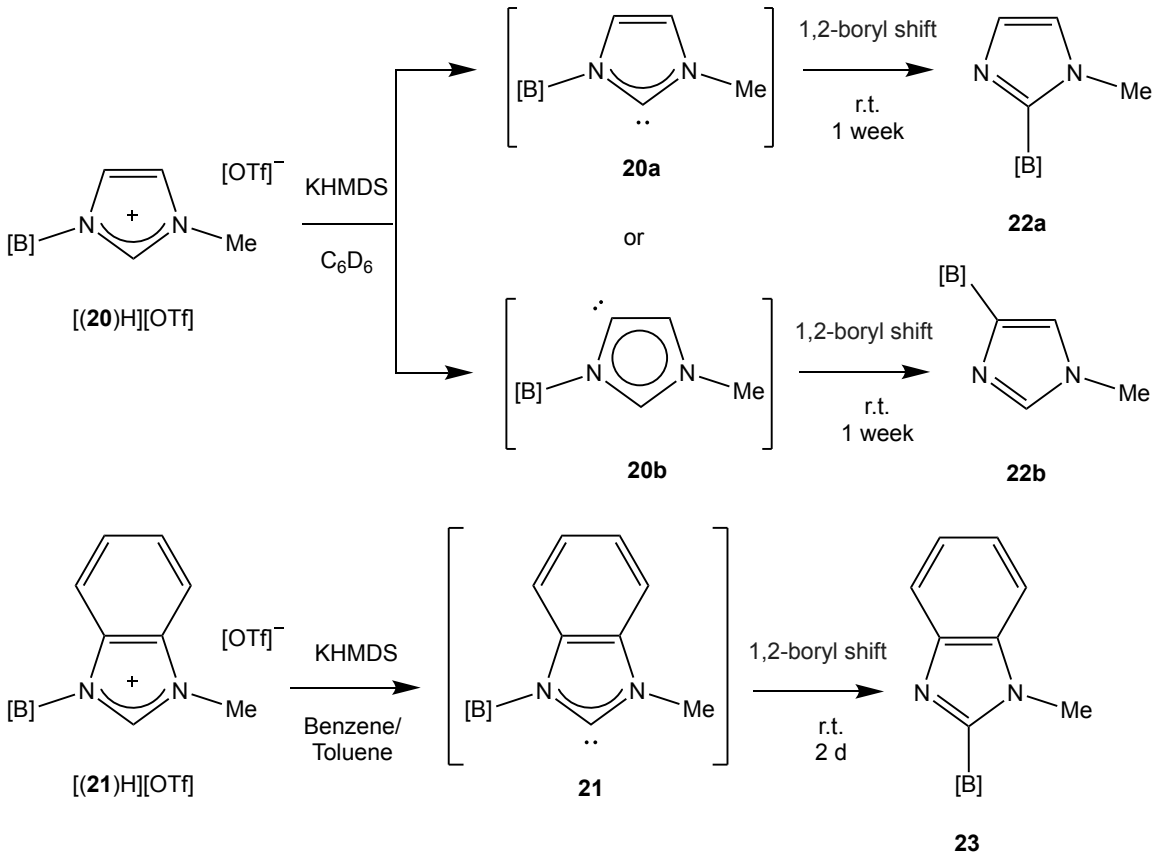

Scheme 4.11 *In situ* deprotonation of [(20)H][OTf] and [(21)H][OTf] to give 20 and 21 with subsequent 1,2-migration of the *N*-substituted boryl groups at room temperature.

This behaviour, in which a characteristic signal for a carbene is observed, which then slowly disappears, is reminiscent of the 1,2-rearrangement observed for **14**. Similar behaviour is postulated for both **20** and **21**. Attempts to obtain single crystals suitable for X-ray crystallography of the carbenes (**20** and **21**) or the rearranged species (**22** and **23**) were, however, unsuccessful. [(**21**)H][OTf] has only one proton on the imidazole heterocycle and thus the boryl group is expected to migrate to C2 to give **23**. [(**20**)H][OTf], on the other hand, has three acidic imidazolium protons, on C2, C4 and C5. C2 is arguably the most acidic proton but without a solid-state structure of **20**, the position of the carbenic centre is unknown and so structures **20a** and **20b** in Scheme 4.11 are both plausible. The ^{13}C chemical shift of **20** (231.8 ppm) is closer to the shifts of unsaturated NHCs than abnormal NHCs,[30,31] but no further evidence supports deprotonation at C2 over the backbone sites. As the solid-state structure of **22** has not been obtained, migration to the backbone cannot be excluded, since the boryl group in putative carbene **4** is known to migrate to the backbone to give **7** (section 3.2.2). A simple experiment to confirm whether the boryl group migrates to the C2 position (**22a**) or the backbone (**22b**), was therefore carried out. The reaction of **22** with methyl trifluoromethanesulfonate was studied by ^{1}H NMR spectroscopy. If the boryl group migrates to C2 (**22a**; Scheme 4.12), then the product of subsequent methylation (**24a**; Scheme 4.12) would be expected to possess a plane of symmetry and the two *N*-methyl and the two backbone C*H*s would be chemically equivalent. If, on the other hand, the boryl group migrates to the backbone of the imidazole (**22b**; Scheme 4.12), methylation should result in a lower symmetry product (**24b**; Scheme 4.12), possessing inequivalent *N*-methyl groups, as well as two 1H singlets for the imidazolium protons. The ^{1}H NMR spectrum of the methylated species suggests that it is **24a** and therefore that the deprotonation of $[(\mathbf{20})]^{+}$ generates carbene **20a**,

which then rearranges *via* boryl group migration to C2 in a similar manner to **14**.

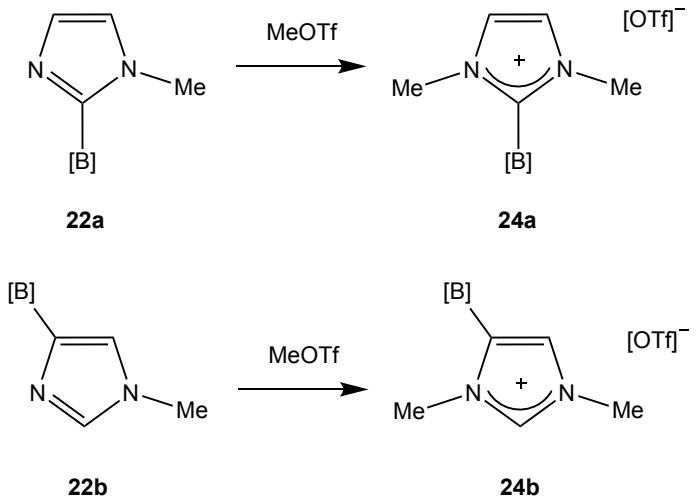

Scheme 4.12 Methylation of 22 with the aim of establishing its structure.

The rearrangement of **20** was monitored as a function of time in a similar manner as described for **14**, in order to probe the kinetics of the 1,2-shift. The change in intensity of six peaks in the ^{1}H NMR spectrum were monitored (Figure 4.15): the imidazole backbone protons of carbene **20** (a; 6.43 and 5.94 ppm), the boryl backbone protons of carbene **20** (b; 6.09 ppm), one imidazole backbone proton of **22** (c; 6.15 ppm), the protons on the backbone of the boryl group of **22** (d; 6.33 ppm) and the protons of the *N*-substituted methyl group of **22** (e; 2.79 ppm).

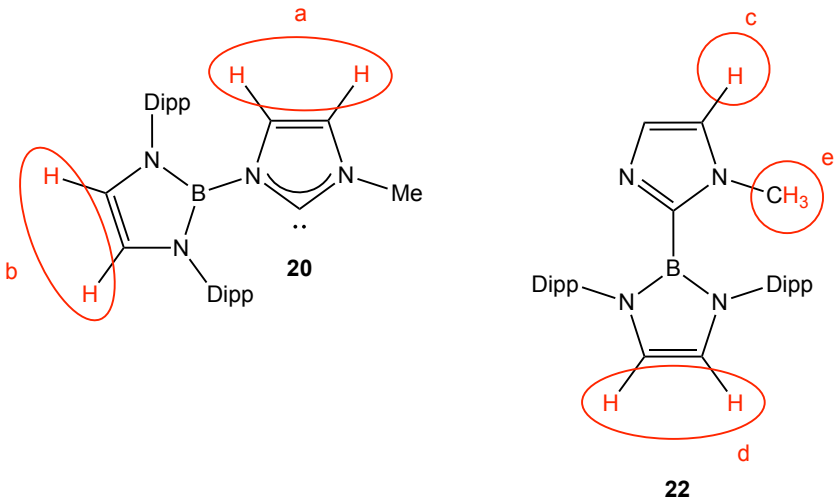

Figure 4.15 The protons of 20 and 22 chosen to monitor with time.

The percentage of carbene **20** and migrated species **22** at any given time was calculated from the integrals of the resonances listed above and plotted with respect to time (Figure 4.16). An exponential plot is obtained when the percentage of the free carbene is plotted with respect to time, and the plot is linear (R^2 = 0.998) for the natural logarithm of the proportion of the free carbene with respect to time (as with carbene **14**). This data suggests that the rate determining steps of the 1,2-rearrangement in carbene **20** is also intramolecular. From the line of best fit in the semi-logarithmic plot, the rate constant, k = (3.9 ± 0.1) x 10^{-6} s^{-1}, and half-life, $t_{½}$ = 49 ± 1 h, could be obtained.[26,27]

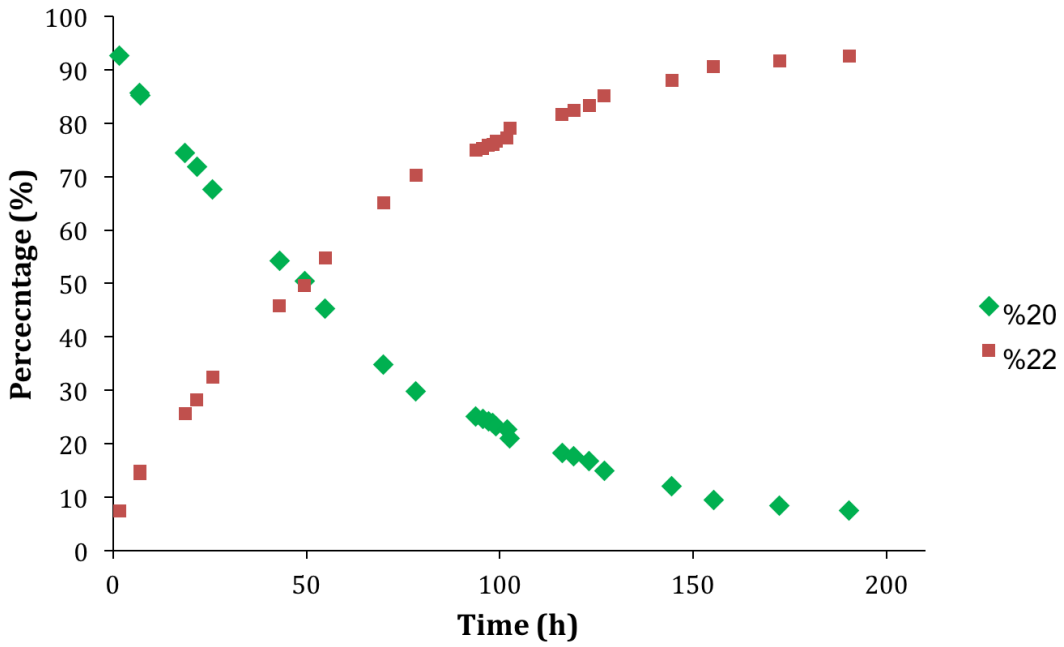

Figure 4.16 Percentage free carbene 20 and rearranged species 22 with respect to time.

DFT calculations to assess the viability of an intramolecular 1,2-rearrangement in **20** were carried out by Dr. Petra Vasko (of the Aldridge group), using the same method as for **14**. The enthalpy and entropy of activation derived from DFT calculations are: $\Delta H^{‡}$ = 85 kJ mol^{-1} and $\Delta S^{‡}$ = -48 J mol^{-1} K^{-1} and the activation barrier is $\Delta G^{‡}$ = 99 kJ mol^{-1} at 298 K. The increase in the free energy of activation compared

to **14** (92 kJ mol^{-1})is in agreement with the longer experimentally determined half-life (**20**: $t_{½}$ = 49 ± 1 h; **14**: $t_{½}$ = 4.01 ± 0.04 h).

The structure of the transition state is depicted in Figure 4.17. As is the case with the transition state located for the 1,2-shift in **14**, the boryl group lies nearly perpendicular to the imidazole heterocycle and the boron atom is projected 43.8° out of the imidazole heterocycle plane (Θ([B^a-N^a-C^a]; Figure 4.17). The bond lengths within the imidazole heterocycle also do not imply significant dearomatization of the ring. This is similar to what is observed in the corresponding transition state derived from **14** and, as discussed earlier, could allow for stabilization of the migrating boryl 'cation' both through interactions between the formally vacant boron σ-orbital and the aromatic π-system, and between the vacant boron $p_π$-orbital and the lone pairs of N^a and C^a.

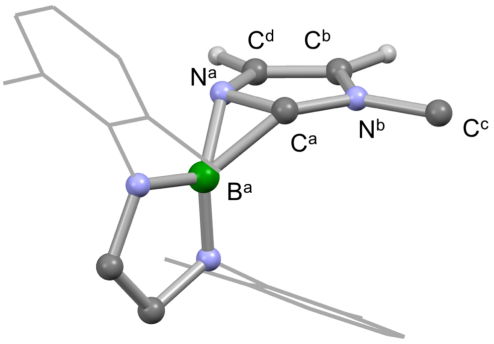

	(Å)/(°)
d(B^a–N^a)	1.611
d(B^a–C^a)	1.696
d(C^a–N^a)	1.356
d(C^a–N^b)	1.356
d(N^a–C^d)	1.382
d(N^b–C^b)	1.376
d(C^b–C^d)	1.356
∠(N^a–C^a–N^b)	106.6
Θ([B^a])	87.8
Θ([B^a-N^a-C^a])	43.8

Figure 4.17 (Left) Molecular structure of the transition state for the 1,2-shift of the boryl group in the Xyl analogue of 20 as determined by DFT calculations. Most hydrogen atoms omitted, and Xyl groups shown in wireframe format for clarity. (Right) Table of key structural parameters. Θ([B^a]) indicates the angle between the plane of the boryl group and the imidazole heterocycle. Θ([B^a-N^a-C^a]) indicates the angle between the plane of the B^a–N^a and B^a–C^a bonds and the imidazole heterocycle.

Unfortunately, the ^{1}H NMR spectroscopic data for the 1,2-rearrangement of **21** was not of good quality and thorough kinetics studies could therefore not be carried out. Analysis of preliminary experiments, however, suggest a half-life of approximately 9-12 h for **21** at room temperature, which is longer than for **14** but shorter than for **20**.

The rates of the 1,2-rearrangement of the three carbene systems explored, **14**, **20** and **21**, are different, with half-lives of 4.01 ± 0.04 h and 49 ± 1 h for **14** and **20**, respectively, and *ca*. 9-12 h for **21** but it is unclear what causes the difference in the rates. The presence of the strongly σ-donating boryl group at the backbone position of **14** is likely to render the imidazole heterocycle somewhat more electron rich compared to **20**. This in turn might result in increased stabilization of the corresponding transition state, thereby lowering the activation barrier and increasing the rate of the rearrangement.

4.2.4 Coordination of Carbene 14 to Transition Metals and Selenium

Metal complexes, as well as phosphorus and selenium adducts, of free carbenes have previously been used to great effect to gauge experimentally their steric and electronic properties (sections 1.2.3, 1.2.4 and 4.1). The binding of carbene **14** to gold, rhodium and selenium was therefore of considerable interest. The syntheses of these metal complexes and the selenium adduct, along with their spectroscopic properties are discussed below.

The percentage buried volume for a carbene ligand is most often calculated from the respective AuCl complex and with like-for-like comparison of the steric properties of **14** in mind, the coordination of **14** to the AuCl fragment was of significant interest. Accordingly, gold complex (**14**)AuCl was synthesized by reacting **14** (generated *in*

situ) with (THT)AuCl, and isolated in 34% yield (Scheme 4.13). In terms of characterization data, a singlet at 177.0 ppm is observed in the ^{13}C NMR spectrum, which is consistent with other gold carbene complexes.[7] The isopropyl methine groups give rise to a broad signal in the ^{1}H NMR spectrum at room temperature, which can be resolved at 333 K. This is presumably caused by restriction in the rotation of the Dipp groups of the *N*-boryl substituent due to steric interaction with the AuCl fragment. Colourless single crystals suitable for X-ray crystallography could be obtained by recrystallization from hexane. The solid-state structure so obtained is depicted in Figure 4.18 and confirms successful coordination of carbene **14** to gold(I) to form complex (**14**)AuCl. In contrast with the imidazolium precursor ([(**14**)H][OTf]), the *N*-bound boryl group lies nearly perpendicular to the imidazole heterocycle (87.7°), presumably due to enhanced steric interactions with the AuCl fragment (*cf*. H).

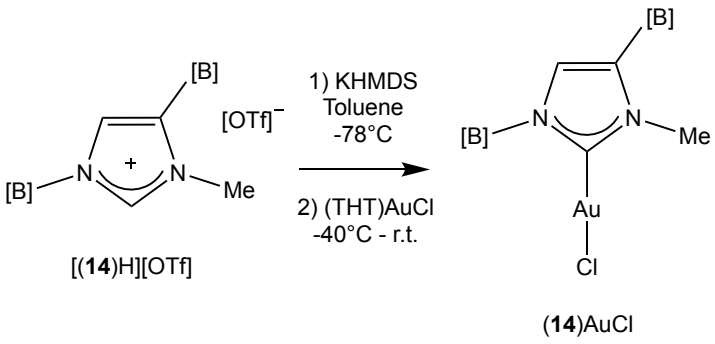

Scheme 4.13 *In situ* synthesis of (14)AuCl.

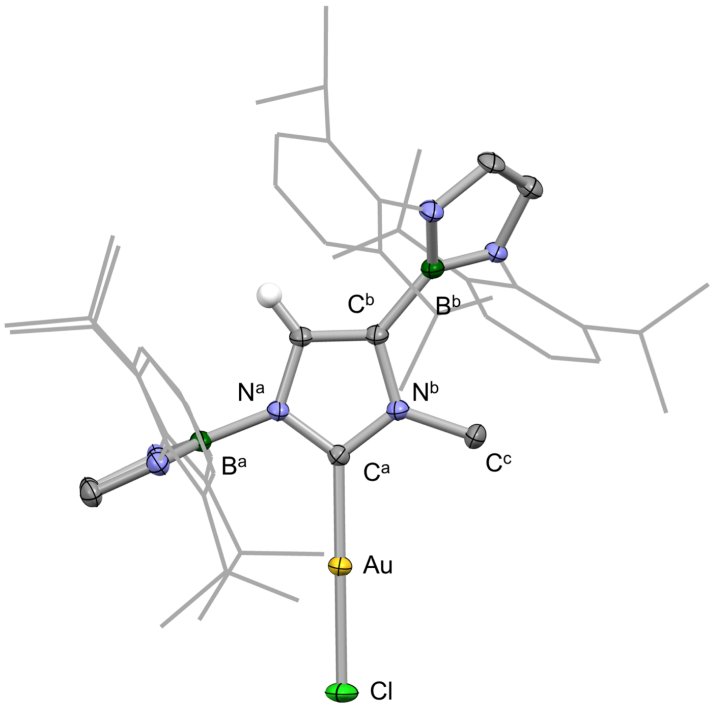

	(Å)/(°)
d(B^a–N^a)	1.485(4)
d(B^b–C^b)	1.557(5)
d(C^a–N^a)	1.352(3)
d(C^a–N^b)	1.339(4)
d(C^a–Au)	1.980(3)
∠(N^a–C^a–N^b)	106.0(2)
Θ([B^a])	87.7
Θ([B^b])	52.9

Figure 4.18 (Left) Molecular structure of (14)AuCl in the solid state, as determined by X-ray crystallography. Most hydrogen atoms omitted, and Dipp groups shown in wireframe format for clarity. Thermal ellipsoids set at the 40% probability level. (Right) Table of key structural parameters.

Using the SambVca 2.0 program,[2] the percentage buried volume of **14** was calculated (see sections 1.2.4 and 4.1 for more details). This method yields a $\%V_{bur}$ of 50.0%, which places carbene **14** among the bulkier carbenes reported to date (Table 4.1). The steric profile of the carbene is intriguing, particularly given that only one of the boryl groups provides steric bulk immediately adjacent to the gold centre. A topographic steric map was also obtained using the SambVca 2.0 software, and is depicted in Figure 4.20. One side of the metal centre is in effect blocked by the boryl group, whereas the other side is reasonably open. This steric profile could allow for interesting stoichiometric and/or catalytic activity of metal complexes of the carbene.

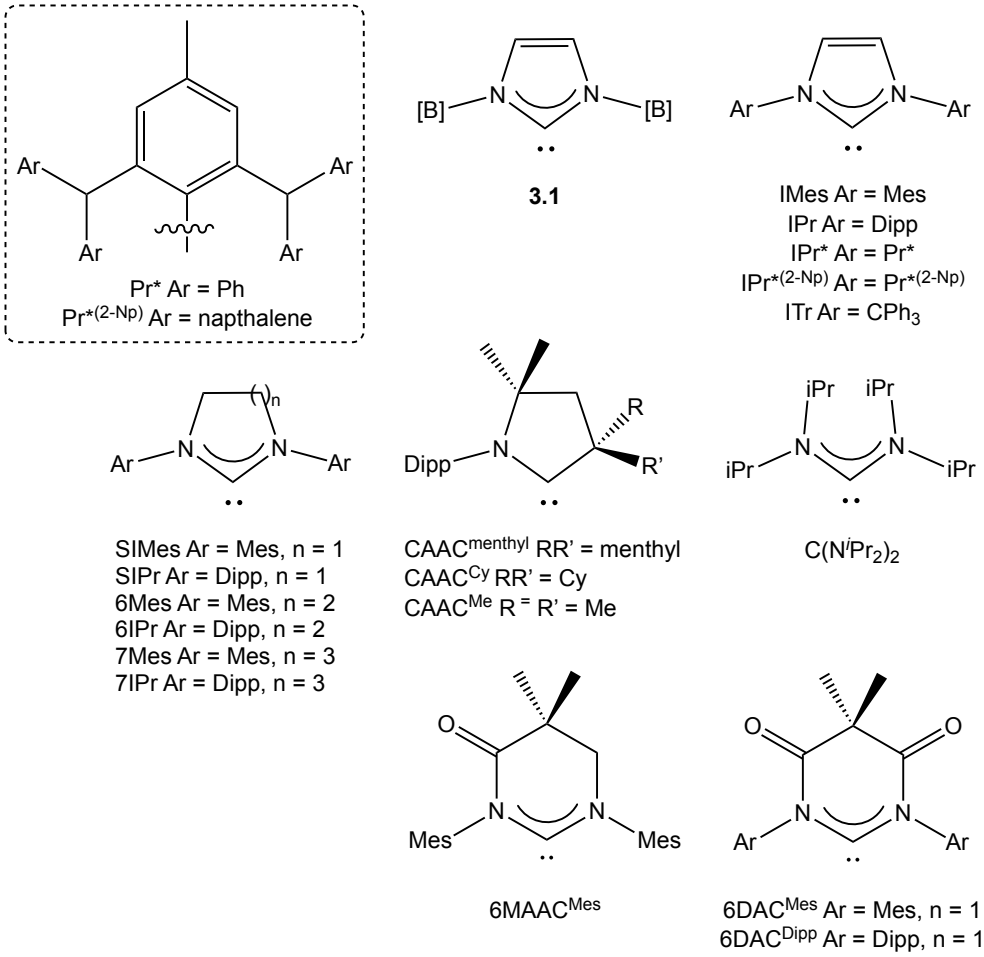

Figure 4.19 Structures of various carbenes used for comparison of data in Tables 4.1, 4.2 and 4.3.

Carbene	$\%V_{bur}$	Carbene	$\%V_{bur}$
14	50.0	**CAAC^{Menthyl}**	51.0[5]
3.1	[a]70.4	**7IPr**	52.6[32]
IPr	44.5[3]	**IPr*$^{(2-Np)}$**	[b]57.4[33]
IPr*	50.4[34]	**ITr**	57.3[35]
6IPr	50.8[32]		

Table 4.1 $\%V_{bur}$ (%) for AuCl complexes of 14 and other carbenes outlined in Figure 4.19.

[a]Obtained from a structure calculated by DFT. [b]Calculated for a AgCl complex.

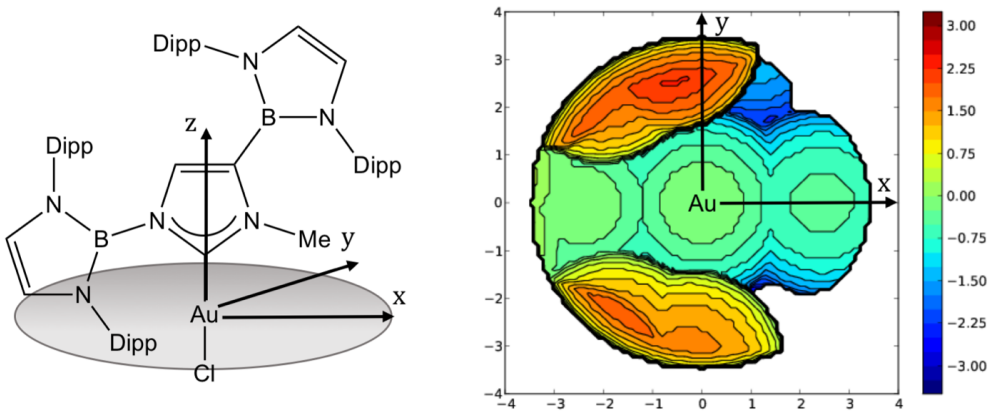

Figure 4.20 Topographic steric map of carbene 14 as a ligand bound to a AuCl complex.[2]

The electronic properties of **14** were also of interest. Carbene complexes of $[Rh(CO)_2Cl]$ are often employed to calculate the Tolman Electronic Parameter (TEP), which gives insight into their electronic properties (see sections 1.2.3 and 4.1 for more detail). $LRh(cod)Cl$ complexes are common precursors to access the $LRh(CO)_2Cl$ systems,[36] and (**14**)Rh(cod)Cl was therefore synthesized and isolated in 40% yield by reacting **14**, generated *in situ*, with $[Rh(cod)Cl]_2$ (Scheme 4.14). Spectroscopically, the appearance of a doublet in the ^{13}C NMR spectrum at 189.0 ppm ($^1J_{RhC}$ = 52.0 Hz) indicates successful coordination of the carbene to the rhodium centre.[36] The ^1H NMR signals for the *N*-boryl group are very broad (to greater extent even than for (**14**)AuCl), presumably reflecting restricted rotation around the Dipp groups of the *N*-boryl substituent due to steric interactions with the [Rh(cod)Cl] fragment. Not all of the signals can be resolved at elevated temperatures. Yellow single crystals suitable for X-ray crystallography could be obtained by recrystallization from pentane. The solid-state structure so obtained is depicted in Figure 4.21 and confirms successful coordination of carbene **14** to the rhodium centre to form (**14**)Rh(cod)Cl. As with (**14**)AuCl, the *N*-boryl group is aligned nearly perpendicular (at 86.9°) to the imidazole heterocycle on account of the steric interaction with the [Rh(cod)Cl] fragment.

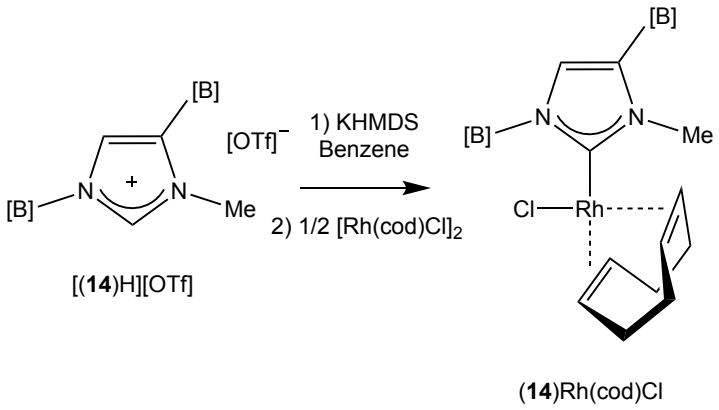

Scheme 4.14 *In situ* synthesis of (14)Rh(cod)Cl.

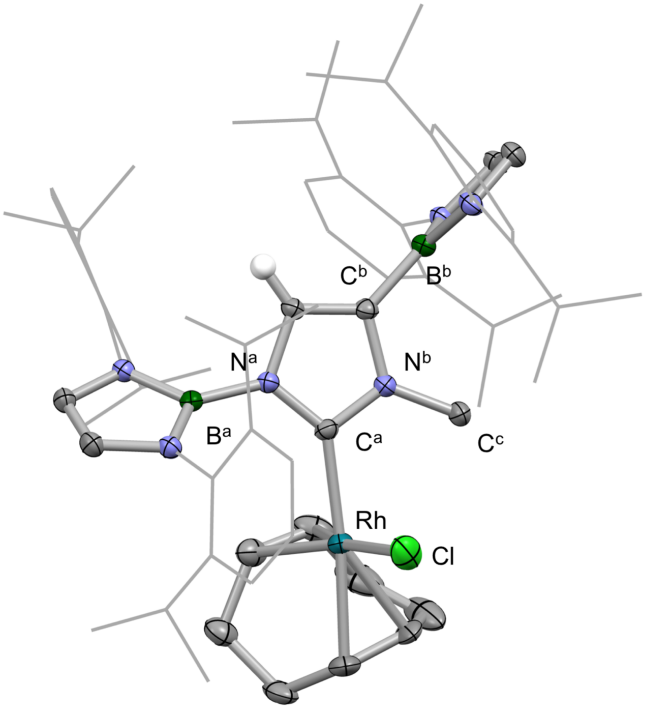

	(Å)/(°)
d(B^a–N^a)	1.481(3)
d(B^b–C^b)	1.572(4)
d(C^a–N^a)	1.372(3)
d(C^a–N^b)	1.342(3)
d(C^a–Rh)	2.063(3)
∠(N^a–C^a–N^b)	105.1(2)
Θ([B^a])	86.9
Θ([B^b])	49.9

Figure 4.21 (Left) Molecular structure of (14)Rh(cod)Cl in the solid state, as determined by X-ray crystallography. Most hydrogen atoms omitted, and Dipp groups shown in wireframe format for clarity. Thermal ellipsoids set at the 40% probability level. (Right) Table of key structural parameters.

The percentage buried volume of **14** calculated based on the structure of (**14**)Rh(cod)Cl (40.2%) is significantly lower than that based on the gold complex (50.0%). This suggests that the carbene is fairly flexible as a ligand. This is well known for other NHCs: the $\%V_{bur}$ calculated for IPr based on the Rh(cod)Cl fragment, for

example, drops significantly compared to (IPr)AuCl (34.0% *vs* 44.5%).[3]

With the aim of accessing the corresponding $[Rh(CO)_2Cl]$ complex, (**14**)Rh(cod)Cl was reacted with CO in C_6D_6.[36] The ^1H NMR spectrum of the reaction mixture indicates full consumption and conversion to a new product (Scheme 4.15). The ^{13}C NMR spectrum contains three doublets in the range 180-190 ppm (two of which are overlapping), consistent with a carbene centre coordinated to a rhodium complex containing two inequivalent carbonyl groups.[36] Again, the ^1H NMR spectrum indicates restriction in rotation around the Dipp group of the *N*-boryl group as its isopropyl groups give rise to broad signals which can be resolved at 343 K.

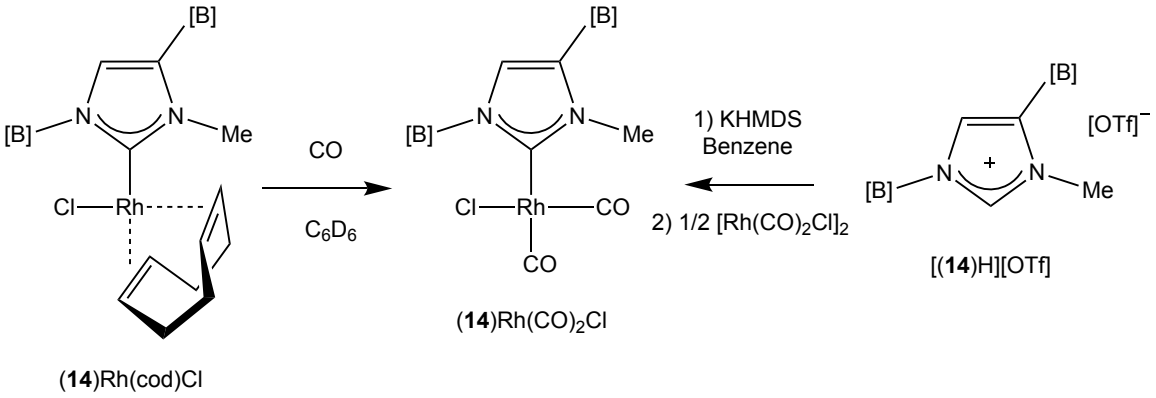

Scheme 4.15 Syntheses of (14)$Rh(CO)_2Cl$, either by addition of CO to (14)Rh(cod)Cl or *in situ* directly from $[Rh(CO)_2Cl]_2$.

As (**14**)Rh(cod)Cl was isolated in rather low yields due to high solubility, it was thought beneficial to synthesize (**14**)$Rh(CO)_2Cl$ directly from $[Rh(CO)_2Cl]_2$. The ^1H and ^{13}C NMR spectra of the reaction mixture of **14** (prepared *in situ*) and $[Rh(CO)_2Cl]_2$ (Scheme 4.15) match that of the product from the reaction of (**14**)Rh(cod)Cl and CO. Moreover, in this case, single crystals suitable for X-ray crystallography could be grown from hexane. The solid-state structure so obtained is depicted in Figure 4.22 and confirms successful coordination of carbene **14** to the rhodium centre. Unfortunately, the data is not of adequate quality to allow for the discussion of structural parameters.

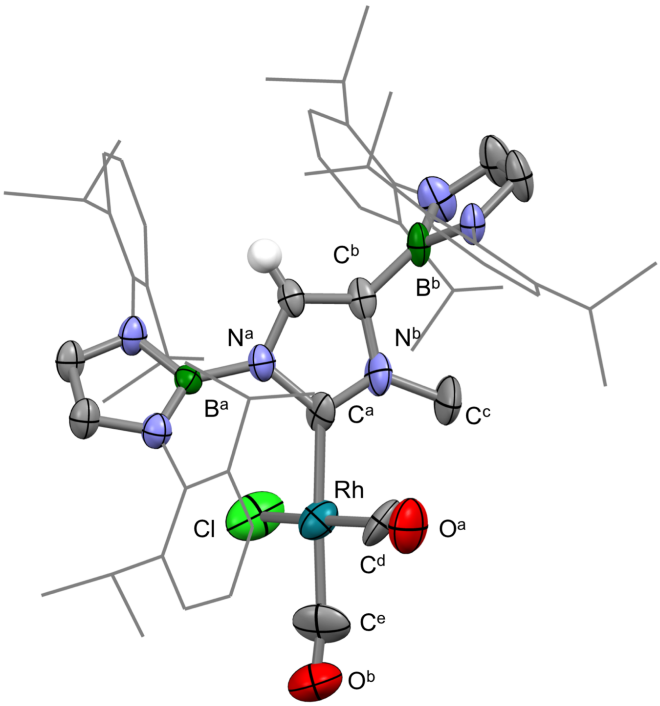

Figure 4.22 Molecular structure of (14)Rh(CO)$_2$Cl in the solid state, as determined by X-ray crystallography. Solvate molecule and most hydrogen atoms omitted, and Dipp groups shown in wireframe format for clarity. Thermal ellipsoids set at the 40% probability level.

The IR spectrum of (**14**)Rh(CO)$_2$Cl in dichloromethane contains two peaks at 1990 cm^{-1} and 2069 cm^{-1}, assigned to the CO stretches of the two distinct carbonyl ligands. The average CO stretching frequency of the rhodium complex, $\nu_{Av}(CO)_{[Rh]}$ = 2030 cm^{-1}, can then be used to derive the Tolman electronic parameter (TEP), which in this case is 2043 cm^{-1}, according to the following equation:[5,6]

$$TEP = 0.782 \cdot \nu_{Av}(CO)_{[Rh]} + 456\ cm^{-1} \quad (4.1)$$

Comparison of the TEP of carbene **14** with other related carbenes is discussed in section 4.2.5.

As discussed in sections 1.2.3 and 4.1, selenium adducts of carbenes offer a useful probe for estimating π-acidity. (**14**)Se was therefore synthesized from *in situ* generated **14** and elemental selenium powder in 66% isolated yield (Scheme 4.16). The ^{1}H NMR spectrum indicates restriction in rotation for the Dipp groups as was

found for the gold and rhodium complexes. The ^{77}Se chemical shift of (**14**)Se in acetone-d_6 is 67 ppm. Comparison with the ^{77}Se chemical shifts of selenium adducts of other related carbenes is examined in section 4.2.5. Single crystals suitable for X-ray crystallography could be obtained by recrystallization from benzene. The solid-state structure so obtained is depicted in Figure 4.23 and confirms successful synthesis of the selenium adduct of carbene **14**.

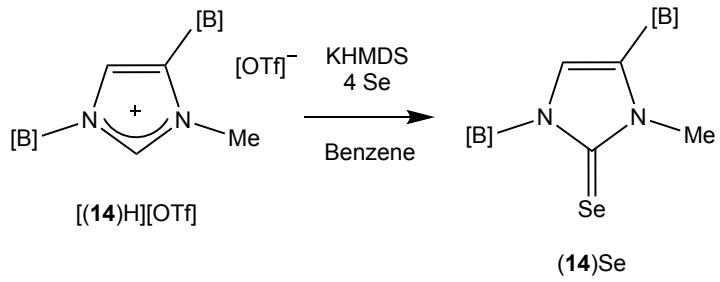

Scheme 4.16 *In situ* synthesis of (14)Se.

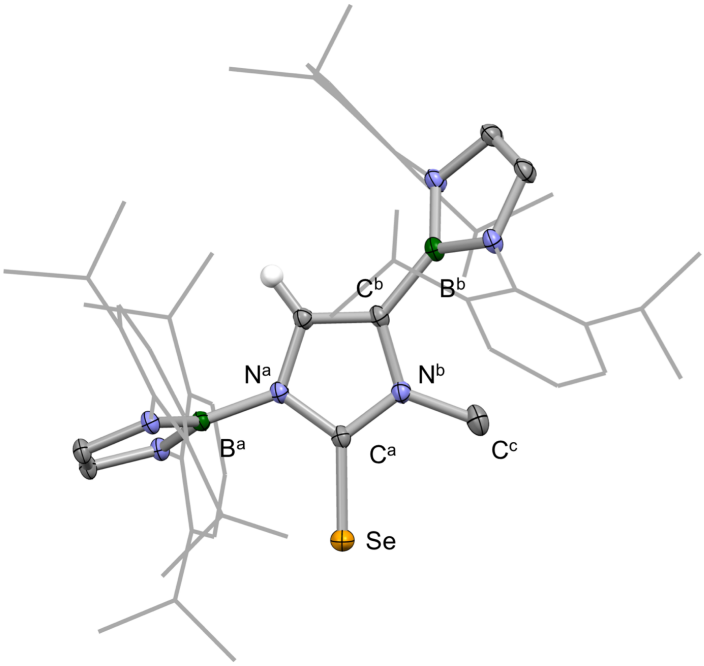

	(Å)/(°)
d(Bᵃ–Nᵃ)	1.497(3)
d(Bᵇ–Cᵇ)	1.573(4)
d(Cᵃ–Nᵃ)	1.366(3)
d(Cᵃ–Nᵇ)	1.348(3)
d(Cᵃ–Se)	1.845(2)
∠(Nᵃ–Cᵃ–Nᵇ)	107.1(2)
Θ([Bᵃ])	77.1
Θ([Bᵇ])	50.6

Figure 4.23 (Left) Molecular structure of (14)Se in the solid state, as determined by X-ray crystallography. Most hydrogen atoms omitted, and Dipp groups shown in wireframe format for clarity. Thermal ellipsoids set at the 40% probability level. (Right) Table of key structural parameters.

4.2.5 Discussion on the Electronic Properties of Carbene 14

Carbene (L)	Free Carbene		LRh(cod)Cl		LSe
	$\delta^{13}C$	TEP	$\delta^{13}C$	$^1J_{RhC}$	$\delta^{77}Se$
14	225.8	2043	[e]189.0	[e]52.0	67[38]
IMes	220.6[30]	[c]2051[6]	183.5[39]	52.5[39]	[f]87[38]
SIMes	243.8[30]	2048[40]	211.6[40]	48.2[40]	[g]181[38]
6Mes	244.9[41]	2042[40]	211.5[40]	46.9[40]	271[38]
7Mes	257.3[41]	2041[40]	[e]224.0[40]	[e]46.7[40]	
6MAAC^{Mes}	260.6[42]	2050[42]			472[38]
6DAC^{Mes}	[a]278.4[43]	2055[44]	245.2[44]	49.1[44]	847[45]
CAAC^{Cy}	[b]309.4[46]	2051[47]	272.9[48]	45[48]	[b,h]492[49]
C(N^{i}Pr$_2$)$_2$	255.5[50]	[d]2050[51]	233.6[51]	67.8[51]	593[38]

Table 4.2 Key spectroscopic data relating to the electronic properties of 14 and related carbenes (see Figure 4.19, section 4.2.3). ^{13}C NMR chemical shifts (ppm) of the carbenic centres of various free carbenes measured in C_6D_6. Tolman Electronic Parameter (TEP, cm^{-1}) of the carbenes calculated by linear regression from the experimentally measured $\nu_{Av}(CO)_{[Rh]}$ of the respective $[Rh(CO)_2Cl]$ complexes, measured in dichloromethane. ^{13}C NMR chemical shifts (ppm) and ^{103}Rh-^{13}C coupling constants (Hz) for the carbenic centres in [Rh(cod)Cl] complexes, measured in $CDCl_3$. ^{77}Se NMR chemical shifts of the selenium adducts of the carbenes, measured in acetone-d_6. [a]Value for 6DAC^{Dipp}. [b]Measured in THF-d_8. [c]Calculated by linear regression from the experimentally measured $\nu_{Av}(CO)_{[Ir]}$ for the $[Ir(CO)_2Cl]$ complex. [d]Measured in KBr. [e]Measured in C_6D_6. Values for [f]IPr, [g]SIPr and [h]CAAC^{Me}.

Table 4.2 lists spectroscopic data for carbene **14** (together with other carbenes) and their respective rhodium and selenium adducts. These data can be interpreted to give insight into the electronic properties of each carbene. The TEP value of **14**, for example, is lower than that for IMes, suggesting increased electron density at the rhodium metal centre; it is very similar to the value determined for SIMes. Superficially, this suggests that **14** is a better σ-donor than IMes, and comparable to SIMes. One must, however, bear in mind that the saturated NHCs typically also have enhanced π-acidity compared with unsaturated NHCs,[12,37] which reduces the overall electron density at the metal centre and thus increases the value of TEP. To allow for

better comparison between ligands, estimation of the π-acidity of **14** was therefore deemed to be relevant.

The ^{77}Se NMR chemical shift of (**14**)Se is a great deal lower than those of SIMes, 6Mes and 7Mes. This would imply that **14** is significantly less π-accepting than the saturated NHCs. Moreover, the ^{77}Se NMR shift is similar to that of IMes, implying that the π-acidity of **14** is not greatly affected by the presence of the boryl group. As outlined in section 1.2.3, ^{77}Se chemical shifts can depend on concentration and tend to be lower at lower concentrations (by up to 9 ppm).[52] As (**14**)Se is only sparingly soluble in acetone-d_6, this may affect the chemical shift, although presumably not substantially compared to the ^{77}Se chemical range (800 ppm).[12]

With the estimation of the π-acidity of carbene **14** in hand, the TEP value can now be better compared with other NHCs. The π-acidity of **14** is similar to IMes and so comparison of the two TEP values would imply that the presence of the boryl groups in **14** augments the σ-donor abilities. Since the π-acidity of **14** is lower than that of the saturated carbenes, the fact that the TEP values of **14** and SIMes are very similar indicates that the σ-donor properties of **14** are also likely to be somewhat lower than SIMes.

As mentioned in sections 1.2.3 and 4.1, the ^{13}C chemical shifts of free carbenes are often used to evaluate their σ-donor properties, with higher shifts typically being associated with greater p-character in the σ-orbital. However, the chemical shift is also influenced by the energy of LUMO, the size of the singlet-triplet energy gap and the angle at the carbene centre.[7–10] As these factors are interrelated, the downfield shift is not definitive, but can give an indication of the electronic properties of the carbene centre to some degree. The ^{13}C chemical shift of **14** (225.8 ppm) lies between

the values for IMes (220.6 ppm) and SIMes (243.8 ppm), indicating that the σ-donor properties lie in that range. This is in agreement with the combined results of the TEP and the ^{77}Se chemical shift of **14** discussed above.

DFT calculations on **14** and other NHCs were performed by Haoyu Niu, of the Aldridge group, in an attempt to corroborate the experimental studies of the electronic structure.[53] The calculated structure of **14** is depicted in Figure 4.24 and its calculated HOMO and LUMO shown in Figure 4.25. The structure of *trans*-(**14**)Ni(PMe_3)$_2$Br was also calculated (Figure 4.26) and its structural properties compared to related complexes of other carbenes (Table 4.3). The Ni–Br bond length gives an indication of the *trans*-influence of the respective carbenes: the longer the Ni–Br bond, the stronger σ-donor the carbene is. In addition, the Ni–C bond length relates to the s/p ratio of the carbene σ-bond: the lower the s/p ratio is, the more p-character at carbon and the longer the Ni–C will be. Strong σ-donor properties are typically associated with greater p-character at C and hence with longer Ni–C bonds.[54] In section 1.2.3, the quantum-chemically calculated quantity of instantaneous interaction energy, ΔE_{orb} was introduced. Of interest in this section are $\Delta E_{orb}(\sigma)$ and $\Delta E_{orb}(\pi)$, the σ- and π-orbital interaction energies, which give information about the σ-donor and π-acceptor properties of the carbene. A more negative value of $\Delta E_{orb}(\sigma)$ indicates more σ-donation from the carbene, and a more negative $\Delta E_{orb}(\pi)$ is indicative of greater π-acceptor properties.

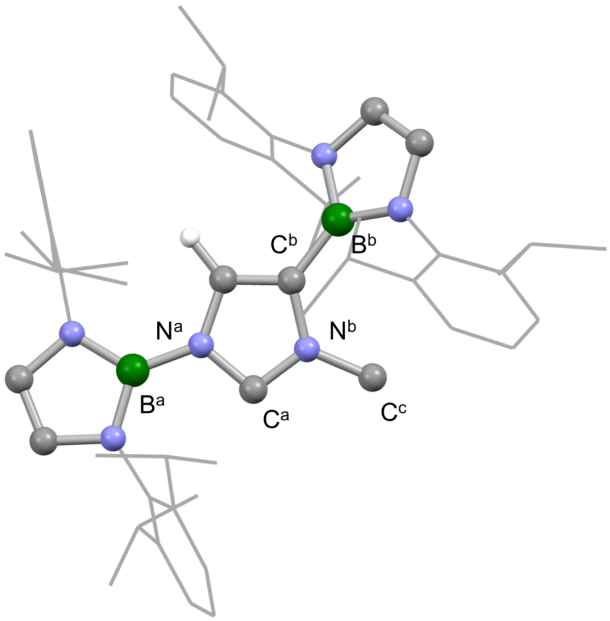

	(Å)/(°)
d(Bᵃ–Nᵃ)	1.469
d(Bᵇ–Cᵇ)	3.806
d(Cᵃ–Nᵃ)	1.390
d(Cᵃ–Nᵇ)	1.358
∠(Nᵃ–Cᵃ–Nᵇ)	102.9
Θ([Bᵃ])	9.0
Θ([Bᵇ])	29.4

Figure 4.24 (Left) Molecular structure of 14 as determined by DFT calculations. Most hydrogen atoms omitted, and Dipp groups shown in wireframe format for clarity. (Right) Table of key structural parameters.

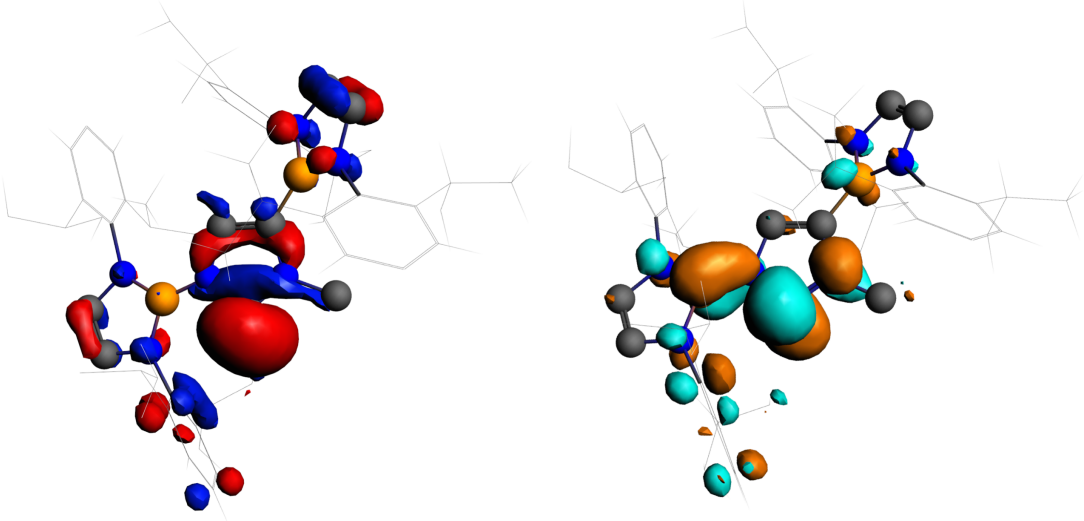

Figure 4.25 Calculated (left) HOMO (-440.8 kJ mol^{-1}) and (right) LUMO (-42.5 kJ mol^{-1}) for 14.

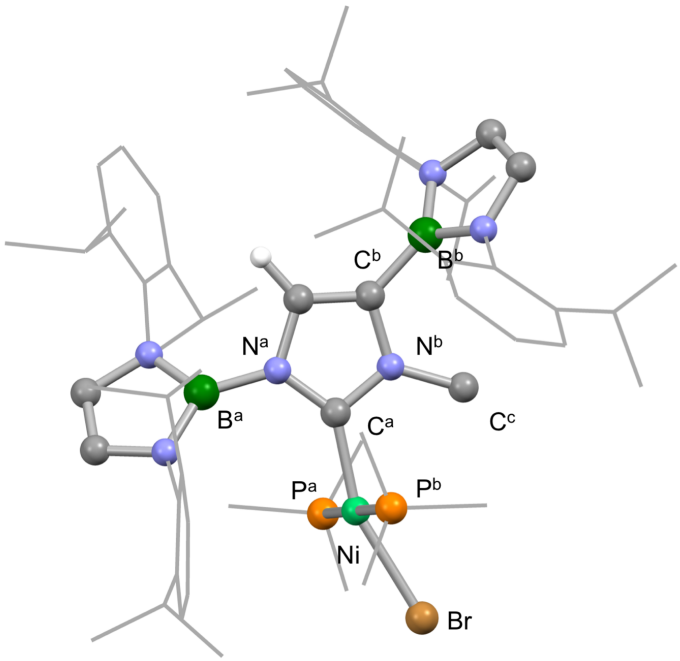

	(Å)/(°)
d(B^a–N^a)	1.495
d(B^b–C^b)	1.567
d(C^a–N^a)	1.383
d(C^a–N^b)	1.366
d(C^a–Ni)	1.903
d(Ni–Br)	2.393
∠(N^a–C^a–N^b)	104.8
Θ([B^a])	44.1
Θ([B^b])	60.7

Figure 4.26 (Left) Molecular structure of (14)Ni(PMe_3)$_2$Br as determined by DFT calculations. Most hydrogen atoms omitted, and Dipp groups and PMe_3 methyl groups shown in wireframe format for clarity. (Right) Table of key structural parameters.

According to the calculations, the HOMO of **14** as the free carbene lies at -440.8 kJ mol^{-1}, which, compared with other saturated and unsaturated NHCs (Table 4.3), suggests higher σ-donor abilities compared with both IMes (-475.0 kJ mol^{-1}) and SIMes (-462.0 kJ mol^{-1}), but lower than the expanded ring NHCs 6Mes (-421.2 kJ mol^{-1}). Compared with the spectroscopic data discussed earlier, these results indicate slightly higher σ-donor abilities, suggesting that **14** is better σ-donor than SIMes. Notably, hypothetical carbene **3.1** (Figure 4.18), which has two *N*-bound boryl groups has an even higher lying HOMO (-420.5 kJ mol^{-1}), presumably due to closer proximity of the second boryl group to the carbene centre. Studying the Ni–Br bond length in *trans*-(**14**)Ni(PMe_3)$_2$Br and comparing with the other nickel complexes suggests that carbene **14** has similar σ-donor properties to SIMes. These results are in line with the experimental results, which suggest that the σ-donor ability of carbene **14** is

augmented with the presence of the two boryl groups on the imidazole heterocycle. $\Delta E_{orb}(\sigma)$ suggests σ-donor properties far higher than the other experimental and computational values suggest, with values that lie outside what has been observed above, and with σ-donor capabilities which greatly exceed those of the other NHCs.

	Free Carbene			$LNi(PMe_3)_2Br$			
L	**HOMO**	**LUMO**	**ΔE**	**d(Ni−Br)**	**d(Ni−C)**	**$\Delta E_{orb}(\sigma)$**	**$\Delta E_{orb}(\pi)$**
14	-440.8	-42.5	398.3	2.393	1.903	-200	-47
3.1	-420.5	-28.9	398.3				
IMes	-475.0	-33.1	441.9	2.383	1.905	-171	-48
SIMes	-462.9	-33.4	429.5	2.391	1.901	-176	-52
6Mes	-421.2	-41.9	379.3	2.416	1.930	-182	-48

Table 4.3 DFT calculations of the frontier orbitals of carbene 14 and other NHCs (see Figure 4.19), both as free carbenes and as ligands bound to $[Ni(PMe_3)_2Br]$. The table lists the energy of the HOMO (kJ mol^{-1}) and the LUMO (kJ mol^{-1}) of the free carbenes in the gas phase and their energetic separation, ΔE (kJ mol^{-1}). The Ni−Br and Ni−C bond lengths (Å) in the calculated structure of the nickel complex in the gas phase and the energy of orbital interaction energies involving both the σ- and π-orbitals, $\Delta E_{orb}(\sigma)$ and $\Delta E_{orb}(\pi)$ (kJ mol^{-1}), are also listed.

The differences between the values for the energy of the LUMOs and $\Delta E_{orb}(\pi)$ between all of the carbenes are not significant and do thus not offer much insight into the π-acidity of **14**.

4.3 Conclusions

Two different carbene systems have been targeted *via* the deprotonation of imidazolium precursors bearing two pendant boryl functions. In the pursuit of an abnormal carbene, in which both boryl groups are adjacent to the carbene centre, methylation at C2 was accomplished and deprotonation investigated. However, the resulting species (compound **16**) can be shown by NMR spectroscopy to be an *N*-heterocyclic olefin (NHO), presumably formed by deprotonation by the amide base at

the newly installed methyl group. Attempts to access a 1,4-diboryl-3-methyl-2-phenylimidazolium salt (**4.6**; Scheme 4.6), an alternative precursor, were unsuccessful.

An unsymmetrical, bisborylated carbene, **14**, has been successfully synthesized *via* deprotonation at C2 and characterized *in situ*. The carbene undergoes a facile 1,2-rearrangement at room temperature with a half-life of $t_{½}$ = 4.01 ± 0.04 h. Kinetic data reveals a first-order rate determining step and an entropy of activation close to zero, suggesting an intramolecular 1,2-rearrangement. Such (intramolecular) processes have not been reported previously for aromatic carbenes and have, until now, been considered thermodynamically unfavourable. Experimental data allow for determination of the enthalpy and entropy of activation, $\Delta H^{‡}$ = 97 ± 2 kJ mol^{-1} and $\Delta S^{‡}$ = -3.1 ± 0.2 J mol^{-1} K^{-1}, values which are in close agreement with DFT calculations. The activation barrier calculated for an intramolecular 1,2-shift, $\Delta G^{‡}$ = 92 kJ mol^{-1}, is significantly lower than has been calculated for other systems, and suggests that this might be a feasible mechanistic pathway for **14**. Experimental and computational data for the rearrangement of a related carbene (**20**) are also consistent with an intramolecular pathway – with a slightly higher activation barrier being determined both experimentally and computationally.

Metal complexes and a selenium adduct of **14** have been successfully synthesized and structurally characterized by X-ray crystallography. The percentage buried volume (50.0%) has been calculated from the structural parameters of (**14**)AuCl, placing it amongst the more sterically demanding carbenes known. A topographic steric map of the ligand reveals an unsymmetrical steric loading around the metal centre.

Comparison of the TEP value and the carbenic ^{13}C chemical shift of **14** and the ^{77}Se

NMR chemical shift of its selenium adduct with other carbenes suggests that as a ligand, **14** is more σ-donating than traditional unsaturated NHCs due to the electron donating boryl groups. On the other hand, the presence of the boryl group does not seem to have a significant effect on the π-acidity of the carbene centre, presumably due to the non-parallel alignment of the respective heterocycle planes. DFT calculations of the HOMO on carbene **14** as well as the Ni−Br bond length and $\Delta E_{orb}(\sigma)$ in (**14**)Ni$(PMe_3)_2$Br support the assertion that the σ-donor ability of carbene **14** is augmented with the presence of the two boryl groups on the imidazole heterocycle.

The results reported in this chapter have shown that the *N*-methyl group in carbene **14** offers kinetic stability and slows down the 1,2-rearrangement of the boryl group which has allowed for detection of the carbene *in situ* and isolation of its metal complexes. One can thus envision that with greater steric hindrance (*e.g.* from a second *N*-boryl group), the rearrangement could be slowed down or even prevented, which could allow for the isolation of a carbene bearing a pendant *N*-boryl substituent. Chapter 3 reported on the 1,2-rearrangement of the *N*-substituted boryl group to the backbone of the imidazole heterocycle and examined the possibility of blocking the backbone CH sites to avoid such migration and force deprotonation at C2. Another approach could be to use a saturated backbone as these are typically less acidic than unsaturated ones. This could force deprotonation at C2 and, with steric protection from the bulky boryl groups, allow for isolation of the desired carbene. Furthermore, heavier Group 14 carbene analogues are likely to be more stable towards 1,2-rearrangement on account of a larger HOMO-LUMO energy gap, for example. Chapter 5 focuses therefore on *N*,*N*'-bisborylated saturated *N*-heterocyclic carbenes and their heavier analogues.

4.4 Experimental Procedures

Preparation of [(14)H][OTf]

Method (a): To a solution of **7** (0.50 g, 0.59 mmol) in benzene (20 mL) was added methyl trifluoromethanesulfonate (0.67 μL, 0.59 mmol) and the resulting mixture stirred for 3 h. The ^{1}H NMR spectrum of an aliquot taken from the reaction mixture at this point indicates full conversion to a new product. Volatiles were removed *in vacuo* and the residue washed with pentane to yield the crude product as an off-white solid. Yield: 0.48 g, 76%. Colourless single crystals suitable for X-ray crystallography could be obtained by layering a benzene solution with pentane.

Method (b): A mixture of **1** (5.0 g, 11 mmol), imidazole (0.36 g, 5.3 mmol) and potassium bis(trimethylsilyl)amide (2.1 g, 11 mmol) was dissolved in pentane (100 mL) and the reaction mixture stirred overnight. The ^{1}H NMR spectrum of an aliquot taken from the reaction mixture at this point indicates full conversion to a new product. Methyl trifluoromethanesulfonate (0.67 mL, 5.9 mmol) was then added, which resulted in the immediate formation of a white precipitate. The reaction mixture was stirred overnight and filtered. The white solid was washed with pentane (5 x 20 mL) and dried *in vacuo* yielding the product as a white solid. Yield: 4.8 g, 84%.

Spectroscopic Data for [(14)H][OTf]

^{1}H NMR (C_6D_6, 400 MHz, 298 K): δ_H 8.57 (1H, br s, NC*H*N), 7.24-7.28 (2H, m, *p*-*H* of *N*-boryl ligand), 7.07-7.12 (6H, overlapping m, *m*-*H* of *N*-boryl ligand and *p*-*H* of *C*-boryl ligand), 6.91-6.93 (4H, m, *m*-*H* of *C*-boryl ligand), 6.27 (1H, d, $^{4}J_{HH}$ = 1.4 Hz, NC*H*C[B]N of imidazole), 6.12 (2H, s, N(C*H*)$_2$N of *C*-boryl ligand), 5.90 (2H, s, N(C*H*)$_2$N of *N*-boryl ligand), 3.70 (3H, s, N*Me*), 2.77-2.90 (8H, overlapping m, C*H*Me$_2$ of *C*- and *N*-boryl

ligand), 1.10 (12H, d, $^{3}J_{HH}$ = 6.8 Hz, CH*Me*$_2$ of *N*-boryl ligand), 1.00 (12H, d, $^{3}J_{HH}$ = 6.8 Hz, CH*Me*$_2$ of *C*-boryl ligand), 0.96 (12H, d, $^{3}J_{HH}$ = 6.9 Hz, CH*Me*$_2$ of *N*-boryl ligand), 0.78 (12H, d, $^{3}J_{HH}$ = 6.9 Hz, CH*Me*$_2$ of *C*-boryl ligand) ppm. ^{1}H NMR (toluene-d$_8$, 400 MHz, 298 K): δ_H 8.54 (br s, 1H, NC*H*N), 7.23-7.27 (2H, m, *p-H* of Dipp of *N*-boryl ligand), 7.08-7.12 (2H, m, *p-H* of Dipp of *C*-boryl ligand), 7.05-7.07 (4H, m, *m-H* of Dipp of *N*-boryl ligand), 6.90-6.92 (4H, m, *m-H* of Dipp of *C*-boryl ligand), 6.25 (1H, d, $^{4}J_{HH}$ = 1.3 Hz, NC*H*C[B]N of imidazole), 6.12 (2H, s, N(C*H*)$_2$N of *C*-boryl ligand), 5.93 (2H, s, N(C*H*)$_2$N of *N*-boryl ligand), 3.65 (3H, s, N*Me*), 2.75-2.85 (8H, overlapping m, C*H*Me$_2$ of *C*- and *N*-boryl ligand), 1.10 (12H, d, $^{3}J_{HH}$ = 6.8 Hz, CH*Me*$_2$ of *N*-boryl ligand), 1.01 (12H, d, $^{3}J_{HH}$ = 6.8 Hz, CH*Me*$_2$ of *C*-boryl ligand), 0.94 (12H, d, $^{3}J_{HH}$ = 6.9 Hz, CH*Me*$_2$ of *N*-boryl ligand), 0.77 (12H, d, $^{3}J_{HH}$ = 6.9 Hz, CH*Me*$_2$ of *C*-boryl ligand) ppm. ^{13}C{^{1}H} NMR (C$_6$D$_6$, 101 MHz, 298 K): δ_C 145.1 (*o-C* of Dipp of *N*-boryl ligand), 144.7 (*o-C* of Dipp of *C*-boryl ligand), 141.3 (N*C*HN), 136.9 (*i-C* of Dipp of *C*-boryl ligand), 135.0 (*i-C* of Dipp of *N*-boryl ligand), 129.8 (*p-C* of Dipp of *N*-boryl ligand), 128.7 (*p-C* of Dipp of *C*-boryl ligand), 126.7 (N*C*HC[B]N of imidazole), 125.3 (*m-C* of Dipp of *N*-boryl ligand), 124.6 (*m-C* of Dipp of *C*-boryl ligand), 121.5 (N(*C*H)$_2$N of *C*-boryl ligand), 120.3 (N(*C*H)$_2$N of *N*-boryl ligand), 37.2 (N*Me*), 28.9 (*C*HMe$_2$ of *N*-boryl ligand), 28.7 (*C*HMe$_2$ of *C*-boryl ligand), 25.5 (CH*Me*$_2$ of *C*-boryl ligand), 24.8 (CH*Me*$_2$ of *N*-boryl ligand), 23.8 (CH*Me*$_2$ of *N*-boryl ligand), 23.2 (CH*Me*$_2$ of *C*-boryl ligand) ppm. *C*[B] cannot be observed. ^{11}B NMR (C$_6$D$_6$, 128 MHz, 298 K): δ_B 19 (br s, *C*- and *N*-boryl ligands) ppm. ^{19}F NMR (C$_6$D$_6$, 377 MHz, 298 K): δ_F -77.63 ppm. MS (ESI): *m/z* (assignment, %) 841 ([M]$^+$, 96%). Acc. Mass ESI: calc. for $C_{56}H_{77}B_2N_6$: 855.6408; found: 855.6525. Elemental microanalysis: found (calc. for $C_{57}H_{77}B_2F_3N_6O_3S$): C 67.79 (68.13)%, H 7.86 (7.72)%, N 8.23 (8.36)%.

Crystallographic Data for [(14)H][OTf]

a = 14.8618(1) Å, b = 22.3715(2) Å, c = 17.4851(1) Å, α = γ = 90°, β = 96.6656(7)°, V = 5774.16(7) Å^3, Monoclinic, $P2_1/n$, Z = 4, R_1 for 10819 [data intensity $I > 2\sigma(I)$] unique data = 0.060, wR_2 (all 11914 unique data) = 0.153.

Preparation of [(15)H][OTf]

A mixture of [(**14**)H][OTf] (1.0 g, 0.94 mmol) and potassium bis(trimethylsilyl)amide (200 mg, 0.98 mmol) was dissolved in toluene (50 mL) at -78 °C and the resulting mixture stirred at -78 °C for 30 min. Methyl trifluoromethanesulfonate (22 µL, 0.20 mmol) was added and the resulting mixture stirred at room temperature for 20 min. After filtration, the filtrate was concentrated to 5-10 mL and the product triturated by addition of pentane (40 mL). The suspension was stirred, allowed to settle and then filtered. The residual solid was washed with pentane (2 x 25 mL) and dried *in vacuo* to yield the product as an off-white solid. Yield: 650 mg, 65%. Colourless single crystals suitable for X-ray crystallography could be obtained by layering a benzene solution with pentane.

Spectroscopic Data for [(15)H][OTf]

^{1}H NMR (MeCN-d$_3$, 500 MHz, 298 K): δ_H 7.08-7.14 (4H, overlapping m, *p*-*H* of Dipp of *C*- and *N*-boryl ligand), 6.92 (8H, overlapping m, *m*-*H* of Dipp of *C*- and *N*-boryl ligand), 6.27 (4H, overlapping s, N(C*H*)$_2$N of *C*- and *N*-boryl ligand), 6.14 (1H, s, NC*H*C[B]N of imidazolium), 3.07 (3H, s, N*Me*), 2.58 (4H, sept, $^3J_{HH}$ = 6.8 Hz, C*H*Me$_2$ of *C*-boryl ligand), 2.51 (4H, sept, $^3J_{HH}$ = 6.8 Hz, C*H*Me$_2$ of *N*-boryl ligand), 1.98 (3H, s, C*Me*), 0.87 (24H, overlapping d, CH*Me*$_2$ of *C*- and *N*-boryl ligand), 0.58 (12H, d, $^3J_{HH}$ = 6.9 Hz, CH*Me*$_2$ of *C*-boryl ligand), 0.52 (12H, d, $^3J_{HH}$ = 6.9 Hz, CH*Me*$_2$ of *N*-boryl ligand) ppm. ^{13}C{^{1}H}

NMR (MeCN-d_3, 126 MHz, 298 K): δ_C 150.2 (N*C*MeN), 145.8 (*o-C* of Dipp of *C*-boryl ligand), 145.5 (*o-C* of Dipp of *N*-boryl ligand), 137.4 (*i-C* of Dipp of *C*-boryl ligand), 135.3 (*i-C* of Dipp of *N*-boryl ligand), 129.8 (*p-C* of Dipp of *N*-boryl ligand), 129.2 (*p-C* of Dipp of *C*-boryl ligand), 126.8 (N*C*HC[B]N of imidazolium), 125.4 (*m-C* of Dipp of *N*-boryl ligand), 125.0 (*m-C* of Dipp of *C*-boryl ligand), 122.6 (N(*C*H)$_2$N of *C*- or *N*-boryl ligand), 121.6 (N(*C*H)$_2$N of *C*- or *N*-boryl ligand), 35.8 (N*Me*), 29.3 (*C*HMe$_2$ of *N*-boryl ligand), 29.2 (*C*HMe$_2$ of *C*-boryl ligand), 25.8 (overlapping s, CH*Me*$_2$ of *C*- and *N*-boryl ligand), 23.4 (CH*Me*$_2$ of *C*-boryl ligand), 23.2 (CH*Me*$_2$ of *N*-boryl ligand), 12.4 (C*Me*) ppm. *C*[B] cannot be observed. ^{11}B NMR (MeCN-d_3, 160 MHz, 298 K): δ_B 20-21 (overlapping br s, *C*- and *N*-boryl ligand) ppm. ^{19}F NMR (C_6D_6, 470 MHz, 298 K): δ_F -79.34 (s) ppm. MS (EI): *m/z* (assignment, %) 869.7 ([M]$^+$, 99 %). Acc. Mass EI: calc. for $C_{57}H_{79}{}^{10}BN_4$: 867.6619; found: 867.6673. Elemental microanalysis: found (calc. for $C_{58}H_{79}B_2N_6F_3O_3S$): C 68.85 (68.37)%, H 8.21 (7.81) %, N 8.28 (8.25) %.

Crystallographic Data for [(15)H][OTf]

a = 12.1045(2) Å, *b* = 49.6218(7) Å, *c* = 19.9160(2) Å, α = γ = 90°, β = 91.582(1)°, V = 11957.9(3) Å^3, Monoclinic, $P2_1/c$, *Z* = 4, R_1 for 22113 [data intensity $I > 2\sigma(I)$] unique data = 0.067, wR^2 (all 24911 unique data) = 0.148.

Reaction of 16

A mixture of [(**15**)H][OTf] (30 mg, 0.028 mmol) and potassium bis(trimethylsilyl)amide (7 mg, 0.03 mmol) in a J. Young's NMR tube was dissolved in C_6D_6 (0.5 mL) and the tube shaken. ^{1}H NMR spectroscopy indicates full consumption of the imidazolium salt and conversion to a new product after 10 min (with < 5% of unknown impurities).

Spectroscopic Data for 16

^{1}H NMR (C_6D_6, 500 MHz, 298 K): δ_H 7.14-7.20 (6H, overlapping m, *p-H* of Dipp of *C*- and *N*-boryl ligand and C_6D_5H), 7.07-7.08 (4H, m, *m-H* of Dipp of *N*-boryl ligand), 7.02-7.03 (4H, m, *m-H* of Dipp of *C*-boryl ligand), 6.17 (2H, s, N(C*H*)$_2$N of *C*-boryl ligand), 6.14 (2H, s, N(C*H*)$_2$N of *N*-boryl ligand), 5.50 (1H, s, NC*H*C[B]N of imidazole), 3.28 (4H, sept, $^{3}J_{HH}$ = 6.8 Hz, C*H*Me$_2$ of *N*-boryl ligand), 3.14 (4H, sept, $^{3}J_{HH}$ = 6.9 Hz, C*H*Me$_2$ of *C*-boryl ligand), 2.91 (1H, d, $^{2}J_{HH}$ = 2.1 Hz, C=CH_2), 2.43 (1H, d, $^{2}J_{HH}$ = 2.1 Hz, C=CH_2), 2.41 (3H, s, N*Me*), 1.17 (12H, d, $^{3}J_{HH}$ = 6.8 Hz, CH*Me*$_2$ of *C*- or *N*-boryl ligand), 1.12 (12H, d, $^{3}J_{HH}$ = 6.8 Hz, CH*Me*$_2$ of *C*- or *N*-boryl ligand), 1.09 (12H, d, $^{3}J_{HH}$ = 6.9 Hz, CH*Me*$_2$ of *C*- or *N*-boryl ligand), 0.97 (12H, d, $^{3}J_{HH}$ = 6.9 Hz, CH*Me*$_2$ of *C*- or *N*-boryl ligand) ppm. Integration of *p-H* of Dipp of *C*- and *N*-boryl ligand is slightly higher than expected due to partial overlap with C_6D_5H. ^{13}C{^{1}H} NMR (C_6D_6, 126 MHz, 298 K): δ_C 154.4 (*C*=CH$_2$), 145.4 (*o-C* of Dipp of *C*- or *N*-boryl ligand), 145.2 (*o-C* of Dipp of *C*- or *N*-boryl ligand), 139.2 (*i-C* of Dipp of *C*-boryl ligand), 138.2 (*i-C* of Dipp of *N*-boryl ligand), 127.5 (*p-C* of Dipp of *C*- or *N*-boryl ligand), 127.4 (*p-C* of Dipp of *C*- or *N*-boryl ligand), 124.1 (overlapping s, *m-C* of Dipp of *C*- and *N*-boryl ligand), 120.5 (N(*C*H)$_2$N of *C*-boryl ligand), 119.6 (N*C*HC[B]N of imidazolium), 119.5 (N(*C*H)$_2$N of *N*-boryl ligand), 46.6 (C=*C*H$_2$), 34.0 (N*Me*), 28.6 (*C*HMe$_2$ of *N*-boryl ligand), 28.5 (*C*HMe$_2$ of *C*-boryl ligand), 25.9 (CH*Me*$_2$ of *C*- or *N*-boryl ligand), 25.7 (CH*Me*$_2$ of *C*- or *N*-boryl ligand), 23.8 (CH*Me*$_2$ of *C*- or *N*-boryl ligand), 23.5 (CH*Me*$_2$ of *C*- or *N*-boryl ligand) ppm. *C*[B] cannot be observed. ^{11}B NMR (C_6D_6, 128MHz, 298 K): δ_B 22 (br s, *C*- and *N*-boryl ligand) ppm.

Preparation of 17

To a solution of 2-phenylimidazole (42 mg, 0.29 mmol) in THF (15 mL) at -78 °C was added dropwise ^{n}BuLi (0.22 mL of a 1.5 M solution in hexane, 0.32 mmol). The

resulting mixture was stirred while slowly reaching room temperature and then stirred at room temperature overnight. At this point, **1** (150 mg, 0.32 mmol) was added and the solution stirred for further 30 h. Volatiles were removed *in vacuo* and the product extracted into benzene. After filtration, volatiles were again removed *in vacuo* to afford the product as an off-white solid. Yield: 90 mg, 59%.

Spectroscopic Data for 17

^{1}H NMR (C_6D_6, 400 MHz, 298 K): δ_H 7.91 (2H, d, $^3J_{HH}$ = 7.2 Hz, *o*-*H* of Ph), 7.12 (1H, br s, NC*H*CHN of imidazole), 7.04-7.09 (4H, overlapping m, *p*-*H* of Dipp and *m*-*H* of Ph), 6.96-7.01 (5H, overlapping m, *m*-*H* of Dipp and *p*-*H* of Ph), 6.83 (1H, br s, NC*H*CHN of imidazole), 6.22 (2H, s, N(C*H*)$_2$N of boryl ligand), 3.18 (4H, sept, $^3J_{HH}$ = 6.8 Hz, C*H*Me$_2$), 1.12 (12H, d, $^3J_{HH}$ = 6.8 Hz, CH*Me$_2$*), 0.93 (12H, d, $^3J_{HH}$ = 6.8 Hz, CH*Me$_2$*) ppm.

***In Situ* Reaction of 17 with Methyl Trifluoromethanesulfonate**

To a solution of **17** (50 mg, 0.095 mmol) in CD_2Cl_2 (0.5 mL) in J. Young's NMR tube was added methyl trifluoromethanesulfonate (11 µL, 0.095 mmol), the tube shaken and the solution allowed to stand for 6 h at room temperature. Full consumption of the starting material and conversion to a new species was observed by ^{1}H NMR spectroscopy. After filtration, volatiles were removed *in vacuo* and the product extracted into C_6D_6.

Spectroscopic Data for the *In Situ* Reaction of 17 with Methyl Trifluoromethanesulfonate

^{1}H NMR (C_6D_6, 400 MHz, 298 K): δ_H 7.98 (1H, d, $^3J_{HH}$ = 2.1 Hz, NC*H*CHN of imidazole), 7.19-7.23 (2H, m, Ar-*H* of Ph), 7.08-7.12 (1H, m, Ar-*H* of Ph), 6.99-7.05 (6H, overlapping m, *p*- and *m*-*H* of Dipp), 6.91 (1H, d, $^3J_{HH}$ = 2.0 Hz, NC*H*CHN of imidazole),

6.63-6.65 (2H, m, Ar-*H* of Ph), 6.06 (2H, s, N(C*H*)$_2$N of boryl ligand), 3.31 (3H, s, N*Me*), 2.79 (4H, sept, $^3J_{HH}$ = 6.7 Hz, C*H*Me$_2$), 1.01 (12H, d, $^3J_{HH}$ = 6.7 Hz, CH*Me$_2$*), 0.95 (12H, d, $^3J_{HH}$ = 6.9 Hz, CH*Me*$_2$) ppm.

In Situ Preparation of 14

A mixture of [(**14**)H][OTf] (40 mg, 0.037 mmol) and potassium bis(trimethylsilyl)amide (10 mg, 0.050 mmol) in a J. Young's NMR tube was dissolved in toluene-d$_8$ (0.5 mL) at -78 °C and the tube shaken intermittently at -78 °C. The resulting precipitate was collected at the top of the tube using a centrifuge. The *in situ* ^{1}H and ^{13}C NMR spectra measured immediately show clean conversion to the free carbene, which is stable in solution at -80 °C but rearranges with a half-life of $t_{1/2}$ = 4 h at room temperature. Attempts to crystalize the product at -80°C from diethyl ether, hexane or toluene from scaled-up syntheses were unsuccessful.

Spectroscopic Data for 14

^{1}H NMR (toluene-d$_8$, 400 MHz, 283 K): δ_H 7.07-7.16 (5H, overlapping m, *p*-H of Dipp of *C*- and *N*-boryl ligand and C$_6$D$_4$*H*CD$_3$), 6.94-7.02 (9H, overlapping m, *m*-H of Dipp of *C*- and *N*-boryl ligand and C$_6$D$_4$*H*CD$_3$), 6.23 (1H, s, NC*H*C[B]N of imidazole), 6.17 (2H, s, N(C*H*)$_2$N of *C*- or *N*-boryl ligand), 5.97 (2H, s, N(C*H*)$_2$N of *C*- or *N*-boryl ligand), 3.15-3.21 (7H, overlapping m, C*H*Me$_2$ of *C*- or *N*-boryl ligand and N*Me*), 3.02 (4H, br m, C*H*Me$_2$ of *C*- or *N*-boryl ligand), 1.19 (12H, br m, CH*Me*$_2$ of *C*- or *N*-boryl ligand, 1.08 (12H, br m, CH*Me*$_2$ of *C*- or *N*-boryl ligand), 0.99 (12H, br m, CH*Me*$_2$ of *C*- or *N*-boryl ligand), 0.80 (12H, br m, CH*Me*$_2$ of *C*- or *N*-boryl ligand) ppm. Integration of *p*-*H* and *m*-*H* of Dipp of both *C*- and *N*-boryl ligand is slightly higher than expected due to partial overlap with C$_6$D$_4$HCD$_3$. ^{13}C{^{1}H} NMR (toluene-d$_8$, 126 MHz, 298 K): δ_C 225.8 (br s, N*C*N), 146.2 (*o*-*C* of Dipp of *C*- or *N*-boryl ligand), 145.4 (*o*-*C* of Dipp of *C*- or *N*-

boryl ligand), 140.0 (*i-C* of Dipp of *C*- or *N*-boryl ligand), 139.3 (*i-C* of Dipp of *C*- or *N*-boryl ligand), 128.5-127.9 (overlapping signals, *p-C* of *C*- or *N*-boryl ligand and toluene-d_8), 127.9 (*p-C* of *C*- or *N*-boryl ligand), 127.6 (N*C*HC[B]N of imidazole), 124.5 (*m-C* of *C*- or *N*-boryl ligand), 124.1 (*m-C* of *C*- or *N*-boryl ligand), 120.8 (N(*C*H)$_2$N of *C*- or *N*-boryl ligand), 119.4 (N(*C*H)$_2$N of *C*- or *N*-boryl ligand), 38.5 (N*Me*), 29.3 (*C*HMe$_2$ of *C*- or *N*-boryl ligand), 29.0 (*C*HMe$_2$ of *C*- or *N*-boryl ligand), 25.8 (CH*Me*$_2$ of *C*- or *N*-boryl ligand), 25.1 (CH*Me*$_2$ of *C*- or *N*-boryl ligand), 24.2 (CH*Me*$_2$ of *C*- or *N*-boryl ligand), 23.7 (CH*Me*$_2$ of *C*- or *N*-boryl ligand) ppm. *C*[B] cannot be observed. ^{11}B NMR (toluene-d_8, 128 MHz, 253 K): δ_B 22 (br s, *C*- and *N*-boryl ligand) ppm.

Preparation of 19

A mixture of [(**14**)H][OTf] (300 mg, 0.028 mmol) and potassium bis(trimethylsilyl)amide (56 mg, 0.028 mmol) was dissolved in benzene (10 mL) and the resulting solution stirred at 80 °C for 20 min. After filtration, volatiles were removed *in vacuo* and the residue dissolved in a minimal amount of acetonitrile at 80 °C. The solution was allowed to cool slowly in the oil bath, producing colourless needle-like crystals. After filtration, the crystals were washed with acetonitrile (4 x 5 mL) to yield the product as a white crystalline solid. Yield: 120 mg, 45%. Colourless single crystals suitable for X-ray crystallography were grown from diethyl ether at -20 °C.

Spectroscopic Data for 19

^{1}H NMR (C_6D_6, 400 MHz, 298 K): δ_H 7.09-7.16 (4H, overlapping m, *p-H* of Dipp of *C2*- and *C4*-boryl ligand), 7.03-7.05 (4H, m, *m-H* of Dipp of *C2*-boryl ligand), 6.98-7.00 (4H, m, *m-H* of Dipp of *C4*-boryl ligand), 6.72 (1H, s, NC*H*C[B]N of imidazole), 6.27 (2H, s, N(C*H*)$_2$N of *C2*-boryl ligand), 6.20 (2H, s, N(C*H*)$_2$N of *C4*-boryl ligand), 3.31 (4H, sept, $^3J_{HH}$ = 6.8 Hz , C*H*Me$_2$ of *C2*-boryl ligand), 3.10 (4H, sept, $^3J_{HH}$ = 6.8 Hz, C*H*Me$_2$ of *C4*-

boryl ligand), 2.94 (3H, s, N*Me*), 1.16 (12H, d, $^3J_{HH}$ = 6.8 Hz, CH*Me*$_2$ of *C2*-boryl ligand), 1.20 (12H, d, $^3J_{HH}$ = 6.8 Hz, CH*Me*$_2$ of *C4*-boryl ligand), 1.07 (12H, d, $^3J_{HH}$ = 6.8 Hz, CH*Me*$_2$ of *C2*-boryl ligand), 0.82 (12H, d, $^3J_{HH}$ = 6.8 Hz, CH*Me*$_2$ of *C4*-boryl ligand) ppm. $^{13}C\{^1H\}$ NMR (C_6D_6, 125.7 MHz, 298 K): δ_C 145.9 (*o-C* of Dipp of *C2*-boryl ligand), 145.7 (*o-C* of Dipp of *C4*-boryl ligand), 140.6 (N*C*HC[B]N of imidazole), 139.4 (*i-C* of Dipp of *C4*-boryl ligand), 138.8 (*i-C* of Dipp of *C2*-boryl ligand), 128.4 (bs, N*C*[B]N), 127.6 and 127.8 (*p-C* of Dipp of *C2*- and *C4*-boryl ligand), 124.0 (*m-C* of Dipp of *C4*-boryl ligand), 123.6 (*m-C* of Dipp of *C2*-boryl ligand), 120.3 (overlapping s, N(*C*H)$_2$N of *C2*- and *C4*-boryl ligand), 34.4 (N*Me*), 28.7 (*C*HMe$_2$ of *C2*-boryl ligand), 28.6 (*C*HMe$_2$ of *C4*-boryl ligand), 25.8 (CH*Me*$_2$ of *C2*-boryl ligand), 25.6 (CH*Me*$_2$ of *C4*-boryl ligand), 23.5 (CH*Me*$_2$ of *C2*-boryl ligand), 23.2 (CH*Me*$_2$ of *C4*-boryl ligand). NCH*C*[B]N cannot be observed. ^{11}B NMR (C_6D_6, 128 MHz, 298 K): δ_B 23 (br s, *C*- and *N*-boryl ligands) ppm. MS (EI): *m/z* (assignment, %) 854.6 ([M]$^+$, 9%). Acc. Mass EI: calc. for $C_{56}H_{76}{}^{10}B_2N_6$: 852.6385; found: 852.6364. Elemental microanalysis: found (calc. for $C_{56}H_{76}B_2N_6$): C 78.83 (78.68)%, H 8.61 (8.96)%, N 9.74 (9.83)%.

Crystallographic Data for 19

a = 13.4666(3) Å, *b* = 20.5721(5) Å, *c* = 19.0832(4) Å, α = γ = 90°, β = 100.008(2)°, V = 5206.3(2) Å^3, Monoclinic, $P2_1/c$, *Z* = 4, R_1 for 8541 [data intensity $I > 2\sigma(I)$] unique data = 0.094, wR_2 (all 10726 unique data) = 0.296.

Preparation of [(20)H][OTf]

To a solution of **3** (95 mg, 0.18 mmol) in hexane (3 mL) was added methyl trifluoromethanesulfonate (22 μL, 0.20 mmol) and the resulting mixture stirred for 4 h. The solution was filtered and the residue washed with hexane (3 x 2 mL) and dried *in vacuo* to yield the product as an off-white powder. Yield: 110 mg, 85%. Colourless

single crystals suitable for X-ray crystallography could be obtained by dissolving the product in a minimal amount of hexane at 60 °C and allowing the solution to cool slowly in the oil bath.

Spectroscopic Data for [(20)H][OTf]

^{1}H NMR (C_6D_6, 400 MHz, 298 K): δ_H 7.53 (1H, s, NC*H*N), 7.29 (2H, m, *p*-*H* of Dipp), 7.15-7.16 (5H, overlapping m, *m*-*H* of Dipp, NCHC*H*N of imidazole and C_6D_5H), 6.30 (1H, s, NC*H*CHN of imidazole), 5.95 (2H, s, N(C*H*)$_2$N of boryl ligand), 3.41 (3H, s, N*Me*), 2.93 (4H, sept, $^{3}J_{HH}$ = 6.8 Hz, C*H*Me$_2$), 1.08-1.11 (24H, overlapping d, CH*Me*$_2$) ppm. ^{13}C{^{1}H} NMR (C_6D_6, 101 MHz, 298 K): δ_C 145.8 (*o*-*C* of Dipp), 137.0 (N*C*HN), 135.5 (*i*-*C* of Dipp), 130.0 (*p*-*C* of Dipp), 126.2 (N*C*HCHN of imidazole), 125.2 (*m*-*C* of Dipp), 121.4 (NCH*C*HN of imidazole), 120.0 (N(*C*H)$_2$N of boryl ligand), 36.7 (N*Me*), 28.9 (*C*HMe$_2$), 24.8 (CH*Me*$_2$), 23.4 (CH*Me*$_2$) ppm. ^{11}B NMR (C_6D_6, 128 MHz, 298 K): δ_B 19 (bs, boryl ligand) ppm. ^{19}F NMR (MeCN-d_3, 470 MHz, 298 K): δ_F -63.26 ppm. MS (EI): *m/z* (assignment, %) 469.4 ([M]$^+$, 99%). Acc. Mass EI: calc. for $C_{29}H_{40}{}^{10}BN_4$: 469.3502; found: 469.3607.

Crystallographic Data for [(20)H][OTf]

a = 11.9339(3) Å, *b* = 14.2524(4) Å, *c* = 19.9236(4) Å, α = β = γ = 90°, V = 3388.74(14) Å^3, Orthorhombic, $P2_12_12_1$, *Z* = 4, R_1 for 5993 [data intensity $I > 2\sigma(I)$] unique data = 0.089, wR_2 (all 6425 unique data) = 0.255.

Preparation of [(21)H][OTf]

To a solution of **9** (170 mg, 0.33 mmol) in hexane (5 mL) was added methyl trifluoromethanesulfonate (41 µL, 0.37 mmol) and the resulting mixture stirred overnight. After filtration, the residue was washed with hexane (2 x 3 mL) and dried

in vacuo to yield the product as an off-white powder. Yield: 190 mg, 87%. Colourless single crystals suitable for X-ray crystallography could be grown by dissolving the product in a minimal amount of acetonitrile at 80 °C and allowing the solution to cool slowly in the oil bath.

Spectroscopic Data for [(21)H][OTf]

^{1}H NMR (C_6D_6, 500 MHz, 298 K): δ_H 9.34 (1H, s, NC*H*N), 7.03-7.08 (4H, overlapping m, NCC*H* and *p*-*H* of Dipp), 6.99-7.00 (4H, m, *m*-*H* of Dipp), 6.86-6.89 (1H, ddd, $^{3}J_{HH}$ = 8.2 Hz, $^{3}J_{HH}$ = 7.3 Hz, $^{4}J_{HH}$ = 1.1 Hz, [B]NCCHC*H*), 6.81-6.84 (1H, ddd, $^{3}J_{HH}$ = 8.1 Hz, $^{3}J_{HH}$ = 7.3 Hz, $^{4}J_{HH}$ = 1.2 Hz, MeNCCHC*H*), 6.25 (2H, s, N(C*H*)$_2$N of boryl ligand), 3.58 (3H, s, N*Me*), 3.20 (4H, sept, $^{3}J_{HH}$ = 6.8 Hz, C*H*Me$_2$), 1.19 (12H, d, $^{3}J_{HH}$ = 6.9 Hz, CH*Me*$_2$), 1.17 (12H, d, $^{3}J_{HH}$ = 6.8 Hz, CH*Me*$_2$) ppm. ^{13}C{^{1}H} NMR (C_6D_6, 126 MHz, 298 K): δ_C 145.9 (*o*-*C* of Dipp), 144.7 (N*C*HN), 135.4 (*i*-*C* of Dipp), 132.7 (MeN*C*CH), 129.3 ([B]N*C*CH), 127.1 ([B]NCCH*C*H), 126.8 (MeNCCH*C*H), 124.7 (*m*-*C* of Dipp), 121.0 (N(*C*H)$_2$N of boryl ligand), 114.2 (MeNC*C*H), 114.0 ([B]NC*C*H), 33.8 (N*Me*), 29.1 (*C*HMe$_2$), 26.0 (CH*Me*$_2$), 23.5 (CH*Me*$_2$) ppm. ^{11}B NMR (C_6D_6, 128 MHz, 298 K): δ_B 21 (bs, boryl ligand) ppm. ^{19}F NMR (C_6D_6, 377 MHz, 298 K): δ_F -77.65 ppm. MS (EI): *m/z* (assignment, %) 519.4 ([M]$^+$, 97%). Acc. Mass EI: calc. for $C_{34}H_{44}BN_2$: 519.3660; found: 519.3761. Elemental microanalysis: found (calc. for $C_{35}H_{44}BN_4F_3O_3S$): C 62.90 (62.87)%, H 6.54 (6.63)%, N 8.71 (8.38)%.

Crystallographic Data for [(21)H][OTf]

a = 12.5831(3) Å, *b* = 46.9310(9) Å, *c* = 18.9096(4) Å, α = γ = 90°, β = 108.096(2)°, V = 10614.5(4) Å^3, Monoclinic, *Cc*, *Z* = 12, R_1 for 13329 [data intensity $I > 2\sigma(I)$] unique data = 0.032, wR_2 (all 13951 unique data) = 0.087.

In Situ Preparation of 20

A mixture of [(**20**)H][OTf] (30 mg, 0.057 mmol) and potassium bis(trimethylsilyl)amide (14 mg, 0.068 mmol) in a J. Young's NMR tube was dissolved in C_6D_6 (0.5 mL) and the tube shaken. The resulting precipitate was collected at the top of the tube using a centrifuge. The *in situ* ^{1}H and ^{13}C NMR spectra measured immediately show clean conversion to the free carbene, which is stable in solution at -80 °C but rearranges with a half-life of $t_{1/2}$ = 47 h at room temperature.

Spectroscopic Data for 20

^{1}H NMR (C_6D_6, 500 MHz, 298 K): δ_H 7.19-7.22 (2H, m, *p-H* of Dipp), 7.13-7.16 (4H, m, *m-H* of Dipp), 6.43 (1H, s, NC*H*CHN of imidazole), 6.09 (2H, s, N(C*H*)$_2$N of boryl ligand), 5.94 (1H, s, NC*H*CHN of imidazole), 3.34 (4H, sept, $^{3}J_{HH}$ = 7.0 Hz, C*H*Me$_2$), 3.09 (3H, s, N*Me*), 1.23 (12H, d, $^{3}J_{HH}$ = 6.9 Hz, CH*Me*$_2$), 1.19 (12H, d, $^{3}J_{HH}$ = 6.9 Hz, CH*Me*$_2$) ppm. $^{13}C\{^{1}H\}$ NMR (C_6D_6, 126 MHz, 298 K): δ_C 223.6 (N*C*N), 146.4 (*o-C* of Dipp), 139.4 (*i-C* of Dipp), 127.9-128.3 (overlapping signals, *p-C* of Dipp and *C*$_6$D$_6$) 123.9 (*m-C* of Dipp), 120.9 and 119.7 (N*C*H*C*HN), 119.0 (N(*C*H)$_2$N of boryl ligand), 37.4 (N*Me*), 28.9 (*C*HMe$_2$), 24.7 (CH*Me*$_2$), 23.6 (CH*Me*$_2$) ppm. ^{11}B NMR (C_6D_6, 160 MHz, 298 K): δ_B 23 (bs, boryl ligand) ppm.

In situ Preparation of 22

A mixture of [(**20**)H][OTf] (19 mg, 0.027 mmol) and potassium bis(trimethylsilyl)amide (6 mg, 0.03 mmol) in a J. Young's NMR tube was dissolved in C_6D_6 (0.5 mL) and the solution heated at 80 °C for 2 h. ^{1}H NMR spectroscopy indicated complete conversion to the migrated species.

Spectroscopic Data for 22

^{1}H NMR (C_6D_6, 400 MHz, 298 K): δ_H 7.16-7.19 (4H, overlapping m, *p-H* of Dipp and C_6D_5H), 7.11 (4H, m, *m-H* of Dipp), 7.00 (1H, s, MeNCHC*H*NB), 6.33 (2H, s, N(C*H*)$_2$N of boryl ligand), 6.15 (1H, s, MeNC*H*CHNB), 3.37 (4H, sept, $^{3}J_{HH}$ = 6.7 Hz, C*H*Me$_2$), 2.79 (3H, s, N*Me*), 1.22 (12H, d, $^{3}J_{HH}$ = 6.8 Hz, CH*Me*$_2$), 1.14 (12H, d, $^{3}J_{HH}$ = 6.8 Hz, CH*Me*$_2$) ppm. Integration of *p-H* of Dipp is slightly higher than expected due to partial overlap with C_6D_5H. ^{13}C{^{1}H} NMR (C_6D_6, 126 MHz, 298 K): δ_C 146.0 (*o-C* of Dipp), 139.2 (*i-C* of Dipp), 131.3 (MeNCH*C*HNB), 123.8 (overlapping s, *m-C* and *p-C* of Dipp), 121.1 (MeN*C*HCHNB), 120.4 (N(*C*H)$_2$N of boryl ligand), 33.2 (N*Me*), 28.8 (*C*HMe$_2$), 25.5 (CH*Me*$_2$), 23.6 (CH*Me*$_2$) ppm. *C*[B] cannot be observed. ^{11}B NMR (C_6D_6, 128 MHz, 298 K): δ_B 23 (bs, boryl ligand) ppm.

***In Situ* Preparation of 21**

A mixture of [(**21**)H][OTf] (26 mg, 0.038 mmol) and potassium bis(trimethylsilyl)amide (10 mg, 0.050 mmol) in a J. Young's NMR tube was dissolved in toluene-d_8 (0.5 mL) at -78 °C and the tube shaken intermittently at -78 °C. The resulting precipitate was collected at the top of the tube using a centrifuge. The *in situ* ^{1}H and ^{13}C NMR spectra measured immediately show clean conversion to the free carbene, which is stable in solution at -80 °C but rearranges with a half-life of *ca*. 9-12 h at room temperature.

Spectroscopic Data for 21

^{1}H NMR (toluene-d_8, 400 MHz, 193 K): δ_H 7.43 (1H, d, $^{3}J_{HH}$ = 7.8 Hz, MeNCC*H*), 6.97-7.00 (5H, overlapping m, *p-H* of Dipp, [B]NCCHC*H* and $C_6D_4HCD_3$), 6.91-6.93 (4H, m, *m-H* of Dipp), 6.78 (1H, m, MeNCCHC*H*), 6.37 (2H, s, N(C*H*)$_2$N of boryl ligand), 6.32

(1H, d, $^3J_{HH}$ = 7.8 Hz, [B]NCC*H*), 3.70 (4H, br m, C*H*Me$_2$), 2.96 (3H, s, N*Me*), 1.28-1.30 (24H, overlapping d, CH*Me*$_2$) ppm. Integration of *p-H* of Dipp and [B]NCCHC*H* is slightly higher than expected due to partial overlap with $C_6D_4HCD_3$. ^{1}H NMR (C_6D_6, 400 MHz, 298 K): δ_H 7.27 (1H, d, $^3J_{HH}$ = 7.9 Hz, MeNCC*H*), 7.00-7.09 (6H, overlapping m, *p-H* and *m-H* of Dipp), 6.90 (1H, dd, $^3J_{HH}$ = 7.8 and 7.8 Hz, [B]NCCHC*H*), 6.70 (1H, dd, $^3J_{HH}$ = 7.8 and 7.8 Hz, MeNCCHC*H*), 6.58 (1H, d, $^3J_{HH}$ = 7.8 Hz, [B]NCC*H*), 6.36 (2H, s, N(C*H*)$_2$N of boryl ligand), 3.63 (4H, sept, $^3J_{HH}$ = 6.8 Hz, C*H*Me$_2$), 3.17 (3H, s, N*Me*), 1.26 (12H, d, $^3J_{HH}$ = 6.8 Hz, CH*Me*$_2$), 1.22 (12H, d, $^3J_{HH}$ = 6.8 Hz, CH*Me*$_2$) ppm. ^{13}C{^{1}H} NMR (Toluene-*d*$_8$, 101 MHz, 298 K): δ_C 231.8 (N*C*N), 145.8 (*o-C* of Dipp), 137.0-138.1 (overlapping signals, *i-C* of Dipp, *i-C* of toluene-d$_8$ and [B]N*C*CH), 134.8 (MeN*C*CH), 127.4-128.1 (overlapping signals, *p-C* of Dipp and *m-C* of toluene-d$_8$), 123.6 (*m-C* of Dipp), 121.1 (MeNCCH*C*H), 120.7 ([B]NCCH*C*H), 119.2 (N(*C*H)$_2$N of boryl ligand), 111.5 (MeNC*C*H), 109.5 ([B]NC*C*H), 34.0 (N*Me*), 28.7 (*C*HMe$_2$ of boryl ligand), 25.9 (CH*Me*$_2$ of boryl ligand), 23.5 (CH*Me*$_2$ of boryl ligand) ppm. ^{11}B NMR (C_6D_6, 128 MHz, 298 K): δ_B 23 (br s, boryl ligand) ppm.

Preparation of 23

A mixture of [(**21**)H][OTf] (100 mg, 0.15 mmol) and potassium bis(trimethylsilyl)amide (33 mg, 0.16 mmol) was dissolved in benzene (5 mL) and the resulting mixture stirred at room temperature for 3 d. After filtration, volatiles were removed *in vacuo* and the residue dissolved in a minimal amount of acetonitrile at 80 °C. The solution was allowed to cool slowly in the oil bath, producing small colourless crystals. After filtration, the crystals were washed with acetonitrile (2 x 2 mL) and dried *in vacuo* to yield the product as a white powder. Yield: 25 mg, 32%.

Spectroscopic Data for 23

^{1}H NMR (C_6D_6, 500 MHz, 298 K): δ_H 7.71 (1H, m, MeNCC*H*), 7.13-7.16 (4H, overlapping m, *p-H* of Dipp and C_6D_5H), 7.06-7.08 (4H, m, *m-H* of Dipp), 6.97-7.03 (2H, m, NCCH(C*H*)$_2$), 6.80-6.82 (m, 1H, C=NCC*H*), 6.37 (2H, s, N(C*H*)$_2$N of boryl ligand), 3.43 (4H, sept, $^{3}J_{HH}$ = 6.9 Hz, C*H*Me$_2$), 3.08 (3H, s, N*Me*), 1.22 (12H, d, $^{3}J_{HH}$ = 6.9 Hz, CH*Me*$_2$), 1.11 (12H, d, $^{3}J_{HH}$ = 6.9 Hz, CH*Me*$_2$) ppm. Integration of *p-H* of Dipp is slightly higher than expected due to partial overlap with C_6D_5H. ^{13}C{^{1}H} NMR (C_6D_6, 126 MHz, 298 K): δ_C 146.0 (*o-C* of Dipp), 138.7 (*i-C* of Dipp), 135.9 (MeN*C*CH), 127.9-128.4 (overlapping signals, *p-C* of Dipp and *C*$_6$D$_6$), 123.9 (*m-C* of Dipp), 122.4 (MeNCCH*C*H), 121.7 (C=NCCH*C*H), 120.9 and 120.8 (MeNC*C*H and N(*C*H)$_2$N of boryl ligand), 109.1 (C=NC*C*H), 30.8 (N*Me*), 28.8 (*C*HMe$_2$), 25.7 (CH*Me*$_2$), 23.5 (CH*Me*$_2$) ppm. The signals for N*C*[B]N and C=N*C*CH cannot be located. ^{11}B NMR (C_6D_6, 160 MHz, 298 K): δ_B 23 (br s, boryl ligand) ppm. MS (EI): *m/z* (assignment, %) 518.4 ([M]$^+$, 8%). Acc. Mass EI: calc. for $C_{34}H_{43}BN_2$: 518.3581; found: 518.3597.

***In Situ* Preparation of 24**

To a solution of **22** (26mg, 0.057 mmol) in C_6D_6 (0.5 mL) in a J. Young's NMR tube was added methyl trifluoromethanesulfonate (8 µL, 0.07 mmol) and the tube shaken. ^{1}H NMR spectroscopy indicates complete conversion to the product after 15 min.

Spectroscopic Data for 14

^{1}H NMR (C_6D_6, 400 MHz, 298 K): δ_H 7.80 (2H, s, N(C*H*)$_2$N of imidazole), 7.11 (2H, m, *p-H* of Dipp), 6.96 (4H, m, *m-H* of Dipp), 6.28 (2H, s, N(C*H*)$_2$N of boryl ligand), 3.42 (6H, s, N*Me*), 2.80 (4H, sept, $^{3}J_{HH}$ = 6.8 Hz, C*H*Me$_2$), 1.01 (12H, d, $^{3}J_{HH}$ = 6.6 Hz, CH*Me*$_2$), 0.86 (12H, d, $^{3}J_{HH}$ = 6.8 Hz, CH*Me*$_2$) ppm. ^{13}C{^{1}H} NMR (C_6D_6, 101 MHz, 298 K): δ_C 144.4

(*o-C* of Dipp), 135.8 (*i-C* of Dipp), 129.1 (*p-C* of Dipp), 126.7 (N(*C*H)$_2$N of imidazole), 125.0 (*m-C* of Dipp), 122.0 (N(*C*H)$_2$N of boryl ligand), 36.3 (N*Me*), 29.0 (*C*HMe$_2$), 26.3 (CH*Me*$_2$), 22.7 (CH*Me*$_2$) ppm. *C*[B] cannot be observed. ^{11}B NMR (C_6D_6, 128 MHz, 298 K): δ_B 19 (br s, boryl ligand) ppm. ^{19}F NMR (C_6D_6, 376 MHz, 298 K): δ_F -63.26 ppm.

Preparation of (14)AuCl

A mixture of [(**14**)H][OTf] (310 mg, 0.29 mmol) and potassium bis(trimethylsilyl)amide (58 mg, 0.29 mmol) was dissolved in toluene at -40 °C and the resulting solution stirred for 20 min. The coagulated solution was then filtered onto (THT)AuCl (93 mg, 0.29 mmol) and the resulting mixture stirred at -40 °C for 30 min before being allowed to slowly warm to room temperature. Volatiles were removed *in vacuo* and the residue dissolved in a minimal amount of acetonitrile at 80 °C. The solution was allowed to cool slowly to room temperature producing colourless crystals. After filtration, the crystals were washed three times with a minimal amount of acetonitrile, and then dried *in vacuo* to yield the product as a white solid. Further crops of the product could be obtained by recrystallization from a concentrated solution of the filtrate stored at -20 °C. Yield: First crop – 70 mg, 22%; second crop – 36 mg, 12%. Colourless single crystals suitable for X-ray crystallography were grown from a concentrated solution in hexane.

Spectroscopic Data for (14)AuCl

^{1}H NMR (C_6D_6, 400 MHz, 298 K): δ_H 7.12-7.16 (5H, overlapping m, *p-H* of Dipp of *N*-boryl ligand and C_6D_5H), 7.05-7.09 (2H, m, *p-H* of Dipp of *C*-boryl ligand), 6.98-7.00 (4H, m, *m-H* of Dipp of *N*-boryl ligand), 6.88-6.90 (4H, m, *m-H* of Dipp of *C*-boryl ligand), 6.37 (1H, s, NC*H*C[B]N of imidazole), 6.14 (2H, s, N(C*H*)$_2$N of *N*-boryl ligand), 6.08 (2H, s, N(C*H*)$_2$N of *C*-boryl ligand), 3.61 (4H, br m, C*H*Me$_2$ of *N*-boryl ligand), 2.94

(3H, s, N*Me*), 2.85 (4H, sept, $^{3}J_{HH}$ = 6.8 Hz, C*H*Me$_2$ of *C*-boryl ligand), 1.30-1.21 (24H, overlapping m, CH*Me*$_2$ of *N*-boryl ligand), 1.01 (12H, d, $^{3}J_{HH}$ = 6.8 Hz, CH*Me*$_2$ of *C*-boryl ligand), 0.46 (12H, d, $^{3}J_{HH}$ = 6.9 Hz, CH*Me*$_2$ of *C*-boryl ligand) ppm. Integration of *p-H* of Dipp of *N*-boryl ligand is slightly higher than expected due to partial overlap with C_6D_5H. ^{1}H NMR (C_6D_6, 400 MHz, 333 K): δ_H 7.12-7.16 (5H, overlapping m, *p-H* of Dipp of *N*-boryl ligand and C_6D_5H), 7.06-7.10 (2H, m, *p-H* of Dipp of *C*-boryl ligand), 7.00-7.02 (4H, m, *m-H* of Dipp of *N*-boryl ligand), 6.90-6.91 (4H, m, *m-H* of Dipp of *C*-boryl ligand), 6.37 (1H, s, NC*H*C[B]N of imidazole), 6.15 (2H, s, N(C*H*)$_2$N of *N*-boryl ligand), 6.10 (2H, s, N(C*H*)$_2$N of *C*-boryl ligand), 3.60 (4H, sept, $^{3}J_{HH}$ = 6.8 Hz, C*H*Me$_2$ of *N*-boryl ligand), 3.00 (3H, s, N*Me*), 2.86 (4H, sept, $^{3}J_{HH}$ = 6.8 Hz, C*H*Me$_2$ of *C*-boryl ligand), 1.18-1.21 (24H, overlapping d, CH*Me*$_2$ of *N*-boryl ligand), 1.01 (12H, d, $^{3}J_{HH}$ = 6.8 Hz, CH*Me*$_2$ of *C*-boryl ligand), 0.50 (12H, d, $^{3}J_{HH}$ = 6.9 Hz, CH*Me*$_2$ of C-boryl ligand) ppm. Integration of *p-H* of Dipp of *N*-boryl ligand is slightly higher than expected due to partial overlap with C_6D_5H. $^{13}C\{^{1}H\}$ NMR (C_6D_6, 101 MHz, 333 K): δ_C 177.0 (N*C*N), 146.8 (*o-C* of Dipp of *N*-boryl ligand), 144.6 (*o-C* of Dipp of *C*-boryl ligand), 137.7 (*i-C* of Dipp of *C*-boryl ligand), 136.5 (*i-C* of Dipp of *N*-boryl ligand), 127.8-128.3 (overlapping s, *p-C* of Dipp of *C*-boryl and *N*-boryl ligands), 127.6 (N*C*HC[B]N of imidazole), 124.6 (*m-C* of Dipp of *C*-boryl ligand), 124.0 (*m-C* of Dipp of *N*-boryl ligand), 120.9 (N(*C*H)$_2$N of *N*-boryl ligand), 120.3 (N(*C*H)$_2$N of *C*-boryl ligand), 37.8 (N*Me*), 29.2 (*C*HMe$_2$ of *N*-boryl ligand), 28.5 (*C*HMe$_2$ of *C*-boryl ligand), 26.3 (CH*Me*$_2$ of *N*-boryl ligand), 25.2 (CH*Me*$_2$ of *C*-boryl ligand), 24.5 (CH*Me*$_2$ of *N*-boryl ligand), 23.0 (CH*Me*$_2$ of *C*-boryl ligand). *C*[B] cannot be observed. ^{11}B NMR (C_6D_6, 128 MHz, 333 K): δ_B 22 (br s, *C*- and *N*-boryl ligand) ppm. MS (EI): *m/z* (assignment, %) 1086.6 ([M]$^+$, 3%). Acc. Mass EI: calc. for $C_{56}H_{76}{}^{10}B_2N_6AuCl$: 1084.5739; found: 1084.5776. The mass of the molecular ion is outside of the calibrated range for the instrument,

but he isotopic profile is, however, in very close agreement with the calculated profile. Elemental microanalysis: found (calc. for $C_{56}H_{76}B_2N_6AuCl$): C 61.66 (61.86)%, H 7.23 (7.05)%, N 7.84 (7.73)%.

Crystallographic Data for (14)AuCl

a = 18.2495(3) Å, b = 19.4439(4) Å, c = 16.3430(3) Å, α = γ = 90°, β = 103.8521(18)°, V = 5630.52(19) Å^3, Monoclinic, *Cc*, Z = 4, R_1 for 6782 [data intensity $I > 2\sigma(I)$] unique data = 0.018, wR_2 (all 6863 unique data) = 0.046.

Preparation of (14)Rh(cod)Cl

A mixture of [(**14**)H][OTf] (500 mg, 0.47 mmol) and potassium bis(trimethylsilyl)amide (93 mg, 0.47 mmol) in benzene (10 mL) was stirred at room temperature for 5 min. The coagulated solution was then filtered onto $[Rh(cod)Cl]_2$ (115 mg, 0.23 mmol) and the resulting mixture stirred for 30 min. Volatiles were removed *in vacuo* and the residue dissolved in toluene; the solution was then concentrated, resulting in the formation of yellow crystals at -20 °C. After filtration, washing the crystals with a minimal amount of toluene and drying *in vacuo* the product was obtained as yellow crystals. Yield: first crop - 70 mg, 14%; second crop - 80 mg, 16%, third crop - 50 mg, 10%. Yellow single crystals suitable for X-ray crystallography were obtained from a concentrated solution in pentane at -20 °C.

Spectroscopic Data for (14)Rh(cod)Cl

^{1}H NMR (C_6D_6, 400 MHz, 298 K): δ_H 7.14-7.18 (6H, overlapping m, *m-H* and *p-H* of Dipp of *C*- or *N*-boryl ligand and C_6D_5H), 6.95-7.04 (6H, overlapping m, *m-H* and *p-H* of Dipp of *C*- or *N*-boryl ligand), 6.47 (1H, s, NC*H*C[B]N of imidazole), 6.13-6.18 (4H, overlapping m, N(C*H*)$_2$N of *C*- and *N*-boryl ligand), 5.79 (1H, t, $^3J_{HH}$ = 7.5 Hz, C*H* of cod),

4.55-4.60 (4H, overlapping m, C*H* of cod and N*Me*), 3.84 (1H, t, $^3J_{HH}$ = 6.5 Hz, C*H* of cod), 3.12 (4H, sept, $^3J_{HH}$ = 6.8 Hz, C*H*Me$_2$ of *C*-boryl ligand), 2.99 (4H, sept, $^3J_{HH}$ = 6.8 Hz, C*H*Me$_2$ of *C*-boryl ligand), 2.64-2.86 (3H, overlapping m, C*H*Me$_2$ of *N*-boryl ligand and C*H$_2$* of cod), 2.43-2.54 (2H, overlapping m, C*H* and C*H$_2$* of cod), 1.83-2.07 (4H, overlapping m, C*H$_2$* of cod), 1.38-1.47 (3H, overlapping m, 2H, C*H$_2$* of cod), 1.29 (6H, br m, CH*Me$_2$* of *N*-boryl ligand), 1.16 (6H, d, $^3J_{HH}$ = 6.9 Hz, CH*Me$_2$* of *C*-boryl ligand), 1.13 (6H, d, $^3J_{HH}$ = 6.8 Hz, CH*Me$_2$* of *C*-boryl ligand), 1.06 (6H, d, $^3J_{HH}$ = 6.8 Hz, CH*Me$_2$* of *C*-boryl ligand), 1.02 (6H, d, $^3J_{HH}$ = 6.7 Hz, CH*Me$_2$* of *N*-boryl ligand), 0.85 (6H, d, $^3J_{HH}$ = 6.9 Hz, CH*Me$_2$* of *C*-boryl ligand), 0.43 (6H, br m, CH*Me$_2$* of *N*-boryl ligand) ppm. 2H for C*H*Me$_2$ and 6H for CH*Me$_2$* of *N*-boryl ligand could not be observed at room temperature due to restricted rotation of the Dipp groups. Integration of *m*-H and *p*-*H* of Dipp is slightly higher than expected due to partial overlap with C_6D_5H. ^{1}H NMR (C_6D_6, 400 MHz, 333 K): δ_H 7.15-7.19 (9H, overlapping m, *m*-*H* and *p*-*H* of Dipp of *C*- or *N*-boryl ligand and C_6D_5*H*), 6.97-7.06 (6H, overlapping m, *m*-*H* and *p*-*H* of Dipp of *C*- or *N*-boryl ligand), 6.49 (1H, s, NC*H*C[B]N of imidazole), 6.21 (2H, s, N(C*H*)$_2$N of *C*-boryl ligand), 6.14 (2H, br s, N(C*H*)$_2$N of *N*-boryl ligand), 5.73 (1H, br t, $^3J_{HH}$ = 7.5 Hz, C*H* of cod), 4.54-4.60 (4H, overlapping m, C*H* of cod and N*Me*), 3.84 (1H, br t, $^3J_{HH}$ = 6.5 Hz, C*H* of cod), 3.57 (2H, br m, C*H*Me$_2$ of *N*-boryl ligand), 3.14 (2H, sept, $^3J_{HH}$ = 6.8 Hz, C*H*Me$_2$ of *C*-boryl ligand), 3.00 (2H, sept, $^3J_{HH}$ = 6.8 Hz, C*H*Me$_2$ of *C*-boryl ligand), 2.79-2.82 (2H, br m, C*H*Me$_2$ of *N*-boryl ligand), 2.61-2.72 (1H, m, C*H$_2$* of cod), 2.41-2.52 (2H, overlapping m, C*H* and C*H$_2$* of cod), 1.85-2.11 (4H, overlapping m, C*H$_2$* of cod), 1.46-1.52 (8H, overlapping m, CH*Me$_2$* of *N*-boryl ligand and C*H$_2$* of cod), 1.31 (6H, d, $^3J_{HH}$ = 6.5 Hz, CH*Me$_2$* of *C*-boryl ligand), 1.14-1.19 (12H, overlapping m, CH*Me$_2$* of *C*-boryl ligand), 1.03-1.07 (12H, overlapping m, CH*Me$_2$* of *C*-boryl and *N*-boryl ligand), 0.86 (6H, d, $^3J_{HH}$ = 6.8 Hz, CH*Me$_2$* of *C*-boryl ligand), 0.51 (6H, br d, $^3J_{HH}$ = 5.7 Hz, CH*Me$_2$*

of *N*-boryl ligand) ppm. Integration of *m*-H and *p*-*H* of Dipp of *C*- or *N*-boryl ligand is slightly higher than expected due to partial overlap with C_6D_5H. $^{13}C\{^1H\}$ NMR (C_6D_6, 101 MHz, 298 K): δ_C 189.0 (d, $^1J_{RhC}$ = 52.0 Hz, N*C*N), 146.0 (*o*-*C* of Dipp of *C*-boryl ligand), 145.6 (bs, *o*-*C* of Dipp of *N*-boryl ligand), 145.4 and 144.5 (overlapping s, *o*-*C* of Dipp of *C*- and *N*-boryl ligands), 138.2 (*i*-*C* of Dipp of *C*-boryl ligand), 138.0 (*i*-*C* of Dipp of *N*-boryl ligand), 127.8-128.3 (overlapping signals, N*C*HC[B]N of imidazole and C_6D_6), 125.2 (br s, *p*-*C* of Dipp of *C*- or *N*-boryl ligand), 124.1, 124.0 and 123.8 (*m*-*C* of Dipp of *C*- and *N*-boryl ligands and *p*-*C* of Dipp of *C*- or *N*-boryl ligand), 121.4 (N(*C*H)$_2$N of *C*-boryl ligand), 122.0 (br s, N(*C*H)$_2$N of *N*-boryl ligand), 99.7 (d, $^2J_{RhC}$ = 8.2 Hz, *C*H of cod), 99.4 (d, $^2J_{RhC}$ = 7.0 Hz, *C*H of cod), 68.8 (d, $^2J_{RhC}$ = 14.1 Hz, *C*H of cod), 64.7 (d, $^2J_{RhC}$ = 13.9 Hz, *C*H of cod), 40.1 (N*Me*), 36.2 (*C*H$_2$ of cod), 32.5 (*C*H$_2$ of cod), 30.3 (*C*H$_2$ of cod), 29.0 (br s, *C*HMe$_2$ of *N*-boryl ligand), 28.7 (*C*HMe$_2$ of *C*-boryl ligand), 28.7 (*C*HMe$_2$ of *C*-boryl ligand), 26.9 (*C*H$_2$ of cod), 26.5 (br s, CH*Me*$_2$ of *N*-boryl ligand), 26.2 (CH*Me*$_2$ of *C*-boryl ligand), 26.0 (CH*Me*$_2$ of *C*-boryl ligand), 25.7 (br s, CH*Me*$_2$ of *N*-boryl ligand), 25.4 (br s, CH*Me*$_2$ of *N*-boryl ligand) 24.0 (CH*Me*$_2$ of *C*-boryl ligand), 23.7 (CH*Me*$_2$ of *C*-boryl ligand), 22.1 (br s, CH*Me*$_2$ of *N*-boryl ligand) ppm. 1C for *C*HMe$_2$ could not be observed at room temperature due to restricted rotation of the Dipp groups. The second set of peaks for *m*-*C* of Dipp of *C*- and *N*-boryl ligands could not be located but are likely to be overlapping with C_6D_6. $^{13}C\{^1H\}$ NMR (C_6D_6, 101 MHz, 333 K): δ_C 189.5 (d, $^1J_{RhC}$ = 52.0 Hz, N*C*N), 146.1 (*o*-*C* of Dipp of *C*-boryl ligand), 145.6 (*o*-*C* of Dipp of *N*-boryl ligand), 145.9 (*o*-*C* of Dipp of *C*-boryl ligand), 145.5 (*o*-*C* of Dipp of *N*-boryl ligand), 138.4 (*i*-*C* of Dipp of *C*- or *N*-boryl ligand), 138.2 (*i*-*C* of Dipp of *C*- or *N*-boryl ligand), 127.8-128.8 (overlapping signals, N*C*HC[B]N of imidazole and C_6D_6), 125.2 (*p*-*C* of Dipp), 124.2, 124.0 and 123.9 (*m*-*C* and *p*-*C* of Dipp of *C*- or *N*-boryl ligand), 121.5 (N(*C*H)$_2$N of *C*-boryl ligand), 121.2 (N(*C*H)$_2$N of *N*-boryl ligand), 99.7 (d,

$^2J_{RhC}$ = 8.2 Hz, *C*H of cod), 90.8 (d, $^2J_{RhC}$ = 7.0 Hz, *C*H of cod), 68.7 (d, $^2J_{RhC}$ = 14.1 Hz, *C*H of cod), 64.9 (d, $^2J_{RhC}$ = 13.9 Hz, *C*H of cod), 40.2 (N*Me*), 36.1 (*C*H_2 of cod), 32.2 (*C*H_2 of cod), 30.6 (*C*H_2 of cod), 29.1 (*C*HMe_2 of *N*-boryl ligand), 28.8 and 28.7 (*C*HMe_2 of *C*- and *N*-boryl ligands), 27.0 (*C*H_2 of cod), 26.5 (CH*Me*$_2$ of *N*-boryl ligand), 26.1 (CH*Me*$_2$ of *C*-boryl ligand), 25.7 (CH*Me*$_2$ of *N*-boryl and *C*-boryl ligands), 25.3 (CH*Me*$_2$ of *N*-boryl ligand), 24.0 (CH*Me*$_2$ of *C*-boryl ligand), 23.6 (CH*Me*$_2$ of *C*-boryl ligand), 22.4 (CH*Me*$_2$ of *N*-boryl ligand) ppm. The second set of peaks for *m*-*C* of Dipp of *C*- and *N*-boryl ligands could not be located but are likely to be overlapping with C_6D_6. *C*[B] cannot be observed. ^{11}B NMR (C_6D_6, 128 MHz, 298 K): δ_B 22 (br s, *C*- and *N*-boryl ligand) ppm.

Crystallographic Data for (14)Rh(cod)Cl

a = 13.3664(2) Å, *b* = 17.4540(2) Å, *c* = 14.2125(2) Å, α = γ = 90°, β = 115.075(2)°, V = 3003.24(9) Å^3, Monoclinic, *P*2$_1$, *Z* = 2, R_1 for 11118 [data intensity $I > 2\sigma(I)$] unique data = 0.030, wR_2 (all 11526 unique data) = 0.078.

Preparation of (14)Rh(CO)$_2$Cl

Method (a) (*in situ*): (**14**)Rh(cod)Cl was dissolved in C_6D_6 (0.5 mL) in a J. Young's NMR tube and the solution degassed *via* three freeze-pump-thaw cycles prior to backfilling the tube with CO. The ^{1}H NMR spectrum measured at this point indicated complete conversion to the desired product.

Method (b) (preparative scale): A mixture of [(**14**)H][OTf] (400 mg, 0.37 mmol) and potassium bis(trimethylsilyl)amide (75 mg, 0.37 mmol) was dissolved in benzene (10 mL) and the resulting mixture stirred for 5 min at room temperature. The coagulated solution was then filtered onto [Rh(CO)$_2$Cl]$_2$ (66 mg, 0.17 mmol) and the resulting

mixture stirred for 10 min. The ^{1}H NMR spectrum of an aliquot taken from the solution at this point indicated complete conversion to the desired product (with < 5% impurities). Volatiles were removed *in vacuo* and the residue dissolved in hot hexane. The resulting solution was allowed to cool slowly to room temperature in the oil bath and then further cooled to -20 °C to yield a crystalline product. Isolated yields of the product were very low due to the high solubility of the product in compatible media. Single crystals suitable for X-ray crystallography were obtained by recrystallization from hexane at -20 °C.

Spectroscopic Data for (14)Rh(CO)$_2$Cl

^{1}H NMR (C_6D_6, 400 MHz, 298 K): δ_H 6.98-7.16 (21H, overlapping m, *p*-*H* and *m*-*H* of Dipp of *C*- and *N*-boryl ligand and C_6D_5H), 6.59 (1H, s, NC*H*C[B]N of imidazole), 6.21 (2H, s, N(C*H*)$_2$N of *C*-boryl ligand), 6.18 (2H, br s, N(C*H*)$_2$N of *N*-boryl ligand), 4.02 (3H, s, N*Me*), 3.26 (4H, br m, C*H*Me$_2$ of *N*-boryl ligand), 2.98 (4H, br m, C*H*Me$_2$ of *C*-boryl ligand), 0.72-1.36 (62H, overlapping m, CH*Me*$_2$ of *C*- and *N*-boryl ligand and coordinated *n*-hexane) ppm. Integration of the signals for *m*-*H* and *p*-*H* is slightly higher than expected due to partial overlap with C_6D_5H, the sum is greater. ^{1}H NMR (C_6D_6, 400 MHz, 343 K): δ_H 7.12-7.18 (20H, overlapping m, *p*-*H* of Dipp of *C*- and *N*-boryl ligand and C_6D_5H), 7.06-7.08 (4H, m, *m*-*H* of Dipp of *N*-boryl ligand), 7.00-7.02 (4H, m, *m*-*H* of Dipp of *C*-boryl ligand), 6.59 (1H, s, NC*H*C[B]N of imidazole), 6.20 (2H, s, N(C*H*)$_2$N of *C*-boryl ligand), 6.17 (2H, br s, N(C*H*)$_2$N of *N*-boryl ligand), 3.98 (3H, s, N*Me*), 3.22 (4H, br m, C*H*Me$_2$ of *N*-boryl ligand), 2.99 (4H, sept, $^{3}J_{HH}$ = 6.9 Hz, C*H*Me$_2$ of *C*-boryl ligand), 1.23-1.29 (8H, overlapping m, CH_2 of coordinated *n*-hexane), 1.03-1.13 (42H, overlapping d, CH*Me*$_2$ of *C*- and *N*-boryl ligand), 0.88 (6H, t, $^{3}J_{HH}$ = 6.8 Hz, CH_3 of coordinated *n*-hexane) ppm. Integration of the signals for *m*-*H* and *p*-*H* of Dipp

is slightly higher than expected due to partial overlap with C_6D_5H. $^{13}C\{^1H\}$ NMR (C_6D_6, 101 MHz, 343 K): δ_C 187.5 (d, $^2J_{RhC}$ = 55.0 Hz, Rh*C*O), 182.5-183.5 (overlapping d, Rh*C*O and N*C*N), 145.5 (*o-C* of Dipp of *N*-boryl ligand), 145.4 (*o-C* of Dipp of *C*-boryl ligand), 138.4 (*i-C* of Dipp of *N*-boryl ligand), 137.8 (*i-C* of Dipp of *C*-boryl ligand), 129.4 (N*C*HC[B]N of imidazole), 127.8-128.3 (overlapping signals, *p-C* of Dipp of *C*- and *N*-boryl ligand and C_6D_6), 125.0 (*m-C* of Dipp of *N*-boryl group), 124.2 (*m-C* of Dipp of *C*-boryl group), 121.3 (N(*C*H)$_2$N of *C*-boryl ligand), 120.3 (N(*C*H)$_2$N of *N*-boryl ligand), 39.9 (N*Me*), 31.9 (*C*H$_2$CH$_2$CH$_3$ of coordinated *n*-hexane), 28.8 (*C*HMe$_2$ of *C*-boryl ligand), 28.7 (*C*HMe$_2$ of *N*-boryl ligand), 26.0 (CH*Me*$_2$ of *C*-boryl ligand), 25.8 (br s, CH*Me*$_2$ of *N*-boryl ligand), 23.7 (CH*Me*$_2$ of *C*-boryl ligand), 23.5 (br s, CH*Me*$_2$ of *N*-boryl ligand), 23.0 (*C*H$_2$CH$_3$ of coordinated *n*-hexane), 14.2 (*C*H$_3$ of coordinated *n*-hexane) ppm. *C*[B] cannot be observed. ^{11}B NMR (C_6D_6, 128 MHz, 343 K): δ_B 21-23 (br s, *C*- and *N*-boryl ligand) ppm. Elemental microanalysis: found (calc. for $C_{58}H_{76}RhB_2ClN_6O_2$): C 66.38 (66.39)%, H 7.61 (7.30)%, N 8.33 (8.01)%. IR (CH_2Cl_2): 1990 (s, C–O stretch) and 2069 (s, C–O stretch) cm^{-1}.

Crystallographic Data for (14)Rh(CO)$_2$Cl

a = 12.6301(5) Å, *b* = 20.2377(8) Å, *c* = 24.9748(10) Å, α = γ = 90°, β = 103.187(4)°, V = 6215.3(4) Å^3, Monoclinic, *P2$_1$/n*, *Z* = 4, R_1 for 5418 [data intensity $I > 2\sigma(I)$] unique data = 0.177, wR_2 (all 7173 unique data) = 0.99.

Preparation of (14)Se

To a mixture of [(**21**)H][OTf] (500 mg, 0.47 mmol), sodium bis(trimethylsilyl)amide (94 mg, 0.51 mmol) and selenium powder (150 mg, 1.9 mmol) was added benzene (7 mL) and the resulting mixture stirred at room temperature for 1 h. After filtration, the volume of the filtrate was reduced until incipient precipitation. The solution was then

warmed until all the precipitate dissolved, and the solution then allowed to cool slowly to room temperature in the oil bath, producing colourless single crystals suitable for X-ray crystallography. After filtration, the remaining crystals were dried *in vacuo* to yield the product as a white solid. Yield: 290 mg, 66 %.

Spectroscopic Data for (14)Se

^{1}H NMR (C_6D_6, 400 MHz, 298 K): δ_H 7.17-7.21 (12H, overlapping m, *p-H* of Dipp of *C*-boryl ligand and C_6D_5H), 7.08 (6H, overlapping m, *p-H* and *m-H* of Dipp *N*-boryl ligand), 6.93 (4H, m, *m-H* of Dipp of *C*-boryl ligand), 6.32 (1H, s, NC*H*C[B]N of imidazole), 6.21 (2H, s, N(C*H*)$_2$N of *N*-boryl ligand), 6.16 (2H, s, N(C*H*)$_2$N of *C*-boryl ligand), 3.64 (4H, br m, CH*Me*$_2$ of *N*-boryl ligand), 3.20 (3H, s, N*Me*), 2.99 (4H, sept, $^{3}J_{HH}$ = 6.8 Hz, CH*Me*$_2$ of *C*-boryl ligand), 1.17 (12H, d, $^{3}J_{HH}$ = 6.8 Hz, CH*Me*$_2$ of *C*-boryl ligand), 1.12 (12H, br m, CH*Me*$_2$ of *C*-boryl ligand), 1.05 (12H, d, $^{3}J_{HH}$ = 6.8 Hz, CH*Me*$_2$ of *N*-boryl ligand), 0.69 (12H, d, $^{3}J_{HH}$ = 6.9 Hz, CH*Me*$_2$ of *N*-boryl ligand). The integration for the signal for *p-H* of Dipp of *C*-boryl ligand is slightly higher than expected due to partial overlap with C_6D_5H. ^{13}C{^{1}H} NMR (C_6D_6, 126 MHz, 298K): δ_C 163.7 (*C*=Se), 146.6 (*o-C* of Dipp of *C*-boryl ligand), 144.7 (*o-C* of Dipp of *N*-boryl ligand), 138.0 (*i-C* of Dipp of *C*-boryl ligand), 137.3 (*i-C* of Dipp of *N*-boryl ligand), 128.4-127.9 (overlapping signals, C_6D_6, *p-C* of Dipp of *C*-boryl ligand and *p-C* or *m-C* of Dipp of *N*-boryl ligand), 125.0 (N*C*HC[B]N of imidazole), 124.4 (*m-C* of Dipp of *C*-boryl ligand), 124.0 (*p-C* or *m-C* of Dipp *N*-boryl ligand), 120.8 (N(*C*H)$_2$N of *C*-boryl ligand), 119.9 (N(*C*H)$_2$N of *N*-boryl ligand), 36.8 (N*Me*), 28.7 (*C*HMe$_2$ of *N*-boryl ligand), 28.5 (*C*HMe$_2$ of boryl ligand of *C*-boryl ligand), 26.6 (CH*Me*$_2$ of *C*-boryl ligand), 25.4 (CH*Me*$_2$ of *N*-boryl ligand), 24.0 (CH*Me*$_2$ of *C*-boryl ligand), 23.1 (CH*Me*$_2$ of *N*-boryl ligand) ppm. *C*[B] cannot be observed. ^{11}B NMR (C_6D_6, 128 MHz, 298 K): δ_B 22 (br s, *C*- and *N*-

boryl ligand) ppm. ^{77}Se NMR (Acetone-d_6, 95 MHz, 298 K): δ_{Se} 67 ppm. MS (EI): *m/z* (assignment, %) 934.6 ([M]$^+$, 3%). Acc. Mass EI: calc. for $C_{56}H_{76}{}^{10}B^{11}BN_6Se$: 954.5519; found: 954.5595. The mass of the molecular ion is outside of the calibrated range for the instrument, but he isotopic profile is, however, in very close agreement with the calculated profile. Elemental microanalysis: found (calc. for $C_{56}H_{76}B_2N_6Se$): C 71.72 (72.03)%, H 8.32 (8.20)%, N 9.20 (9.00)%.

Crystallographic Data for (14)Se

a = 20.3192(3) Å, b = 12.4493(1) Å, c = 22.9607(3) Å, α = γ = 90°, β = 113.317(1)°, V = 5333.78(12) Å^3, Monoclinic, $P2_1/n$, Z = 4, R_1 for 9793 [data intensity $I > 2\sigma(I)$] unique data = 0.047, wR_2 (all 11090 unique data) = 0.130.

4.5 References

1 A. C. Hillier, W. J. Sommer, B. S. Yong, J. L. Petersen, L. Cavallo and S. P. Nolan, *Organometallics*, 2003, **22**, 4322–4326.
2 L. Falivene, R. Credendino, A. Poater, A. Petta, L. Serra, R. Oliva, V. Scarano and L. Cavallo, *Organometallics*, 2016, **35**, 2286–2293.
3 H. Clavier and S. P. Nolan, *Chem. Commun.*, 2010, **46**, 841–861.
4 C. A. Tolman, *Chem. Rev.*, 1977, **77**, 313–348.
5 A. Gómez-Suárez, D. J. Nelson and S. P. Nolan, *Chem. Commun.*, 2017, **53**, 2650–2660.
6 R. A. Kelly, H. Clavier, S. Giudice, N. M. Scott, E. D. Stevens, J. Bordner, I. Samardjiev, C. D. Hoff, L. Cavallo and S. P. Nolan, *Organometallics*, 2008, **27**, 202–210.
7 D. Tapu, D. A. Dixon and C. Roe, *Chem. Rev.*, 2009, **109**, 3385–3407.
8 M. Nonnenmacher, D. Kunz, F. Rominger and T. Oeser, *Chem. Commun.*, 2006, **386**, 1378–1380.
9 A. J. Arduengo, *Acc. Chem. Res.*, 1999, **32**, 913–921.
10 R. W. Alder and M. E. Blake, *J. Phys. Chem. A*, 1999, **103**, 11200–11211.
11 O. Back, M. Henry-Ellinger, C. D. Martin, D. Martin and G. Bertrand, *Angew. Chem. Int. Ed.*, 2013, **52**, 2939–2943.
12 A. Liske, K. Verlinden, H. Buhl, K. Schaper and C. Ganter, *Organometallics*, 2013, **32**, 5269–5272.
13 S. V. C. Vummaleti, D. J. Nelson, A. Poater, A. Gómez-Suárez, D. B. Cordes, A. M. Z. Slawin, S. P. Nolan and L. Cavallo, *Chem. Sci.*, 2015, **6**, 1895–1904.

14 S. Dutta, B. Maity, D. Thirumalai and D. Koley, *Inorg. Chem.*, 2018, **57**, 3993–4008.
15 H. Jacobsen, A. Correa, A. Poater, C. Costabile and L. Cavallo, *Coord. Chem. Rev.*, 2009, **253**, 687–703.
16 M. M. D. Roy and E. Rivard, *Acc. Chem. Res.*, 2017, **50**, 2017–2025.
17 S. M. I. Al-Rafia, A. C. Malcolm, S. K. Liew, M. J. Ferguson, R. McDonald and E. Rivard, *Chem. Commun. (Camb).*, 2011, **47**, 6987–6989.
18 J. Clayden, N. Greeves and S. Warren, *Organic Chemistry*, Oxford University Press, New York, 2nd edn., 2012.
19 S. Solé, H. Gornitzka, O. Guerret and G. Bertrand, *J. Am. Chem. Soc.*, 1998, **120**, 9100–9101.
20 J. W. Storer and K. N. Houk, *J. Am. Chem. Soc.*, 1993, **115**, 10426–10427.
21 M. T. H. Liu, *Acc. Chem. Res.*, 1994, **27**, 287–294.
22 C. Heinemann and W. Thiel, *Chem. Phys. Lett.*, 1994, **217**, 11–16.
23 J. A. Montgomery, K. Raghavdchari, M. A. Alaham, V. G. Zakrzewski, E. S. Replogle, R. Gomperts, R. L. Martin, D. J. Fox, J. S. Binkley, G. Maier, J. Endres and H. P. Reisenauer, *Angew. Chem. Int. Ed.*, 1997, **36**, 69451–69454.
24 W. C. Liu, Y. H. Liu, T. S. Lin, S. M. Peng and C. W. Chiu, *Inorg. Chem.*, 2017, **56**, 10543–10548.
25 X. Cattoën, H. Gornitzka, F. S. Tham, K. Miqueu, D. Bourissou and G. Bertrand, *Eur. J. Org. Chem.*, 2007, **2007**, 912–917.
26 J. E. House, *Principles of Chemical Kinetics*, Elsevier Science & Technology, San Diego, 2007.
27 E. V. Anslyn and D. A. Dougherty., *Modern physical organic chemistry*, University Science Books, Sausalito, California, 2006.
28 D. W. Urry, *Math. Model.*, 1982, **3**, 503–522.
29 G. A. McGibbon, C. Heinemann, D. J. Lavorato and H. Schwarz, *Angew. Chemie Int. Ed. English*, 1997, **36**, 1478–1481.
30 A. J. Arduengo, R. Krafczyk, R. Schmutzler, H. A. Craig, J. R. Goerlich, W. J. Marshall and M. Unverzagt, *Tetrahedron*, 1999, **55**, 14523–14534.
31 E. Aldeco-Perez, A. J. Rosenthal, B. Donnadieu, P. Parameswaran, G. Frenking and G. Bertrand, *Science*, 2009, **326**, 556–560.
32 J. J. Dunsford, K. J. Cavell and B. M. Kariuki, *Organometallics*, 2012, **31**, 4118–4121.
33 S. Dierick, D. F. Dewez and I. E. Markó, *Organometallics*, 2014, **33**, 677–683.
34 A. Gómez-Suárez, R. S. Ramón, O. Songis, A. M. Z. Slawin, C. S. J. Cazin and S. P. Nolan, *Organometallics*, 2011, **30**, 5463–5470.
35 M. M. D. Roy, P. A. Lummis, M. J. Ferguson, R. McDonald and E. Rivard, *Chem. Eur. J.*, 2017, **23**, 11249–11252.
36 A. R. Chianese, X. Li, M. C. Janzen, J. W. Faller and R. H. Crabtree, *Organometallics*, 2003, **22**, 1663–1667.
37 O. Back, M. Henry-Ellinger, C. D. Martin, D. Martin and G. Bertrand, *Angew. Chem. Int. Ed.*, 2013, **52**, 2939–2943.
38 A. Liske, K. Verlinden, H. Buhl, K. Schaper and C. Ganter, *Organometallics*, 2013, **32**, 5269–5272.

39 M. Ahmed, C. Buch, L. Routaboul, R. Jackstell, H. Klein, A. Spannenberg and M. Beller, *Chem. Eur. J.*, 2007, **13**, 1594–1601.
40 M. Iglesias, D. J. Beetstra, B. Kariuki, K. J. Cavell, A. Dervisi and I. A. Fallis, *Eur. J. Inorg. Chem.*, 2009, **2009**, 1913–1919.
41 M. Iglesias, D. J. Beetstra, J. C. Knight, L. L. Ooi, A. Stasch, S. Coles, L. Male, M. B. Hursthouse, K. J. Cavell, A. Dervisi and I. A. Fallis, *Organometallics*, 2008, **27**, 3279–3289.
42 G. A. Blake, J. P. Moerdyk and C. W. Bielawski, *Organometallics*, 2012, **31**, 3373–3378.
43 T. W. Hudnall and C. W. Bielawski, *J. Am. Chem. Soc.*, 2009, **131**, 16039–16041.
44 V. César, N. Lugan and G. Lavigne, *Eur. J. Inorg. Chem.*, 2010, **2010**, 361–365.
45 K. Verlinden, H. Buhl, W. Frank and C. Ganter, *Eur. J. Inorg. Chem.*, 2015, **2015**, 2416–2425.
46 V. Lavallo, Y. Canac, C. Präsang, B. Donnadieu and G. Bertrand, *Angew. Chem. Int. Ed.*, 2005, **44**, 5705–5709.
47 V. Lavallo, Y. Canac, A. DeHope, B. Donnadieu and G. Bertrand, *Angew. Chem. Int. Ed.*, 2005, **44**, 7236–7239.
48 Y. Wei, B. Rao, X. Cong and X. Zeng, *J. Am. Chem. Soc.*, 2015, **137**, 9250–9253.
49 M. Tretiakov, Y. G. Shermolovich, A. P. Singh, P. P. Samuel, H. W. Roesky, B. Niepötter, A. Visscher and D. Stalke, *Dalton Trans.*, 2013, **42**, 12940–12946.
50 R. W. Alder, P. R. Allen, M. Murray and A. G. Orpen, *Angew. Chem. Int. Ed.*, 1996, **35**, 1121–1123.
51 K. Denk, P. Sirsch and W. A. Herrmann, *J. Organometalic Chem.*, 2002, **649**, 219–224.
52 H. Duddeck, *Prog. Nucl. Magn. Reson. Spectrosc.*, 1995, **27**, 1–323.
53 H. Niu, R. J. Mangan, A. V. Protchenko, N. Phillips, W. Unkrig, C. Friedmann, E. L. Kolychev, R. Tirfoin, J. Hicks and S. Aldridge, *Dalton Trans.*, 2018, Accepted Manuscript. DOI: 10.1039/C8DT01661E
54 J. Zhu, Z. Lin and T. B. Marder, *Inorg. Chem.*, 2005, **44**, 9384–9390.

Chapter V

Syntheses and Reactivity of *N,N*'-Bisborylated Saturated *N*-Heterocyclic Carbenes and Group 14 Tetrelenes

---

5.1 Introduction

Attempts to isolate an *N*,*N*'-bisborylated carbene and/or its metal complexes have not been successful; as discussed in section 3.2.4, 1,2-migration of the boryl group to the backbone has prevented isolation of the target NHCs. One strategy to avoid deprotonation of the backbone involved blocking the backbone CH sites of the imidazole heterocycle to promote deprotonation at C2 but all attempts to access such carbenes were, unfortunately, unsuccessful. Another possibility to promote deprotonation at C2 could be the use of a saturated backbone, the protons of which are not as acidic as those of unsaturated backbones. The syntheses of precursors to carbenes of this type (*e.g.* **5.1**) might be accomplished by borylation of imidazoline or 3,4,5,6-tetrahydropyrimidine (Scheme 5.1).

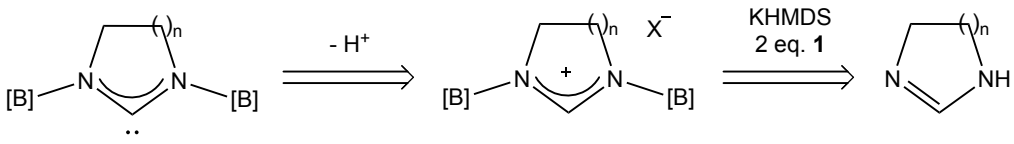

5.1 **5.2** **5.3**

Scheme 5.1 Borylation of imidazoline (n = 1) or 3,4,5,6-tetrahydropyrimidine (n = 2) and subsequent deprotonation as potential routes to *N,N*'-bisborylated saturated NHCs.

In addition to using the corresponding protonated salts as carbene precursors (as discussed in section 3.1), cyclic thioureas are often employed to access free carbenes

and can, for example, be synthesized by reacting bifunctional diamines with CS_2 or thiophosgene (Scheme 5.2),[1–3] followed by reduction of the C=S bond using K or KC_8.[3–5] As this method does not rely on deprotonation, the backbone of the heterocycle is not expected to be implicated, thereby driving carbene formation at C2. Such a carbene might also be kinetically stabilized towards 1,2-rearrangement on the basis of the steric disincentive for migration of a boryl group to C2.

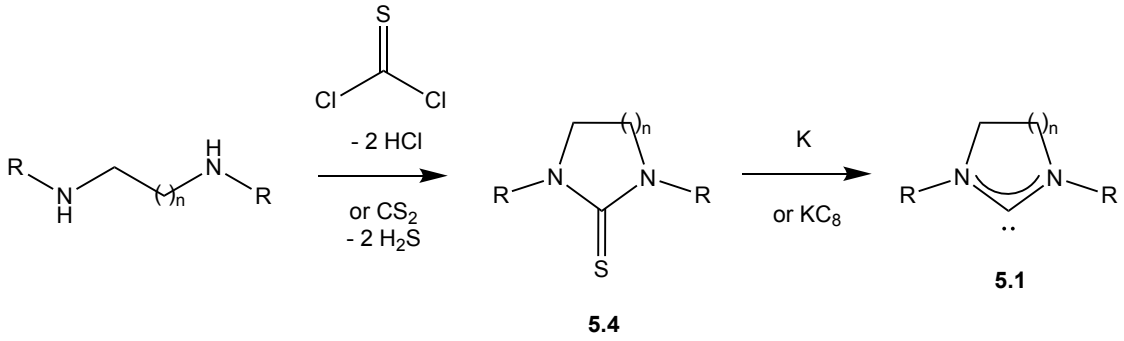

Scheme 5.2 Synthetic approach to access cyclic thioureas from diamines and either thiophosgene or CS_2 and subsequent reduction to form free carbenes.[1–5]

Unlike carbenes, the heavier Group 14 carbene analogues; silylenes, germylenes, stannylenes and plumbylenes can be accessed directly from their respective dihalides (*e.g.* IPr·$SiCl_2$, IPr·$SiBr_2$, $GeCl_2$·dioxane, $SnCl_2$, $SnBr_2$, SnI_2, $PbCl_2$, $PbBr_2$, PbI_2) *via* halide metathesis (an example is shown in Scheme 5.3).[6–9] This synthetic strategy has the advantages of avoiding unwanted side reactions arising, for example, from backbone deprotonation, nucleophilic attack of a base at the tetralene centre or over-reduction. Nonetheless, it is worth noting that, as a side product, IPr is formed in metathesis reactions using IPr·$SiCl_2$ or IPr·$SiBr_2$, and is often difficult to separate from the target silylene. Separation strategies including sequestration by CO_2 or $SiBr_4$ have been reported, although these are contingent on these reagents not reacting with the target silylene itself.[6]

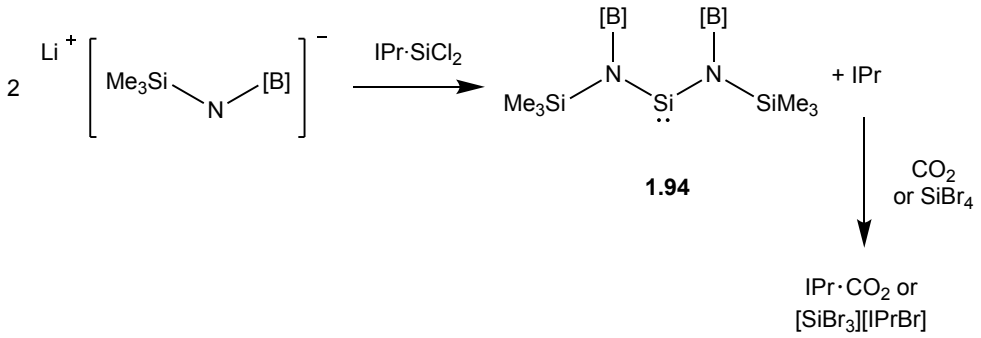

Scheme 5.3 An example of a salt metathesis reaction to form a Group 14 tetrelene. The scheme shows the synthesis of acyclic diaminosilylene 1.94 from IPr·$SiCl_2$ where IPr is formed as a side product. CO_2 or $SiBr_4$ could be used to sequester IPr.[6]

An alternative method to access silylenes, which does not result in the formation of IPr as a side product, is the reduction of Si(IV) precursors. This method was used before silylenes could be accessed *via* salt metatheses, for example in the synthesis of the first isolable silylene, **1.60** (Scheme 5.4).[10] Sen *et al.* reported a milder reduction of a Si(IV) precursor which proceeded *via* base-induced elimination of HCl from the corresponding Si(IV)(hydrido)chloride (**5.7**; Scheme 5.5).[11]

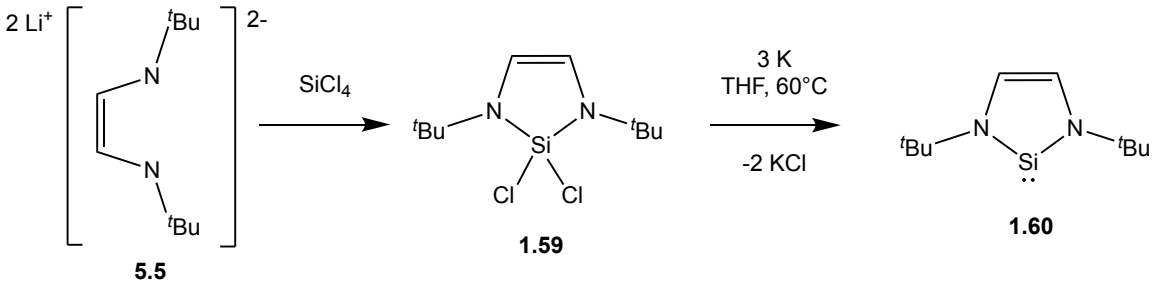

Scheme 5.4 Synthesis of silylene 1.60 by reduction of Si(IV) precursor 1.59.[10,12]

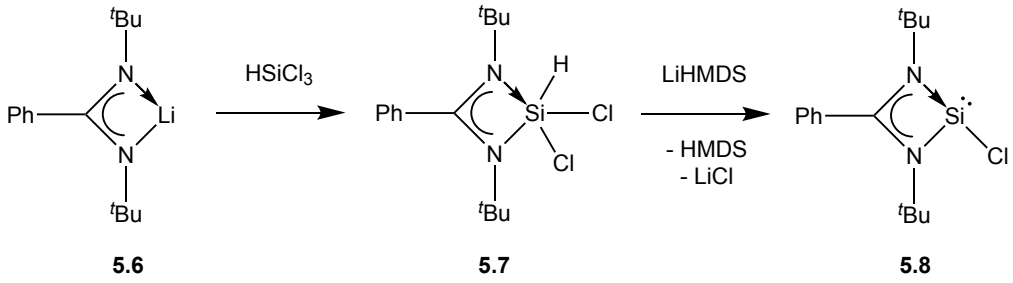

Scheme 5.5 Synthesis of a base-stabilized silylene (5.8) by elimination of HCl from 5.7.[11]

Ketones usually exist in the monomeric form, but the heavier analogues have a tendency to oligomerize or polymerize due to weaker E-O π-bonding and the greater bond polarity.[13] To date, only one stable, unsupported, monomeric germanone has been isolated – featuring the extremely bulky Eind substituents (Eind = 1,1,3,3,5,5,7,7-octaethyl-s-hydrindacen-4-yl) (**1.68**; Scheme 1.23).[14] Furthermore, during the course of this work, the first unsupported silanones were isolated by Alvarado-Beltran and Rosas-Sánchez *et al*. (**1.75** and **1.76**; Scheme 1.25).[15,16] Due to the tendency of the silanones and germanones to oligomerize, sterically bulky substituents are needed to offer kinetic stabilization. With this in mind, the bulky Dipp-substituted boryl groups were thought to represent viable kinetically stabilizing substituents.

At the outset, the aim of the research reported in this chapter was the syntheses of *N*-heterocyclic carbenes, silylenes, germylenes and stannylenes of types **5.1** and **5.9** (Figure 5.1). The reactivity of the tetrelenes was then to be studied with a particular focus on the aim of synthesizing an unsupported germanone **5.10** (Figure 5.1), with steric stabilization by the peripheral boryl groups. The tetrelene chemistry reported in this chapter was carried out in close collaboration with Nicola Oldroyd (Part 2 student), Rachel Grabiner (Part 2 student) and Andreas Heilmann (summer student), who worked under my supervision in the Aldridge group.

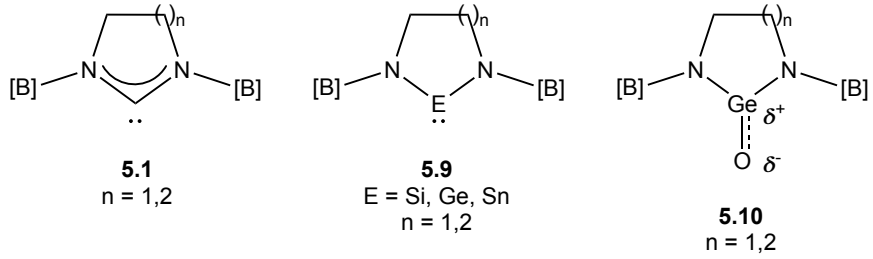

5.1
n = 1,2

5.9
E = Si, Ge, Sn
n = 1,2

5.10
n = 1,2

Figure 5.1 Targeted five- and six-membered *N*-heterocyclic carbenes (5.1) and the corresponding heavier analogues (5.9); a target germanone (5.10).

5.2 Results and Discussion

5.2.1 Attempted Synthesis of an *N*,*N*'-Bisborylated Six-Membered NHC

The C2 proton is the most acidic proton on 3,4,5,6-tetrahydropyrimidium salts. Bisborylated 3,4,5,6-tetrahydropyrimidium salts therefore have the potential to afford (at least *in situ*) a free carbene with two adjacent boryl substituents. Due to the steric bulk of the boryl substituents and the implied 1,2 regiochemistry of the rearrangement product, migration of one of the boryl groups to the C2 position was considered unlikely on steric grounds. At the very least, it was hypothesized that such migration might have a high enough kinetic barrier to allow for detection and/or trapping of the carbene *in situ*.

Bisborylated pyrimidium salt [(**25**)H][BPh_4] was readily synthesized from 3,4,5,6-tetrahydropyrimidine in 59% yield (Scheme 5.6) in a similar fashion to [(**4**)H][BPh_4] and [(**11**)H][BPh_4] (sections 3.2.1 and 3.2.4). The backbone protons of the pyrimidium heterocycle give rise to two broad multiplets in the ^{1}H NMR spectrum at 2.28 and -0.29 ppm, which integrate to four and two protons, respectively. Furthermore, the backbone protons of the boryl substituents give rise to one singlet at 5.60 ppm that integrates to four protons and one septet and two doublets can be observed at 2.50 (8H), 1.01 and 0.77 ppm (24H each) for the isopropyl methine and methyl protons, respectively. This is consistent with a symmetrical pyrimidium heterocycle containing two equivalent boryl groups. In addition to NMR spectroscopy, mass spectroscopy (including accurate mass, m/z = 857.6592 ($[C_{56}H_{79}B_2N_6]^+$)) and elemental microanalysis are consistent with successful synthesis of [(**25**)H][BPh_4]. Single crystals suitable for X-ray crystallography unfortunately could not be obtained despite multiple attempts.

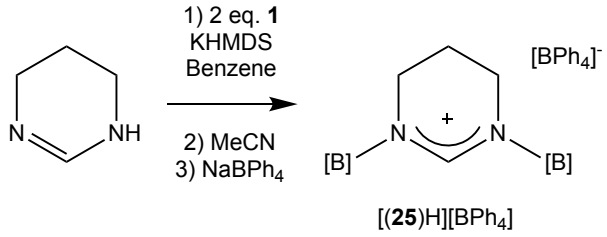

[(**25**)H][BPh$_4$]

Scheme 5.6 Bisborylation of 3,4,5,6-tetrahydropyrimidine to give pyrimidium salt [(25)H][BPh$_4$].

With the aim of accessing the target free carbene, [(**25**)H][BPh$_4$] was reacted with potassium bis(trimethylsilyl)amide. Two different species (**26** and **27**, in roughly 40:60 ratio) are observed in the ^{1}H NMR spectrum of the reaction mixture (Figure 5.2). Each species seems to feature two inequivalent boryl groups: four singlets are observed for the boryl backbone protons. The signals at 5.86 and 6.04 ppm are assigned to **26**, and those at 5.87 and 6.11 ppm to **27** on the basis of matching integral intensities. Three additional multiplets (at 5.35, 4.55 and 4.29 ppm) seem to belong to **26**; each integrates to half the intensity of the 2H singlets at 5.86 and 6.04 ppm, and are therefore assigned to single proton environments. The position of these resonances suggest that **26** is an alkenic species. Moreover, a 1H singlet at 7.51 ppm is also assigned to **26**, this resonance having a chemical shifts reminiscent of the NC*H*N proton in a formamidine.

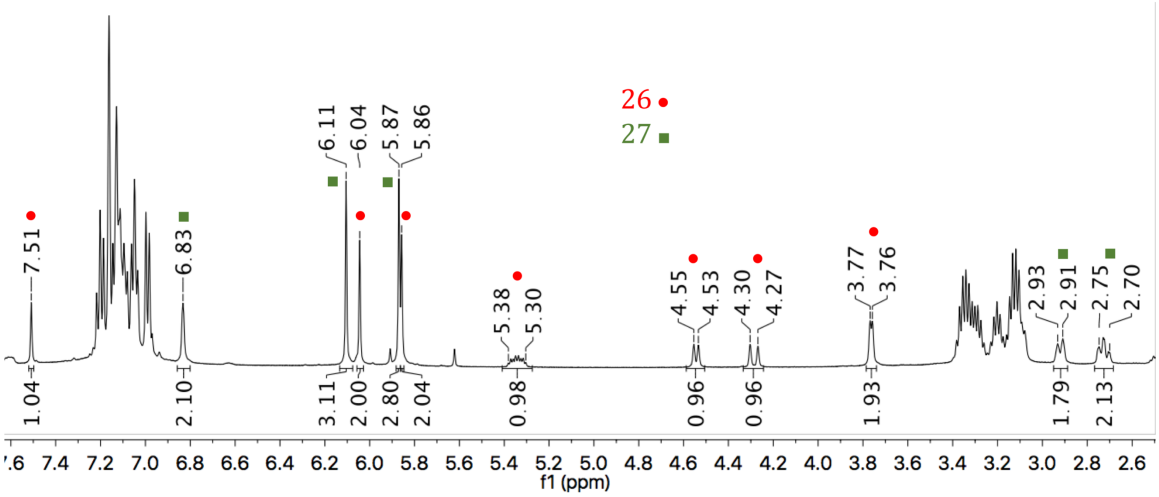

Figure 5.2 The *in situ* ^{1}H NMR spectrum of the reaction mixture of [(25)H][BPh_4] and potassium bis(trimethylsilyl)amide in C_6D_6. The integrations of the signals are referenced according to the minor species, 26.

After filtration and removal of volatiles, colourless single crystals suitable for X-ray crystallography were grown from a hot acetonitrile solution and provided the solid-state structure of one of the species (Figure 5.3). The structure so obtained reveals ring-opening of the six-membered ring to give an *N*,*N*'-bisborylated formamidine featuring a pendant allyl function. Instead of deprotonation at C2, one of the C5 protons is removed, which leads to a 1,4-Hofmann elimination and ring-opening *via* N–C bond cleavage (Scheme 5.7). The ^{1}H NMR spectrum of the crystals redissolved in C_6D_6 matches the chemical shifts assigned to the minor species (**26**) in the reaction mixture. Kolychev *et al*. observed an analogous 1,4-Hofmann elimination when reacting a seven membered formamidinium salt with Ag_2O.[17] Additionally, the Aldridge group observed C–N cleavage in a six-membered NHC coordinated to an iridium centre, where excess carbene acts as a base and removes the C5 proton with subsequent 1,4-Hofmann elimination.[18]

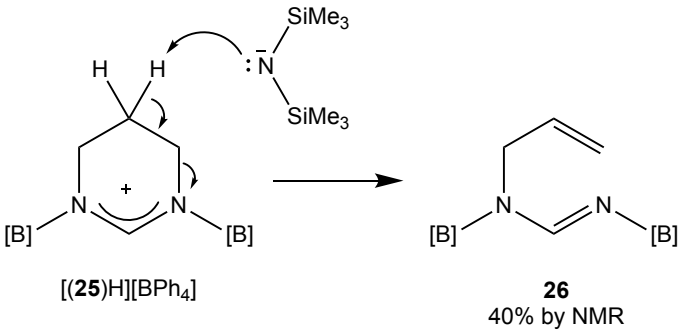

Scheme 5.7 Suggested mechanism towards 26, which is one of two main products from the reaction of pyrimidium salt [(25)H][BPh$_4$] and potassium bis(trimethylsilyl)amide.

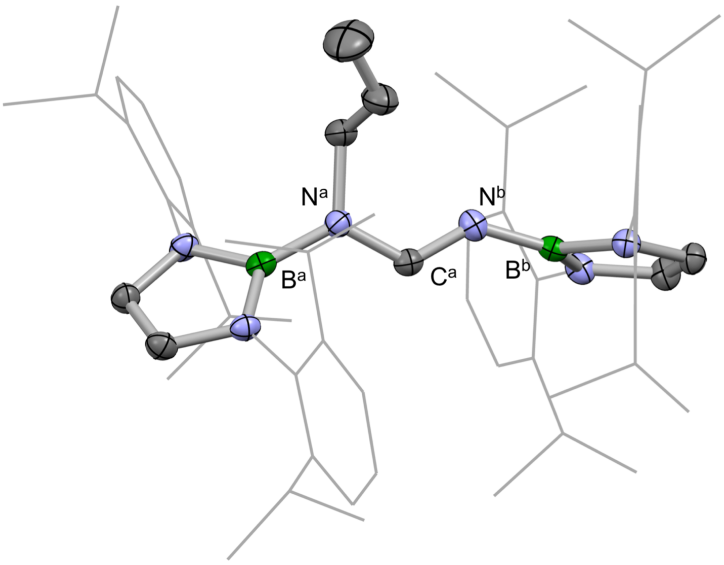

	(Å)/(°)
d(B^a–N^a)	1.465(2)
d(B^b–N^b)	1.433(2)
d(C^a–N^a)	1.367(2)
d(C^a–N^b)	1.264(2)
∠(N^a–C^a–N^b)	123.9(1)

Figure 5.3 (Left) Molecular structure of 26 in the solid state, as determined by X-ray crystallography. Most hydrogen atoms omitted, and Dipp groups shown in wireframe format for clarity. Thermal ellipsoids set at the 40% probability level. (Right) Table of key structural parameters.

Deprotonation of pyrimidium salt [(**25**)H][BPh$_4$] at C5 could potentially be attributed to the size of the base. Potassium bis(trimethylsilyl)amide is sterically bulky and the pocket around the proton at C2 is very small due to the bulky adjacent boryl groups. Therefore, [(**25**)H][BPh$_4$] was reacted with a smaller base – potassium hydride – in THF. Unfortunately, this leads to the formation of the monoborylated 3,4,5,6-tetrahydropyrimidine, suggesting nucleophilic attack of the hydride on the

boryl group.

Isolation of the major species (**27**) from the reaction mixture of pyrimidium salt [(**25**)H][BPh_4] and potassium bis(trimethylsilyl)amide was unsuccessful as samples obtained by recrystallization were invariably contaminated with **26** and clean ^{1}H and ^{13}C NMR spectra could not be obtained. Although a number of signals in the reaction mixture can be assigned to **27** (by comparison of the spectra of an authentic sample of **26**), it is apparent that several signals overlap with those of **26**. The spectra of **27** are therefore difficult to assign unambiguously and the structure of **27** cannot be definitively established. Possible candidates are, however, discussed below.

In the presence of a Lewis acid, allyl formamidines similar to **26** are known to ring-close in 5-*endo*-trig fashion (Scheme 5.8).[19] Similarly, given the electrophilicity of the boryl group, one could envision 5-*endo*-trig or even 6-*exo*-trig ring-closure of **26** taking place with accompanying (intra- or intermolecular) nucleophilic attack on the boryl group to give **27a** or **27b** (Scheme 5.9). Other potential structures for **27** can also be envisaged (Scheme 5.9) derived from: (a) deprotonation at C2 to give the target free carbene (**27c**); (b) formation of **27c** followed by 1,2-migration of one of the boryl groups to the C2 position (**27d**); or (c) formation of **27c**, followed by C–H activation of one of the isopropyl groups (**27e**).

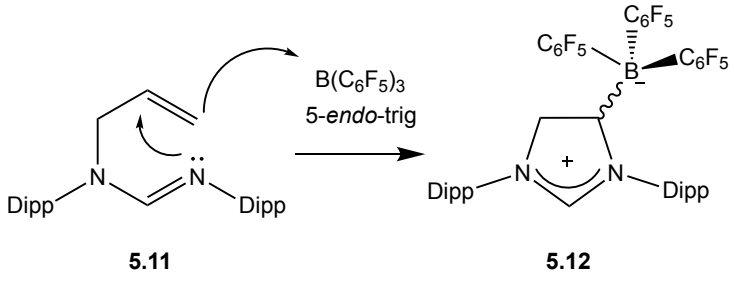

Scheme 5.8 Nucleophilic attack of allyl formamidine 5.11 on the Lewis acidic $B(C_6F_5)_3$ *via* 5-*endo*-trig ring closure to give a zwitter-ionic imidazolium.[19]

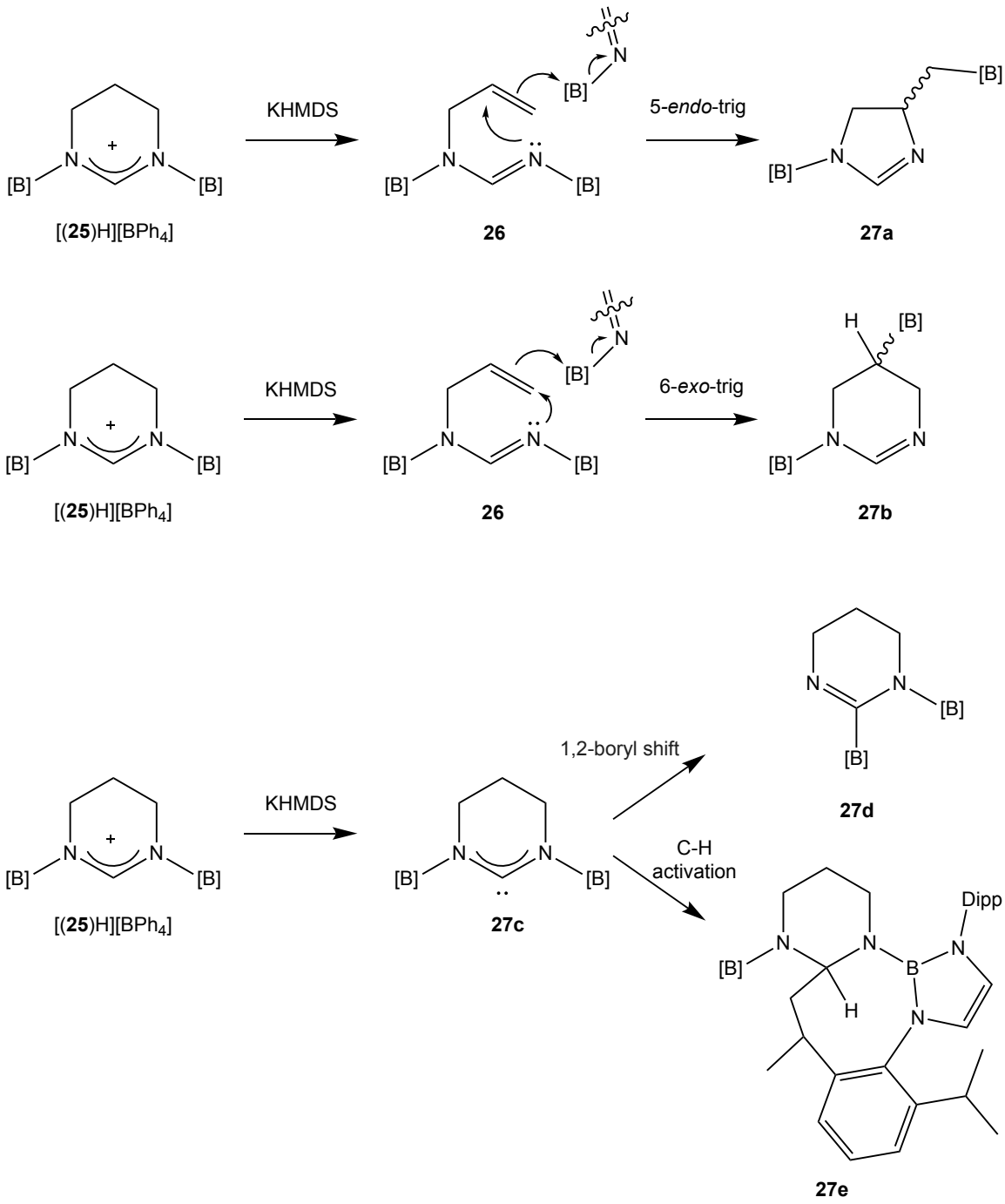

Scheme 5.9 Potential structures of the major species (27) in the reaction mixture of [(25)H][BPh$_4$] and potassium bis(trimethylsilyl)amide. For the ring-closure mechanisms, the N–[B] bond is depicted separately for illustrative purposes.

Of particular relevance is a broad signal at 6.83 ppm integrating to one proton. According to the COSY NMR spectrum, this proton couples to a proton with a chemical shift of 3.01 ppm and not to any proton in the aromatic region. This suggests that the

proton is not an aromatic proton and in addition, the chemical shift is similar to expected chemical shift of the NC*H*N proton of a formamidine. This could support either **27a** or **27b** as the second product, as this proton would not be present in **27c**, **27d** nor **27e**. The presence of this resonance, as well as lack of a signal above 150 ppm in the ^{13}C NMR spectrum and lowered symmetry in both the ^{1}H and ^{13}C NMR spectra strongly suggest that the target carbene (**27c**) has not been obtained. Unfortunately, neither kinetic experiments nor the ^{1}H and ^{13}C NMR spectra could establish the structure of **27**.

It is clear that the *N*,*N*'-bisborylated six-membered NHC cannot be accessed *via* the corresponding pyrimidine salt due to backbone deprotonation. As discussed in section 5.1, NHCs can also be accessed by reduction of cyclic thioureas, a method which does not rely on deprotonation to access the free carbene. The syntheses of bisborylated cyclic thioureas (for example by reacting boryl-functionalized diamines with CS_2 or thiophosgene) were therefore of some interest.[1,3] With this in mind, access to the requisite bisborylated diamines was sought and is the topic of the following section.

5.2.2 Syntheses of *N*,*N*'-Bisborylated Diamides

The syntheses of *N*,*N*'-bisborylated diamines are of interest as they can be used as starting materials for cyclic thioureas and are also potential starting materials in the syntheses of the targeted Group 14 tetrelenes (**5.9**; Figure 5.1). This section focuses therefore both on the syntheses of *N*,*N*'-bisborylated diamines, based on 1,2-diaminoethane and 1,3-diaminopropane backbones, and on methods of deprotonation to access the corresponding dianionic species.

N,*N*'-Bisborylated 1,2-diaminoethane and 1,3-diaminopropane, (**28**)H_2 and (**29**)H_2, were synthesized *via* the reaction of **1** with the respective diamine, using

triethylamine as a base to sequester the generated HBr, and isolated in yields of 81% and 93%, respectively (Scheme 5.10). Colourless crystals suitable for X-ray crystallography were obtained by recrystallization from pentane and hexane, respectively. The solid-state structures so obtained (Figures 5.4 and 5.5) confirm successful bisborylation of the diamines.

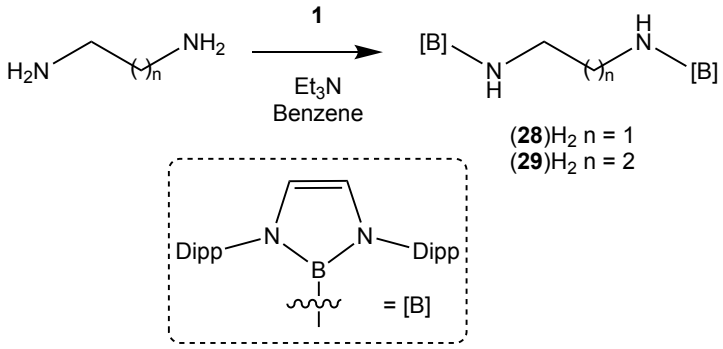

Scheme 5.10 Syntheses of bisborylated diamines (28)H_2 and (29)H_2.

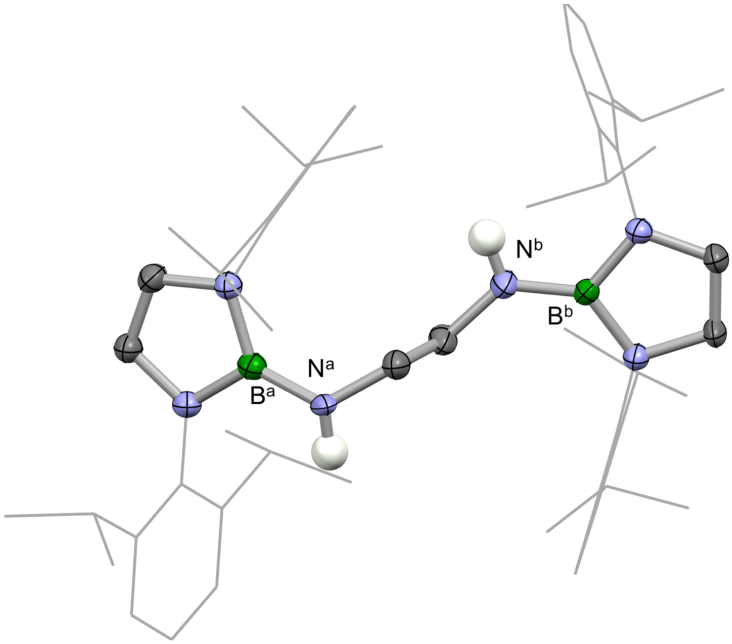

	(Å)/(°)
d(B^a–N^a)	1.454(6)
d(B^b–N^b)	1.409(6)

Figure 5.4 (Left) Molecular structure of (28)H_2 in the solid state, as determined by X-ray crystallography. Most hydrogen atoms omitted, and Dipp groups shown in wireframe format for clarity. Thermal ellipsoids set at the 40% probability level. (Right) Table of key structural parameters.

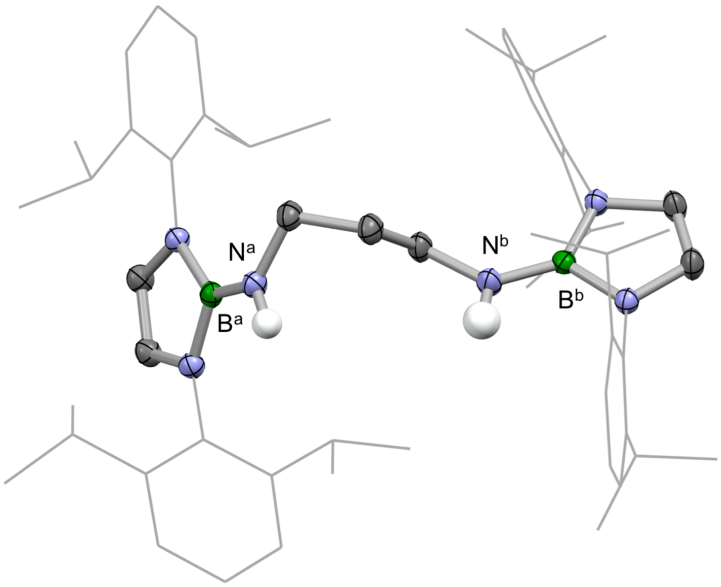

	(Å)/(°)
d(B^a–N^a)	1.411(2)
d(B^b–N^b)	1.406(2)

Figure 5.5 (Left) Molecular structure of (29)H_2 in the solid state, as determined by X-ray crystallography. Most hydrogen atoms omitted, and Dipp groups shown in wireframe format for clarity. Thermal ellipsoids set at the 40% probability level. (Right) Table of key structural parameters.

Considerable efforts were expended in the search for an appropriate base for the deprotonation of protio-ligands (**28**)H_2 and (**29**)H_2. In the case of phenyllithium for example, addition of four equivalents of phenyllithium was needed for the reaction with (**28**)H_2 to progress to a single species, which is proposed to be the dilithiated compound Li_2(**28**)·(OEt_2)$_2$ (Scheme 5.11).

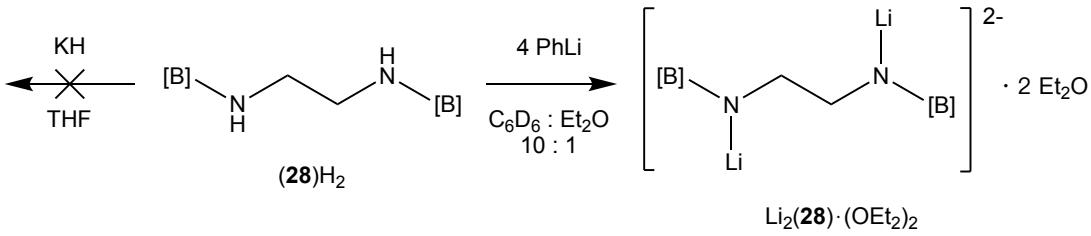

Scheme 5.11 (28)H_2 does not react with KH but can be deprotonated using excess phenyllithium, albeit with the latter reaction only proving workable on a small scale.

A key indicator that the double deprotonation has occurred is the absence of the N–H protons, both in the ^{1}H and COSY NMR spectra. A large downfield shift of the CH_2

groups of the diamine linker, from 2.27 ppm to 2.94 ppm, is also observed along with slight shifts in the resonances of the isopropyl groups and the boryl backbone. Despite prolonged exposure to vacuum, two equivalents of diethyl ether are still retained, implying that the product is the diethyl ether solvate. It is proposed that the diethyl ether is coordinated to the lithium atoms. Attempts to obtain crystals from both hexane and diethyl ether were unsuccessful

Attempts to repeat this synthesis on a larger scale were unsuccessful. Despite the addition of a large excess of phenyllithium, the reaction did not progress cleanly to the dilithiated species and the ^{1}H NMR spectrum indicates only partial consumption of the protio-ligand. Attempts were also made to deprotonate (**29**)H_2 *in situ* on a small scale in the presence of phenyllithium, but no consumption of the protio-ligand was observed by ^{1}H NMR spectroscopy. The use of phenyllithium was therefore abandoned in favour of finding a more reliable route capable of deprotonating both (**28**)H_2 and (**29**)H_2 on a larger scale.

Attempts to deprotonate (**28**)H_2 using potassium hydride in THF were unsuccessful and so the potential of using ^{n}BuLi as a base was investigated. The ^{1}H NMR spectrum of a mixture of (**28**)H_2 and ^{n}BuLi in diethyl ether at room temperature or after heating in hexane at 50 °C for three days, shows no consumption of the diamine. When the reaction was carried out in toluene, a mixture of species formed, but according to the ^{1}H NMR spectrum of the reaction mixture, heating at 80 °C for three days did not result in the clean conversion to a single species.

^{n}BuLi exists as a hexamer in solution but in the presence of TMEDA (*N*,*N*,*N*'*N*'-tetramethylethylenediamine), it is a solvated tetramer, which increases availability of the butyl group and thus the reactivity of ^{n}BuLi.[20] With this in mind, deprotonation of

the protio-ligands was attempted using ^{n}BuLi in the presence of TMEDA. The ^{1}H NMR spectrum of an aliquot taken from the reaction mixture of (**28**)H_2, ^{n}BuLi and one equivalent of TMEDA is similar to that of Li_2(**28**)·(OEt_2)$_2$ (derived from the reaction with phenyllithium). This suggests successful synthesis of the bisborylated diamide (Scheme 5.12), but excess ^{n}BuLi is needed for full deprotonation. As before, a key indicator that the targeted double deprotonation has occurred is the absence of the N–H protons, both in the ^{1}H and COSY NMR spectra. Signals at 1.56 ppm, 1.71 ppm, 1.76 ppm, 5.93 ppm, 6.25 ppm and 6.71 ppm in the ^{1}H NMR spectrum indicate that one equivalent of TMEDA and one equivalent of toluene are coordinated to the dilithiated product giving an overall formulation Li_2(**28**)·(C_6H_5Me)(TMEDA).

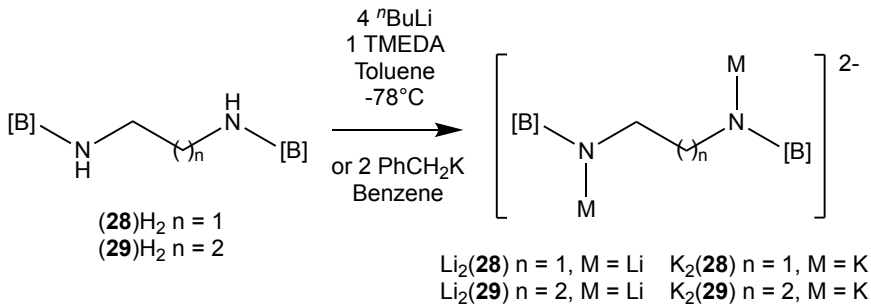

Scheme 5.12 Successful deprotonation of bisborylated diamines using either excess ^{n}BuLi in the presence of TMEDA, or benzyl potassium.

Small, colourless crystals suitable for X-ray crystallography were obtained by recrystallization from the reaction mixture in hexane. The solid-state structure so obtained reveals the structure of a monolithiated species, Li(**28**)H·(TMEDA), which has one equivalent of TMEDA coordinated at the lithium centre (Figure 5.6). This is presumably not the product observed by the ^{1}H NMR spectrum but has been isolated due to exposure to a sub-stoichiometric amount of adventitious water during manipulation of the solution. The N^{b}–Li bond length is 1.904(9) Å, which is statistically equal to the sum of the single-bond covalent radii (1.99(8) Å) for Li and

N, and therefore indicates covalent character in the bonding.[21]

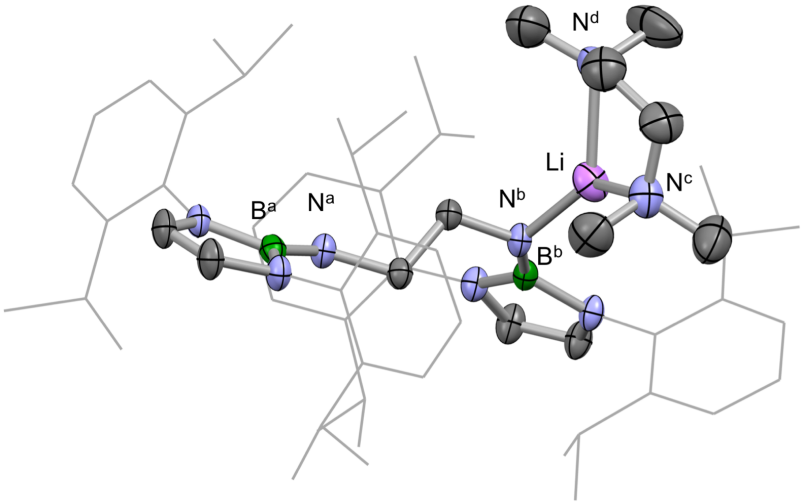

	(Å)/(°)
d(B^a–N^a)	1.409(5)
d(B^b–N^b)	1.388(5)
d(N^b–Li)	1.904(9)

Figure 5.6 (Left) Molecular structure of Li(28)HLi·(TMEDA) in the solid state, as determined by X-ray crystallography. Most hydrogen atoms omitted, and Dipp groups shown in wireframe format for clarity. Thermal ellipsoids set at the 40% probability level. (Right) Table of key structural parameters.

Li_2(**29**)·(C_6H_5Me)(TMEDA) was prepared in an analogous fashion from (**29**)H_2 and excess ^{n}BuLi in the presence of TMEDA (Scheme 5.12). In this case too, the ^{1}H NMR spectrum is consistent with coordination of one equivalent of TMEDA and one equivalent of toluene. As both Li_2(**28**)·(C_6H_5Me)(TMEDA) and Li_2(**29**)·(C_6H_5Me)(TMEDA) are highly soluble and readily decompose to form (**28**)H_2 and (**29**)H_2, respectively, attempts to isolate either product were unsuccessful. Reactions of the products with Group 14 dihalides (reported in sections 5.2.5 and 5.2.6), however, support that these reactions have indeed resulted in complete deprotonation at N.

In view of using the ligands in the syntheses of tetrelenes, the need for excess base is not ideal as excess Group 14 element precursor would likely also be needed in subsequent metathesis chemistry. A base that can successfully deprotonate the

diamines stoichiometrically would therefore be beneficial. The addition of two equivalents of benzyl potassium to (**28**)H_2 or (**29**)H_2 in C_6D_6 leads to full conversion to a single new species (in each case) as indicated by ^{1}H NMR spectroscopy. Formation of a toluene signal at 2.11 ppm indicates protonation of the benzyl potassium, which suggests successful deprotonation. The ^{1}H chemical shifts of the remaining signals in the reaction mixtures are similar to those of Li_2(**28**) and Li_2(**29**). Furthermore, successful deprotonation is also indicated by the absence of the N–H protons, both in the ^{1}H and COSY spectra. Reactions of the product with Group 14 dihalides (reported in sections 5.2.5 and 5.2.6) also support that these reactions have indeed resulted in successful deprotonation at N. It therefore seems apparent that bisborylated diamides K_2(**28**) and K_2(**29**) can be successfully synthesized without the use of excess base (Scheme 5.12).

5.2.3 Bisborylated Cyclic Thioureas

With the bisborylated diamines (**28**)H_2 and (**29**)H_2 at hand, the corresponding cyclic thioureas could be pursued as precursors to bisborylated carbenes as outlined in Scheme 5.2. The ^{1}H NMR spectrum of an aliquot of the reaction mixture of (**28**)H_2 and CS_2 in pyridine indicates no reactivity, even after refluxing the solution for multiple days. The only new species apparent in the spectrum are decomposition products derived from the boryl group. Diamides Li_2(**28**) and Li_2(**29**) could be feasible candidates to access the cyclic thioureas as they are expected to be more nucleophilic than the corresponding diamines. (**28**)H_2 was reacted with excess phenyllithium in C_6D_6:Et_2O (10:1). When full deprotonation was confirmed by ^{1}H NMR spectroscopy, 1.1 equivalents of CS_2 were added. Complete consumption of the diamide is observed by ^{1}H NMR spectroscopy, but the spectrum does not indicate clean conversion to a

single species. Colourless single crystals suitable for X-ray crystallography could be obtained from the reaction mixture C_6D_6. The solid-state structure reveals a monoborylated imidazole moiety which is coordinated to a Li–S cluster (**30**; Figure 5.7). This indicates successful installation of the C=S fragment to form the target bisborylated thiourea, but with subsequent removal of one of the boryl groups (Scheme 5.13). The excess phenyllithium present is likely acting as a nucleophile and attacking the boryl group, similar to the chemistry observed in the reaction of bisborylated imidazolium salt [(**4**)H][BPh_4] with phenyllithium (section 3.2.2). As the target bisborylated thiourea could not be accessed *via* this method, other routes were explored.

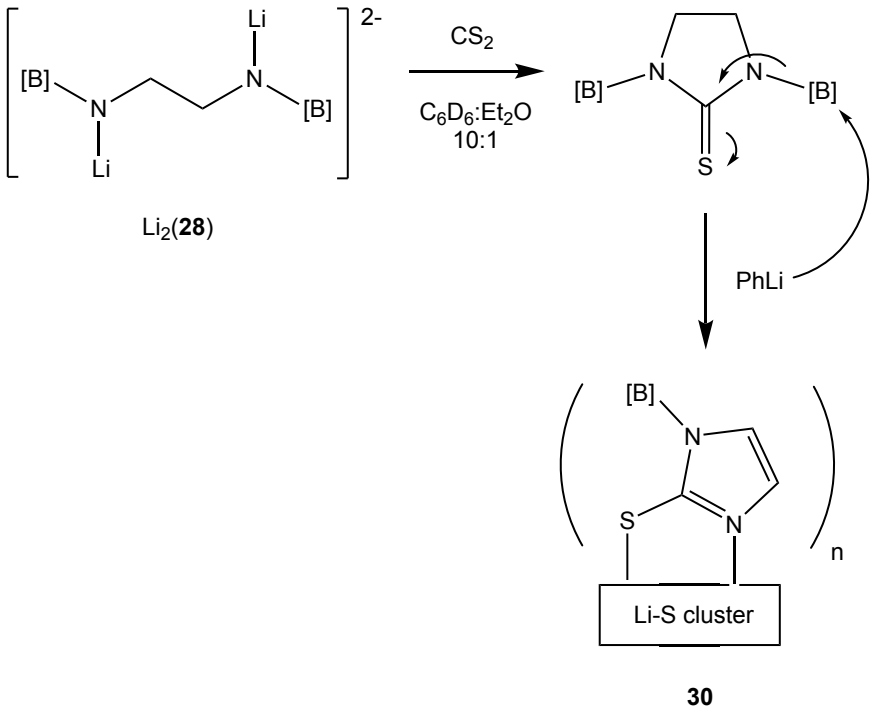

Scheme 5.13 Suggested mechanism for the formation of Li–S cluster 30 *via* nucleophilic attack of excess phenyllithium on one of the boryl groups.

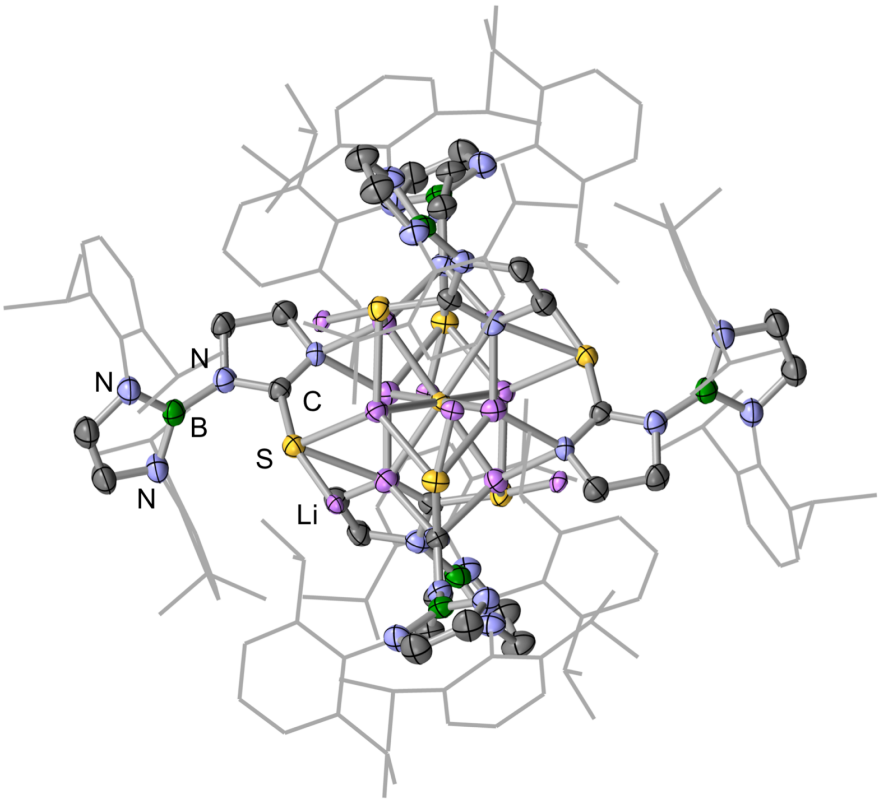

Figure 5.7 Preliminary molecular structure of Li-S cluster 30 in the solid state, as determined by X-ray crystallography. Hydrogen atoms omitted and Dipp groups shown in wireframe format for clarity. Thermal ellipsoids set at the 40% probability level.

Thionocarbonyl-1,1′-diimidazole is a well-established source of an electrophilic source of the CS fragment and was therefore thought to be a potential reagent to generate the target cyclic thiourea when reacted with diamines (**28**)H_2 or (**29**)H_2. The leaving group in this case, imidazolide, is basic and thus prior deprotonation of the diamine could potentially be circumvented. The ^{1}H NMR spectrum of the reaction mixture derived from thionocarbonyl-1,1′-diimidazole and (**29**)H_2 in toluene-d_8 shows no consumption of the staring material at room temperature but a new product appears when the reaction mixture is heated at 110 °C. Complete consumption of the starting material is observed after heating the reaction mixture for two weeks. Only one major species is observed in the spectrum but the propyl

linker between the two amino groups can, however, not be observed. Instead, the signals of the major species in the spectrum match that of monoborylated imidazole **3** (section 3.2.1). Formation of the target bisborylated thiourea is proposed to take place (albeit slowly), with subsequent (fast) nucleophilic attack of the imidazole leaving group at the boryl functionalities yielding one equivalent of 3,4,5,6-tetrahydro-2-pyrimidinethiol (which apparently has low solubility in toluene-d_8) and two equivalents of monoborylated imidazole **3** (Scheme 5.14).

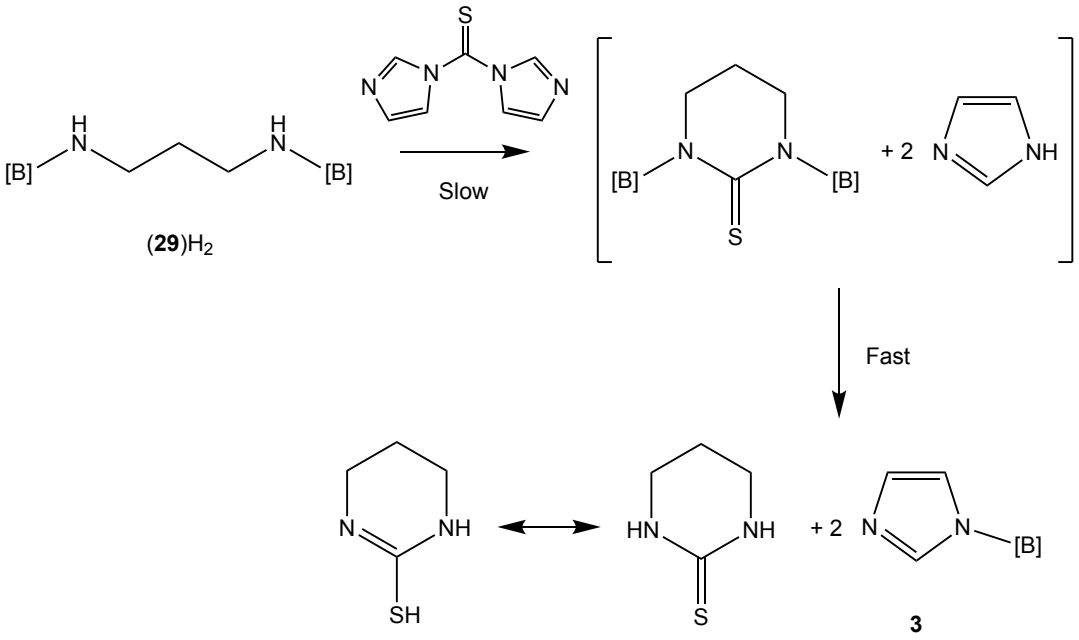

Scheme 5.14 Suggested mechanism for the reaction of thionocarbonyl-1,1′-diimidazole and (29)H_2 with subsequent removal of the boryl groups from the transient cyclic thiourea by imidazolide.

The formation of 3,4,5,6-tetrahydro-2-pyridinethiol in this reaction prompted the investigation of it as a potential starting material for the bisborylated cyclic thiourea, by borylation in a similar fashion to the imidazoles examined in Chapter 3. The *in situ* measured ^{1}H NMR spectrum of the reaction between 3,4,5,6-tetrahydro-2-pyridinethiol and one equivalent of both potassium bis(trimethylsilyl)amide and **1** shows complete consumption of **1** and conversion to a single new species (**31**) after

heating at 80 °C for 25 days. The ^{1}H NMR spectrum suggests lowering of symmetry in the six-membered heterocycle, due to the presence of three multiplets at 2.78, 2.08 and 0.85 ppm, each of which integrate to two protons. **31** could be isolated in 28% yield (Scheme 5.15). Colourless single crystals suitable for X-ray crystallography could be obtained by recrystallization from hot acetonitrile. The solid-state structure so obtained confirms successful borylation at the nitrogen of the cyclic thiourea and is depicted in Figure 5.8.

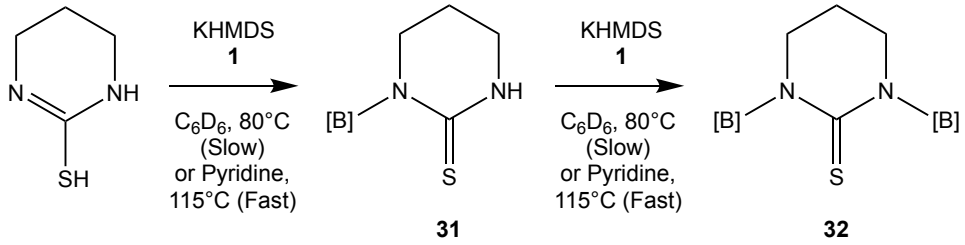

Scheme 5.15 Borylation of 3,4,5,6-tetrahydro-2-pyridinethiol to give thiones 31 and 32.

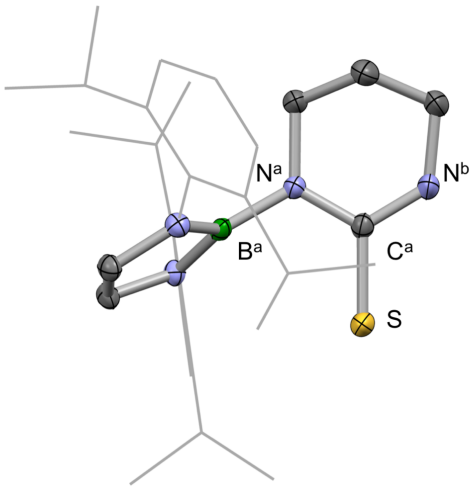

	(Å)/(°)
d(B^{a}–N^{a})	1.4814(15)
d(C^{a}–N^{a})	1.3548(15)
d(C^{a}–N^{b})	1.3289(15)
d(C^{a}–S)	1.6990(12)
∠(N^{a}–C^{a}–N^{b})	119.36(10)
Θ([B^{a}])	69.3

Figure 5.8 (Left) Molecular structure of 31 in the solid state, as determined by X-ray crystallography. Solvate molecule and most hydrogen atoms omitted, and Dipp groups shown in wireframe format for clarity. Thermal ellipsoids set at the 40% probability level. (Right) Table of key structural parameters.

Upon addition of a second equivalent of potassium bis(trimethylsilyl)amide and **1**

to the reaction mixture containing **31**, immediate consumption of **31** and conversion to a single new species is observed by ^{1}H NMR spectroscopy. However, the bromoborane (**1**) seems to be unreacted. This observation would be consistent with immediate deprotonation of thione **31**. Extensive heating is then needed to add the second boryl group and after heating the reaction mixture for three weeks at 80 °C, only 60% consumption of **1** is observed with conversion to a new product (**32**). The ^{1}H NMR spectrum of the new product suggests higher symmetry than **31**, with only two multiplets being observed for the $CH_2CH_2CH_2$ backbone (at 2.28 and -0.29 ppm), integrating to four and two protons, respectively. Furthermore, the boryl backbone protons give rise to only one singlet that integrates to four protons and only one isopropyl methine septet (8H) and two isopropyl doublets (24H each) are seen. This suggests a symmetrical product featuring two equivalent boryl groups and that both nitrogen atoms are borylated (**32**; Scheme 5.15). A signal at 182.6 ppm in the ^{13}C NMR spectrum matches the chemical shift of other cyclic thioureas.[2]

The reduced reactivity of the thiourea towards **1** can potentially be attributed to the thione-thiol tautomerism; the nitrogens are presumably less nucleophilic compared with imidazole for example. As discussed in section 3.2.4, carrying out borylation chemistry in pyridine can potentially increase the electrophilicity of the boryl group. As such, the chemistry was examined using pyridine as an alternative reaction medium. The *in situ* ^{1}H NMR spectrum of a reaction mixture comprised of 3,4,5,6-tetrahydro-2-pyridinethiol, two equivalents of both potassium bis(trimethylsilyl)amide and **1** in pyridine-d_5 indicates full conversion to **32** after heating the reaction mixture at 115 °C for only 1 h. This is much faster compared to the analogous reaction in benzene, in agreement with the hypothesis of an increase in electrophilicity of the boryl group in the presence of pyridine.

Colourless single crystals of **32** suitable for X-ray crystallography could be obtained by recrystallization from hot acetonitrile. The solid-state structure so obtained confirms the uptake of two boryl groups to give the bisborylated cyclic thiourea and is depicted in Figure 5.9.

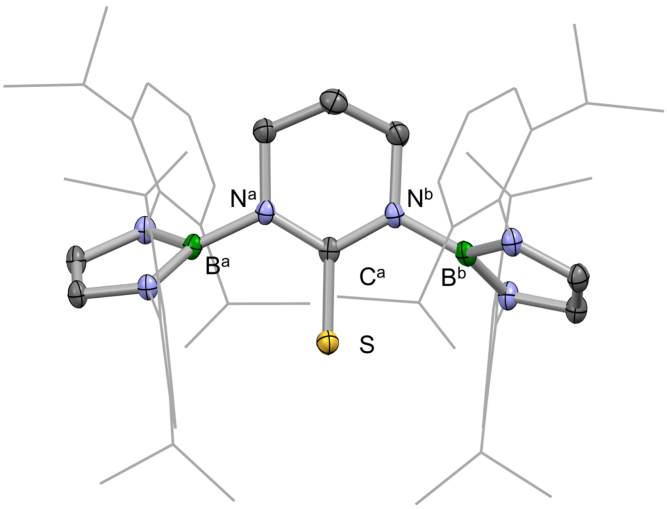

	(Å)/(°)
d(B^a–N^a)	1.484(3)
d(B^b–N^b)	1.492(3)
d(C^a–N^a)	1.363(3)
d(C^a–N^b)	1.353(3)
d(C^a–S)	1.678(3)
∠(N^a–C^a–N^b)	120.0(2)
Θ([B^a])	72.8
Θ([B^b])	58.1

Figure 5.9 (Left) Molecular structure of 32 in the solid state, as determined by X-ray crystallography. Most hydrogen atoms omitted, and Dipp groups shown in wireframe format for clarity. Thermal ellipsoids set at the 40% probability level. (Right) Table of key structural parameters.

Having accessed the precursor bisborylated thiourea, reduction of the C=S bond was attempted in the pursuit of a free carbene of type **5.1** (Figure 5.1), with both potassium and potassium graphite being examined as potential reductants. The ^{1}H NMR spectrum of a reaction mixture comprised of **32** and potassium in THF-d_8 indicates the formation of a single species after heating at 80 °C for one week. Only one singlet is observed for the backbone of the boryl group in addition to one isopropyl methine septet and two isopropyl methyl doublets. This suggests that the new species only contains one boryl environment and is thus either symmetrical or contains only one boryl group. The protons of the backbone of the six-membered ring

can, however, not be observed and no signal is observed above 150 ppm in the ^{13}C NMR spectrum. This latter observation is not consistent with the formation of a free carbene. Furthermore, addition of (THT)AuCl to the reaction mixture does not give rise to a change in the ^{1}H NMR spectrum, as would be expected if the putative free carbene were to coordinate to the gold. Repetition of the reaction in THF resulted in a mixture of unidentifiable species. This, combined with the absence of the backbone of the six-membered ring in the ^{1}H NMR suggests that **32** is over-reduced in the presence of potassium and decomposes. The search for another suitable reducing agent was therefore continued and potassium graphite was explored.

The ^{1}H NMR spectrum of a reaction mixture of **32** and potassium graphite in C_6D_6 shows no consumption at room temperature, but that **32** is slowly consumed upon heating the reaction mixture at 80 °C. After two days the reaction has gone to completion but the ^{1}H NMR spectrum indicates the formation of multiple species, the relative amounts of which do not change upon further heating. Two sets of single crystals suitable for X-ray crystallography were grown from a hexane solution of the reaction mixture. The solid-state structures so obtained reveal the formation of *N*,*N*′-bis(2,6-diisopropylphenyl)-1,4-diazabutadiene and 2-(2,6-diisopropylphenyl)-3,4,5,6-tetrahydropyrimine (**2.2** and **33**; Figure 5.10). The boryl group thus seems to be cleaved by the potassium graphite.

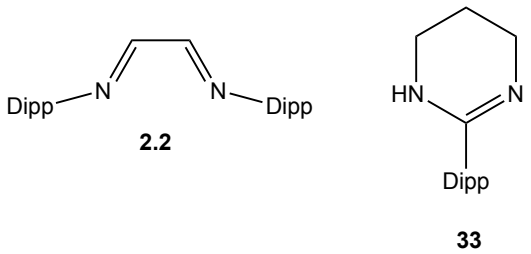

2.2 **33**

Figure 5.10 Decomposition products from the reaction of 32 and potassium graphite.

Potassium and potassium graphite do not seem to be suitable reducing agents for reducing cyclic thiourea **32** to give the target carbene and a milder reducing agent is likely needed. Recently, Tomás-Mendivil *et al*. reported the synthesis of bicyclic (alkyl)(amino)carbenes (BICAACs), which were shown to be more electrophilic and nucleophilic than monocyclic CAACs.[22] Due to the increased π-acidity, ligand exchange was observed when heating the selenium adduct of CAAC^{Et} (**5.13**) with BICAAC^{Me}, which reaches equilibrium containing 70% of the selenium adduct of BICAAC^{Me} (**5.14**) (Scheme 5.16). This chemistry reflects a stronger carbene–Se bond in BICAACs compared with CAACs, which in turn is attributed to the higher π-acidity of the former. This could potentially be a method to generate free carbenes from the corresponding selenium adducts. A C=S double bond is stronger than a C=Se double bond,[23] but it would be interesting to see if the disparity in the π-acidity of BICAAC^{Me} and poor π-acceptors (for example saturated NHCs) would be sufficient to remove sulphur from cyclic thioureas to give the corresponding free saturated NHCs (Scheme 5.17).

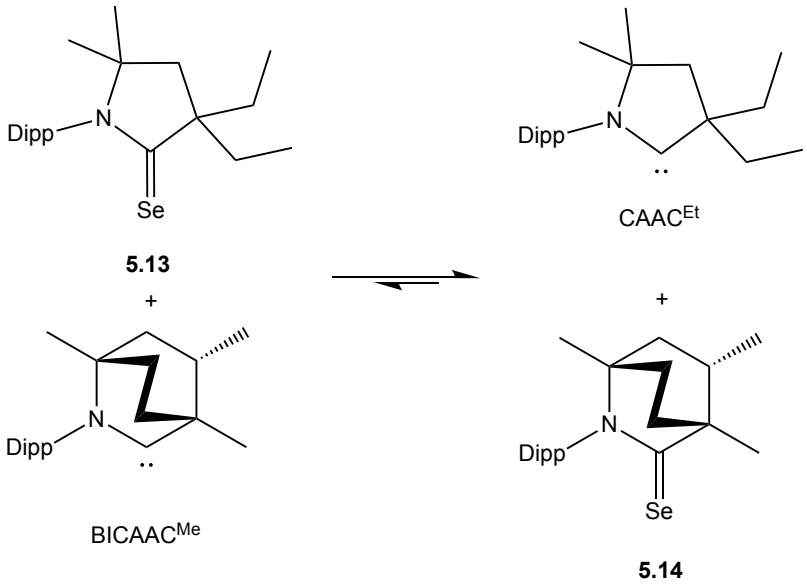

Scheme 5.16 Ligand exchange reaction on a selenium centre.[22]

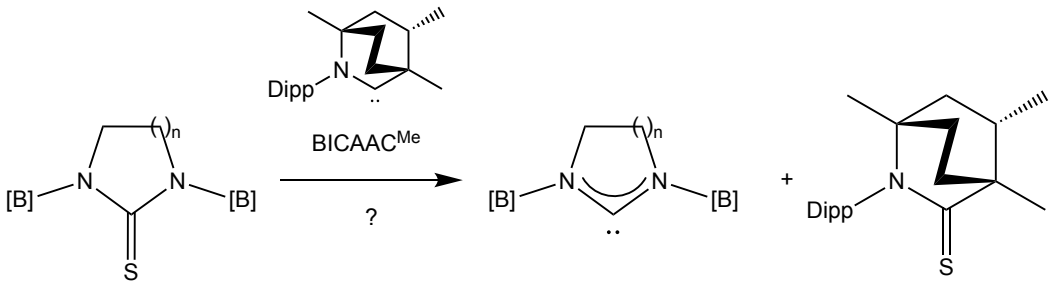

Scheme 5.17 The potential use of BICAACs to reduce cyclic thioureas.

The reaction of cyclic thiourea **32** and BICAAC^{Me} was therefore of interest. The ^{1}H NMR spectrum of the reaction mixture comprising of cyclic thiourea **32**, iminium salt [(BICAAC^{Me})H][BF_4] and potassium bis(trimethylsilyl)amide in C_6D_6 indicates immediate formation of free carbene BICAAC^{Me} at room temperature but no indication of the consumption of **32**. The reaction mixture was heated to 60 °C but this resulted in slow decomposition of BICAAC^{Me} to an unknown species. It seems that the C=S bond in **32** is too strong to be cleaved, even by the very π-acidic BICAAC^{Me} under such conditions. The selenium analogue of **32** was therefore of interest, as substituent exchange involving selenium is likely to be more facile.

Woollins' reagent (see Scheme 5.18) is used in selenocarbonyl syntheses from carbonyl starting materials (*e.g.* Scheme 5.18)[24] and it was therefore of interest to see if it could be used to convert thiourea **32** to selenourea. Accordingly, **32** and Woollins' reagent were refluxed in several different solvents; C_6D_6 (three days), $CDCl_3$ (overnight), CD_2Cl_2 (overnight), THF-d_8 (overnight) and mesitylene (one week) but no change was observed in either the ^{1}H or ^{31}P NMR spectra in any case. Unfortunately, the synthesis of the selenourea was unsuccessful and thus the use of BICAAC^{Me} to access a free carbene of type **5.1** in Figure 5.1 was not possible.

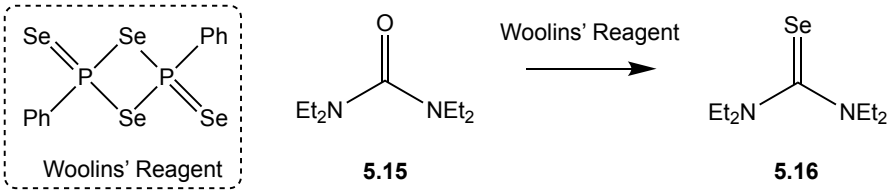

Scheme 5.18 Selenourea 5.16 synthesized from urea 5.15 using Woollins' reagent.[24]

All attempts to access *N*,*N*'-bisborylated carbenes and/or their metal complexes reported in this thesis have been unsuccessful. The remainder of this chapter will focus on attempts to access heavier analogues of such carbenes, namely *N*,*N*'-bisborylated *N*-heterocyclic Group 14 tetrelenes. Tetrelenes can be accessed *via* metathesis reactions involving metallated diamides and readily available Group 14 dihalides and thus do not rely on deprotonation or reduction, which have proven to be very problematic in the case of the carbenes.

5.2.4 Attempted Syntheses of *N*-*N*'-Bisborylated *N*-Heterocyclic Silylenes

Silylenes can be accessed by salt metathesis involving anionic substituents and (for example) IPr·$SiCl_2$ (Scheme 5.3; section 5.1). Bisborylated amides (**28**) and (**29**) are therefore potential precursors for accessing *N*,*N*'-bisborylated *N*-heterocyclic silylenes of type **5.9** (Figure 5.1). Section 5.2.2 described the syntheses of bisborylated amides (**28**) and (**29**), which can be accessed by deprotonation of protio-ligands (**28**)H_2 and (**29**)H_2.

Given the more efficient deprotonation, benzyl potassium was chosen as a base to deprotonate (**28**)H_2 and (**29**)H_2 prior to salt metathesis. Upon successful deprotonation of (**28**)H_2 or (**29**)H_2, one equivalent of IPr·$SiCl_2$ was added. The ^{1}H NMR spectra of the reaction mixtures indicate complete consumption of the diamides within 30 min and conversion to a single new species (in each case), in addition to the liberated free carbene, IPr, and *ca.* 20-25% of the protio-ligand, (**28**)H_2 or (**29**)H_2

(Scheme 5.19). The new species are both symmetrical with one singlet for the boryl backbone protons and one isopropyl environment. The protons of the respective saturated backbones are also consistent with a symmetrical environment: in the case of (**28**)H_2 only one multiplet integrating to four protons is observed, and in the case of (**29**)H_2 two multiplets integrating to four and two protons are assigned to the backbone. In addition, singlets at 137 and 122 ppm, respectively, are present in the ^{29}Si NMR spectra, which fall within the range of chemical shifts reported for other silylenes and suggests successful generation of (**28**)Si and (**29**)Si (Figure 5.11).

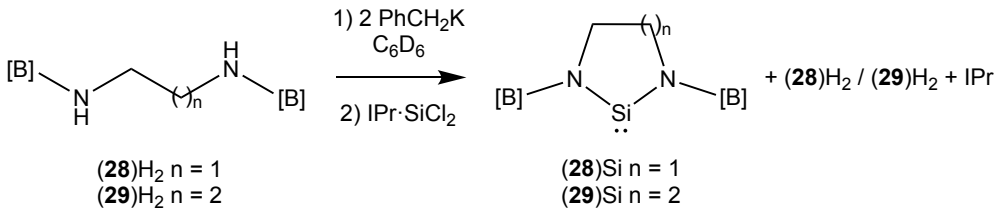

Scheme 5.19 ***In situ*** **syntheses of (28)Si and (29)Si.**

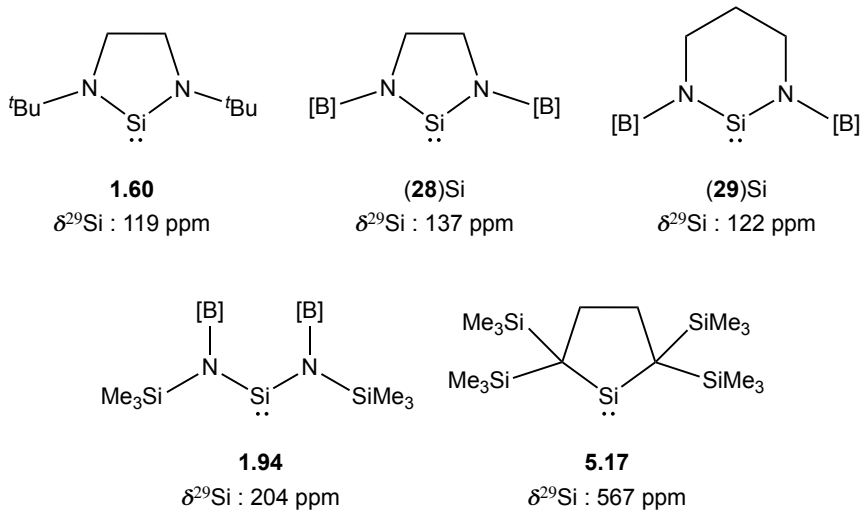

Figure 5.11 ^{29}**Si NMR chemical shifts of various silylenes.**[6,10,25]

There is a large range reported for ^{29}Si NMR chemical shifts of silylenes due to the variety of different substituents used to stabilize them.[10,25] Figure 5.11 lists a number of silylenes of interest along with their ^{29}Si NMR chemical shifts. As with comparison of ^{13}C chemical shifts for carbenes, one needs to be careful in interpreting ^{29}Si chemical

shifts as they are influenced by many factors. The shifts are thus not definitive but can give implication of the electronic properties of the silylene to some degree. The acyclic silylene **1.94** features similar boryl-amido ligands to (**28**)Si and (**29**)Si. Its ^{29}Si chemical shift (204 ppm) is downfield compared with (**28**)Si and (**29**)Si. This is attributed to the chelating backbones of (**28**) and (**29**) that are likely to cause the N–Si–N angle to narrow compared with **1.94**, thereby increasing the s-character of the lone pair on the tetrelene centre. Increased s-character leads to more electron density closer to the Si centre and hence greater shielding and an upfield shift. Consistent with this idea, a comparison of (**28**)Si with (the non-borylated) five-membered *N*-heterocyclic silylene **1.60** shows that the two compounds have much more similar shifts.

The formation of significant amounts of protio-ligand in the attempted syntheses of silylenes, has previously been observed by the Bertrand group[26] and was reported by Hadlington *et al.* in the synthesis of silylene **1.94** (Scheme 5.3; section 5.1) when reacting two equivalents of the extremely bulky [{SiMe$_3$}{B(NDippCH)$_2$}N]$^-$ ligand and one equivalent of IPr·SiCl$_2$.[6] Interestingly, the problem was solved by reacting two equivalents of IPr·SiCl$_2$ with the ligand, whereupon clean conversion to the silylene was observed. With this in mind, K$_2$(**29**) was reacted with two equivalents of IPr·SiCl$_2$. This did, however, not lead to improvement in the amount of protio-ligand contamination.

It was speculated whether a change in counterion (Li *vs* K) might affect the amount of protio-ligand formed, and so attempts were made to synthesize the silylenes *via* the lithiated ligand backbones. Unfortunately, all attempts resulted in a mixture of unidentified species in the ^{1}H NMR spectrum, even when the reactions were carried out at low temperatures. It is likely that careful control of stoichiometry is of importance, which is not possible in this case (due to the need of excess ^{n}BuLi).

Due to similar solubilities, putative silylenes (**28**)Si and (**29**)Si, and the IPr co-product are difficult to separate. Hadlington *et al.* did, however, manage to separate **1.94** from IPr by the addition of CO_2 to form an insoluble zwitterionic IPr·CO_2 adduct, since the silylene in their case was unreactive to CO_2.[6] Upon addition of CO_2 to the *in situ* reaction mixture containing (**29**)Si in a J. Young's NMR tube, a precipitate forms and no (**29**)Si is observed in the ^{1}H NMR spectrum after 10 min, while both the protio-ligand and IPr remain untouched. After one hour, however, the resonances assigned to IPr have disappeared as well. This indicates that the silylene reacts with CO_2 faster than IPr does, and that this is therefore not a viable method for separating the free carbene from the silylenes and the respective protio-ligands.

$B(C_6F_5)_3$ is also known to form an adduct with IPr[27] and could be used as an alternative Lewis acid to sequester the carbene as the steric bulk of (**28**)Si and (**29**)Si might hinder the formation of their corresponding adducts with $B(C_6F_5)_3$. ^{1}H and ^{19}F NMR spectra measured after the addition of $B(C_6F_5)_3$ to the reaction mixture of (**29**)Si show the formation of IPr·$B(C_6F_5)_3$,[27] while the resonances assigned to the silylene remain unchanged. IPr·$B(C_6F_5)_3$ was crystallized from pentane but some IPr·$B(C_6F_5)_3$ was still present in the supernatant and a second recrystallization was needed to remove the remaining adduct. Unfortunately, due to similar solubility of the silylene and the protio-ligand and the high moisture sensitivity of the silylene, multiple attempts to isolate the silylene from the remaining supernatant were unsuccessful and single crystals suitable for X-ray crystallography could not be obtained.

The formation of IPr and protio-ligands in the salt metatheses to access (**28**)Si and (**29**)Si is problematic. The route relies on extensive manipulation of the reaction mixture to remove IPr, which results in increased decomposition of the putative

silylenes. To circumvent this problem and in an attempt to find another method that does not lead to such a high contamination with the protio-ligands, syntheses of the silylenes from Si(IV) species were pursued. Addition of $HSiCl_3$ or $SiBr_4$ to K_2(**29**) (generated *in situ*) unfortunately, however, led to decomposition and full conversion to the protio-ligand, (**29**)H_2 (Scheme 5.20).

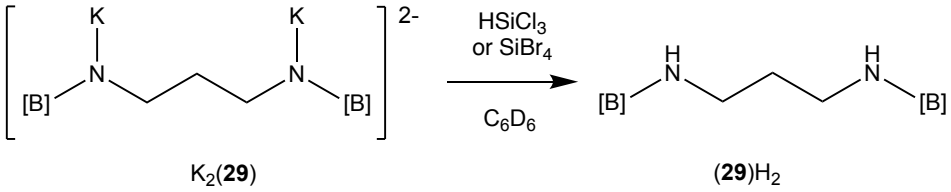

Scheme 5.20 Attempted syntheses of (29)SiHCl or (29)$SiBr_2$ resulted in decomposition of the diamide.

5.2.5 Syntheses of *N*-*N*'-Bisborylated *N*-Heterocyclic Germylenes

In a similar manner to silylenes, germylenes can be synthesized by salt metathesis of the respective ligand(s) and $GeCl_2$·dioxane. This adduct represents a convenient precursor as it is commercially available and the free dioxane donor is easier to remove than IPr.

In a J. Young's NMR tube, (**28**)H_2 or (**29**)H_2 were deprotonated using two equivalents of benzyl potassium in C_6D_6. The ^{1}H NMR spectra after the addition of 1.1 equivalents of $GeCl_2$·dioxane to the reaction mixtures indicate complete consumption of the diamides and conversion to a single new species (in each case), in addition to 30% and 25% of the respective protio-ligand. The new species are both symmetrical with one singlet for the protons on the backbone of the boryl groups and one isopropyl environment. The signals if the protons of the saturated backbones ar also consistent with the formation of a symmetrical species: in the case of **28**, one multiplet integrating to four protons is observed, while in the case of **29**, only two

multiplets integrating to four and two protons are seen. Attempts were made to ascertain if the addition of THF would reduce the amount of protio-ligand but no significant differences were noticed for either ligand. (**28**)Ge and (**29**)Ge could not be crystallized for isolation on a bulk scale from pentane or hot acetonitrile due to high contamination with the protio-ligand, although a few yellow single crystals of (**29**)Ge suitable for X-ray crystallography were obtained from pentane. The solid-state structure so obtained is depicted in Figure 5.12 and confirms successful coordination of the bisborylated diamide to the germanium centre to give the target germylene.

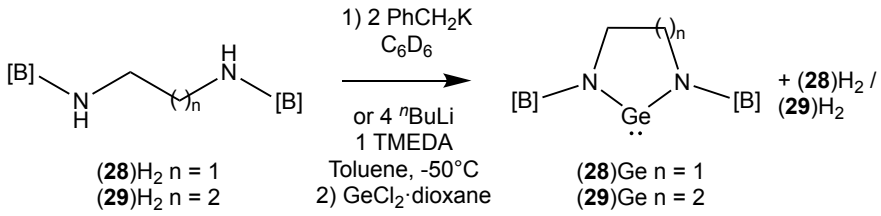

Scheme 5.21 Syntheses of (28)Ge and (29)Ge.

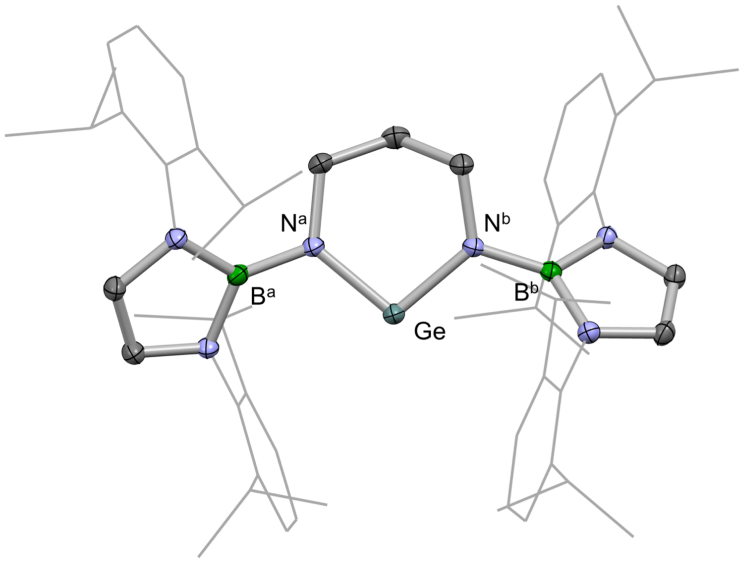

	(Å)/(°)
d(B^a–N^a)	1.443(3)
d(B^b–N^b)	1.443(2)
d(Ge–N^a)	1.866(1)
d(Ge–N^b)	1.846(1)
∠(N^a–Ge–N^b)	99.85(6)
Θ ([B^a])	37.8
Θ ([B^b])	37.2

Figure 5.12 (Left) Molecular structure of (29)Ge in the solid state, as determined by X-ray crystallography. Solvate molecule and most hydrogen atoms omitted, and Dipp groups shown in wireframe format for clarity. Thermal ellipsoids set at the 40% probability level. (Right) Table of key structural parameters.

An attempt to reduce the amount of protio-ligand was made by using Li_2(**28**) and Li_2(**29**) (obtained by deprotonation with excess ^{n}BuLi) for the salt metathesis steps. (**28**)H_2 or (**29**)H_2 were deprotonated using four equivalents of ^{n}BuLi in the presence of TMEDA and 3.5 equivalents of $GeCl_2$·dioxane added. This resulted in full conversion to the germylenes, (**28**)Ge and (**29**)Ge, with lower contamination by the respective protio-ligands. This allowed for isolation of germylenes (**28**)Ge and (**29**)Ge, in 51% and 40% yields, respectively. Yellow single crystals of (**28**)Ge suitable for X-ray crystallography were obtained by recrystallization from pentane. The solid-state structure so obtained is depicted in Figure 5.13 and confirms to formation of the target germylene.

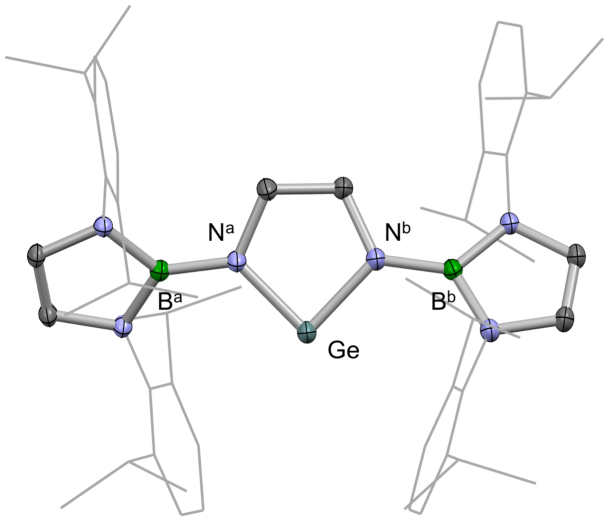

	(Å)/(°)
d(B^a–N^a)	1.4341(15)
d(B^b–N^b)	1.4362(15)
d(Ge–N^a)	1.8541(9)
d(Ge–N^b)	1.8650(9)
∠(N^a–Ge–N^b)	88.03(4)
Θ ([B^a])	35.0
Θ ([B^b])	28.6

Figure 5.13 (Left) Molecular structure of (28)Ge in the solid state, as determined by X-ray crystallography. Solvate molecule and most hydrogen atoms omitted, and Dipp groups shown in wireframe format for clarity. Thermal ellipsoids set at the 40% probability level. (Right) Table of key structural parameters.

The N–Ge bond lengths measure for (**28**)Ge and (**29**)Ge (1.4341(15) and 1.4362(15) Å for (**28**)Ge and 1.443(3) and 1.443(2) Å for (**29**)Ge) are slightly shorter than the sum of the respective covalent radii (1.91(5) Å),[21] consistent with a

description as essentially single covalent N–Ge bonds. As expected, the N–Ge–N angle increases significantly upon lengthening of the backbone (99.85(6)° for (**28**)Ge, 88.03(4)° for (**29**)Ge). The boryl groups in both (**28**)Ge and (**29**)Ge are significantly twisted compared with the germylene heterocycle and thus not likely to affect the energy of the germanium-centred LUMOs to any degree.

5.2.6 Syntheses of *N,N'*-Bisborylated *N*-Heterocyclic Stannylenes

As with germylenes, stannylenes can be synthesized by salt metathesis from commercially available precursors ($SnCl_2$ or $SnBr_2$, in this case) without IPr being formed as a side product. Stannylenes are also generally more stable than germylenes and thus stannylenes (**28**)Sn and (**29**)Sn were seen as viable synthetic targets.

The ^{1}H NMR spectrum of the reaction of K_2(**29**) (formed *in situ*) and $SnCl_2$ in C_6D_6 indicates no consumption of the diamide, but after heating at 80 °C for five days, full conversion to the protio-ligand is observed with no sign of a new product being formed. The procedure was modified *via* the addition of several drops of THF to the reaction mixture. After heating the reaction mixture at 80°C for six hours, a noticeable colour change from yellow to dark brown was observed and the ^{1}H NMR spectrum indicates complete consumption of the amide and conversion to a new species, in addition to 40% of the protio-ligand, (**29**)H_2. The new species has similar ^{1}H NMR chemical shifts to (**29**)Ge and a broad singlet at 457-459 ppm is present in the ^{119}Sn NMR spectrum, which suggests successful generation of (**29**)Sn (Scheme 5.22).

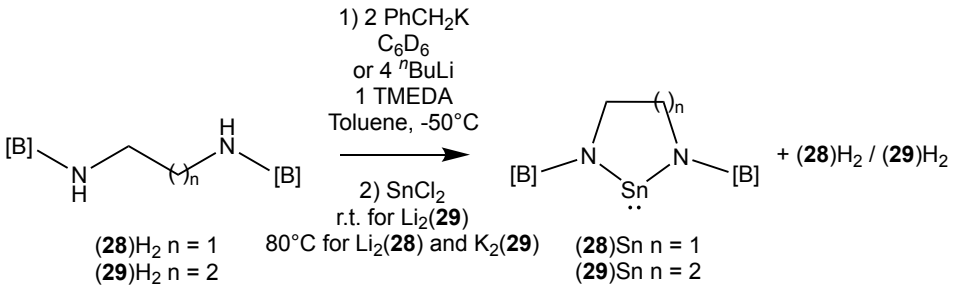

Scheme 5.22 Syntheses of (28)Sn and (29)Sn.

The use of dilithiated precursors Li_2(**28**) and Li_2(**29**) improved the yields of both (**28**)Ge and (**29**)Ge, and so the syntheses of (**28**)Sn and (**29**)Sn from the same dilithio precursors were studied. The ^{1}H NMR spectrum of the reaction mixture comprised of excess $SnCl_2$ and Li_2(**28**) (prepared *in situ* from excess ^{n}BuLi) in toluene-d_8 shows no consumption of the amide at room temperature. On heating the reaction mixture to 80 °C for 24 h, however, complete consumption of Li_2(**28**) was observed with approximately 90% conversion to a new species and only 10% contamination by the protio-ligand. The new species has similar ^{1}H chemical shifts to (**28**)Ge and a broad singlet at 527-529 ppm is present in the ^{119}Sn NMR spectrum, which suggests successful generation of (**28**)Sn (Scheme 5.22).

When the reaction was scaled up and carried out in a Schlenk tube, the ^{1}H NMR spectrum of an aliquot taken from the reaction mixture shows 25% contamination of the protio-ligand. The increased contamination compared with the *in situ* reaction indicates that (**28**)Sn is likely to partially decompose to (**28**)H_2 during the process of taking an aliquot from the reaction mixture and is thus probably very moisture sensitive. The product could not be crystallized for isolation on a bulk scale due to high solubility, moisture sensitivity and contamination by (**28**)H_2. A few orange crystals suitable for X-ray crystallography could, however, be obtained by slow evaporation of a hexane solution. The solid-state structure so obtained is depicted in

Figure 5.14 and confirms successful coordination of the bisborylated diamide to the tin centre to give the target stannylene. Unfortunately, the data is not of adequate quality to allow for the discussion of structural parameters.

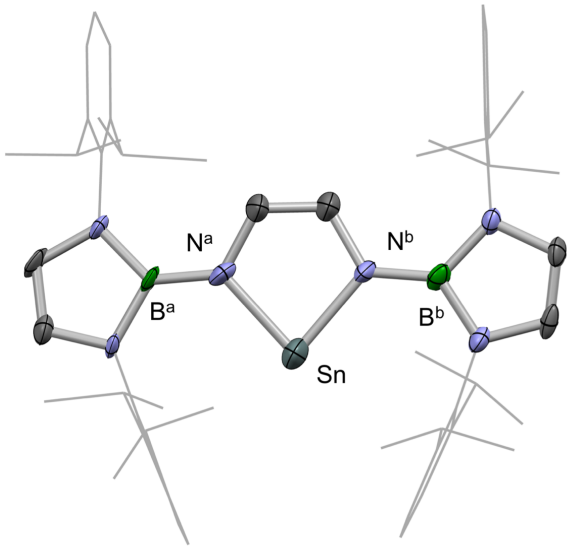

Figure 5.14 (Left) Molecular structure of (28)Sn in the solid state, as determined by X-ray crystallography. Most hydrogen atoms omitted, and Dipp groups shown in wireframe format for clarity. Thermal ellipsoids set at the 40% probability level.

The synthesis of (**29**)Sn from the lithiated amide follows a very similar protocol to that of (**28**)Sn, using *in situ* prepared Li_2(**29**) and excess $SnCl_2$ (Scheme 5.24). In contrast to (**28**)Sn, the synthesis did not require heating and complete conversion was observed by ^{1}H NMR spectroscopy after 24 h at room temperature. The reactivity of Li_2(**29**) is also quite different compared with K_2(**29**), which needed heating at 80 °C with $SnCl_2$ for 6 h for the reaction to go to completion. The ^{1}H and ^{119}Sn NMR chemical shifts match the product that was formed in the reaction of K_2(**29**) and $SnCl_2$. (**29**)Sn was isolated in 35% yield but contaminated by 15 % of protio-ligand (**29**)H_2, as observed by ^{1}H NMR spectroscopy. Orange single crystals suitable for X-ray crystallography were obtained from pentane. The solid-state structure so obtained is depicted in Figure 5.15 and confirms successful coordination of the bisborylated

diamide to the tin centre to give the target stannylene.

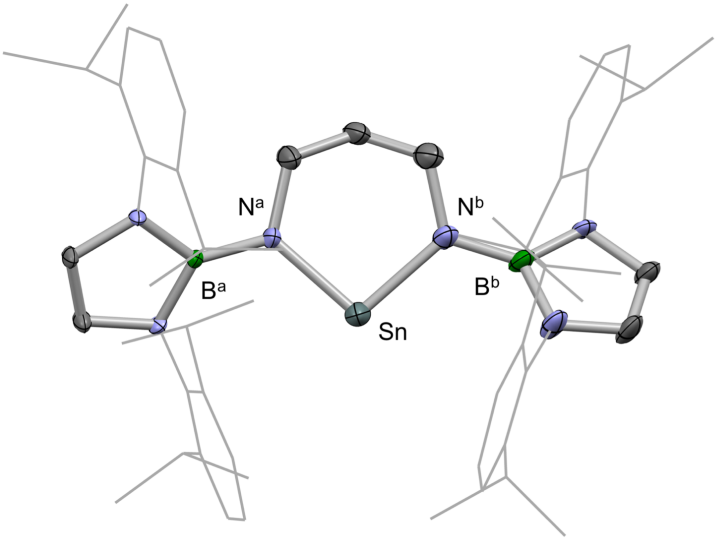

	(Å)/(°)
d(Bᵃ–Nᵃ)	1.428(5)
d(Bᵇ–Nᵇ)	1.435(6)
d(Sn–Nᵃ)	2.063(4)
d(Sn–Nᵇ)	2.087(4)
∠(Nᵃ–Sn–Nᵇ)	93.3(2)
Θ([Bᵃ])	34.3
Θ([Bᵇ])	33.7

Figure 5.15 (Left) Molecular structure of (29)Sn in the solid state, as determined by X-ray crystallography. Most hydrogen atoms omitted, and Dipp groups shown in wireframe format for clarity. Thermal ellipsoids set at the 40% probability level. (Right) Table of key structural parameters.

The N–Sn bond lengths are statistically equivalent to the respective covalent radii (2.10(5) Å),[21] consistent with a description as essentially single covalent N–Sn bonds. The N–Sn–N angle (93.3(2)°) is more acute compared with the corresponding germylene ((**29**)Ge: 99.85(6)°), as expected upon descending group 14. The boryl groups are significantly twisted with respect to the stannylene heterocycle and thus not likely to affect the energy of the LUMOs of the stannylene centre.

A different approach to access the target stannylenes might involve reacting the protio-ligands (**28**)H_2 or (**29**)H_2 with $Sn\{N(SiMe_3)_2\}_2$. $[N(SiMe_3)_2]^-$ can act as a base and therefore deprotonation of the protio-ligands prior to the reactions not needed. The ^1H NMR spectrum of the reaction mixture comprised of (**28**)H_2 and $Sn\{N(SiMe_3)_2\}_2$ in toluene-d_8 shows no consumption of the protio-ligand and no new product can be observed even after heating at 110 °C for three days.

5.2.7 Reactivity of Bisborylated *N*-Heterocyclic Germylenes and Stannylenes

Haoyu Niu, of the Aldridge group, carried out DFT calculations of the frontier orbitals of (**28**)E and (**29**)E as well as the related bis(monodentate) systems, {^{t}Bu[B(NDippCH)$_2$]N}$_2$E ((**5.18**)$_2$E; Figure 5.16), (E = Si, Ge, Sn). The results are shown in Table 5.1. In each case, the lone pair on the tetrelene centre is the HOMO-2 and the empty p-orbital at E is the LUMO. The HOMO and HOMO-1 are associated with the π-systems of the boryl groups and the amido nitrogens.

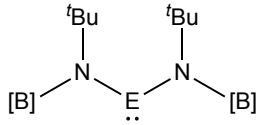

(**5.18**)$_2$E E = Si, Ge, Sn

Figure 5.16 Tetrelenes (5.18)$_2$E.

L	M	N–E–N Angle	HOMO-2	LUMO	ΔE
(**28**)E	Si	91	-502	-171	331
	Ge	87	-533	-204	329
	Sn	81	-535	-231	304
(**29**)E	Si	102	-497	-139	358
	Ge	100	-527	-185	342
	Sn	95	-530	-218	312
(**5.18**)$_2$E	Si	121	-436	-107	329
	Ge	113	-441	-200	241
	Sn	112	-473	-266	207

Table 5.1 The N–E–N angles (°) of various tetrelenes (E = Si, Ge, Sn) obtained from their calculated structures, along with the energy of the frontier orbitals, HOMO-2 and LUMO (kJ mol^{-1}) and their energy difference ΔE.

Upon descending Group 14, the angle at the tetrelene centre decreases, in accordance with expected trends upon descending the Main Group. For all three ligand systems, the largest change between tetrelene centres can be seen in the energy of LUMO, which decreases for the heavier tetrelenes. This is the opposite trend to that expected based on the heavier tetrelenes having higher energy valence p-

orbitals. These observations can be explained by considering the degree of N-to-E π-donation, which serves to raise the LUMO. The p-orbital overlap of the nitrogen and the tetrelene centre and E is greatest in the silylene complexes as the nitrogen and silicon orbitals are more similar in size (relative to nitrogen and the heavier analogues) resulting in improved N-to-E π-donation. For the heavier elements, germanium, and particularly tin, the N–E π-overlap is much poorer and π-donation from the adjacent nitrogen atoms thus less prominent – which results in the LUMO not being destabilized to the same degree. As there is not as pronounced change in the energy of the HOMO-2, the decreasing LUMO energy explains why the (HOMO-2)-LUMO gap (ΔE) actually decreases down the group despite the HOMO-2 lowering in energy.

The energy gaps (ΔE) for the cyclic tetrelenes are generally bigger than for the acyclic systems. This implies that the cyclic systems are more stable, but as a consequence less reactive. Trends in both the HOMO-2 and LUMO account for this. (**28**)E and (**29**)E have narrower N–E–N bond angles than (**5.18**)$_2$E due to their cyclic nature, and this is reflected in the energy of the HOMO-2 which is lower in the cyclic systems as there is greater s-character. In accordance with the discussion of acyclic carbenes in section 1.2.5, the adjacent nitrogen atoms in acyclic tetrelenes are not constrained in a plane with the tetrelene centre and can thus pyramidalize, which results in poorer overlap of the π-orbitals of the nitrogen and the tetrelene centre, thereby lowering the energy of the p_π-orbital. For the cyclic systems, the nitrogens are more likely to be constrained in plane with the tetrelene centre and thus less pyramidalized.

Following theoretical studies, the reactivity of the novel germylenes and the

stannylenes was explored experimentally. The ^{1}H NMR spectra of the reaction mixtures comprising of (**28**)Ge, (**28**)Sn or (**29**)Sn and H_2 (in C_6D_6 or toluene-d_8 in J. Young's NMR tubes) indicate no reactivity even after heating at temperatures up to 110 °C over several days. The same is true when the reaction of (**29**)Sn and (**29**)Ge with trimethylsilyl azide were explored.

Of fundamental interest is the reactivity of the germylenes with oxygen transfer agents with the potential aim of accessing a germanone (**5.10**; Figure 5.1). As such, the reactions of (**28**)Ge and (**29**)Ge with a range of *N*-oxides were explored. The ^{1}H NMR spectrum of the reaction mixture comprised of (**29**)Ge and Me_3NO shows complete consumption of the germylene at room temperature and conversion to a new product. The isopropyl methine groups give rise to two overlapping septets and the isopropyl methyl groups appear as four doublets, but the boryl backbone protons give rise to only one singlet. This suggests that the two boryl groups are equivalent but restriction in rotation might give rise to the different environments observed by the isopropyl groups. The ^{13}C NMR spectrum supports this, as two sets of signals for the *ortho*- and *meta*-carbons can be observed but only one for the *ipso*- and *para*-carbons. These features indicate a product with restricted rotation of the Dipp groups. This product then slowly converts to another species featuring higher symmetry. It was hypothesized that the slow formation of the second species might be due to the build-up of NMe_3 in the sealed system. Therefore, several freeze-pump-thaw cycles were carried out to drive the reaction to completion. Single crystals suitable for X-ray crystallography of the second species were obtained by slow evaporation of a benzene solution. The solid-state structure so obtained (Figure 5.17) establishes that the second product is the germanediol, (**29**)$Ge(OH)_2$ (Scheme 5.23) consistent with the formal

uptake of two hydroxide groups at the germanium centre. It seems likely that moisture was introduced into the reaction during the degassing steps and that the lack of moisture was the limiting factor in the (initially slow) formation of the second product.

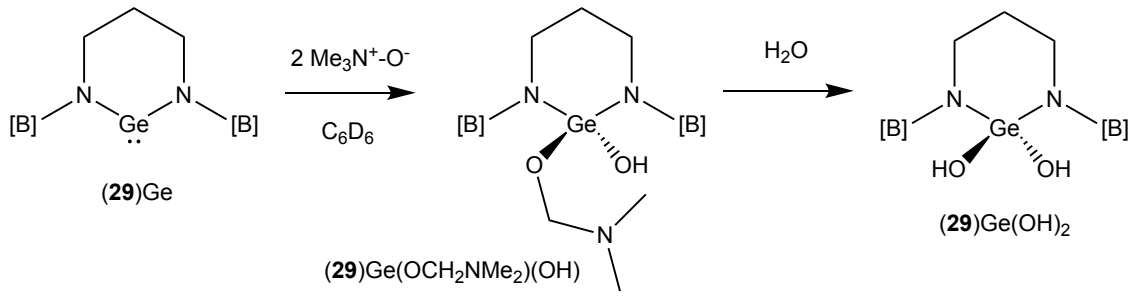

Scheme 5.23 Reaction of (29)Ge with Me_3NO to give (29)Ge(OCH_2NMe_2)(OH) and subsequent hydrolysis to form germanediol in the presence of adventitious water.

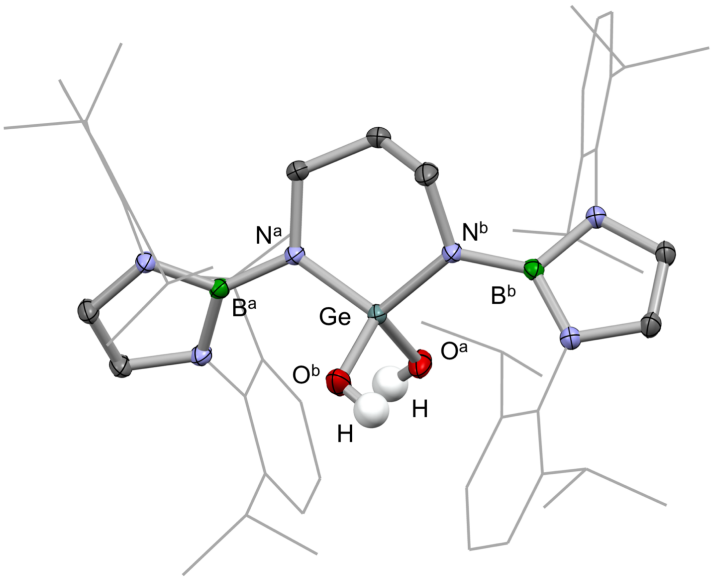

	(Å)/(°)
d(B^a–N^a)	1.4410(15)
d(B^b–N^b)	1.4422(15)
d(Ge–N^a)	1.8083(10)
d(Ge–N^b)	1.8148(9)
d(Ge–O^a)	1.7654(9)
d(Ge–O^b)	1.7561(9)
∠(N^a–Ge–N^b)	108.70(4)
Θ([B^a])	32.9
Θ([B^b])	42.7

Figure 5.17 (Left) Molecular structure of (29)Ge$(OH)_2$ in the solid state, as determined by X-ray crystallography. Most hydrogen atoms omitted, and Dipp groups shown in wireframe format for clarity. Thermal ellipsoids set at the 40% probability level. (Right) Table of key structural parameters.

The reaction of Me_3NO and (**29**)Ge was therefore repeated with minimal manipulation being employed during the work up in order to avoid hydrolysis and allow for isolation of the initially formed product. Accordingly, single crystals suitable

for X-ray crystallography could be obtained by slow evaporation of a cyclohexane solution. Figure 5.18 depicts the solid-state structure so obtained and shows a tetravalent Ge(IV) compound featuring OH and OCH_2NMe_2 ligands (*i.e.* (**29**)Ge(OCH_2NMe_2)(OH)). The N–Ge–N bond angle has increased slightly from 99.85(6)° in the parent germylene to 103.40(8)° in (**29**)Ge(OCH_2NMe_2)(OH). This widening is consistent with the change in oxidation state from Ge(II) to Ge(IV), and the need in angular terms to push the bulky ancillary ligands further apart. The presence of the bulky $OCHNMe_2$ group attached to the germanium centre and the reduced size of Ge(IV) compared to Ge(II) presumably underpins the restricted rotation of the Dipp groups observed by NMR spectroscopy.

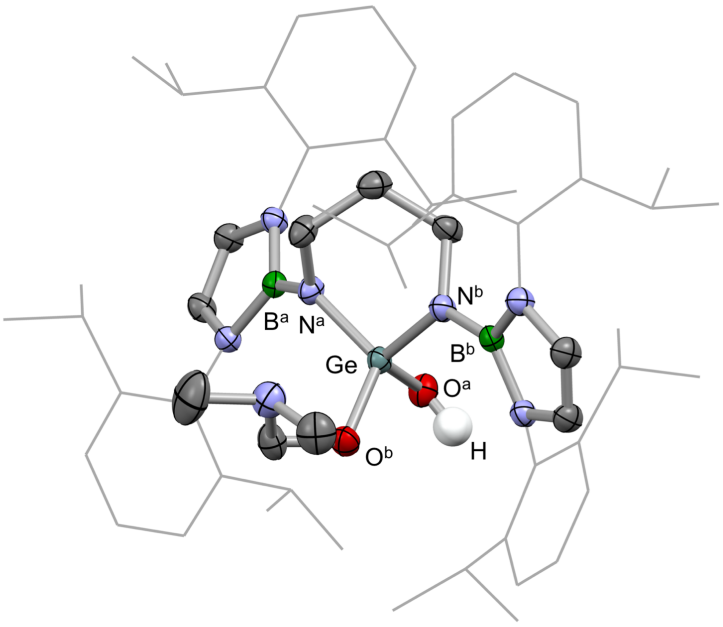

	(Å)/(°)
d(B^a–N^a)	1.443(3)
d(B^b–N^b)	1.435(3)
d(Ge–N^a)	1.810(2)
d(Ge–N^b)	1.823(2)
d(Ge–O^a)	1.762(2)
d(Ge–O^b)	1.765(2)
∠(N^a–Ge–N^b)	103.40(8)
Θ([B^a])	51.3
Θ([B^b])	34.8

Figure 5.18 (Left) Molecular structure of (29)Ge(OCH_2NMe_2)(OH) in the solid state, as determined by X-ray crystallography. Most hydrogen atoms omitted, and Dipp groups shown in wireframe format for clarity. Thermal ellipsoids set at the 40% probability level. (Right) Table of key structural parameters.

The structure of (**29**)Ge(OCH_2NMe_2)(OH) suggests that two equivalents of Me_3NO are required for the reaction to go to completion. When the reaction is carried out on

an NMR scale it is difficult to precisely control the ratios of reactants due to the low molecular weight of Me_3NO. Therefore, in order to study the amount of Me_3NO consumed in the reaction, the reaction was repeated on a larger scale. The ^1H NMR spectrum of a reaction mixture comprised of equimolar amount of Me_3NO and (**29**)Ge shows that 50% of the germylene is left unreacted; upon addition of a further equivalent of Me_3NO the reaction proceeds to completion. Similar results have been reported by Veith *et al.*,[28] who suggest that the reaction of their germylene with Me_3NO proceeds through a transient germanone that reacts with a second equivalent of Me_3NO. A similar mechanism is proposed for the reaction of (**29**)Ge and Me_3NO, with initial formation of the germanone, being followed by coordination of another molecule of Me_3NO at the highly electrophilic germanium centre and proton transfer (Scheme 5.24). Ejection, then reassimilation of an iminium fragment by C–O bond formation would then account for the observed product.

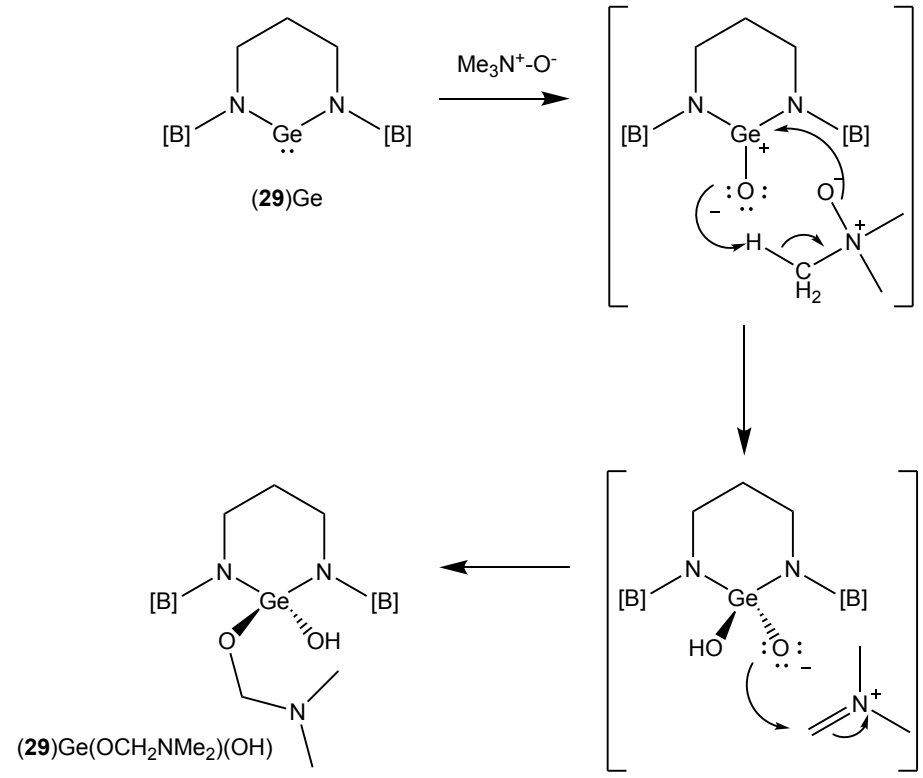

Scheme 5.24 Suggested mechanism for the reaction of (29)Ge and Me_3NO.

Pyridine *N*-oxide was selected as a potential alternative oxygen transfer agent, due to the reduced acidity of its β-protons compared with Me_3NO, a factor which might hinder reaction with a second equivalent of the oxygen transfer agent. The ^1H NMR spectra of the reaction mixtures comprised of equimolar amount of pyridine *N*-oxide and either (**28**)Ge or (**29**)Ge show no consumption of the germylenes at room temperature. Upon heating to 110 °C, however, a single new product appears in each case. After three days of heating, no further conversion is observed but 50% of the reaction mixtures consist of the respective unreacted germylene. Upon addition of a further equivalent of pyridine *N*-oxide and heating, both reactions proceed to completion. This indicates that each germylene reacts with two equivalents of pyridine *N*-oxide. Furthermore, the ^1H NMR spectra of the new products suggest restricted rotation of the Dipp groups, consistent with coordination of a sterically demanding group at the germanium centre. For the reaction mixture of (**28**)Ge and pyridine *N*-oxide, there are two broad doublets for the alkyl bridging backbone at 3.19 and 2.85 ppm with geminal couplings apparent in the ^1H NMR spectrum and similarly, for the reaction mixture of (**29**)Ge and pyridine *N*-oxide, two sets of broad doublets for the NCH_2 protons of the alkyl backbone are apparent in the ^1H NMR spectrum (the signal for NCH_2CH_2 overlaps with the isopropyl methyl groups).

Single crystals from the product of the reaction of (**29**)Ge and pyridine *N*-oxide suitable for X-ray crystallography were obtained by recrystallization from hexane. Figure 5.19 depicts the solid-state structure so obtained and shows a tetravalent Ge(IV) compound featuring OH and C_5H_4NO ligands (*i.e.* (**29**)Ge(C_5H_4NO)(OH)). A pathway similar to the reaction with Me_3NO is suggested (*i.e. via* a transient germanone) with subsequent C–H activation of a second pyridine *N*-oxide molecule yielding the final product (Scheme 5.25).

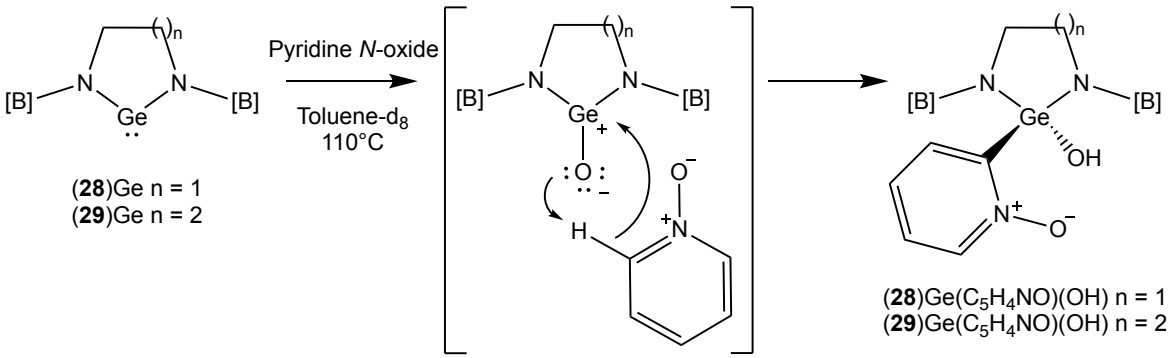

Scheme 5.25 Suggested mechanism for the reaction of pyridine *N*-oxide and (28)Ge or (29)Ge.

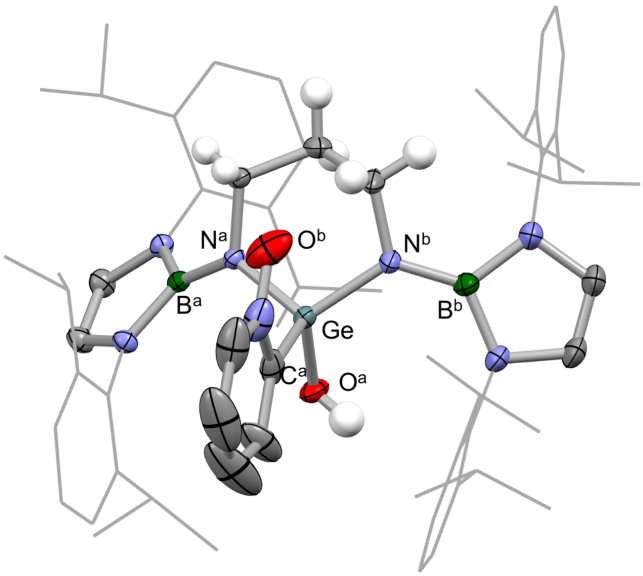

	(Å)/(°)
d(B^a–N^a)	1.431(5)
d(B^b–N^b)	1.439(6)
d(Ge–N^a)	1.811(3)
d(Ge–N^b)	1.832(4)
d(Ge–O^a)	1.766(3)
d(Ge–C^a)	1.957(4)
∠(N^a–Ge–N^b)	107.2(1)
Θ([B^a])	47.22
Θ([B^b])	26.61

Figure 5.19 (Left) Molecular structure of (29)Ge(C_5H_4NO)(OH) in the solid state, as determined by X-ray crystallography. Most hydrogen atoms omitted, and Dipp groups shown in wireframe format for clarity. Thermal ellipsoids set at the 40% probability level. (Right) Table of key structural parameters.

Compared with the parent germylene ((**29**)Ge), the N–Ge–N bond angle gets significantly wider and the Ge–N bonds get shorter. This is due to the Ge centre becoming smaller on oxidation from Ge(II) to Ge(IV).

The product from the reaction mixture of (**28**)Ge and pyridine N-oxide has been characterized *in situ* by ^{1}H NMR spectroscopy as attempts to isolate it *via* multiple methods and in a range of solvents including pentane, hexane, heptane and toluene

were unsuccessful. Two equivalents of pyridine N-oxide are needed for the reaction to go to completion, and the spectroscopic features of this product are very similar to the analogous reaction product (**29**)Ge(C_5H_4NO)(OH); it is therefore hypothesized that an analogous product has been formed (*i.e.* (**28**)Ge(C_5H_4NO)(OH); Scheme 5.25).

Trimethylamine *N*-oxide and pyridine *N*-oxide seem to successfully generate the target germanone, but subsequent reactivity with another molecule of the oxygen transfer agent is problematic and prevents isolation of the germanone. Therefore, the reactivity of the germylenes with other oxygen transfer agents was explored. Lutidine *N*-oxide and 2,6-dichloropyridine *N*-oxide were selected due to larger steric bulk compared with pyridine *N*-oxide and the absence of β-hydrogens, both of which might help prevent C–H activation of a second molecule of the *N*-oxide following generation of the target germanone.

The ^{1}H NMR spectra comprised of the reaction mixtures of (**28**)Ge or (**29**)Ge and lutidine *N*-oxide show partial consumption of the germylenes and conversion to a mixture of species when heated in toluene-d_8 at 110 °C. Upon further heating, full decomposition to the respective protio-ligands is observed. No reaction was observed in the reaction of (**29**)Ge with 2,6-dichloropyridine *N*-oxide even when heated in toluene-d_8 at 110 °C for five days. Lutidine *N*-oxide and 2,6-dichloropyridine *N*-oxide are less reactive oxygen transfer agents compared with pyridine *N*-oxide due to steric and/or electronic factors which in this case, presumably prevent the initial oxygen transfer from occurring and thus no productive reactivity is observed.

Given the undesired activation of Me_3NO and pyridine *N*-oxide by transiently formed germanones, and the lack of reactivity with lutidine *N*-oxide or 2,6-dichloropyridine *N*-oxide, alternative oxygen sources were considered. N_2O, CO_2 and

O_2 are all oxygen transfer agents which have previously been reported to react with tetrelenes.[6,29,30] None are sterically demanding, unlike the *N*-oxides, and in addition they generate N_2 and CO as by-products which are very unreactive, or in the case of O_2, no by-product is formed. Unfortunately, no reaction is observed by ^{1}H NMR spectroscopy when heating the germylenes in the presence of these oxygen transfer agents, even when heated for extended periods of time.

The target putative germanones appear to be too reactive to be isolated in the presence of a sufficiently active oxygen transfer reagent, and thus efforts to synthesize the less reactive sulphur analogues were made. Germanethiones are generally synthesized *via* the reactions of germylenes and 1/8 of an equivalent of sulphur.[28,31] Due to the low molecular mass of sulphur, however, large amount of germylene would be needed to ensure such a stoichiometry and therefore excess sulphur was used. Both (**28**)Ge and (**29**)Ge show reactivity towards excess sulphur when heated at 80 °C (Scheme 5.26). The reaction of (**28**)Ge and S_8 takes a significantly longer time to go to completion than that of (**29**)Ge (18 days compared with 8 days).

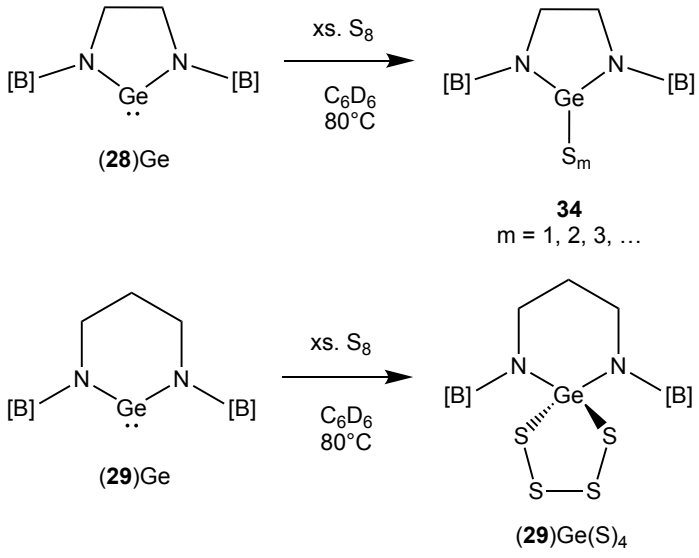

Scheme 5.26 Reactions of (28)Ge and (29)Ge and elemental sulphur.

Single crystals suitable for X-ray crystallography of the product from the reaction of (**29**)Ge and S_8 were obtained by slow evaporation from a pentane solution. The solid-state structure so obtained is depicted in Figure 5.20 and reveals a tetravalent germanium centre featuring a five membered GeS_4 ring (*i.e.* (**29**)Ge$(S)_4$). The ^{1}H NMR spectrum of (**29**)Ge$(S)_4$ reveals evidence for partially restricted rotation of the Dipp groups: the doublet at 1.36 ppm assigned to isopropyl methine groups appears as a broad multiplet at room temperature, but is a sharp doublet at elevated temperatures.

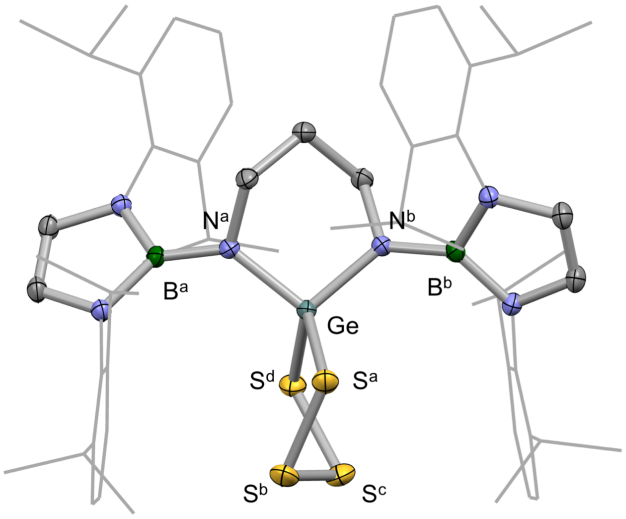

	(Å)/(°)
d(B^a–N^a)	1.450(2)
d(B^b–N^b)	1.449(2)
d(Ge–N^a)	1.814(1)
d(Ge–N^b)	1.812(1)
d(Ge–S^a)	2.2459(4)
d(Ge–S^d)	2.2420(4)
∠(N^a–Ge–N^b)	100.89(6)
Θ([B^a])	44.7
Θ([B^b])	44.0

Figure 5.20 (Left) Molecular structure of (29)Ge$(S)_4$ in the solid state, as determined by X-ray crystallography. Solvate molecules and most hydrogen atoms omitted, and Dipp groups shown in wireframe format for clarity. Thermal ellipsoids set at the 40% probability level. (Right) Table of key structural parameters.

Attempts were made to crystallize the product of the reaction between (**28**)Ge and S_8 (**34**) from a variety of solvents but all were unsuccessful, and therefore the compound was characterized *in situ* by NMR spectroscopy. The spectroscopic features of this product are very similar to the analogous reaction product (**29**)Ge$(S)_4$ and thus it is hypothesized that the uptake of sulphur has taken place at the germanium centre, although, without a solid-state structure of **34**, the number of

sulphur atoms incorporated in the product is unknown.

Several other tetrathiagermolanes have been reported by Okazaki *et al.* and several can undergo desulfurization to produce germanethiones (Scheme 5.27).[33] Following a similar procedure, (**29**)$Ge(S)_4$ was reacted with three equivalents of triphenylphosphine. The ^1H and ^{31}P NMR spectra reveal complete consumption of both (**29**)$Ge(S)_4$ and triphenylphosphine. A singlet at 42.7 ppm is observed in the ^{31}P NMR spectrum, which matches the ^{31}P chemical shift of triphenylphosphine sulfide.[33] The ^1H NMR spectrum indicates conversion of the germanium species to a single boryl containing species which is not the parent germylene and has same patterns as the parent tetrathiagermolane but with slightly different shifts and sharper signals, which could indicate increased rotation around the Dipp groups and thus less steric bulk at the germanium centre. Single crystals of the product were not obtained but the formation of triphenylphosphine sulfide and indications of unrestricted rotation around the Dipp groups are consistent with removal of (one or more) sulphur atoms from the tetrathiagermolane. Furthermore, the absence of the parent germylene in the ^1H NMR spectrum suggests that over-reduction has not taken place. Without the solid-state structure, however, the number of sulphur atoms present at the germanium centre cannot be definitively established.

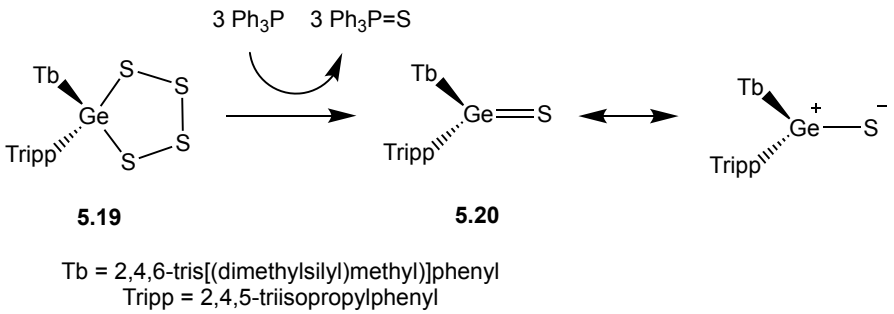

Scheme 5.27 Desulphurization of tetrathiagermolane 5.19 by Ozaki *et al.*[32]

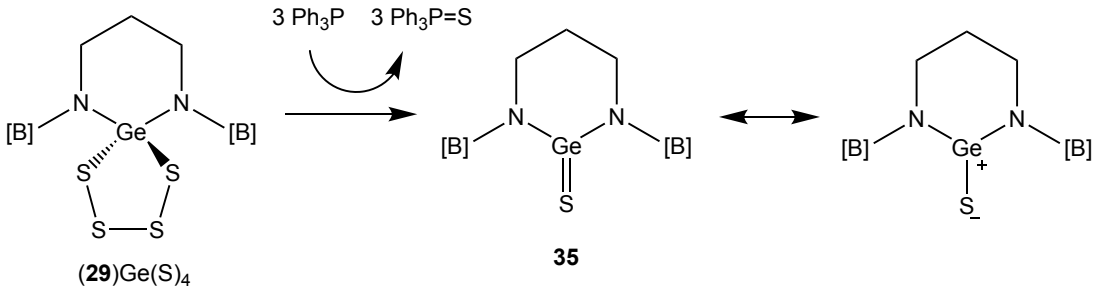

Scheme 5.30 Proposed desulphurization of (29)Ge(S)$_4$ by triphenylphosphine.

5.3 Conclusions

The bisborylated 3,4,5,6-tetrahydropyrimidium salt ([(**25**)H][BPh$_4$]) was successfully synthesized by borylation of 3,4,5,6-tetrahydropyrimidine. Reaction with potassium bis(trimethylsilyl)amide, however, does not result in the formation of the target free carbene (**25**) but leads instead to the formation of two different species, one of which (the *N*-allyl formamidine **26**) is formed *via* backbone deprotonation and subsequent ring-opening, and has been structurally characterized by X-ray crystallography. Attempts to access the free NHC *via* reduction of a bisborylated cyclic thiourea were also made. 3,4,5,6-Tetrahydro-2-pyridinethiol was successfully borylated to give bisborylated cyclic thiourea **32**. Unfortunately, reduction using K or KC$_8$ leads to decomposition products. The carbene was also pursued *via* a ligand exchange with BICAAC^{Me}, but no reactivity of the two species was observed.

The heavier analogues of the bisborylated carbene were considered to be more easily accessed as their syntheses do not rely on deprotonation or reduction and the heavier analogues are thermodynamically more stable. Although the tetrelenes could be synthesized, they are very moisture sensitive and due to similar solubility with the respective protio-ligands, difficult to isolate. NMR spectroscopy, and ^{29}Si in particular, suggest successful *in situ* generation of *N*,*N*'-bisborylated 5- and 6-membered *N*-

heterocyclic silylenes, (**28**)Si and (**29**)Si. Thir isolation in pure form was, however, unsuccessful due to the large amounts of protio-ligand and the presence of IPr as a side product, which was not easily separated from the target product. *N*,*N*'-Bisborylated 5- and 6- membered *N*-heterocyclic germylenes and stannylenes, (**28**)Ge, (**29**)Ge, (**28**)Sn and (**29**)Sn, were successfully isolated and structurally characterized by X-ray crystallography.

The reactivity of the germylenes and stannylenes was studied. (**29**)Ge, (**28**)Sn and (**29**)Sn do not react with dihydrogen and neither do (**29**)Ge or (**29**)Sn with trimethylsilyl azide. Reactions of the germylenes with oxygen transfer agents (Me_3NO and pyridine *N*-oxide) are thought to proceed through the target germanones (**5.10**; Figure 5.1), which then activate a second equivalent of the oxygen transfer agent to yield tetravalent Ge(IV) species ((**29**)Ge(OCH_2NMe_2)(OH) and (**29**)Ge(C_5H_4NO)(OH); Figures 5.18 and 5.19). No reaction was observed with lutidine *N*-oxide, 2,6-dichloropyridine *N*-oxide, N_2O, CO_2 or O_2. (**29**)Ge reacts with excess S_8 to give (**29**)Ge$(S)_4$, which most likely undergoes desulfurization in the presence of triphenylphosphine to give a germanethione, although the product has not been structurally characterized by X-ray crystallography.

To summarize, *N*,*N*'-bisborylated *N*-heterocyclic tetrelenes are easier to access compared with to the corresponding bisborylated NHCs, as they can be prepared directly *via* salt metathesis, and thus do not rely on deprotonation or reduction under harsh conditions.

5.4 Experimental Procedures

Preparation of [(25)H][BPh_4]

A mixture of 3,4,5,6-tetrahydropyrimidine (43 μL, 0.54 mmol), **1** (0.50 g, 1.1 mmol) and potassium bis(trimethylsilyl)amide (0.11 g, 0.54 mmol) was dissolved in benzene (10 mL) and the resulting mixture stirred at room temperature for 30 min. Volatiles were removed *in vacuo* and the residue redissolved in acetonitrile (10 mL). The resulting mixture was stirred for 15 min, Na[BPh_4] (0.11 g, 0.32 mmol) added and the solution stirred for a further 15 min. Volatiles were again removed *in vacuo* and the residue dissolved in dichloromethane (15 mL). After filtration, the volume of the supernatant was reduced to 5 mL *in vacuo* and the product triturated with hexane (30 mL). After filtration, the precipitate was washed with pentane (2 x 10 mL) and dried *in vacuo* to yield the product as an off-white solid. Yield: 0.32 g, 59%.

Spectroscopic Data for [(25)H][BPh_4]

^{1}H NMR (C_6D_6, 400 MHz, 298 K): δ_H 7.99-8.01 (8H, m, *o*-H of [BPh_4]$^-$), 7.19-7.23 (4H, m, *p*-*H* of Dipp), 7.13 (1H, s, NC*H*N), 7.04-7.07 (8H, m, *m*-*H* of [BPh_4]$^-$), 6.69-7.00 (8H, m, *m*-*H* of Dipp), 7.85-7.89 (4H, m, *p*-*H* of [BPh_4]$^-$), 5.60 (4H, s, N(C*H*)$_2$N of boryl ligand), 2.50 (8H, septet, $^3J_{HH}$ = 6.7 Hz, C*H*Me$_2$), 2.28 (4H, br m, NCH_2), 1.01 (24H, d, $^3J_{HH}$ = 6.6 Hz, CH*Me*$_2$), 0.77 (24H, d, $^3J_{HH}$ = 6.8 Hz, CH*Me*$_2$), -0.29 (2H, br m, CH_2(CH_2N)$_2$) ppm. ^{13}C{^{1}H} NMR (C_6D_6, 101 MHz, 298 K): δ_C 165.3 (q, $^1J_{CB}$ = 49.0 Hz, *i*-*C* of [BPh_4]$^-$), 145.6 (*o*-*C* of Dipp), 136.7 (*i*-*C* of Dipp), 135.4 (*o*-*C* of [BPh_4]$^-$), 129.7 (*p*-*C* of Dipp), 126.2-126.3 (*m*-*C* of [BPh_4]$^-$ and N*C*HN), 125.0 (*m*-*C* of Dipp), 121.9 (*p*-*C* of [BPh_4]$^-$), 120.9 (N(*C*H)$_2$N of boryl ligand), 44.3 (N*C*H$_2$), 28.9 (*C*HMe$_2$), 25.3 (CH*Me*$_2$), 23.5

(CH*Me*$_2$), 14.4 (*C*H$_2$(CH$_2$N)$_2$) ppm.^{11}B NMR (C_6D_6, 128 MHz, 298 K): δ_B 21 (br s, boryl ligand), -7 (s, [BPh$_4$]$^-$) ppm. MS (EI): *m/z* (assignment, %) 857.7 ([M]$^+$, 64%). Acc. Mass EI: calc. for $C_{56}H_{79}B_2N_6$: 857.6564; found: 857.6592. Elemental microanalysis: found (calcd. for $C_{56}H_{76}B_2N_6$): C 81.04 (81.30)%, H 8.42 (8.72)%, N 7.48 (7.20)%.

Reaction of [(25)H][BPh$_4$] and Potassium Bis(trimethylsilyl)amide

A mixture of [(**25**)H][BPh$_4$] (230 mg, 0.23 mmol) and potassium bis(trimethylsilyl)amide (36 mg, 0.23 mmol) was dissolved in benzene (5 mL) and the resulting solution stirred for 1 h. After filtration, volatiles were removed *in vacuo* and the residue dissolved in minimal acetonitrile at 80 °C. The solution was allowed to cool slowly to room temperature in the oil bath, producing colourless single crystals of **26** suitable for X-ray crystallography. After filtration, the remaining crystals were dried *in vacuo* to yield **26** as a white crystalline powder with 5-10% contamination by **27** (as determined by ^{1}H NMR spectroscopy). Yield: 15 mg, 25%. A second recrystallization resulted in 1:1 co-crystallization of **26** and **27**.

Spectroscopic Data for 26

^{1}H NMR (C_6D_6, 400 MHz, 298 K): δ_H 7.51 (1H, s, NC*H*N), 7.18-7.22 (2H, m, *p*-*H* of Dipp of *C*- or *N*-boryl ligand), 7.08-7.13 (6H, m, *m*-*H* of Dipp of *C*- or *N*-boryl ligand and *p*-*H* of Dipp of *C*- or *N*-boryl ligand), 6.78-7.00 (4H, m, *m*-*H* of Dipp of *C*- or *N*-boryl ligand), 6.04 (2H, s, N(C*H*)$_2$N of *C*- or *N*-boryl ligand), 5.86 (2H, s, N(C*H*)$_2$N of *C*- or *N*-boryl ligand), 5.35 (1H, m, NCH$_2$C*H*), 4.55 (1H, br m, NCH$_2$CHC*H*$_2$), 4.29 (1H, br m, NCH$_2$CHC*H*$_2$), 3.77 (2H, br m, NC*H*$_2$), 3.36 (4H, sept, $^3J_{HH}$ = 6.8 Hz, C*H*Me$_2$ of *C*- or *N*-boryl ligand), 3.12 (4H, sept, $^3J_{HH}$ = 6.8 Hz, C*H*Me$_2$ of *C*- or *N*-boryl ligand), 2.28 (4H, br m, NC*H*$_2$), 1.23 (12H, d, $^3J_{HH}$ = 6.8 Hz, CH*Me*$_2$ of *C*- or *N*-boryl ligand), 1.15 (12H, d, $^3J_{HH}$ = 6.8 Hz, CH*Me*$_2$ of *C*- or *N*-boryl ligand), 1.11 (12H, d, $^3J_{HH}$ = 6.8 Hz, CH*Me*$_2$ of *C*- or *N*-

boryl ligand), 1.01 (12H, d, $^{3}J_{HH}$ = 6.8 Hz, CH*Me*$_2$ of *C*- or *N*-boryl ligand) ppm. $^{13}C\{^{1}H\}$ NMR (C_6D_6, 101 MHz, 298 K): δ_C 147.2 (N*C*HN), 146.3 (*o*-*C* of Dipp of *C*- or *N*-boryl ligand), 145.6 (*o*-*C* of Dipp of *C*- or *N*-boryl ligand), 140.0 (*i*-C of Dipp of *C*- or *N*-boryl ligand), 138.9 (*i*-C of Dipp of *C*- or *N*-boryl ligand), 136.3 (NCH$_2$*C*H), 127.9-128.4 (overlapping signals, *p*-*C* of Dipp of *C*- or *N*-boryl ligand and C_6D_6), 126.8 (*p*-*C* of Dipp of *C*- or *N*-boryl ligand), 124.3 (*m*-*C* of Dipp of *C*- or *N*-boryl ligand), 123.5 (*m*-*C* of Dipp of *C*- or *N*-boryl ligand), 119.4 (N(*C*H)$_2$N of *C*- or *N*-boryl ligand), 118.2 (N(*C*H)$_2$N of *C*- or *N*-boryl ligand), 113.8 (NCH$_2$CH*C*H$_2$), 45.5 (N*C*H$_2$) 28.7 (*C*HMe$_2$ of *C*- or *N*-boryl ligand), 28.6 (*C*HMe$_2$ of *C*- or *N*-boryl ligand), 25.2 (CH*Me*$_2$ of *C*- or *N*-boryl ligand), 24.6 (CH*Me*$_2$ of *C*- or *N*-boryl ligand), 24.1 (CH*Me*$_2$ of *C*- or *N*-boryl ligand), 23.5 (CH*Me*$_2$ of *C*- or *N*-boryl ligand) ppm. ^{11}B NMR (C_6D_6, 128 MHz, 298 K): δ_B 22 (br s, boryl ligand) ppm. MS (EI): *m/z* (assignment, %) 813.6 ([M]$^+$, 14 %). Acc. Mass EI: calc. for $C_{56}H_{78}{}^{10}B_2N_6$: 854.6541; found: 854.6509.

Crystallographic Data for 26

a = 19.4525(4) Å, *b* = 12.4276(2) Å, *c* = 22.3324(5) Å, α = γ = 90°, β = 98.825(2)°, V = 5334.90(19) Å^3, Monoclinic, *P*2$_1$/*n*, *Z* = 4, R_1 for 8957 [data intensity $I > 2\sigma(I)$] unique data = 0.052, wR_2 (all 11059 unique data) = 0.150.

Spectroscopic Data for 27

^{1}H NMR (C_6D_6, 400 MHz, 298 K): δ_H 6.98-7.22 (38H, overlapping m, Ar-*H* of **26** and **27** and C_6D_5H), 6.83-6.84 (1H, br m, NC*H*N), 6.11 (2H, s, N(C*H*)$_2$N of boryl ligand), 5.87 (2H, s, N(C*H*)$_2$N of boryl ligand), 3.09-3.39 (20H, overlapping m, C*H*Me$_2$ of both **26** and **27** and aliphatic proton originated from backbone), 2.90-2.95 (1H, br m, aliphatic protons originated from backbone), 2.73 (1H, dt, $^{3}J_{HH}$ = 3.5 Hz, $^{3}J_{HH}$ = 11.9 Hz, aliphatic protons originated from backbone), 2.49-1.55 (1H, m, aliphatic protons originated from

backbone), 0.89-1.41 (120H, overlapping m, CH*Me*$_2$ of both **26** and **27** and aliphatic protons originated from backbone) ppm. Integration of Ar-*H* of **26** and **27** is slightly higher than expected due to partial overlap with C_6D_5H. $^{13}C\{^1H\}$ NMR (C_6D_6, 126 MHz, 298 K): δ_C 147.3, 146.8, 146.6, 146.1, 146.1, 145.0, 139.4, 139.2, 127.5, 124.1, 123.9, 123.4, 119.5, 118.7, 43.1, 28.7, 28.5, 28.5, 25.9, 25.5, 25.2, 24.9, 23.7, 23.6, 23.4, 23.3 ppm. ^{11}B NMR (C_6D_6, 128 MHz, 298 K): δ_B 22 (br s, boryl ligands of **26** and **27**) ppm.

Preparation of (28)H$_2$

1,2-diaminoethane (0.22 mL, 3.2 mmol) was dissolved in triethylamine (3 mL) and the resulting solution added to a solution of **1** (3.0 g, 6.4 mmol) in benzene (15 mL). The resulting orange mixture was stirred at room temperature for 1 h, whereupon a white precipitate formed immediately. After filtration, volatiles were removed *in vacuo,* and the residue washed with acetonitrile (3 x 10 mL) and dried *in vacuo,* yielding (**28**)H_2 as a white powder. Yield: 2.2 g, 81%. Colourless crystals suitable for X-ray crystallography could be obtained by recrystallization from a pentane solution at -20 °C.

Spectroscopic Data for (28)H$_2$

^1H NMR (C_6D_6, 400 MHz, 298 K): δ_H 6.96-7.12 (12H, overlapping m, *m-H* and *p-H of* Dipp), 5.99 (s, 4H, N(C*H*)$_2$N of boryl ligand), 3.30 (8H, sept, $^3J_{HH}$ = 6.9 Hz, C*H*Me$_2$), 2.27 (4H, m, NC*H*$_2$), 1.43 (2H, t, $^3J_{HH}$ = 7.2 Hz, N*H*), 1.19 (24H, d, $^3J_{HH}$ = 6.9 Hz, CH*Me*$_2$), 1.15 (24H, d, $^3J_{HH}$ = 6.9 Hz, CH*Me*$_2$) ppm. $^{13}C\{^1H\}$ NMR (C_6D_6, 101 MHz, 298 K): δ_C 147.1 (*o-C* of Dipp), 139.0 (*i-C* of Dipp), 127.5 (*p-C* of Dipp), 123.7 (*m-C* of Dipp), 117.4 (N(*C*H)$_2$N of boryl ligand), 45.0 (N*C*H$_2$), 28.5 (*C*HMe$_2$), 24.8 (CH*Me*$_2$), 23.7 (CH*Me*$_2$) ppm. ^{11}B NMR (C_6D_6, 128 MHz, 298 K): δ_B 23 (br s, boryl ligand) ppm. MS (CI): *m/z* (assignment, %) 833.7 ([M]H$^+$, 20%). Acc. Mass ESI: calc. for $[C_{54}H_{79}{}^{10}B_2N_6]^+$: 831.6625; found: 831.6615.

Crystallographic Data for (28)H_2

a = 14.2417(2) Å, *b* = 22.3662(4) Å, *c* = 16.4812(3) Å, α = γ = 90°, β = 97.5685(8)°, V = 5204.06(15) Å^3, Monoclinic, *P*2$_1$, *Z* = 4, R_1 for 8834 [data intensity $I > 2\sigma(I)$] unique data = 0.061, wR_2 (all 12110 unique data) = 0.156.

Preparation of (29)H_2

(**29**)H_2 was synthesized by a similar method to (**28**)H_2 from 1,3-diaminopropane (0.18 mL, 2.1 mmol), triethylamine (2 mL) and **1** (2.0 g, 4.3 mmol). The solution was stirred for 3 h and (**29**)H_2 was obtained as a white powder. Yield: 1.7 g, 93%. Colourless crystals suitable for X-ray crystallography could be obtained by recrystallization from a hexane solution at -20 °C.

Spectroscopic data for (29)H_2

^{1}H NMR (C_6D_6, 400 MHz, 298 K): δ_H 7.11-7.24 (overlapping m, *p-H* and *m-H* of Dipp and C_6D_5H), 5.88 (4H, s, N(C*H*)$_2$N of boryl ligand), 3.34 (8H, sept, $^3J_{HH}$ = 6.9 Hz, C*H*Me$_2$), 2.07 (4H, dt, $^3J_{HH}$ = 7.1 Hz, $^3J_{HH}$ = 6.9 Hz, NC*H*$_2$), 1.23 (24H, d, $^3J_{HH}$ = 6.9 Hz, CH*Me*$_2$), 1.17-1.19 (26H, overlapping m, CH*Me*$_2$, N*H*), 0.57 (2H, quint, $^3J_{HH}$ = 7.1 Hz, C*H*$_2$(CH$_2$N)$_2$) ppm. Integration of *m-H* and *p-H* of Dipp is slightly higher than expected due to partial overlap with C_6D_5H. ^{13}C{^{1}H} NMR (C_6D_6, 101 MHz, 298 K): δ_C 147.3 (*o-C* of Dipp), 139.3 (*i-C* of Dipp), 127.5 (*p-C* of Dipp), 123.6 (*m-C* of Dipp), 117.4 (N(*C*H)$_2$N of boryl ligand), 39.1 (N*C*H$_2$), 37.7 (*C*H$_2$(CH$_2$N)$_2$), 28.5 (*C*HMe$_2$), 24.6 (CH*Me*$_2$), 23.8 (CH*Me*$_2$) ppm. ^{11}B NMR (C_6D_6, 128 MHz, 298 K): δ_B 22 (br s, boryl ligand) ppm. MS (CI): *m/z* (assignment, %) 847.7 ([M]H$^+$, 0.3%). Acc. Mass ESI: calc. for [$C_{55}H_{81}{}^{10}B_2N_6$]$^+$: 845.6781; found: 845.6781. Elemental microanalysis: found (calcd. for $C_{55}H_{80}B_2N_6$): C 76.06 (76.53)%, H 9.42 (9.52)%, N 9.49 (9.92)%.

Crystallographic data for (29)H_2

a = 19.0773(2) Å, *b* = 13.7845(1) Å, *c* = 20.3735(2) Å, α = γ = 90°, β = 99.780(1)°, V = 5279.78(9) Å^3, Monoclinic, $P2_1/c$, *Z* = 4, R_1 for 9261 [data intensity $I > 2\sigma(I)$] unique data = 0.046, wR_2 (all 10581 unique data) = 0.129.

***In Situ* Deprotonation of (28)H_2 with Phenyllithium: Generation of Li_2(28)·$(OEt_2)_2$**

(**28**)H_2 (50 mg, 0.060 mmol) and phenyllithium (20 mg, 0.24 mmol) in a J. Young's NMR tube were dissolved in a mixture of C_6D_6 and diethyl ether (0.5 mL:0.05 mL). The resulting orange solution was shaken and left to stand for 3 h. Volatiles were removed *in vacuo*, and the product extracted into hexane and concentrated. Attempts to crystallize the product at -20 °C were unsuccessful.

Spectroscopic Data for Li_2(28)·$(OEt_2)_2$

^{1}H NMR (C_6D_6, 400 MHz, 298 K): δ_H 7.09-7.25 (overlapping m, *p-H* and *m-H* of Dipp and C_6D_5H). 5.90 (4H, s, N(C*H*)$_2$N of boryl ligand), 3.49 (8H, sept, $^3J_{HH}$ = 6.8 Hz, C*H*Me$_2$), 2.94 (4H, s, NCH_2), 2.88 (12H, q, $^3J_{HH}$ = 6.9 Hz, CH_2 of coordinated Et_2O), 1.26 (24H, d, $^3J_{HH}$ = 6.8 Hz, CH*Me*$_2$), 1.19 (24H, d, $^3J_{HH}$ = 6.8 Hz, CH*Me*$_2$), 0.68 (8H, t, $^3J_{HH}$ = 6.9 Hz, CH_3 of coordinated Et_2O) ppm. Integration of *m-H* and *p-H* of Dipp is slightly higher than expected due to partial overlap with C_6D_5H.

***In Situ* Deprotonation of (28)H_2 with ^{n}BuLi/TMEDA: Generation of Li_2(28)·(C_6H_5Me)(TMEDA)**

To a stirred mixture of (**28**)H_2 (0.20 g, 0.24 mmol) and TMEDA (36 μL, 0.24 mmol) in toluene (2 mL) at -50 °C was added dropwise ^{n}BuLi (0.60 mL of a 1.6 M solution in hexane, 0.96 mmol). The resulting pale orange reaction mixture was warmed to room

temperature and volatiles removed *in vacuo* to afford a yellow oil. The residue was extracted into hexane, concentrated and stored at -20 °C to yield colourless single crystals suitable for X-ray crystallography of the monolithiated ligand (Li(**28**)H·(TMEDA)). Attempts to crystalize the dilithiated species were unsuccessful.

Spectroscopic data for Li_2(28)·(C_6H_5Me)(TMEDA)

^{1}H NMR (C_6D_6, 400 MHz, 298 K): δ_H 6.99-7.18 (overlapping m, *p-H* and *m-H* of Dipp and C_6D_5H), 6.71 (2H, m, *o-H* of coordinated toluene), 6.25 (2H, m, *m-H* of coordinated toluene), 5.93 (1H, m, *p-H* of coordinated toluene), 5.87 (4H, s, N(C*H*)$_2$N of boryl ligand), 3.54-3.60 (8H, br m, C*H*Me$_2$), 2.82-2.85 (4H, br m, NC*H*$_2$), 1.76 (3H, s, C*H*$_3$ of coordinated toluene), 1.71 (12H, s, C*H*$_3$ of coordinated TMEDA), 1.56 (4H, s, C*H*$_2$ of coordinated TMEDA), 1.17-1.35 (48H, overlapping m, CH*Me*$_2$) ppm. Integration of *m-H* and *p-H* of Dipp is slightly higher than expected due to partial overlap with C_6D_5H. ^{13}C{^{1}H} NMR (C_6D_6, 101 MHz, 298 K): δ_C 155.3 (*i-C* of coordinated toluene), 147.2 (*o-C* of Dipp), 143.0 (*i-C* of Dipp), 130.2 (*o-C* of coordinated toluene), 126.7 (*p-C* of Dipp), 124.0 (*m-C* of Dipp), 118.0 (N(*C*H)$_2$N of boryl ligand), 115.5 (*m-C* of coordinated toluene), 107.2 (*p-C* of coordinated toluene), 56.2 (*C*H$_2$ of coordinated TMEDA), 54.5 (N*C*H$_2$), 45.3 (*C*H$_3$ of coordinated TMEDA), 38.8 (*C*H$_3$ of coordinated toluene), 28.5 (*C*HMe$_2$), 25.6 (CH*Me*$_2$), 23.9 (CH*Me*$_2$) ppm. ^{11}B NMR (C_6D_6, 128 MHz, 298 K): δ_B 29 (br s, boryl ligand) ppm. ^{7}Li NMR (C_6D_6, 156 MHz, 298 K): δ_{Li} 1.1 ppm.

Crystallographic data for Li(28)H·(TMEDA)

a = 12.7938(4) Å, *b* = 18.1314(5) Å, *c* = 13.3403(5) Å, α = γ = 90°, β = 103.293(3)°, V = 3011.63(17) Å^3, Monoclinic, *P*2, *Z* = 2, R_1 for 7501 [data intensity $I > 2\sigma(I)$] unique data = 0.067, wR_2 (all 9849 unique data) = 0.186.

In Situ Deprotonation of (29)H_2 with ^{n}BuLi/TMEDA: Generation of Li_2(29)·(C_6H_5Me)(TMEDA)

Li_2(**29**)·(C_6H_5Me)(TMEDA) was prepared by a similar method to Li_2(**28**)·(C_6H_5Me)(TMEDA) from (**29**)H_2 (0.20 g, 0.24 mmol), TMEDA (36 μL, 0.24 mmol) and ^{n}BuLi (0.59 mL of a 1.6 M solution in hexane, 0.95 mmol). Attempts to crystallize the product from hexane at -20 °C were unsuccessful.

Spectroscopic Data for Li_2(29)·(C_6H_5Me)(TMEDA)

^{1}H NMR (C_6D_6, 400 MHz, 298 K): δ_H 7.00-7.20 (overlapping m, *p*-*H* and *m*-*H* of Dipp and C_6D_5H), 6.86 (2H, m, *o*-*H* coordinated toluene), 6.45 (2H, m, *m*-*H* of coordinated toluene), 6.03 (1H, m, *p*-*H* of coordinated toluene), 5.87 (4H, s, N(C*H*)$_2$N of boryl ligand), 3.48 (8H, sept, $^3J_{HH}$ = 6.9 Hz, C*H*Me$_2$), 2.78 (4H, m, NCH_2), 2.08 (3H, s, CH_3 of coordinated toluene), 1.75 (12H, s, CH_3 of coordinated TMEDA), 1.61 (4H, s, CH_2 of coordinated TMEDA), 1.22 (24H, d, $^3J_{HH}$ = 6.9 Hz, CH*Me*$_2$), 1.13 (24H, d, $^3J_{HH}$ = 6.9 Hz, CH*Me*$_2$), 0.96 (2H, m, CH_2(CH$_2$N)$_2$) ppm. Integration of *m*-*H* and *p*-*H* of Dipp is slightly higher than expected due to partial overlap with C_6D_5H. ^{13}C{^{1}H} NMR (C_6D_6, 101 MHz, 298 K): δ_C 147.4 (*i*-*C* of coordinated toluene), 146.8 (*o*-*C* of Dipp), 142.8 (*i*-*C* of Dipp), 130.2 (*o*-*C* of coordinated toluene), 125.7 (*p*-*C* of Dipp), 124.2 (*m*-*C* of Dipp), 117.3 (N(*C*H)$_2$N of boryl ligand), 115.6 (*m*-*C* of coordinated toluene), 106.6 (*p*-*C* of coordinated toluene), 56.4 (*C*H$_2$ of coordinated TMEDA), 47.5 (N*C*H$_2$), 45.3 (*C*H$_3$ of coordinated TMEDA), 40.0 (*C*H$_2$(CH$_2$N)$_2$), 36.8 (*C*H$_3$ of coordinated toluene), 28.7 (*C*HMe$_2$), 24.7 (CH*Me*$_2$), 23.8 (CH*Me*$_2$) ppm. ^{11}B NMR (C_6D_6, 128 MHz, 298 K): δ_B 26 (br s, boryl ligand) ppm. ^{7}Li NMR (156 MHz, C_6D_6, 298 K): δ_{Li} 1.0 ppm.

In situ Deprotonation of (28)H_2 with Benzyl Potassium: Generation of K_2(28)

To a mixture of (**28**)H_2 (48 mg, 0.058 mmol) and benzyl potassium (15 mg, 0.12

mmol) in a J. Young's NMR tube was added C_6D_6 (0.5 mL) and the resulting red solution sonicated for 3 h. The ^{1}H NMR spectrum of the reaction mixture indicates full conversion to K_2(**28**).

Spectroscopic Data for K_2(28)

^{1}H NMR (C_6D_6, 400 MHz, 298 K): δ_H 6.99-7.15 (12H, overlapping m, *m*-*H* and *p*-*H* of Dipp), 5.98 (4H, s, N(C*H*)$_2$N of boryl ligand), 3.61 (8H, sept, $^3J_{HH}$ = 6.9 Hz, C*H*Me$_2$), 2.66 (4H, s, NCH_2), 1.24 (24H, d, $^3J_{HH}$ = 6.9 Hz, CH*Me*$_2$), 1.09 (24H, d, $^3J_{HH}$ = 6.9 Hz, CH*Me*$_2$) ppm.

***In situ* Deprotonation of (29)H_2 with Benzyl Potassium: Generation of K_2(29)**

K_2(**29**) was prepared by a similar method to K_2(**28**) from (**29**)H_2 (50 mg, 0.059 mmol) and benzyl potassium (15 mg, 0.12 mmol). The ^{1}H NMR spectrum of the reaction mixture indicates full conversion to K_2(**29**).

Spectroscopic data for K_2(29)

^{1}H NMR (C_6D_6, 400 MHz, 298 K): δ_H 7.00-7.15 (12H, overlapping m, *m*-*H* and *p*-*H* of Dipp), 5.90 (4H, s, N(C*H*)$_2$N of boryl ligand), 3.61 (8H, sept, $^3J_{HH}$ = 6.9 Hz, C*H*Me$_2$), 2.87 (4H, m, NCH_2), 1.26 (24H, d, $^3J_{HH}$ = 6.9 Hz, CH*Me*$_2$), 1.14 (24H, d, $^3J_{HH}$ = 6.9 Hz, CH*Me*$_2$), 0.94 (2H, m, CH_2(CH_2N)$_2$) ppm.

Preparation of 31

In an ampoule fitted with a J. Young's tap, a mixture of 3,4,5,6-tetrahydro-2-pyrimidinethiol (75 mg, 0.64 mmol), **1** (300 mg, 0.64 mmol) and potassium bis(trimethylsilyl)amide (130 mg, 0.64 mmol) was dissolved in toluene (10 mL) and the resulting mixture stirred at 110 °C for a week. After filtration, volatiles were

removed *in vacuo* and the residue dissolved in hot acetonitrile. The solution was allowed to cool slowly to room temperature in the oil bath, producing colourless single crystals suitable for X-ray crystallography. The remainder of the crystals were isolated by filtration and washed with acetonitrile (2 x 3 mL). Yield: 120 mg, 38%. Note: the reaction progresses faster in refluxing pyridine with complete consumption of the starting materials observed by ^{1}H NMR spectroscopy in under 1 h.

Spectroscopic Data for 31

^{1}H NMR (C_6D_6, 400 MHz, 298 K): δ_H 7.16-7.23 (8H, overlapping m, *p*-*H* and *m*-*H* of Dipp and C_6D_5H), 6.21 (2H, s, N(C*H*)$_2$N of boryl ligand), 3.62 (4H, br m, C*H*Me$_2$), 2.78 (2H, br m, NCH_2), 2.08 (2H, br m, NCH_2), 1.36 (12H, br m, CH*Me*$_2$), 1.20 (12H, d, $^{3}J_{HH}$ = 6.7 Hz, CH*Me*$_2$), 0.85 (2H, br m, CH_2(CH$_2$N)$_2$) ppm. Integration of *m*-*H* and *p*-*H* of Dipp is slightly higher than expected due to partial overlap with C_6D_5H. ^{13}C{^{1}H} NMR (C_6D_6, 126 MHz, 298 K): δ_C 180.1 (*C*=S), 146.8 (bs, *o*-*C* of Dipp), 138.7 (*i*-*C* of Dipp), 127.8 (*p*-*C* of Dipp), 123.9 (bs, *m*-*C* of Dipp), 118.9 (N(*C*H)$_2$N of boryl ligand), 44.4 (N*C*H$_2$), 40.3 (N*C*H$_2$), 28.7 (*C*HMe$_2$), 26.5 (CH*Me*$_2$), 23.6 (bs, CH*Me*$_2$), 20.2 (*C*H$_2$(CH$_2$N)$_2$) ppm. ^{11}B NMR (C_6D_6, 128 MHz, 298 K): δ_B 23 (br s, boryl ligand) ppm. MS (CI): *m/z* (assignment, %) 502.3 ([M]H$^+$, 33%). Acc. Mass ESI: calc. for $C_{30}H_{43}{}^{10}BN_4S$: 501.3332; found: 501.3318.

Crystallographic Data for 31

a = 11.3298(3) Å, *b* = 12.3220(3) Å, *c* = 12.4644(3) Å, α = 69.324(2)°, β = 85.144(2)°, γ = 82.361(2)°, V = 1612.24(7) Å^3, Triclinic, *P*1, *Z* = 2, R_1 for 5400 [data intensity $I > 2\sigma(I)$] unique data = 0.034, wR_2 (all 5559 unique data) = 0.084.

Preparation of 32

In an ampoule fitted with a J. Young's tap, a mixture of 3,4,5,6-tetrahydro-2-pyrimidinethiol (130 mg, 1.1 mmol), **1** (1.3 g, 2.8 mmol) and potassium bis(trimethylsilyl)amide (490 mg, 2.5 mmol) was dissolved in pyridine (20 mL) and the resulting mixture refluxed for 2 h. Volatiles were removed *in vacuo* at 90 °C and the residue dissolved in dichloromethane (15 mL). After filtration, volatiles were again removed *in vacuo* and the residue washed with acetonitrile (2 x 10 mL) to yield the product as a white crystalline solid. Yield: 620 mg, 62%. Slow cooling of a hot acetonitrile solution to room temperature produced colourless single crystals suitable for X-ray crystallography.

Spectroscopic Data for 32

^{1}H NMR (C_6D_6, 400 MHz, 298 K): δ_H 7.19-7.23 (4H, m, *p-H* of Dipp), 7.11-7.13 (8H, m, *m-H* of Dipp), 6.07 (4H, s, N(C*H*)$_2$N of boryl ligand), 3.37 (8H, m, C*H*Me$_2$), 2.80-2.83 (4H, m, NC*H*$_2$), 1.11 (24H, d, $^{3}J_{HH}$ = 6.8 Hz, CH*Me*$_2$), 1.08 (24H, d, $^{3}J_{HH}$ = 6.8 Hz, CH*Me*$_2$), 0.80-0.86 (2H, m, NCH$_2$C*H*$_2$) ppm. ^{13}C{^{1}H} NMR (C_6D_6, 101 MHz, 298 K): δ_C 182.6 (*C*=S), 146.5 (*o-C* of Dipp), 139.1 (*i-C* of Dipp), 127.7 (*p-C* of Dipp), 123.9 (*m-C* of Dipp), 119.1 (N(*C*H)$_2$N of boryl ligand), 45.4 (N*C*H$_2$), 28.6 (*C*HMe$_2$), 26.3 (CH*Me*$_2$), 23.3 (CH*Me*$_2$), 21.2 (NCH$_2$*C*H$_2$) ppm. ^{11}B NMR (C_6D_6, 128 MHz, 298 K): δ_B 22 ppm (br s, boryl ligand). MS (ESI): *m/z* (assignment, %) 502.3 ([M]H$^+$, 20%). Acc. Mass ESI: calc. for $C_{56}H_{78}{}^{10}B_2N_6S$: 886.6262; found: 886.6304. The mass of the molecular ion is outside of the calibrated range for the instrument, but the isotopic profile is, however, in very close agreement with the calculated profile. Elemental microanalysis: found (calcd. for $C_{56}H_{78}B_2N_6S$): C 75.42 (75.66)%, H 8.42 (8.84)%, N 9.32 (9.45)%.

Crystallographic Data for 32

a = 20.6234(3) Å, b = 12.5214(2) Å, c = 22.6684(3) Å, α = γ = 90°, β = 110.6586(17)°, V = 5477.35(15) Å^3, Monoclinic, $P2_1/n$, Z = 4, R_1 for 8975 [data intensity $I > 2\sigma(I)$] unique data = 0.071, wR_2 (all 9829 unique data) = 0.194.

***In Situ* Preparation of (28)Si**

A mixture of (**28**)H_2 (50 mg, 0.060 mmol) and benzyl potassium (15 mg, 0.12 mmol) in a J. Young's NMR tube was dissolved in C_6D_6 (0.5 mL) and the resulting red solution sonicated for 3 h. IPr·$SiCl_2$ (29 mg, 0.060 mmol) was subsequently added and the reaction mixture sonicated for 30 min. Samples prepared this way were invariably contaminated with *ca.* 25% of (**28**)H_2 and the liberated free carbene (IPr).

Spectroscopic data for (28)Si (with 25% of (28)H_2 and Free IPr Carbene)

^{1}H NMR (C_6D_6, 400 MHz, 298 K): δ_H 6.99-7.31 (overlapping m, *p-H* and *m-H* of Dipp and C_6D_5H), 5.96 (4H, s, N(C*H*)$_2$N of boryl ligand), 3.26 (8H, m, C*H*Me$_2$), 2.82 (4H, m, NC*H*$_2$), 1.28-1.10 (48H, overlapping m, CH*Me*$_2$) ppm. ^{29}Si NMR (C_6D_6, 79.4 MHz, 298 K): δ_{Si} 137 (br s) ppm. Integration of *m-H* and *p-H* of Dipp is slightly higher than expected due to partial overlap with C_6D_5H.

***In Situ* Preparation of (29)Si**

(**29**)Si was prepared by a similar method to (**28**)Si from (**29**)H_2 (50 mg, 0.059 mmol), benzyl potassium (15 mg, 0.12 mmol) and IPr·$SiCl_2$ (29 mg, 0.059 mmol). Samples were invariably contaminated with *ca.* 20% of (**29**)H_2 and the liberated free carbene (IPr).

Spectroscopic data for (29)Si (with 20% of (29)H_2 and Free IPr Carbene)

^{1}H NMR (C_6D_6, 400 MHz, 298 K): δ_H 7.00-7.31 (12H overlapping m, *p-H* and *m-H* of

Dipp and C_6D_5H), 5.99 (4H, s, N(C*H*)$_2$N of boryl ligand), 3.25 (8H, sept, $^3J_{HH}$ = 6.9 Hz, C*H*Me$_2$), 2.67 (4H, m, NC*H*$_2$), 0.70-1.29 (50H, overlapping m, CH*Me*$_2$ and NCH$_2$C*H*$_2$) ppm. ^{29}Si NMR (C_6D_6, 79.4 MHz, 298 K): δ_{Si} 122 (br s) ppm. Integration of *m-H* and *p-H* of Dipp is slightly higher than expected due to partial overlap with C_6D_5H.

Preparation of (28)Ge

To a stirred mixture of (**28**)H$_2$ (500 mg, 0.60 mmol) and TMEDA (90 μL, 0.60 mmol) in toluene (10 mL) at -50 °C was added dropwise ^{n}BuLi (1.6 mL of a 1.6 M solution in hexane, 2.5 mmol). The resulting orange reaction mixture was left to reach room temperature and stirred for a further 1 h. GeCl$_2$·dioxane (500 mg, 2.1 mmol) was subsequently added and the resulting reaction mixture stirred overnight, producing a yellow solution with a white precipitate. Volatiles were removed *in vacuo* and the product extracted into pentane and filtered. The filtrate was concentrated and the solution cooled to -20 °C to produce orange crystals. After filtration, the orange crystals were washed with cold pentane (2 x 10 mL) and dried *in vacuo*. Yield: 280 mg, 51% yield. Yellow single crystals suitable for X-ray crystallography could be obtained by recrystallization from pentane at -20 °C.

Spectroscopic Data for (28)Ge

^{1}H NMR (C_6D_6, 400 MHz, 298 K): δ_H 6.01-7.16 (overlapping m, *p-H* and *m-H* of Dipp and C_6D_5H), 5.98 (4H, s, N(C*H*)$_2$N of boryl ligand), 3.28 (8H, sept, $^3J_{HH}$ = 6.8 Hz, C*H*Me$_2$), 2.93 (4H, s, NC*H*$_2$), 1.19 (24H, d, $^3J_{HH}$ = 6.8 Hz, CH*Me*$_2$), 1.11 (24H, d, $^3J_{HH}$ = 6.8 Hz, CH*Me*$_2$) ppm. Integration of *m-H* and *p-H* of Dipp is slightly higher than expected due to partial overlap with C_6D_5H. ^{13}C{^{1}H} NMR (C_6D_6, 101 MHz, 298 K): δ_C 146.5 (*o-C* of Dipp), 140.1 (*i-C* of Dipp), 127.8 (*p-C* of Dipp), 124.0 (*m-C* of Dipp), 118.0 (N(*C*H)$_2$N of boryl ligand), 51.3 (N*C*H$_2$), 28.6 (*C*HMe$_2$), 25.1 (CH*Me*$_2$), 23.4 (CH*Me*$_2$) ppm. ^{11}B NMR

(C_6D_6, 128 MHz, 298 K): δ_B 24 (br s, boryl ligand) ppm. Elemental microanalysis: found (calcd. for $C_{54}H_{76}B_2N_6Ge$): C 71.80 (71.79)%, H 8.69 (8.48)%, N 8.86 (9.30)%.

Crystallographic Data for (28)Ge

a = 12.9973(1) Å, *b* = 20.9096(1) Å, *c* = 21.1512(2) Å, α = γ = 90°, β = 103.4323(7)°, V = 5590.98(8) Å^3, Monoclinic, *P*2$_1$/c, *Z* = 2, R_1 for 10696 [data intensity $I > 2\sigma(I)$] unique data = 0.031, wR_2 (all 11609 unique data) = 0.085.

Preparation of (29)Ge

Method (a): A mixture of (**29**)H_2 (50 mg, 0.059 mmol) and benzyl potassium (15 mg, 0.12 mmol) in a J. Young's NMR tube was dissolved in C_6D_6 (0.5 mL) and the resulting red solution sonicated for 3 h. $GeCl_2$·dioxane (15 mg, 0.064 mmol) was then added and the reaction mixture sonicated for a further 5 h. Samples prepared this way were invariably contaminated with *ca.* 25% of (**29**)H_2. Yellow crystals suitable for X-ray crystallography could be obtained by recrystallization from pentane at -20 °C.

Method (b) (preparative scale): (**29**)Ge could also be prepared from Li_2(**29**) by a similar method to (**28**)Ge, using (**29**)H_2 (0.90 g, 1.1 mmol), TMEDA (160 μL, 1.1 mmol), ^{n}BuLi (2.7 mL of a 1.6 M solution in hexane, 4.3 mmol) and $GeCl_2$·dioxane (0.87 mg, 3.7 mmol) in toluene (5 mL). The product was isolated by recrystallization from hexane at -20 °C. Yield: 0.39 g, 40% yield.

Spectroscopic Data for (29)Ge

^{1}H NMR (C_6D_6, 400 MHz, 298 K): δ_H 7.04-7.20 (overlapping m, *p-H* and *m-H* of Dipp and C_6D_5H), 5.97 (4H, s, N(C*H*)$_2$N of boryl ligand), 3.29 (8H, sept, $^3J_{HH}$ = 6.9 Hz, C*H*Me$_2$), 2.80 (4H, m, NCH_2), 1.12-1.24 (50H, overlapping m, CH*Me*$_2$ and CH_2(NCH$_2$)$_2$) ppm.

Integration of *m-H* and *p-H* of Dipp is slightly higher than expected due to partial overlap with C_6D_5H. $^{13}C\{^1H\}$ NMR (C_6D_6, 101 MHz, 298 K): δ_C 146.0 (*o-C* of Dipp), 140.2 (*i-C* of Dipp), 127.5 (*p-C* of Dipp), 124.0 (*m-C* of Dipp), 118.6 (N(*C*H)$_2$N of boryl ligand), 46.8 (N*C*H$_2$), 33.5 (*C*H$_2$(CH$_2$N)$_2$), 28.7 (*C*HMe$_2$), 25.4 (CH*Me*$_2$), 23.8 (CH*Me*$_2$) ppm. ^{11}B NMR (C_6D_6, 128 MHz, 298 K): δ_B 25 (br s, boryl group) ppm. MS (EI): *m/z* (assignment, %) 918.6 ([M]$^+$, 0.6%). Acc. Mass ESI: calc. for $[C_{55}H_{78}B_2N_6Ge]^+$: 918.5686; found: 918.5714.

Crystallographic Data for (29)Ge

a = 10.6441(2) Å, *b* = 13.4667(4) Å, *c* = 19.8671(5) Å, α = 70.951(2)°, β = 78.3208(19)°, γ = 89.024(2)°, V = 2632.39(12) Å^3, Triclinic, *P*1, *Z* = 2, R_1 for 9790 [data intensity $I > 2\sigma(I)$] unique data = 0.035, wR_2 (all 10828 unique data) = 0.090.

Preparation of (28)Sn

(**28**)Sn was prepared from Li_2(**28**) by a similar method to (**28**)Ge using (**28**)H_2 (0.20 g, 0.24 mmol), TMEDA (36 μL, 0.24 mmol), ^{n}BuLi (0.60 mL of a 1.6 M solution in hexane, 0.96 mmol) and $SnCl_2$ (46 mg, 0.24 mmol) in toluene (2 mL). The hexane filtrate was slowly concentrated to yield a small quantity of orange crystals suitable for X-ray crystallography. The product could not be crystallized for isolation on a bulk scale due to high solubility, moisture sensitivity and contamination of (**28**)H_2. Samples are invariably contaminated with *ca.* 25% of (**28**)H_2.

Spectroscopic Data for (28)Sn (with 25% of (28)H_2)

^1H NMR (C_6D_6, 400 MHz, 298 K): δ_H 7.01-7.13 (overlapping m, *m-C* and *p-C* of Dipp), 5.99 (4H, s, N(C*H*)$_2$N of boryl ligand), 3.35 (8H, sept, $^3J_{HH}$ = 6.8 Hz, C*H*Me$_2$), 3.07 (4H, s, NC*H*$_2$), 1.19 (24H, d, $^3J_{HH}$ = 6.8 Hz, CH*Me*$_2$), 1.15 (24H, d, $^3J_{HH}$ = 6.8 Hz, CH*Me*$_2$) ppm.

^{119}Sn NMR (C_6D_6, 149MHz, 298K): δ_{Sn} 527-529 (br s) ppm.

Preparation of (29)Sn

(**29**)Sn was prepared in a similar method to (**28**)Ge, using (**29**)H_2 (0.50 g, 0.59 mmol), TMEDA (90 μL, 0.59 mmol), ^{n}BuLi (1.5 mL of a 1.6 M solution in hexane, 2.5 mmol) and $SnCl_2$ (0.39 mg, 2.1 mmol) in toluene (4 mL). The reaction mixture was stirred at room temperature for 24 h. Yield: 0.20 g, 35%. Orange single crystals suitable for X-ray crystallography could be obtained by recrystallization from pentane at -20 °C. Samples are invariably contaminated with *ca.* 15% of (**29**)H_2.

Spectroscopic Data for (29)Sn (with 15% of (29)H_2)

^{1}H NMR (C_6D_6, 400 MHz, 298 K): δ_H 7.05-7.22 (12H, overlapping m, *p-H* and *m-H* of Dipp and C_6D_5H), 5.97 (4H, s, N(C*H*)$_2$N of boryl ligand), 3.36 (8H, sept, $^3J_{HH}$ = 6.9 Hz, C*H*Me$_2$), 3.05 (4H, dd, $^3J_{HH}$ = 7.1 Hz, $^3J_{HH}$ = 6.9 Hz, NCH_2), 1.18-1.25 (50H, overlapping m, CH*Me*$_2$ and CH_2(CH$_2$N)$_2$) ppm. Integration of *m-H* and *p-H* of Dipp is slightly higher than expected due to partial overlap with C_6D_5H. ^{13}C{^{1}H} NMR (C_6D_6, 101 MHz, 298 K): δ_C 146.5 (*o-C* of Dipp), 140.7 (*i-C* of Dipp), 127.7 (*p-C* of Dipp), 124.2 (*m-C* of Dipp), 118.3 (N(*C*H)$_2$N of boryl ligand), 47.6 (N*C*H$_2$), 37.7 (*C*H$_2$(CH$_2$N)$_2$), 28.6 (*C*HMe$_2$), 25.4 (CH*Me*$_2$), 23.6 (CH*Me*$_2$) ppm. ^{11}B NMR (C_6D_6, 128 MHz, 298 K): δ_B 25 (br s, boryl ligand) ppm. ^{119}Sn NMR (C_6D_6, 149 MHz, 298 K): δ_{Sn} 457-459 (br s). MS (EI): *m/z* (assignment, %) 964.6 ([M]$^+$, 0.6%). Acc. Mass ESI: calc. for [$C_{55}H_{78}B_2N_6Ge$]$^+$: 964.5496; found: 964.5557.

Crystallographic Data for (29)Sn

a = 10.5800(2) Å, *b* = 13.7902(2) Å, *c* = 36.8584(4) Å, α = γ = 90°, β = 91.0379(12)°, V = 5376.77(14) Å^3, Monoclinic, $P2_1/c$, *Z* = 4, R_1 for 10209 [data intensity $I > 2\sigma(I)$]

unique data = 0.100, wR_2 (all 11123 unique data) = 0.295.

Preparation of (29)Ge(OCH$_2$NMe$_2$)(OH)

A mixture of (**29**)Ge (51 mg, 0.056 mmol) and trimethylamine *N*-oxide (6 mg, 0.08 mmol) in a J. Young's NMR tube was dissolved in C_6D_6 and the resulting solution sonicated for 3 h, at which point it had turned pale yellow. Single crystals suitable for X-ray crystallography could be obtained by recrystallization from cyclohexane at -20 °C. The remainder of the crystals were isolated for characterization by filtration of the supernatant but are invariably contaminated with *ca.* 7% of germanediol, (**29**)Ge(OH)$_2$.

Spectroscopic Data for (29)Ge(OCH$_2$NMe$_2$)(OH) (with 7% of (29)Ge(OH)$_2$)

^{1}H NMR (C_6D_6, 400 MHz, 298 K): δ_H 7.10-7.20 (12H, overlapping m, *m-H* and *p-H* of Dipp), 5.92 (4H, s, N(C*H*)$_2$N of boryl ligand), 3.45 (2H, s, OC*H*$_2$), 3.31-3.44 (8H, overlapping sept, C*H*Me$_2$), 2.89 (4H, m, NC*H*$_2$), 2.20 (6H, s, N*Me*$_2$), 1.17 (12H, d, $^3J_{HH}$ = 6.7 Hz, CH*Me*$_2$), 1.20 (12H, d, $^3J_{HH}$ = 6.7 Hz, CH*Me*$_2$), 1.30 (12H, d, $^3J_{HH}$ = 6.7 Hz, CH*Me*$_2$), 1.35 (12H, d, $^3J_{HH}$ = 6.7 Hz, CH*Me*$_2$), 0.85-0.67 (2H, m, C*H*$_2$(CH$_2$N)$_2$), 0.24 (1H, s, O*H*) ppm. ^{13}C{^{1}H} NMR (C_6D_6, 101 MHz, 298 K): δ_C 147.1 (*o-C* of Dipp), 147.0 (*o-C* of Dipp), 140.4 (*i-C* of Dipp), 127.6 (*p-C* of Dipp), 123.8 (*m-C* of Dipp), 123.7 (*m-C* of Dipp), 119.1 (N(*C*H)$_2$N of boryl ligand), 82.9 (O*C*H$_2$), 47.3 (N*C*H$_2$), 41.7 (N*Me*$_2$), 31.5 (*C*H$_2$(CH$_2$N)$_2$), 28.6 (*C*HMe$_2$), 28.5 (*C*HMe$_2$), 26.3 (CH*Me*$_2$), 26.3 (CH*Me*$_2$), 23.7 (CH*Me*$_2$), 23.5 (CH*Me*$_2$) ppm.

Crystallographic Data for (29)Ge(OCH$_2$NMe$_2$)(OH)

a = 13.4539(2) Å, *b* = 18.6682(2) Å, *c* = 23.0037(3) Å, α = β = γ = 90°, V = 5777.61(13) Å^3, Orthorhombic, $P2_12_12_1$, *Z* = 4, R_1 for 11432 [data intensity $I > 2\sigma(I)$] unique data = 0.038, wR_2 (all 12005 unique data) = 0.099.

Hydrolysis of (29)Ge(OCH_2NMe_2)(OH)

Upon exposure to moisture, (**29**)Ge(OCH_2NMe_2)(OH) is hydrolysed to form germanediol, (**29**)Ge$(OH)_2$. Single crystals suitable for X-ray crystallography could be obtained by recrystallization by slow evaporation of a benzene solution.

Spectroscopic data for (29)Ge$(OH)_2$

^{1}H NMR (C_6D_6, 400 MHz, 298 K): δ_H 7.13-7.22 (12H, overlapping m, *m-H* and *p-H* of Dipp), 6.02 (4H, s, N(C*H*)$_2$N of boryl ligand), 3.43 (8H, sept, $^3J_{HH}$ = 6.9 Hz, C*H*Me$_2$), 2.85 (4H, m, NCH_2), 1.30 (24H, d, $^3J_{HH}$ = 6.9 Hz, CH*Me*$_2$), 1.20 (24H, d, $^3J_{HH}$ = 6.9 Hz, CH*Me*$_2$), 0.87 (2H, m, CH_2($CH_2N)_2$), -0.10 (2H, s, Ge(O*H*)$_2$) ppm. ^{13}C{^{1}H} NMR (C_6D_6, 101 MHz, 298 K): δ_C 147.2 (*o-C* of Dipp), 139.9 (*i-C* of Dipp), 127.6 (*p-C* of Dipp), 123.9 (*m-C* of Dipp), 118.5 (N(*C*H)$_2$N of boryl ligand), 47.5 (N*C*H$_2$), 32.2 (*C*H_2($CH_2N)_2$), 28.6 (*C*HMe$_2$), 26.0 (CH*Me*$_2$), 23.4 (CH*Me*$_2$) ppm. ^{11}B NMR (C_6D_6, 128 MHz, 298 K): δ_B 23 (br s, boryl ligand) ppm.

Crystallographic Data for (29)Ge$(OH)_2$

a = 10.74425(14) Å, *b* = 13.38809(14) Å, *c* = 37.3049(5) Å, α = γ = 90°, β = 90.2315(12)°, V = 5366.08(11) Å^3, Monoclinic, $P2_1/c$, *Z* = 4, R_1 for 10263 [data intensity $I > 2\sigma(I)$] unique data = 0.031, wR_2 (all 11122 unique data) = 0.081.

Preparation of (28)Ge(C_5H_4NO)(OH)

A mixture of (**28**)Ge (45 mg, 0.049 mmol) and pyridine *N*-oxide (10 mg, 0.11 mmol) in a J. Young's NMR tube was dissolved in toluene-d_8 and the resulting mixture heated at 110 °C for 3 days. The ^{1}H NMR spectrum measured at this point indicates complete consumption of the germylene and conversion to a new product. Attempts to obtain single crystals suitable for X-ray crystallography were unsuccessful.

In Situ Spectroscopic Data for (28)Ge(C_5H_4NO)(OH)

^{1}H NMR (toluene-d_8, 400 MHz, 298 K): δ_H 6.77-7.20 (overlapping m, *p-H* and *m-H* of Dipp and toluene-d_8), 7.73 (1H, m, Ge{C(CH)$_3$C*H*(NO)}), 7.36 (2H, overlapping m, Ge{CC*H*(CH)$_3$(NO)} and Ge{C(CH)$_2$C*H*CH(NO)}), 5.64 (1H, m, Ge{CCHC*H*(CH)$_2$(NO)}), 5.87 (4H, s, N(C*H*)$_2$N of boryl ligand), 3.45 (4H, sept, $^3J_{HH}$ = 6.8 Hz, C*H*Me$_2$), 3.33 (4H, sept, $^3J_{HH}$ = 6.8 Hz, C*H*Me$_2$), 3.19 (2H, br m, NC*H*$_2$), 2.89 (2H, br m, NC*H*$_2$), 1.35 (12H, d, $^3J_{HH}$ = 6.8 Hz, CH*Me*$_2$), 1.18 (12H, d, $^3J_{HH}$ = 6.8 Hz, CH*Me*$_2$), 1.15 (12H, d, $^3J_{HH}$ = 6.8 Hz, CH*Me*$_2$), 1.12 (12H, d, $^3J_{HH}$ = 6.8 Hz, CH*Me*$_2$), 0.75 (1H, s, O*H*) ppm. Integration of *m-H* and *p-H* of Dipp is slightly higher than expected due to partial overlap with toluene-d_8.

Preparation of (29)Ge(C_5H_4NO)(OH)

(**29**)Ge(C_5H_4NO)(OH) was prepared in a similar method to (**28**)Ge(C_5H_4NO)(OH) using (**29**)Ge (23 mg, 0.025 mmol) and pyridine *N*-oxide (5 mg, 0.05 mmol) in toluene-d_8 (0.5 mL). Single crystals suitable for X-ray crystallography were grown from a hexane solution at -20°C.

Spectroscopic Data for (29)Ge(C_5H_4NO)(OH)

^{1}H NMR (toluene-d_8, 400 MHz, 298 K): δ_H 6.81-7.24 (overlapping m, *p-H* and *m-H* of Dipp and toluene-d_8), 7.45 (1H, m, Ge{C(CH)$_3$C*H*(NO)}), 6.14 (2H, overlapping m, Ge{CC*H*(CH)$_3$(NO)} and Ge{C(CH)$_2$C*H*CH(NO)}), 5.90 (4H, s, N(C*H*)$_2$N of boryl ligand), 5.64 (1H, m, Ge{CCHC*H*(CH)$_2$(NO)}) 3.41 (8H, overlapping m, C*H*Me$_2$), 3.80 (2H, br m, NC*H*$_2$), 3.25 (2H, br m, NC*H*$_2$), 1.35 (12H d, $^3J_{HH}$ = 6.7 Hz, CH*Me*$_2$), 1.16-1.23 (38H, overlapping m, CH*Me*$_2$ and C*H*$_2$(CH$_2$N)$_2$), 0.79 (1H, s, O*H*) ppm. Integration of *m-H* and *p-H* of Dipp is slightly higher than expected due to partial overlap with toluene-d_8. ^{13}C{^{1}H} NMR (C_6D_6, 101 MHz, 298 K): δ_C 148.1 (Ge{*C*(CH)$_4$(NO)}), 146.7 (*o-C* of Dipp),

146.5 (*o-C* of Dipp), 141.0 (*i-C* of Dipp), 136.1 (Ge{C(CH)$_3$*C*H(NO)}), 131.5 (Ge{C(CH)$_2$*C*HCH(NO)}), 129.0 (*p-C* of Dipp), 128.0 (*m-C* of Dipp), 127.2 (*m-C* of Dipp), 123.9 and 123.8 (Ge{C*C*H(CH)$_3$(NO)} and Ge{C(CH)$_2$*C*HCH(NO)}), 118.9 (N(*C*H)$_2$N of boryl ligand), 47.8 (N*C*H$_2$), 33.4 (*C*H$_2$(CH$_2$N)$_2$), 28.8 (*C*HMe$_2$), 28.5 (*C*HMe$_2$), 26.5 (CH*Me*$_2$), 26.0 (CH*Me*$_2$), 23.6 (CH*Me*$_2$), 22.6 (CH*Me*$_2$) ppm. ^{11}B NMR (C_6D_6, 128 MHz, 298 K): δ_B 24 (br s, boryl ligand) ppm.

Crystallographic Data for (29)Ge(C_5H_4NO)(OH)

a = *b* = 42.2093(12) Å, *c* = 13.8670(5) Å, α = β = γ = 90°, V = 24705.8(13) Å^3, Tetragonal, *I4$_1$/a*, *Z* = 16, R_1 for 10060 [data intensity $I > 2\sigma(I)$] unique data = 0.070, wR_2 (all 12712 unique data) = 0.99.

Preparation of 34

A mixture of (**28**)Ge (30 mg, 0.33 mmol) and excess S_8 in a J. Young's NMR tube was dissolved in C_6D_6 (0.5 mL) and the resulting reaction mixture heated at 80 °C for 18 d. The ^{1}H NMR spectrum of an aliquot taken from the reaction mixture measured at this point indicates complete consumption of the germylene and conversion to a new product. Attempts to obtain single crystals suitable for X-ray crystallography were unsuccessful.

***In Situ* Spectroscopic Data for 34**

^{1}H NMR (C_6D_6, 400 MHz, 298 K): δ_H 7.01-7.18 (overlapping m, *p-H* and *m-H* of Dipp and C_6D_5H), 5.96 (4H, s, N(C*H*)$_2$N of boryl ligand), 3.31 (8H, sept, $^3J_{HH}$ = 6.8 Hz, C*H*Me$_2$), 3.80 (2H, br m, NC*H*$_2$), 3.25 (2H, br m, NC*H*$_2$), 1.25 (24H, br d, $^3J_{HH}$ = 6.8 Hz, CH*Me*$_2$), 1.10 (24H, d, $^3J_{HH}$ = 6.8 Hz, CH*Me*$_2$) ppm. Integration of *m-H* and *p-H* of Dipp is slightly higher than expected due to partial overlap with C_6D_5H.

Preparation of (29)Ge(S)$_4$

(**29**)Ge(S)$_4$ was prepared in a similar method to **34** from (**29**)Ge (25 mg, 0.027 mmol) and excess S_8 in C_6D_6 (0.5 mL). The reaction was completed after heating the reaction mixture at 80 °C for 8 days. Single crystals suitable for X-ray crystallography were grown by slow evaporation of a hexane solution.

Spectroscopic Data for (29)Ge(S)$_4$

^{1}H NMR (C_6D_6, 400 MHz, 313 K): δ_H 7.01-7.16 (overlapping m, *p-H* and *m-H* of Dipp and C_6D_5H), 6.03 (4H, s, N(C*H*)$_2$N of boryl ligand), 3.33 (8H, sept, $^3J_{HH}$ = 6.8 Hz, C*H*Me$_2$), 3.20 (4H, m, NCH_2), 1.36 (24H, d, $^3J_{HH}$ = 6.8 Hz, CH*Me*$_2$), 1.14 (24H, d, $^3J_{HH}$ = 6.8 Hz, CH*Me*$_2$), (0.07, m, CH_2(CH$_2$N)$_2$) ppm. Integration of *m-H* and *p-H* of Dipp is slightly higher than expected due to partial overlap with C_6D_5H. ^{13}C{^{1}H} NMR (C_6D_6, 101 MHz, 298 K): δ_C 147.2 (*o-C* of Dipp), 139.8 (*i-C* of Dipp), 127.5 (*p-C* of Dipp), 123.7 (*m-C* of Dipp), 118.9 (N(*C*H)$_2$N of boryl ligand), 45.8 (NCH$_2$), 28.8 (*C*H$_2$(CH$_2$N)$_2$), 28.6 (*C*HMe$_2$), 24.7 (CH*Me*$_2$), 23.9 (CH*Me*$_2$) ppm. ^{11}B NMR (C_6D_6, 128 MHz, 298 K): δ_B 24 (br s, boryl ligand) ppm.

Crystallographic Data for (29)Ge(S)$_4$

a = 25.9885(7) Å, *b* = 12.7722(2) Å, *c* = 40.4419(9) Å, α = γ = 90°, β = 99.221(2)°, V = 13250.4(5) Å^3, Monoclinic, *I*2/*c*, *Z* = 8, R_1 for 12411 [data intensity $I > 2\sigma(I)$] unique data = 0.034, wR_2 (all 13747 unique data) = 0.087.

Preparation of 35

A mixture of (**29**)Ge(S)$_4$ (12 mg, 0.013 mmol) and triphenylphosphine (10 mg, 0.039 mmol) in a J. Young's NMR tube was dissolved in C_6D_6 and the resulting mixture sonicated for 24 h. The ^{1}H NMR spectrum of the reaction mixture measured at this

point indicates complete consumption of (**29**)Ge(S)$_4$ and conversion to a new product.

Spectroscopic Data for 35

^{1}H NMR (C_6D_6, 400 MHz, 313 K): δ_H 7.11-7.22 (overlapping m, *p-H* and *m-H* of Dipp and C_6D_5H), 5.87 (4H, s, N(C*H*)$_2$N of boryl ligand), 3.33 (8H, br m, C*H*Me$_2$), 2.89 (2H, br m, NCH_2), 2.07 (2H, br m, NCH_2), 1.17-1.23 (48H, overlapping d, CH*Me*$_2$) ppm. Integration of *m-H* and *p-H* of Dipp is slightly higher than expected due to partial overlap with C_6D_5H. ^{31}P NMR (C_6D_6, 162 MHz, 298 K): δ_P 42.7 (PPh_3S) ppm.

5.5 References

1 C. Li, S. L. Mella and A. C. Sartorelli, *J. Med. Chem*, 1981, **1241**, 1089–1092.
2 F. Aminals, M. K. Denk, S. Gupta, J. Brownie and S. Tajammul, *Chem. Eur. J.*, 2001, **7**, 4477–4486.
3 P. de Frémont, N. Marion and S. P. Nolan, *Coord. Chem. Rev.*, 2009, **253**, 862–892.
4 M. K. Denk, A. Thadani, K. Hatano and A. J. Lough, *Angew. Chem. Int. Ed.*, 1997, **36**, 2607–2609.
5 B. Gehrhus, P. B. Hitchcock and M. F. Lappert, *J. Chem. Soc. Dalton Trans.*, 2000, **2**, 3094–3099.
6 T. J. Hadlington, J. A. B. Abdalla, R. Tirfoin, S. Aldridge and C. Jones, *Chem. Commun.*, 2016, **52**, 1717–1720.
7 P. J. Davidson and M. F. Lappert, *J. Chem. Soc., Chem. Commun.*, 1973, **0**, 317.
8 R. S. Ghadwal, H. W. Roesky, S. Merkel, J. Henn and D. Stalke, *Angew. Chem. Int. Ed.*, 2009, **48**, 5683–5686.
9 A. C. Filippou, O. Chernov and G. Schnakenburg, *Angew. Chem. Int. Ed.*, 2009, **48**, 5687–5690.
10 M. Denk, R. Lennon, R. Hayashi, R. West, A. V. Belyakov, H. P. Verne, A. Haaland, M. Wagner and N. Metzler, *J. Am. Chem. Soc.*, 1994, **116**, 2691–2692.
11 S. S. Sen, H. W. Roesky, D. Stern, J. Henn and D. Stalke, *J. Am. Chem. Soc.*, 2010, **132**, 1123–1126.
12 H. tom Dieck and M. Zettlitzer, *Chem. Ber.*, 1987, **120**, 795–801.
13 J. Küpp, M. Remko and P. von R. Schleyer, *J. Am. Chem. Soc.*, 1996, **1118**, 5745–5751.
14 L. Li, T. Fukawa, T. Matsuo, D. Hashizume, H. Fueno, K. Tanaka and K. Tamao, *Nat. Chem.*, 2012, **4**, 361–365.
15 I. Alvarado-Beltran, A. Rosas-Sánchez, A. Baceiredo, N. Saffon-Merceron, V.

Branchadell and T. Kato, *Angew. Chem. Int. Ed.*, 2017, **56**, 10481–10485.
16 A. Rosas-Sánchez, I. Alvarado-Beltran, A. Baceiredo, N. Saffon-Merceron, S. Massou, D. Hashizume, V. Branchadell and T. Kato, *Angew. Chem. Int. Ed.*, 2017, **56**, 15916–15920.
17 E. L. Kolychev, I. A. Portnyagin, V. V. Shuntikov, V. N. Khrustalev and M. S. Nechaev, *J. Organomet. Chem.*, 2009, **694**, 2454–2462.
18 N. Phillips, R. Tirfoin and S. Aldridge, *Chem. Eur. J.*, 2014, **20**, 3825–3830.
19 N. Phillips, R. Tirfoin and S. Aldridge, *Dalton Trans.*, 2014, **43**, 15279–15282.
20 R. K. Haynes, S. C. Vonwiller and M. R. Luderer, in *Encyclopedia of Reagents for Organic Synthesis*, ed. L. A. Paquette, J. Wiley & Sons, New York, 2006.
21 B. Cordero, V. Gómez, A. E. Platero-Prats, M. Revés, J. Echeverría, E. Cremades, F. Barragán and S. Alvarez, *Dalton Trans.*, 2008, **0**, 2832.
22 E. Tomás-Mendivil, M. M. Hansmann, C. M. Weinstein, R. Jazzar, M. Melaimi and G. Bertrand, *J. Am. Chem. Soc.*, 2017, **139**, 7753–7756.
23 A. D. Johnson, *Some Thermodynamic Aspects of Inorganic Chemistry*, Cambridge University Press, Cambridge, 2nd edn., 1982.
24 P. Bhattacharyya and J. D. Woollins, *Tetrahedron Lett.*, 2001, **42**, 5949–5951.
25 M. Kira, S. Ishida, T. Iwamoto and C. Kabuto, *J. Am. Chem. Soc.*, 1999, **121**, 9722–9723.
26 C. Weinstein and G. Bertrand, *Unpubl. Results*.
27 P. A. Chase, A. L. Gille, T. M. Gilbert and D. W. Stephan, *Dalton Trans.*, 2009, **0**, 7179–7188.
28 M. Veith and A. Rammo, *Zeitschrift fur Anorg. und Allg. Chemie*, 1997, **623**, 861–872.
29 S. Yao, Y. Xiong and M. Driess, *Chem. Eur. J.*, 2010, **16**, 1281–1288.
30 A. V. Protchenko and S. Aldridge, *Unpubl. Results*.
31 L. Wang, Y. S. Lim, Y. Li, R. Ganguly and R. Kinjo, *Molecules*, 2016, **21**, 990–1000.
32 N. Tokitoh, T. Matsumoto, K. Manmaru and R. Okazaki, *J. Am. Chem. Soc.*, 1993, **115**, 8855–8856.
33 G. Baccolini, C. Boga and M. Mazzacurati, *J. Org. Chem.*, 2005, **70**, 4774–4777.

Chapter VI

Conclusions

6.1 Conclusions and Future Work

Chapter III focused on the syntheses of various borylated imidazoles and imidazolium salts, with the aim of accessing an *N*,*N*'-bisborylated NHC or its metal complexes. The reactivity of the bisborylated imidazolium salts ([(**4**)H]$^+$) with alkali metal bis(trimethylsilyl)amides leads to deprotonation of the imidazolium moiety, but at C5 rather than at the desired C2 position. Due to a lack of steric protection at the backbone positions, a facile 1,2-migration of one of the boryl groups takes place. This 1,2-shift occurs too quickly to allow for the detection, isolation or trapping of intermediates. Attempts were made to access the C2-centred carbene by blocking the backbone CH sites. Benzimidazole and 4,5-diphenylimidazole were unfortunately not suitable building blocks for the respective bisborylated imidazolium salts as a second boryl group could not be attached due to the reduced nucleophilicity of the imidazole core. This is attributed to the electron-withdrawing nature of the backbone substituents. 4,5-Dimethylimidazole did, on the other hand, prove to be a suitable precursor to a bisborylated imidazolium salt. On treatment with a base, however, one of the backbone-substituted methyl groups was deprotonated, followed by a 1,3-shift of one of the boryl groups to give an unsymmetrical charge neutral species featuring a backbone activated methyl group (**12**). Wynberg *et al*. have reported a synthetic procedure for 4,5-di-*tert*-butylimidazole,[1] which could be a potential precursor for the target NHC as the *tert*-butyl group is not electron-withdrawing and does not

possess an acidic proton. It could therefore be an ideal candidate to block the backbone sites.

The aim of the research reported in chapter IV was two-fold: (a) the synthesis of an abnormal NHC with boryl substituents attached to each of the atoms α to the carbene centre (**4.1**), and (b) syntheses of unsymmetrical NHCs bearing one *N*- boryl group, with the second *N*-substituent being an alkyl group (**4.2**). Unfortunately, a bisborylated abnormal NHC could not be accessed; deprotonation of a 1,4-bisborylated imidazolium salt with *N*- and *C2*-bound methyl groups ([(**15**)H]$^+$) leads instead to the formation of an *N*-heterocyclic olefin (**16**). NHOs make up an attractive ligand class and it would be interesting to investigate further the properties of this unsymmetrical bisborylated NHO. Attempts to access a similar imidazolium precursor, with a *C2*-bound phenyl group (from 2-phenylimidazole) were unsuccessful on account of the electron-withdrawing properties of the phenyl group. Again, a *tert*-butyl group might be a suitable substituent at the C2 position as 2-*tert*-butylimidazole is readily synthesized[2] and could be used as a building block for an imidazolium salt of type [(**4.1**)H]$^+$.

The synthesis of unsymmetrical NHCs bearing an *N*-substituted boryl group was more successful, leading, for example, to an unsymmetrical 1,4-bisborylated NHC (**14**). The *N*-bound methyl group offers adequate kinetic stability towards the 1,2-migration of the *N*-bound boryl group, and the resulting carbene can be observed and characterized both *in situ* and in a range of trapping experiments. The relatively slow 1,2-rearrangement ($t_{½}$ = 4.01 ± 0.04 h at room temperature) allows for assessment of the kinetics of this migration process. The kinetic data reveal a first-order rate determining step and an entropy of activation close to zero, suggesting an

intramolecular 1,2-rearrangement. Such intramolecular processes have not been reported previously for aromatic carbenes and have, until now, been considered kinetically unfavourable with calculated activation barriers close to double that determined for **14** (both experimentally and computationally). Experimental and computational studies of a related *N*-borylated system (**20**) are also consistent with an intramolecular rearrangement, with a slightly higher activation barrier. Transition metal complexes and a selenium adduct of carbene **14** have been successfully synthesized and structurally characterized by X-ray crystallography, and their structural/spectroscopic studies used to give insight into the electronic and steric properties of the carbene. The experimental and computational data are consistent with the pendant boryl groups leading to enhanced σ-donor properties for the carbene. Furthermore, the *N*-bound boryl group offers great steric protection, resulting in a carbene with a $\%V_{bur}$ of 50.0%, despite the *N*-bound substituent (a methyl group) not being very sterically demanding. In terms of future work, it is likely that related *N*-borylated carbenes bearing a bulkier second *N*-substituent (*i.e*. bigger than Me) might (a) be stable towards 1,2-rearrangement, which would allow for the isolation of a 'free' borylated NHC; and (b) in terms of steric properties, exceed the bulkiest carbenes reported to date.

Chapter V reports on attempts to synthesize saturated *N*,*N*'-bisborylated saturated NHCs and closely related heavier Group 14 tetrelenes. It was thought that using a saturated backbone might favour deprotonation at C2 to give the target NHC, which could be kinetically stable towards a 1,2-rearrangement. Deprotonation of the backbone of a six-membered bisborylated pyrimidium salt, however, leads to a 1,4-Hofmann elimination and ring-opening of the pyrimidine heterocycle *via* C–N bond cleavage. While 5-membered CAACs are well known and easily accessed, the 6-

membered analogues have proven to be difficult to synthesize on account of similar ring-opening on deprotonation of the precursor.[3] This suggests that the 5-membered saturated systems are more stable towards 1,4-Hofmann elimination and it would be interesting to see if deprotonation of an *N,N*'-bisborylated imidazolinium might take place at the C2 position to give the target NHC. *N*,*N*'-bisborylated *N*-heterocyclic germylenes and stannylenes were successfully synthesized and structurally characterized. NMR spectroscopic studies *in situ* suggest the successful synthesis of related *N*,*N*'-bisborylated *N*-heterocyclic silylenes, but their isolation was unsuccessful on account of high degrees of contamination by the respective protio-ligands and the by-product, IPr. Syntheses of target germanones from germylenes (**28**)Ge and (**29**)Ge were unsuccessful as the proposed transient germanone appears to be too reactive and activates a second molecule of the respective oxygen transfer agent.

In conclusion, the reactions of borylated *N*-heterocyclic systems examined in this thesis have highlighted the lability of the exocyclic N–B bonds, and electrophilicity of the boryl group; displacement or migration of the boryl group was repeatedly observed. Attempts to isolate an *N*,*N*'-bisborylated NHC were unsuccessful but *N*,*N*'-bisborylated *N*-heterocyclic tetrelenes were successfully synthesized and isolated as they can be prepared directly *via* salt metathesis, and thus do not rely on deprotonation or reduction under harsh conditions.

6.2 References

1 H. Wynberg and A. de Groot, *Chem. Commun.*, 1966, **0**, 171.

2 J. Dong, S. Chen, R. Li, W. Cui, H. Jiang, Y. Ling, Z. Yang and W. Hu, *Eur. J. Med. Chem.*, 2016, **108**, 605–615.

3 C. Weinstein and G. Bertrand, *Unpubl. Results*.